RESEARCH ON IMPROVING TERMINAL TRAFFIC FLOW EFFICIENCY AND AIRPORT CAPACITY THROUGH DATA-DRIVEN AND DEEP LEARNING-BASED DYNAMIC AIRCRAFT WAKE SEPARATION PREDICTION

NANA CHU

PhD

The Hong Kong Polytechnic University

2025

The Hong Kong Polytechnic University

Department of Aeronautical and Aviation Engineering

Research on Improving Terminal Traffic Flow Efficiency and Airport Capacity Through Data-driven and Deep Learning-based Dynamic Aircraft Wake Separation Prediction

Chu Nana

A thesis submitted in partial fulfilment of requirements for the degree of Doctor of Philosophy

Dec 2024

CERTIFICATE OF ORGINALITY

I hereby declare that this thesis is my own work and that, to the best of my knowledge and belief, it reproduces no materials previously published or written, nor material that has been accepted for the award of any other degree or diploma, except where due acknowledgement has been made in the text.

_____ _____ (Signed)

Chu Nana (Name of student)

Abstract

Improving traffic flow efficiency and runway throughput has always been crucial to dealing with heavy traffic. The trajectory-based operational concept provides an alternate option to achieve highly collaborative air traffic management, among which four-dimensional flight trajectory prediction and time-based separation build the foundation. With the development of computer technology and the accumulation of massive historical flight information and other separation-related data, emerging data-driven machine learning techniques have gained great popularity for civil air traffic operations. Despite extensive deep learning implementations in flight traffic prediction and optimisation problems, they generally focus on model development rather than the applicational scenarios, and the flight procedures and distance-based separation requirements are conservative and static, with restrictions on the efficiency of traffic dispatch. Therefore, this thesis intends to investigate the potential of deep learning in terminal traffic flow optimisation and runway scheduling, particularly from the perspective of predicting dynamic wake separation. Novel deep learning approaches are developed to improve efficiency and safety in terminal approach management and enhance their reliability and trustworthiness for these safety-critical air traffic operations.

As the lifetime and movement characteristics of aircraft wake turbulence are crucial determinants of dynamic wake separation and they are highly related to aircraft weight and meteorological conditions, deep convolutional neural networks are developed for near- real-time vortex locations and strength recognition using Light Detection and Ranging (LiDAR) -scanned wake images in the first stage. Data pre-processing, analysis, and pattern learning based on machine learning (ML) and deep learning techniques are involved and pinpointed to identify wake pairs. The first step

consists of vortex core locating utilising the Convolutional Neural Network (CNN), and the second step predicts vortex strength within the Region of Interest (ROI), derived from raw images based on the initial core locating results. This study primarily processes the wake features and builds preconditions for the second-stage wake prediction.

In the second stage, the dynamic time-based flight separation in the final approach for avoiding aircraft wake turbulence encounters is studied through long-term wake evolution prediction regarding the spatial-temporal attributes of aircraft wake vortices in their future decay and transport process, utilising the probabilistic sequential prediction models. First, the wake vortex sequences are sectored with the relevant aircraft information, such as the flight speed, heading and aircraft type, and ambient weather information mapped in the final approach. In the offline model training phase, the Attention-based Temporal Convolutional Networks (ATCN) are built and trained using the historical LiDAR dataset to achieve optimal performance. Next, the trained CNN and wake prediction models are fused to achieve long-term wake decay forecasts in actual flight scenarios. Finally, the dynamic aircraft separation minima in relation to wind conditions in the final approach is assessed with wake encounter safety analysis. Furthermore, the model decision processes are explained by feature relevance analysis of both image-based and sequential prediction-based models to enhance the trustworthiness of the deep learning model, and the prediction uncertainty of the model is estimated to improve the robustness of deep learning models.

The third part assesses the effect of time-based dynamic wake separation on runway capacity improvement at both the theoretical and operational levels. The dynamic wake vortex separation model that adjusts separation criteria in response to varying atmospheric conditions and flight pairs is trained. The runway sequencing and

scheduling model is constructed and solved with the Branch and Bound algorithm under dynamic wake separation matrices. Furthermore, the performance improvement of time-based wake separation is verified under the First-come, First-serve strategy and runway optimisation and compared with the traditional RECAT-EU wake separation standard.

The last part of this thesis develops an integrated approach for optimising runway and terminal traffic management by performing dynamic wake separation matrixes. The study evaluates the contributions of time-based and weather-related wake separation in runway operation efficiency and assesses its implications for terminal area operations during high traffic density without compromising safety and ensuring conflict-free airspace.

The overall research presents new attempts at improving traffic flow efficiency and safety of the terminal approach and enhancing the runway capacity using reliable and trustworthy data-driven deep learning-supported models and algorithms. We expect to find a comprehensive understanding of the trade-offs between efficiency gains of aircraft separation reduction under dynamic wind situations and safety considerations. This research may facilitate the development of dynamic flight separation indicators in the final approach and the robust, proactive decision-support tool for runway and terminal approach operations to benefit air traffic controllers and airport managers.

Supervisor: Prof. Kam K.H. Ng

Co-supervisor: Prof. Hsu Li-ta

Publications arising from the thesis

Journal articles (in reverse chronological order)

Chu, N., Ng, K. K. H., Liu, Y., Hon, K. K., Chan, P. W., Li, J., & Zhang, X. (2024). Assessment of approach separation with probabilistic aircraft wake vortex recognition via deep learning. Transportation Research Part E: Logistics and Transportation Review, 181, 103387. https://doi.org/https://doi.org/10.1016/j.tre.2023.103387

Chu, N., Ng, K. K., Zhu, X., Liu, Y., Li, L., & Hon, K. K. (2024). Towards dynamic flight separation in final approach: A hybrid attention-based deep learning framework for long-term spatiotemporal wake vortex prediction. Transportation Research Part C: Emerging Technologies, 169. https://doi.org/10.1016/j.trc.2024.104876

Manuscript under review and preparation (in reverse chronological order)

Chu, N., Delahaye, D., Luo, Q., Liu, Y., Zhang, C., Ng, K. K., (2024). Advanced data-driven integrated arrival optimisation in the terminal manoeuvring area leveraging intelligent dynamic wake separation prediction: Enhancing arrival performance at Hong Kong International Airport. *Transportation Research Part C: Emerging Technologies (under 1st review).*

Chu, N., Ng, K. K., Liu, Y., Tang, T., Hon, K.K. (2023). Comprehensive review of 4D flight trajectory prediction for trajectory-based air transportation: algorithms, applications and future research opportunities. *Journal of Air Transportation Management (under 1st review).*

Chu, N., Ng, K. K., (2024). Runway capacity improvement strategy: Smart dynamic aircraft wake separation prediction. *Transportation Research Part C: Emerging Technologies (under preparation).*

Chu, N., Ng, K. K., (2024). Diffusion process for aircraft wake evolution and encounter risk analysis. *(under preparation).*

Others (in reverse chronological order)

Liu, Y., Ng, K.K.H., **Chu, N.**, Hon, K.K., Zhang, X. (2023). Spatiotemporal Image-Based Flight Trajectory Clustering Model with Deep Convolutional Autoencoder Network. *Journal of Aerospace Information Systems 20(9)*, 575-587. http://doi.org/10.2514/1.I011194

Conference paper (in reverse chronological order)

Chu, N., Ng, K.K.H. *, Liu, Y., Hon, K.K. (2024). Analyzing the potential of dynamic aircraft wake separation via data-driven aircraft wake region detection. AIAA 2024-4249. AIAA AVIATION FORUM AND ASCEND 2024. July 2024. https://doi.org/10.2514/6.2024-4249 (**Best Student Paper**).

Chu, N., Ng, K.K.H. *, Liu, Y. (2023). Analysis of the impact of crosswind to aircraft wake vortex Transition through deep learning approach. *The 26th ATRS World Conference*. Kobe, Japan, June 2023.

Acknowledgements

First and foremost, I am deeply grateful to my supervisor, Professor Kam Hung Ng, for his invaluable guidance, insightful feedback, and unwavering support throughout my PhD journey. Working under his supervision in the Department of Aeronautical and Aerospace Engineering has been a rewarding experience. Reflecting on my decision to pursue postgraduate studies at our university with him as my mentor, I feel truly fortunate. He has always been there to help, whether in research challenges or daily life. This thesis wouldn't have been possible without him. Professor Ng is deeply invested in the future success of his students, providing opportunities to draft funding proposals, supervising research assistants and MPhil students, gaining industry experience, participating in international conferences, and engaging with aerospace professionals. Additionally, his encouragement to engage with cutting-edge projects and connect with experts in the field has broadened my horizons and enhanced my research skills. I am immensely thankful for his mentorship, which goes beyond academics, instilling in me the values of perseverance and integrity. This journey has not only shaped my career but also enriched my personal growth, for which I am eternally grateful. I am also sincerely grateful to my co-supervisor, Professor Hsu Li-ta, for his guidance and encouragement throughout my thesis process. Additionally, I owe a great debt of gratitude to Professor Daniel Delahaye, my host supervisor at Ecole Nationale de l'Aviation Civile (ENAC), France, for enhancing my learning experience through his shared knowledge and passion for research and teaching.

My heartfelt thanks go to my groupmates, especially Mr. Yin Yuen Chan, Ms. Ye Liu, Mr. Chenliang Zhang, Ms. Senan Yao, Yipeng Zhu, Ms. Xin Yuan, Mr. Zhongyi Jin, Ms. Mr. Congcong Du, Mr. Yeung Tsz Chun, Mr. Tam Tsz Kin, Mr. Changxin Zhu, Mr. Tong Tang, Mr. Zhou Qinyu and Ms. Bu Yuanyuan in Dr. Ng's research group at

Hong Kong Polytechnic University. Your insightful suggestions and lively discussions have been invaluable, and your companionship and laughter have provided immense support during challenging times. I am also grateful to our dedicated technician, Mr. Yin Chiu Kan, for his efficient assistance with research equipment and daily tasks.

I owe special thanks to my boyfriend, Mr. Qianyue Luo, for his suggestions when I have problems with data processing and coding, and for his patience and encouragement during my stressful times. Lastly, I am profoundly thankful to my parents, sister, brother, grandparents, and uncle for their unwavering support and trust, enabling me to focus on my studies without family or financial pressures.

Chu Nana

March 2025

Table of contents

List of Figures

List of Tables

Nomenclature

ADS-B	Automatic Dependent Surveillance-Broadcast
ALP	Aircraft Landing Problem
ANN	Artificial Neural Network
ASSP	Aircraft Sequencing and Scheduling Problem
ATCOs	Air Traffic Control Officers
ATC	Air Traffic Control
ATCN	Attention-based Temporal Convolutional Network
ATM	Air Traffic Management
BADA	EUROCONTROL Base of Aircraft Data
BNN	Bayesian Neural Network
CAA	Civil Aviation Authority
CBAM	Convolutional Block Attention Module
CFD	Computational Fluid Dynamics
CNN	Convolutional Neural Network
CSPR	Closely Spaced Parallel Runway
CPS	Conditional Position Shifting
DBS	Distance-based separation
DCNN	Deep Convolutional Neural Network
DNN	Deep Neural Network
DT	Decision Tree
EASA	European Union Aviation Safety Agency
EUROCONTROL	European Organisation for the Safety of Air Navigation
FAA	Federal Aviation Administration
FAF	Final Approach Fix

FCFS	First Come, First Serve
FTP	Flight Trajectory Prediction
GAN	Generative Adversarial Network
GMM	Gaussian Mixture Model
GRU	Gated Recurrent Unit
Grad-CAM	Grad-regression Activate Map
HKIA	Hong Kong International Airport
HMM	Hidden Markov Model
ICAO	International Civil Aviation Organisation
IFR	Instrument Flight Rules
IAF	Initial Approach Fix
KF	Kalman Filter
KNN	K-nearest Neighbour
LiDAR	Light Detection and Ranging
LSTM	Long-short Term Memory Network
MAE	Mean Absolute Error
MC	Monte Carlo
METAR	Meteorological Aerodrome Report
MIT	Miles in trail
ML	Machine Learning
MLP	Multiple-layer Perception Model
MILP	Mixed-Integer Linear Programming
MRS	Minimum Radar Separation
MSE	Mean Square Error
NAS	National Airspace System

NASA	National Aeronautics and Space Administration
NextGen	Next Generation Air Transportation System
PCA	Principal Component Analysis
PDA	Prediction Difference Analysis
QAR	Quick Access Recorder
R-CNN	Regions with CNN features
RECAT	Recategorisation of Aircraft Weight
RECAT-EU	Recategorisation in European
RMC	Rolling Moment Coefficient
RMSE	Root Mean Square Error
RNN	Recurrent Neural Network
ROT	Runway Occupancy Time
RV	Radial Velocity
SA	Simulated Annealing
SESAR	Single European Sky ATM Research Programme
SHAP	Shapley Additive Explanations
STAR	Standard Terminal Arrival Route
SVM	Support Vector Machine
TBO	Trajectory-based Operation
TBS	Time-based Separation
TCN	Temporal Convolutional Network
TTFP	Terminal Traffic Flow Problem
TMA	Terminal Manoeuvring Area
WVEs	Wake Vortex Encounters
YOLO	You Only Look Once

Chapter 1. Introduction

1.1. Research background

According to the International Air Transport Association, air traffic demand has surged by 70% since 2004 (IATA, 2022), and the overall number of travellers in 2024 is expected to be about 3% higher than in 2019, potentially reaching 4% if recovery accelerates in routes still below pre-pandemic levels (ICAO, 2024). Special care on the level of safety and efficiency is required to achieve sustainable air transportation. To achieve sustainable air transportation, particular attention must be paid to safety and efficiency. Over the past two decades, the air traffic management (ATM) community has shown a great deal of interest in Trajectory-based Operations (ICAO, 2005) as an alternate option, with advanced multinational programmes such as the Single European Sky ATM Research Programme (SESAR) (SESAR, 2007) and the Next Generation air transportation system (NextGen) developed by the National Aeronautics and Space Administration (NASA) and Federal Aviation Administration (FAA) (FAA, 2007). In TBO, airspace users will work cooperatively with ATM service providers to access a collaborative air traffic management system through synchronised flight trajectories for ground and air traffic. Furthermore, the time-based separation will be one efficient measure to realise cooperative trajectory-based operations.

The main objectives of terminal flight optimisation are to minimise fuel consumption, reduce emissions, avoid flight conflict and enhance the overall predictability of aircraft landings (Ng et al., 2018). It involves optimising a wide range of flight parameters, including altitude, speed, descent rate, and flight path angle while accounting for various factors such as weather conditions, air traffic control instructions, and aircraft performance characteristics. Advanced optimisation methods, such as genetic algorithms (Abdelghany et al., 2007; Hu et al., 2004), particle swarm optimisation

(Blasi et al., 2013) and other heuristic approaches (Zhang et al., 2015), have been employed to identify optimal flight trajectories that balance indexes such as fuel efficiency, noise reduction, flight safety and traffic delay. Four-dimensional trajectory prediction, which refers to the estimation of an aircraft's future flight path over time, accounting for its position in three-dimensional space and the fourth dimension being time (Khan et al., 2021), is also crucial for planning and executing terminal flight optimisation strategies effectively and enables pilots and air traffic controllers to plan and adjust flight paths proactively. Estimating arrival time based on flight trajectory prediction will build preconditions for near-real-time scheduling of the final approach.

In the final approach phase of aircraft landing, runway sequencing and scheduling are critical in ensuring safe and efficient operations at busy airports (Samà et al., 2017). During this phase, multiple aircraft must be sequenced and scheduled to land on the same runway while maintaining safe separation distances, maximising runway utilisation and minimizing overall delays. Runway sequencing involves determining the order in which aircraft will land on the runway, considering factors such as aircraft type, size, weight, and approach speed (Prakash et al., 2018). On the other hand, runway scheduling involves allocating specific time slots for each aircraft to commence its final approach and touchdown (Xu, 2017). These processes must consider various factors, including weather conditions, air traffic congestion, and operational constraints, to optimise runway utilisation and enhance overall airport capacity. Effective runway optimisation algorithms and flight operation procedures deserve to be developed under the Trajectory-based Operation (TBO) scenarios to achieve efficient runway operations with improved throughputs (Yang et al., 2020). In addition to the optimisation algorithms such as mixed-integer linear programming (Farhadi et al., 2014), machine learning models and reinforcement learning algorithms can be integrated to deal with

changing conditions and traffic flows and realise the integrated prediction-optimisation methodological framework.

Runway capacity is a major constraint at many international hub airports. The procedural and efficiency aspects of runway operations can increase the performance of airports with constraint capacity (Farhadi et al., 2014). Current research on runway scheduling typically considers the prior static and conservative wake separation as safety-related constraints that prevent optimal traffic flow efficiency. In fact, time-based aircraft separation under dynamic wake separation will improve runway throughput, reduce traffic delay and provide additional flexibility and resilience for runway scheduling during heavy traffic periods and adverse situations, especially for Closely Spaced Parallel Runways (CSPR). Wake turbulence is the by-product of aircraft lift, leading to two counter-rotating vortices tailing behind the aircraft and could induce different degrees of hazard towards the follower aircraft (Hallock et al., 2018). The current flight separation related to the wake vortex is independent of time and meteorological conditions (Demirel, 2023). The atmosphere conditions, especially winds, play a leading role in determining the time of vortex lasting and transport in the background turbulence. Thus, the flight separation time could be reduced when vortices are directly blown out of the flight path by strong wind quickly after its generation.

The terminal area and the final approach zone are two main areas that require efficient flight dispatch. Current research on terminal traffic control and runway scheduling typically considers the prior static and conservative wake separation as safety-related constraints that prevent optimal airport traffic flow efficiency. Dynamic wake separation can be a promising concept for improving runway performance with constrained capacity and configuration. Therefore, the research areas in this work are introduced from detailed to general perspectives, focusing on developing novel

approaches for efficient air traffic control in terminal flight. One aspect is to investigate the potential of weather-related and pairwise aircraft wake separation through deep learning-driven approaches utilising historical wake data from LiDAR at the Hong Kong International Airport (HKIA). The other aspect is to perform intelligent and dynamic runway scheduling and integrated terminal traffic flow optimisation considering the dynamic time-based flight separation under aircraft wake vortex prediction research. This research aims to build preconditions for holistic and continuous traffic planning and facilitate improvement of the overall traffic flow efficiency.

1.2. Research scope and objectives

The contradiction between the increase of flight volume and the saturation of the current operational capacity of airports and terminal areas prompts the development of more efficient traffic flow scheduling methods in each airspace sector and integrated coordination methods for the whole region when the route structures and airport configuration of the airspace cannot be changed. This thesis aims to develop novel data-driven machine-learning approaches for improving traffic flow efficiency and safety of both the terminal area and final approach area under the trajectory-based operational concept. The research objectives of this work are primarily in three aspects:

(1) The first objective of this research is to explore the efficient approach for developing dynamic wake separation related to varying meteorological conditions and aircraft pairs. The novel deep learning approaches for image processing and sequential data prediction will be investigated for their applicational capability in aircraft wake vortex recognition, evolution prediction and dynamic separation determination. Furthermore, approaches for

improving their trustworthiness, explainable ability and prediction robustness will be explored to ensure flight safety and enhance human control over the system and predictive results.

(2) At the runway scheduling level, the research is dedicated to identifying the potential of flight separation minima reduction related to aircraft wake turbulence and exploring its effect in improving the efficiency and throughputs of runway operations at theoretical and actual operational operations under certain traffic situations. The criteria for developing dynamic wake separation without compromising flight safety will be analysed statistically based on vortex encounter safety assessment with verification.

(3) In the macroscope level of terminal airspace, we further aim to explore the impact of runway scheduling through dynamic wake separation on terminal approach scheduling. Using a dynamic wake vortex separation model, which adjusts separation criteria based on atmospheric conditions and aircraft types, the study evaluates how these changes influence runway operations and terminal area management during periods of high traffic density. Most importantly, we investigate whether these efficiency improvements could compromise safety by causing conflicts in the terminal manoeuvring area. The goal is to balance efficiency gains with necessary safety considerations, ensuring conflict-free airspace.

1.3. Organisation of the thesis

The structure and correlation between the work done in this thesis and the four research stages of the overall framework are presented in **Figure 1-1**. After a brief introduction in Chapter 1, the rest of this thesis is organised as follows:

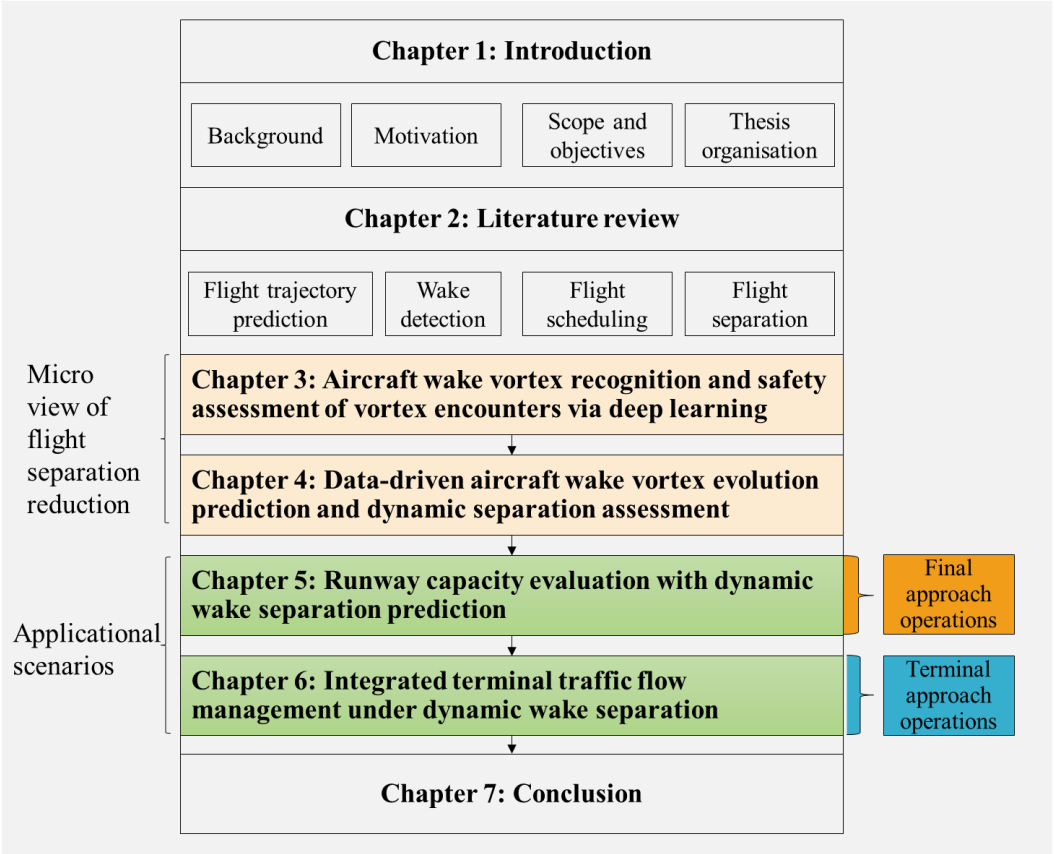

Figure 1-1. The structure of the doctoral thesis.

Chapter 2 proposes a comprehensive and extensive literature review on elements related to terminal traffic flow: flight trajectory predictions; aircraft wake vortex prediction, development of the flight separation standard and the optimisation algorithms of sequencing and scheduling.

Chapter 3 and Chapter 4 aim to simulate the dynamic wake separation time from the wake vortex characteristic analysis perspective, regarding the first objective. The reduction of flight separation minima is investigated by recognising the presence and positions of aircraft wake vortices, their transport, and encounter time at the approach profiles. Specifically, Chapter 3 develops the fast-time and data-driven vortex identification models and explores the effects of crosswinds on the lateral transport of wake vortices. Chapter 4 elucidates the short-term and long-term wake vortex transport

and decay forecasting. The integration of wake vortex recognition in Chapter 3 with vortex evolution prediction is also verified with model performance evaluation, demonstrating both the online vortex monitoring and prediction ability of future vortex movement. This research is a breakthrough in realising deep learning-based vortex feature extraction and quantified recognition of aircraft wake vortices based on the LiDAR technique, which enables real-time vortex presence monitoring and risk assessment of vortex encounters.

The dynamic wake separation predicted based on Chapter 3 and Chapter 4 provides preconditions for developing proactive runway scheduling plans. Chapter 5 explores the contribution of dynamic wake separation in theoretical and operational runway throughput improvement, focusing on the second objective. This research is a microscope-level investigation of the managerial implications of dynamic wake separation strategy.

Chapter 6 further investigates the effect of dynamic wake separation in the final approach on macroscope traffic control in the terminal area and concentrates on the last objective. The feasibility of applying the dynamic wake separation in different traffic demands and meteorological conditions is discussed, and the performance of arrival time, flight delay, and air traffic controllers' workload is assessed.

Finally, Chapter 7 summarises this research and discusses the potential future research directions.

Chapter 2. Literature review

With the development of computer technology and the accumulation of massive volumes of flight data and operational data, data-driven machine learning techniques have gained great popularity in air traffic management, especially the terminal traffic flow management area. This chapter reviews the conventional approaches and novel machine learning algorithms utilised in terminal flight optimisation and runway scheduling problems. The development of aircraft separation standards in the final approach related to aircraft wake vortex, as well as the approaches for wake vortex modelling and prediction, are also examined to understand the physical reason for the approach to flight separation reduction. This chapter could improve our grasp of the connotations and approaches of the target research topics and identify the research gaps that head the research objectives of the following chapters.

2.1. Aircraft wake vortex dynamics, modelling and safety assessment

Wake turbulence is the by-product of aircraft lift, leading to two counter-rotating vortices tailing behind the aircraft in the far end, as shown in **Figure 2-1,** and could induce different degrees of hazard towards the following aircraft when they enter the wake region of the leading aircraft, as depicted in **Figure 2-2** (Shen et al., 2023). **Figure 2-3** shows the two-phase decay and lateral movement of aircraft wake vortices in moderate turbulence.

The research of aircraft wake vortex starts with the development of numerical simulation techniques of Computational Fluid Dynamics (CFD). The early numerical studies for discrete vortex estimation can be traced back to the 1960s (Moore, 1974). In recent years, the pulsed Light Detection and Ranging radar has been implemented for monitoring the behaviour of wake vortices. Therefore, the methodologies of wake

vortex study are mainly two-fold: physical model-based and data-driven model based on LiDAR technique, with the literature research as follows.

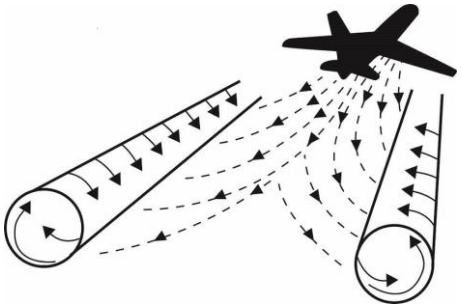

Figure 2-1. Wake turbulence generated behind the aircraft.

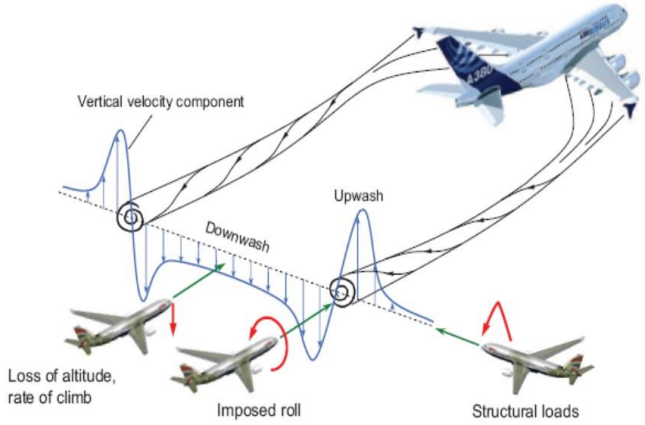

Figure 2-2. Hazards for the following aircraft when getting into the wake region that is generated by the leading heavy aircraft.

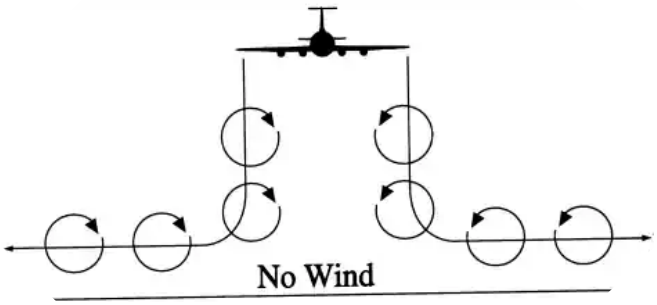

Figure 2-3. Wake decay process under a stable atmosphere without winds.

2.1.1. Physical dynamic-based wake modelling

The wake separation reduction system relies highly on the accuracy of wake detection and modelling of the hazard assessment of aircraft wake turbulence. The two-dimensional (Burnham et al., 1978) and three-dimensional (Robins et al., 1996; Switzer et al.) numerical simulations were applied to identify more and more realistic vortex movement and circulation evolution, with computational methods refinement. Corjon et al. (2012) identified and explained the generation of secondary vortex structures generated by environmental turbulence in the wake vortices' strain field.

A large volume of existing research specialises in the wake vortex prediction from the theoretical model perspective, with the vortex initialised employing analytical models such as the Lamb-Oseen and Burnham-Hallock (Gerz et al., 2002). Models for the rapid predictions of wake vortices are developed further. For instance, the initial fast-time model proposed worked as an illustrative model for later model advancements. The other fast-time prediction models include the Aircraft Vortex Spacing System (AVOSS) (Proctor, 1998), TASS Driven Algorithm for Wake Prediction (TDAWP) (Proctor et al., 2006), Probabilistic Two-phase Wake Vortex Decay model (P2P) (Holzäpfel, 2003) and Deterministic Wake Vortex Model (DVM) in WAKE4D platform (Visscher et al., 2010). To simulate the decrease and decay of vortices, they employ theoretical empirical parameterisations upon wake vortex physics. Adjustments are made to model elements and coefficients based on theoretical factors, the results of computational simulations and field experiments, and validated regarding experimental data. For considering the stochastic features of wake vortices, some physical models incorporate probabilistic aspects that consider the uncertainty and diversity of initial modelling and environmental conditions to forecast the uncertainty range of the vortex behaviour. For example, the physical Wake Vortex Prediction System (WSVS) was

constructed with inputs of aircraft information and atmosphere conditions and demonstrated with the safety level of their model by the Monte Carlo simulation, and its applicability in separation reduction and traffic optimisation was further evaluated (Holzäpfel et al., 2021; Matayoshi et al., 2014). However, such a physical model can only describe ideal tail-vortex generation and performs under certain weather conditions and atmospheric disturbance assumptions. The stochastic feature of the wake turbulence requires techniques to detect and analyse the actual data in real operations.

2.1.2. Wake vortex recognition based on the LiDAR technique

Light Detection and Ranging instruments with rapid wake vortex identification algorithms are considered to support monitoring and analysis of wake behaviour under several weather conditions (Hon et al., 2021; Thobois et al., 2016). The rapid wake vortex location identification based on LiDAR data can be divided into extraction from the Velocity Envelope (VE) and Radial Velocity (RV) categories. VE algorithm locates vortex cores from the velocity envelopes and calculates the circulation based on the given velocity model (Holzäpfel et al., 2003). Both fixed threshold (Rahm et al., 2008) and adaptive threshold to Signal-to-Noise Ratio (SNR) (Wassaf et al., 2011) for estimating vortex parameters from the Doppler spectra were researched. RV method employs radial velocity to identify wake vortex position (Li et al., 2020; Smalikho & Banakh, 2015; Smalikho et al., 2015). Circulation strength indicates the intensity of the wake vortex, which is more difficult to estimate. A method of circulation retrieval is based on vortex position estimation and the downwash velocity model, such as the Burnham-Hallock model. Wu et al. (2019) specifically introduced their measurement of wake core with radial velocity data from LiDAR scan and Fast Fourier Transform (FFT) spectrum distribution and estimation of wake circulation with the Burnham-

Hallock vortex model based on velocity envelope. Other methods for circulation estimation were to build mathematical theoretical velocity models and fit with the LiDAR detection data, such as the Maximum Likelihood estimator (Frehlich et al., 2005; Hallermeyer et al., 2016; Jacob et al., 2011). To the best of our knowledge, these rapid-processing algorithms are universal and may be affected by noise and high-turbulence scenarios.

2.1.3. Data-driven with machine learning models

Data-driven deep learning models such as convolutional neural networks have a strong ability in image processing and identification, which is ideal for wake vortex detection to facilitate the physical LiDAR processing algorithm. Although Machine Learning techniques such as image processing have been applied in LiDAR algorithms for initially identifying the existence of wake vortex and narrowing down the vortex window for wake core localisation before the circulation strength calculation (Hon et al., 2021; Thobois et al., 2016), there are only few studies that straightforwardly perform quantitative practice of wake location and circulation estimation with ML to improve the computational automaticity and speed (Wartha et al., 2022). Pan et al. (2020) employed the Support Vector Machine (SVM) to identify the presence of wake vortices using features of radial wind data from LiDAR and meteorological data such as temperature, air pressure, background wind speed and direction. The classification of the existence of wake vortex achieved 70% accuracy in SVM (Pan et al., 2020) and 94% accuracy in Artificial Neural Networks (ANNs) (Weijun et al., 2019). Regions with CNN features (R-CNN) and You Only Look Once (YOLO)-v5s network structures are also employed for vortex classification and strength category identification (Shen et al., 2023). Another latest research applied Multilayer Perceptrons (MLPs) and

Convolutional Neural Networks to quantitatively estimate the location and strength of wake vortex, which achieved an 86% match rate compared to the benchmarking Radial Velocity (RV) method. However, this research conducted separate training of the pairwise and coupling two-dimensional vortex positions. Furthermore, the performance of their model has no reference to compare with that of other deep learning models. More complicated deep learning models remain to be developed to reveal the intrinsic non-linear features of wake turbulence generation and decay process, considering several weather conditions and information of aircraft types.

2.1.4. Safety assessment of wake encounter

The analysis of Wake Vortex Encounters (WVEs) has advanced significantly, leveraging a variety of methods to address safety and operational efficiency concerns. The risk assessment of the impact of wake turbulence in the rear aircraft is primarily based on the single-parameter and multi-parameter assessment models. In the take-off and landing stage, the vortex intensity is high, and the wake encounter angle is small, which mainly causes rolling motion to the rear aircraft. The rolling moment coefficient (RMC) is primarily used to assess the risk of wake encounters.

Rojas et al. (2021) focused on sensitivity analysis of wake vortex circulation and decay during the en-route phase, utilising a modelling approach to evaluate WV effects based on aircraft mass, altitude, and environmental factors. This research aids in identifying critical scenarios for WVE simulations, and optimising safety assessments by reducing computational redundancies. Baren et al. (2017) validated the RMC as a metric for wake vortex encounter severity through piloted flight simulations. Their findings support the pair-wise separation concept, refining the Recategorisation of Aircraft Weight (RECAT) separation standards by aligning severity levels across

aircraft categories. This method enhances the reliability of safety metrics while addressing operational demands for reduced separations. Pan et al. (2023) employed numerical simulations to explore atmospheric stratification impacts on wake vortex evolution. Utilising Reynolds-averaged Navier–Stokes equations and Brunt–Väisälä (BV) frequency metrics, this study constructs three-dimensional hazard zones and calculates wake separations. The results demonstrate faster decay rates under unstable stratifications, enabling tailored separation adjustments based on environmental conditions. Jiang et al. (2023) integrated quick access recorder (QAR) data with aerodynamic modelling to analyse dynamic wake separation. By considering real-time velocity data and incorporating roll moment coefficients as safety metrics, this approach dynamically adjusts separations for various aircraft classes, achieving significant reductions in separation distances while maintaining adherence to RECAT standards.

The rolling moment coefficient RMC can be expressed as a function of the front and rear wing spread (Treve, 2013):

$$\mathrm{RMC} = \frac{\Gamma_{\mathrm{v}}}{V_f b_f} \frac{AR_f}{AR_f + 4} F\left(\frac{b_1}{b_f}\right) \tag{2-1}$$

Where the Γ_v is the vortex strength of the leading aircraft, V_f is the flight airspeed, AR_f is the wing area of the rear aircraft, b_1 and b_f are the wingspan of the leading and following aircraft, $F\left(\frac{b_1}{b_f}\right) = 1 - 2(2a\frac{b_1}{b_f})[\sqrt{1 + \left(2a\frac{b_1}{b_f}\right)^2} - 2a\frac{b_1}{b_f}]$ and $a = 0.04$.

Multi-parameter assessment criteria can describe aircraft wake hazards comprehensively, such as the Simplified Hazard Area Prediction method (SHAPe) from the German Aerospace Centre (DLR). The hazard encounter criteria include flight

altitude, pilot control commands, starting parameters (sideslip angle and angle of attack), route offset and acceleration, etc.

2.2. Runway operation and terminal traffic flow management with time-based separation

In the case of complex background wind, the evolution and drift of aircraft wake are complicated. Therefore, the static wake interval is unsuitable for upwind, crosswind conditions and application in closely spaced parallel runways. The use of Distance-based Separation (DBS) will greatly reduce the runway utilisation efficiency. In the case of crosswind, the wake of the aircraft may be blown away from the runway, as depicted in **Figure 2-4**, so that the probability of the rear aircraft encountering the wake of the front aircraft could be reduced; thus, the wake interval of the front and rear aircraft can be reduced. Several large European airports, represented by London Heathrow Airport, have proposed the Time-based Separation (TBS) that can increase runway capacity by 14% under moderate upwind conditions. Under strong upwind conditions, the capacity increase is more obvious, and the delay time of aircraft under crosswinds is reduced from 5.9 minutes to 3.4 minutes.

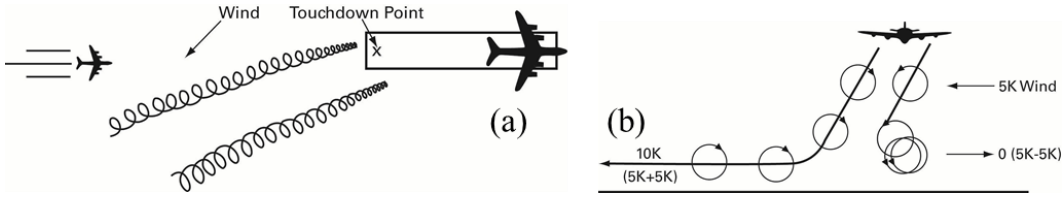

Figure 2-4. Wake vortex lateral transport under crosswind (a) the top view of the flight, (b) the rear view of the flight.

The wake separation is taken as a hard constraint in runway scheduling and optimisation problems. This section reviews the existing literature on runway

scheduling under time-based air traffic management procedure and identifies research gaps and research potential in this topic with the separation reduction developed by methodology in the above section.

2.2.1. Research on runway scheduling under separation constraint

Runway sequencing and scheduling are critical components of air traffic management that focus on determining the optimal order and timing for aircraft to land or take off on one or more runways. These processes aim to maximise the efficiency of runway operations while ensuring safety and minimising delays, by arranging aircraft in a specific order and precise time slots based on factors such as arrival times, departure priorities, runway capacity, weather conditions, aircraft types, separation requirements to avoid conflicts and other operational constraints. The widely used First-Come-First-Served (FCFS) approach often leads to inefficient utilisation of available capacity in the runway sequencing and scheduling problem. The single runway scheduling problem, which involves managing arrivals, departures, and ground aircraft, has been addressed using multi-objective dynamic programming (DP) by researchers focusing on real-time decision support for air traffic controllers (Malik & Jung, 2016). Balakrishnan et al. (2010) proposed the most classical K Constrained Position Shifting (K-CPS) substitution algorithm based on FCFS for runway scheduling under the time-based wake separation regulated by the International Civil Aviation Organisation (ICAO), which enhances flexibility in sequencing. Malik et al. (2016) built the Mixed-Integer Linear Programming (MILP) model for multiple runway scheduling problems under selective CPS. Jacquillat et al. (2017) modelled the mixed take-off and landing of runway configuration and analysed with random queuing theory under approach time uncertainty. The feasible robust optimisation (Samà, et al., 2017) and exact

optimisation algorithms were proposed for different uncertainty models in the approach scenarios (Ng et al., 2021; Ng et al., 2020; Ng et al., 2017). For large-scale landing problems, Pinol et al. (2006) were the first to introduce the Scatter Search (SS) method and the Bionomic algorithm for addressing the Aircraft Landing Problem (ALP) with time window constraints, successfully solving large-scale instances involving 500 aircraft and five runways within a minute. Building on this, Salehipour et al. (2013) combined Simulated Annealing (SA) with Variable Neighbourhood Descent (VND) and Variable Neighbourhood Search (VNS) to tackle the ALP. Further advancements of the VNS algorithm (Salehipour et al., 2013) were made (Ng et al., 2017). This research achieved comparable results to CPLEX but with significantly reduced computational times. The stochastic branch and bound algorithm was applied to solve the stochastic runway scheduling (Sölveling et al., 2014). Dastgerdi et al. (2015) proposed a novel Evolutionary Algorithm (EA) to address congestion at single-runway airports. Additionally, swarm intelligence approaches for the ALP model have been explored. The convergence rate of the Artificial Bee Colony (ABC) algorithm was proposed with a robust optimisation framework proposed for the Aircraft Sequencing and Scheduling Problem (ASSP) by incorporating mixed-mode runway operations to account for uncertainties in arrival and departure times (Ng et al., 2017). In real-world applicational scenarios, the Spot and Runway Departure Advisor (SARDA) is a decision-support tool designed to enhance the efficiency and predictability of airport surface operations by assisting ramp and tower controllers, through collaborations with airline partners and has undergone human-in-the-loop simulations at major airports, such as Dallas-Fort Worth and Charlotte, demonstrating its potential to improve departure pushback operations (Barhydt, 2013).

In fact, these prior researches directly feed the static separation minima in their

algorithms. Performance improvement under reduced wake separation, and even dynamic aircraft separation in runway operations, deserves to be studied. Wake vortex avoidance is the main factor that affects the operational problem with aircraft spacing to increase runway capacity and throughput. Wake vortex separation is a necessary hard constraint for runway operations related to safety. The lateral movement and decay of wake turbulence make the optimisation problem more complex in the closely spaced parallel runway (Dönmez et al., 2022; Liu et al., 2019). For closely spaced parallel runways, the wake vortex generated in one runway may transport to adjacent runways. When combined with the wake characteristics in crosswind, the take-off and landing capacity of the runway could also be significantly improved compared with the existing rules for closely spaced parallel runways.

2.2.2. Terminal traffic flow optimisation problem

The Terminal Traffic Flow Problem (TTFP) extends the framework of the ASSP. Microscopic air traffic flow models enhance the practical applicability and robustness of solutions by providing detailed control over Air Traffic Control (ATC) operations, such as air segment management, holding patterns, runway allocation, and ground movements. Optimising traffic flow within the Terminal Manoeuvring Area (TMA) involves the strategic planning and management of aircraft trajectories during their approach to or departure from a runway, with the goal of maximising airspace utilisation, minimising delays, and ensuring safety (Murça et al., 2015). The terminal approach problems can be modelled as deterministic or stochastic with uncertainty considered, and solved with exact algorithms or heuristic algorithms, respectively. Deterministic TTFP models have been extensively studied for achieving conflict-free approaches and minimising total flow time within the TMA. Rey et al. (2016)

introduced a deterministic conflict resolution model constructed through non-linear optimisation, employing subtle speed adjustments via subliminal speed control. Li et al. (2022) developed a mixed-integer quadratic programming model, enhancing the column generation algorithm to address disrupted flight recovery challenges, incorporating discrete flight duration control and aircraft assignment constraints. To mitigate computational complexity in large-scale instances, meta-heuristics optimisation algorithms are proposed (Ikli et al., 2021; Ng et al., 2018; Samà, et al., 2017).

The inclusion of various uncertainties, practical constraints, and environmental changes significantly increases the complexity of air traffic control decision-making. To address these uncertainties, mitigate delay propagation and reduce the need for reactive rescheduling, two primary approaches are employed: stochastic and robust modelling. In the stochastic approach, uncertainty is modelled using probability distributions derived from historical data (Jacquillat et al., 2015; Jacquillat et al., 2017). By contrast, the robust approach addresses uncertainty through interval-based models, focusing on performance under deviation scenarios rather than statistical distributions (Aissi et al., 2009; Gabrel et al., 2014). As a risk-averse strategy, robust modelling emphasises conservative decision-making, ensuring reliable outcomes despite environmental uncertainties (Ng et al., 2017).

2.2.3. The development of aircraft separation standard

Following the ICAO's initial wake vortex interval standard based on three types of aircraft in the last century, major civil air traffic management programs, represented by the European Single Air Traffic Control Program and the United States Next Generation Air Traffic Control Program, were launched. The representative wake research projects

include EUROWAKE, WAVENC, MFLAME, C-Wake, S-Wake, I-Wake, ATC-Wake, FAR-Wake, FLYSAFE, Green-Wake (Gerz et al., 2002), etc. Through a large number of studies on aircraft wake characteristics and hazard assessment, the possibility of further reduction of wake interval is explored. Some of the research results have been gradually applied to air traffic control and aircraft take-off and landing schedules, and on this basis, the wake interval reduction of aircraft reclassification is proposed.

At present, the RECAT-EU from EASA and the first stage of the RECAT scheme in FAA Order JO 7110.659C aims to optimise the classification of aircraft and divides aircraft weight classes from the traditional three categories into six categories according to aircraft weight and wingspan (forming a 6×6 matching matrix) (FAA, 2016). The latest wake reclassification standards have been widely adopted by some countries, including RECAT-CN under CCAR-93-R5 in 2017; ReCAT-EU under EU 2020/469 ATS in 2013; ReCAT-EU-PWS (Proposal for 2022). However, these standards do not consider the dynamic effects of weather changes on the separation intervals, and they are still conservative.

In 2016, the FAA issued RECAT-II Phase II with the goal of constructing static wake intervals based on flight pairs. A one-to-one aircraft spacing criterion is formed based on the wake of different aircraft and the conditions encountered by the wake, which results in a 1200×1200 pairing matrix representing essentially all aircraft types. The standard is being tested at six U.S. airports. The ultimate goal of Phase III is to achieve dynamic and real-time wake interval adjustment based on flight pairs and weather changes. The dynamic wake vortex interval adjustment adapted to different weather and flight conditions has greater potential to increase airport capacity and is the development trend of air traffic control technology in the future.

2.2.4. Research on time-based aircraft separation

Some state-of-arts directly focus on the aircraft separation problem. Diana (2015b) assessed the impact of time-based flow management procedures on airport performance through an autoregressive conditional duration model. This model reveals the volatility of interarrival duration time in real operational data and its impact on traffic delay and taxi-out time. They also investigated the variation of departure throughputs before and after RECAT implementation using a Markov regime-switching model (Diana, 2015a), in which the results show that the departure will persist in a longer constrained period in the post-implementation. Furthermore, research on the prediction of runway exit time was also developed employing machine learning techniques for aircraft under the ICAO vortex categories based on historical traffic data (Herrema et al., 2019).

As for the flight interval optimisation of parallel runways, preliminary studies have been conducted on the impact of shortening wake vortex intervals on runway operations. Janic (2008) calculated the capacity model of the CSPR model through an analytical model with approaching scenarios considered. Hammer (2000) analysed the basic principle of the approach procedure of the close parallel runway. The study of crosswind analysis mainly focuses on the effect of crosswind conditions (crosswind direction and wind level change) on wake and pairing time intervals. Chen (2019) considered the influence of wind speed on the evolution of the wake vortex based on the P2P wake vortex dissipation model. At the same time, based on the rolling moment coefficient evaluated by wake vortex encounter, the aircraft spacing of B747-400 and B737-700 aircraft during close parallel take-off under the influence of crosswind was determined. In general, these studies adopt a simple crosswind model for the lateral movement of wake and simplify the classification of danger wake region, without considering the sinking characteristics of wake vortex pairs. At the same time, in the flight pair, only

the specific aircraft type matching pair is selected, and the universal real-time matching interval estimation based on dynamic crosswind is not realised.

2.3. Flight trajectory prediction in air transportation

4D trajectory prediction serves as a foundation to support and integrate high-level decision-making systems in TBO, such as arrival and departure management, conflict detection and resolution, and en-route air traffic flow management. In the present literature, aircraft trajectory prediction approaches can be categorised as model-driven and data-driven (Zhang et al., 2020). Several pioneer research on physics-model-based flight trajectory prediction focuses primarily on establishing the relationship between future trajectory with the current aircraft states using aircraft performance models and aircraft intentions. Although sophisticated model-driven Flight Trajectory Prediction (FTP) is capable of describing realistic aircraft movement, these flight-phase-orientated physical models fail to manage the dynamic and time-varying flying environment. Machine learning-based models with data mining techniques show significant advantages in four-dimensional flight trajectory prediction through processing and integrating massive historical trajectory data with trajectory regularity and several flight-related information (Liu et al., 2023b). This section reviews the literature on flight trajectory prediction.

4D flight trajectories can be characterised mathematically as a time-ordered set of trajectory vectors, such as a 4D flight trajectory sequence: $(x_{t-15}, \dots, x_{t-2}, x_{t-1}, x_t, x_{t+1}, \dots, x_{t+15}, t \geq 16)$, where x vector contains spatial properties of trajectory with at least latitude, longitude and altitude, and t represents a temporal property with timestamp or other time intervals.

Suppose given the observed current and historical trajectory vectors

$(x_{t-b-1}, \ldots, x_{t-2}, x_{t-1}, x_t), t \geq b + 2$, prediction of flight trajectories in future a time intervals $(x_{t+1}, \ldots, x_{t+2}, x_{t+a})$ is achieved by trajectory predictors, employing data from observed trajectory vectors and other attributes such as environmental conditions, uncertainty information describing the quality of prediction and information indicating operation modes and aircraft intents of flight guidance systems, etc.(FAA/EUROCONTROL, 2010). b denotes the input length of observed flight trajectories, x represents the trajectory vector. a represents the prediction time horizon, which is the period ahead to which prediction is performed and determines the time scale of prediction (Cheng et al., 2021; Guan et al., 2014; Hrastovec et al., 2016). Prediction of future trajectories within one to several minutes is categorised as short-term. The medium to long-term projection spans minutes to hours into the future. The predicted output might be either deterministic or probabilistic. The deterministic prediction yields single and nominal results without alternatives. The probabilistic prediction exposes prediction uncertainty by considering the stochastic distribution of inputs and model parameters (Pang et al., 2021; Sun et al., 2018).

2.3.1. Physical model-based

(1) Aircraft performance model-based

The most sophisticated model of aircraft performance is the full six-degree-of-freedom kinetic model with aircraft translation and rotation, which describes forces and moments acting on aircraft as well as aircraft movement in detail. In the air traffic operational scale that focuses on kinematics, aircraft can be simplified as a point with mass under certain assumptions in aircraft configuration, with 3-dimensional differential equations following Newton's law without consideration of rotational moments. With the initial states (time, mass, velocity, position, Euler angles and

performance constraints), flight plan, performance parameters and weather data (wind speed, direction, etc.) given, the sequential points of future aircraft trajectory in integrated differential equations can be forecasted.

Estimation of performance parameters and modelling of aircraft intent are two main concerns for model-driven trajectory prediction (Schuster et al., 2012). Aircraft intents are structured instructions that specify unambiguous configuration changes and operational states of the aircraft over a specific time horizon (Schuster et al., 2012). The formal Aircraft Intent Description Language (AIDL) using mathematical expressions of aircraft intents was presented to improve computational synchronisation across multiple predictors (Dupuy et al., 2007; Gallo et al., 2007; Lopez-Leones et al., 2007). Extensive research is based on databases such as EUROCONTROL Base of Aircraft Data (BADA), which provides multiple layers of aircraft performance models and parameter estimation (Nuic et al., 2010). As the flight profiles described in BADA are general cases with certain assumptions, which are unrealistic in actual flights and may induce significant prediction errors (Alligier et al., 2015; Schuster, 2015), the statistical simulation technologies were performed to estimate uncertainty of performance parameters or meteorological conditions, such as Monte Carlo (Lymperopoulos et al., 2010; Sankararaman et al., 2017; Wang et al., 2021) and other estimation methods with reduced computational burden than MC approach (Casado et al., 2017; Subramanian et al., 2022).

(2) State transition model-based

The aircraft kinematic model is another approach to simplify aircraft physical movement, which considers kinematical motions with positions, velocity, and heading, but ignores the physical mechanism of forces. The state transition model in state space

theory is often used to model the kinematic dynamics and forecast trajectory of an aircraft. The Kalman Filter (KF) is a classic recursive approach for single-model estimation that only considers one flight mode (Lin et al., 2008; Thipphavong et al., 2012).

Hidden Markov model (HMM) (Ayhan et al., 2016; Georgiou et al., 2020; Rezaie et al., 2021) and Interacting Multiple Model (IMM) (Roy et al., 2006; Song et al., 2012) are two representative stochastic methods for multi-model estimation that handles multiple flight modes, which is an estimation problem of stochastic linear hybrid system that weighs a hefty cost on computation. Flight trajectories and relevant information (local meteorological data, flight intent, aircraft properties, etc.) are typically modelled as discrete values that comprise HMM states. The trajectory is subsequently updated with transitions between these states, using historical trajectory data and temporal-spatial constraints (Ayhan et al., 2016; Georgiou et al., 2020). In addition to two major components of the initial distribution and the evolution lay of the Markov sequence, Rezaie et al. (2021) developed the dynamic Gaussian conditionally Markov model to estimate trajectories with waypoints. The IMM algorithm allows multiple state hypotheses with multi-filter models to perform state estimation with great performance and low computational cost (Roy et al., 2006; Song et al., 2012). Song et al. (2012) used IMM to estimate aircraft state and updated the transition probability matrix of aircraft intent with a typical trajectory library extracted using a data mining algorithm. Seah et al. (2010) extended the IMM and applied it to monitor the conformity of real trajectories, including turns and descents, with flight plans, utilising KF and Markov chains to update aircraft states and flight modes.

2.3.2. Machine learning model-driven

(1) Machine learning methods

The statistical machine learning methods are also used to estimate aircraft performance data from historical trajectories and have demonstrated improved performance than predicting with the BADA model, such as polynomial regression to estimate thrust law and mass in the climb phase (Alligier et al., 2013), the K-nearest neighbour model (Hrastovec et al., 2016) and gradient boosting machine for predicting aircraft mass and speed (Alligier et al., 2018). Sun et al. (2018) used the Bayesian inference based on Automatic Dependent Surveillance-Broadcast (ADS-B) flight data to calculate the initial aircraft masses based on the total energy model and fuel-flow model. Their results were expanded to a large open-source database of parametric statistical models (Sun et al., 2019). Yu et al. (2019) introduced a physics-based learning method with a recurrent neural network for learning aircraft dynamical behaviour and inherent characteristics, and their model shows superior performance and lower training costs than the data-driven Long-short Term Memory Network (LSTM) model. The Gaussian mixture model was also proposed as a pseudo measurement for state estimation-based prediction with RM-IMM, which achieved better accuracy than the single Gaussian mixture model- and LSTM-based trajectory prediction (Choi et al., 2021). The online trajectory prediction with the physical model was also involved with updated aircraft intents (Schuster et al., 2012; Zhang et al., 2018).

(2) Deep learning neural network-based

The state-of-the-art deep neural networks have been employed by 24 studies for flight trajectory prediction, as shown in Table 5 of the Appendix. The datasets used in the state-of-arts and their features are also listed in Table 3 and Table 4 of the Appendix. Back Propagation Neural Network (BPNN) with few hidden layers was constructed for

trajectory forecasting (Verdonk et al., 2018; Wang et al., 2018; Wu et al., 2020), where the former two focus on the approaching phase while the last for en-route flight, and trajectory clustering is performed in all of them to classify similar trajectories to improve trajectory prediction performance. Clustering plays a pivotal role in flight trajectory pattern identification and prediction (Liu et al., 2023a). Model stacking between BPNN and machine learning models was also employed with enhanced performance compared to prediction based on individual models (Wang et al., 2020). With sophisticated nonlinear transformations obtained from novel deep learning architecture, complicated relationships might be learned over historical trajectory samples.

Recurrent Neural Network (RNN) networks and their variants are the most prevalent approaches for predicting flight trajectory, accounting for 14 out of 24 deep learning networks employed. The feedback connections between states in previous and subsequent steps of the RNN model are capable of capturing variable temporal dependencies. The LSTM model is an important structural variant of RNN that reduces training time and improves the accuracy of time-series data. The added memory function of LSTM with sigmoid and pointwise multiplication enables the ability to solve long-term dependence in sequence data. LSTM model was constructed for take-off and landing trajectory prediction (Zeng et al., 2020), arrival time estimation (Deng et al., 2022) and en-route long-term 4D trajectory prediction (Han et al., 2021), with attributes of aircraft type, standard terminal arrival routes and time of wheel block concatenated, respectively. Bidirectional LSTM was used in (Sahadevan et al., 2022), achieving more accuracy than single-directional LSTM with enhanced relevance in historical and future trajectory data. The model that encoders with 1D convolutional layer and decoders with Gated Recurrent Unit (GRU) was applied (Tran et al., 2022).

A novel model, a generative adversarial network, was applied for long-term probabilistic 4D trajectory prediction (Wu et al., 2022). Conv1D-Generative Adversarial Network (Conv1D-GAN) has the highest prediction similarity to real trajectory compared to two-dimensional convolution-based and LSTM-based generators and discriminators trained on RGB trajectories. Other probabilistic predictions, such as Gaussian process-based DNN and MC Dropout, were implemented for probabilistic separation measurement (Chen et al., 2020) and (Zhang et al., 2020), respectively, where the trajectory prediction results were probabilistic with confidence level rather than deterministic.

Transformer architecture also efficiently manages long-term dependencies. Guo et al. (2023) proposed a novel binary encoding method with a transformer as the backbone network to formulate the FTP task as a multi-binary classification problem. The trajectory embedding module includes an attribute embedding block and an attribute correlation attention block to obtain high-dimensional features and correlations in input attributes.

The properties of different DNN structures confer both advantages and limitations. The advantages of RNN networks in capturing temporal features with memory function, and the good performance of CNN in extracting spatial features from high-dimensional data, make hybrid deep neural networks a promising research direction (Ding et al., 2022; Ma et al., 2020; Sahfienya et al., 2021). In particular, a 1D convolutional network (Ma et al., 2020) and a 3D CNN (Shafienya et al., 2022) were applied for the extraction of a 3-dimensional spatial trajectory. The integration of the BPNN model and the LSTM model can be referred to (Zhang et al., 2020), which achieved both long-term prediction ability and great prediction accuracy.

The above-mentioned trajectory prediction focuses on a single flight. Multi-aircraft

trajectory prediction is also proposed to consider social connections of adjacent flights, the interactions between aircraft and their effect on trajectory prediction. The spatial-temporal interactions were learnt by social pooling layers of the social-LSTM model (Xu et al., 2021), a graph-based spatial transformer module and a temporal module (Pang et al., 2021).

2.4. Concluding remarks

This chapter presents a literature review of methodologies for terminal air traffic control. The flight trajectory prediction approaches are examined to support traffic flow optimisation. The literature review on this research area shows that emerging deep learning models have great advantages for 4D spatial-temporal flight trajectory prediction. The performance of those data-driven models can be further improved by integrating dynamic information related to weather, aircraft intentions and flight procedures. In addition, integrated deep learning models and deep learning-supported physical methods can achieve greater prediction performance. However, these studies focus mainly on model development. The integration and implementation of 4D trajectory prediction in problems such as flight separation assurance and traffic optimisation require further research.

In runway operational scenarios, the literature review starts with aircraft wake vortex modelling and prediction, which relates closely to flight separation in the final approach. The survey also shows the great potential of utilising novel data-driven neural networks for recognising and predicting aircraft wake vortices, which can serve as the verification method for physical vortex research and provide the model foundation for developing dynamic aircraft separation. Furthermore, this separation reduction inferred from the aircraft wake vortex prediction model can be applied to runway scheduling problems

for improving runway throughputs and reducing overall delay, compared to traditional runway scheduling with static separation constraints.

Chapter 3. Aircraft wake vortex recognition and safety assessment of vortex encounters via deep learning

In this chapter, a preliminary empirical study/experiment of aircraft wake vortex recognition is conducted as a prodromal step of the overall research programme. The deep convolutional neural networks are trained to identify the locations and strength of wake vortices. This study has demonstrated the separation reduction potential in weather-related conditions for the final approach without compromising flight safety. Under pre-identified crosswinds, the wake turbulence induced by the leading aircraft can be either conveyed out of the approaching path or decayed to an acceptable level for the follower aircraft to encounter. This separation scheme based on wind conditions indicates the benefits of increasing capacity for runway operations with high intensity, compared with the standard and fixed weather-independent wake separation minima. The proposed methodology was validated in the environment of the Hong Kong International Airport, using both near real-time and fast-time simulation in deep learning models. This separation suggestive tool increases the precision of separation delivery and decreases the number of unorganised temporal separations. The results show that the operational improvement is considerable when the crosswind near the ground is 3 m/s or greater for a continuous period.

3.1. Introduction

3.1.1. Research background

Aircraft wake-related separation reduction becomes a hot direction to improve runway capacity under the "Increasing air traffic movement and improving runway efficiency" concept in air traffic management. Wake turbulence is the by-product of aircraft lift, leading to two counter-rotating vortices tailing behind the aircraft and could induce different degrees of hazard towards the following aircraft (FAA, 2016). In the current National Airspace System (NAS), miles-in-trail (MIT) is widely adopted to maintain a minimum distance measured in miles for aircraft sequencing in the en-route stream (Kopardekar et al., 2003). However, such static separation management assumes the worst-case scenario of wake encounters and may restrict the number of aircraft movements in a particular period in a sub-airspace, which results in delays and delay propagation under severe weather or other uncertain situations. The dynamic and safe wake separation adapted to weather and traffic conditions with wake-vortex research is the current research focus of the air traffic control programs around the world to pursue both economic and environmental benefits, such as the current phase of aircraft recategorisation concept proposed by EASA and FAA (Holzäpfel et al., 2021; Roa et al., 2020).

The RECAT separation is still essentially static and conservative. Dynamic aircraft separation, which involves adjusting the aircraft separation in real-time concerning the characteristics of the decay and movement of wake vortices under specific aircraft pairs and wind conditions, deserves to be researched and applied in runway operations to improve efficiency and safety (Holzäpfel et al., 2021). With the accumulation of a massive amount of LiDAR data, data mining with machine learning techniques shows great advantages in wake behaviour and separation reduction analysis to support

integrated runway optimisation. Some recent research has initially attempted to integrate objective detection algorithms (Shen et al., 2023), artificial neural networks (Wartha et al., 2022), and machine learning techniques such as support vector machine (Pan et al., 2020) in wake presence identification. More advanced deep learning models remain to be developed to quantificationally analyse the decay and movement of the wake vortices.

The research of aircraft wake turbulence focuses predominantly on numerical simulation with computational fluid dynamics (Robins et al., 1996) and physical modelling aspects. Aircraft Vortex Spacing System (AVOSS) (Proctor, 1998), TASS Driven Algorithm for Wake Prediction (TDAWP) (Proctor et al., 2006), Probabilistic Two-phase Wake Vortex Decay model (P2P) (Holzäpfel, 2003) and Deterministic Wake Vortex Model (DVM) in WAKE4D platform (Visscher et al., 2010) are some of the theoretical vortex models. Nevertheless, these analytical models rely on certain parametrical assumptions and function under ideal situations of wake encounters, which may result in deviations between prediction and actual flight scenarios. Light Detection and Ranging instruments with the data processing algorithm (Holzäpfel et al., 2003; Li et al., 2016; Smalikho, et al., 2015) can facilitate behaviour analysis of wake vortex during actual flight operations and serve as a validation tool for vortex analysis. Velocity Envelope (VE) (Holzäpfel et al., 2003) and Radial Velocity (RV) method (Li et al., 2020) are two primary methodological categories for processing LiDAR data to identify the locations and intensity of wake vortex, either velocity envelopes or radial velocities are employed. To our knowledge, these algorithms for the rapid processing of LiDAR data are universal and may be affected by noisy background wind turbulence, resulting in inaccurate positioning and intensity estimation. The stochastic nature of wake turbulence necessitates techniques applicable to a variety of meteorological

conditions encountered in actual operations.

3.1.2. Research gaps, motivations, and objectives

In this context, the research questions that this chapter aims to address are as follows:

(1) How to analyse wake behaviour and recognise wake vortex through a data-driven approach with deep learning?

(2) What is the potential of aircraft separation reduction under several meteorological conditions compared to the RECAT standard?

(3) How to ensure the trustworthiness and interpretability of decisions in deep learning models to facilitate their implementation in the wake separation system?

In this chapter, we consider the above issues starting with developing a two-stage deep-learning framework for wake vortex locating and strength estimation. Next, the potential time reduction of approach separation is assessed upon the probabilistic wake positioning and duration measurement on the approach corridor. Finally, the prediction uncertainty of the proposed deep learning is explained by employing image feature analysis. The principal contributions of this research are primarily fourfold:

(1) In contrast to the research in (Wartha et al., 2022), where each wake-vortex parameter was trained in a single model, we construct a two-stage deep learning-based framework for near real-time locating and strength estimation of wake vortices. The estimation of vortex circulation is performed on a refined region of interest extracted from raw wake images, based on first-stage vortex locating, which achieves significantly higher prediction accuracy compared to estimating directly on the entire wake images.

(2) We explain the model decision process using the gradient-weighted activation map and prediction difference analysis (PDA) without requiring any

architectural changes or re-training of the CNN network. This visual analysis technique identifies the most relevant areas for vortex locating, reveals the shape of wake vortices and facilitates safety assessment by quantifying the safety-critical vortex encounter zone for follower aircraft.

(3) The data-driven wake vortex estimation contributes to the existing literature by providing a deep understanding of vortex behaviour via high-dimensional feature analysis with deep learning models. The proposed CNN models effectively revise recognition errors that may occur with the physical algorithm. Furthermore, our model achieves higher recognition accuracy for estimating vortex locations in one model compared to (Wartha et al., 2022), thereby revealing the coupled relationship among spatial vortex features.

(4) The wake encounter assessment, based on probabilistic vortex positioning at a high confidence level under specific crosswind conditions and certain aircraft weight categories, provides an effective methodological foundation for quantifying the dynamic wake separation. This assessment serves as a supplementary tool for reliable near-real-time wake vortex monitoring and establishes preconditions for developing more efficient and resilient runway scheduling to enhance runway throughputs.

3.2. Backgrounds

3.2.1. Characteristics of aircraft wake behaviour

Wake turbulence is typically a pairwise vortex in a steady atmosphere, counter-rotating in the far end. It is a complicated phenomenon related to many variables, such as weight, wingspan, engine thrust, speed, etc., of the generating aircraft and intervening atmosphere such as crosswind, atmospheric stability and turbulence.

Surrounding meteorological conditions is the predominant determinant of its duration (Hallock et al., 2018). The development process of the wake vortex can be characterised as a two-phase decay in weak to moderate turbulence: the initial diffusion phase with gradual decay and the rapid decay phase that follows shortly. The initial circulation can be described by the below equation:

$$\Gamma_0 = \frac{M_A g}{\rho b_0 V_A} \tag{3-1}$$

Where $M_A, \rho,$ and V_A represent the aircraft mass, the density of air and flight speed, respectively; $b_0 = sB$, in which B is the wingspan and s is the load factor related to the wingspan.

Near the ground, the interaction with the secondary vortex separating from the ground influences the fall, rebound, and decay properties of vortices. The influence of instability and wind on vortex decay is shown to be negligible, with which even a moderate crosswind is sufficient to produce strong asymmetric rebound characteristics (Holzäpfel et al., 2007).

The meteorological conditions, such as crosswind and the background wind turbulence, play a crucial role in specifying how long a vortex remains potentially hazardous and indicating the transport of the wake vortices, as depicted in **Figure 3-1**. Specifically, when the crosswind is roughly equivalent to the initial descent speed, the upwind vortex is likely to halt over the runway, and the decay of the wake pair will be unequal (Lin et al., 2017; Xu et al., 2023). While in a strong crosswind without the adverse headwind, and the prevailing headwind over approximately 5 m/s, the wake vortex will quickly leave the approach path (Holzäpfel et al., 2021). Furthermore, the large-scale and heavy atmospheric turbulence extracts energy from wake vortices while simultaneously diminishing their strengths, thereby accelerating their decay.

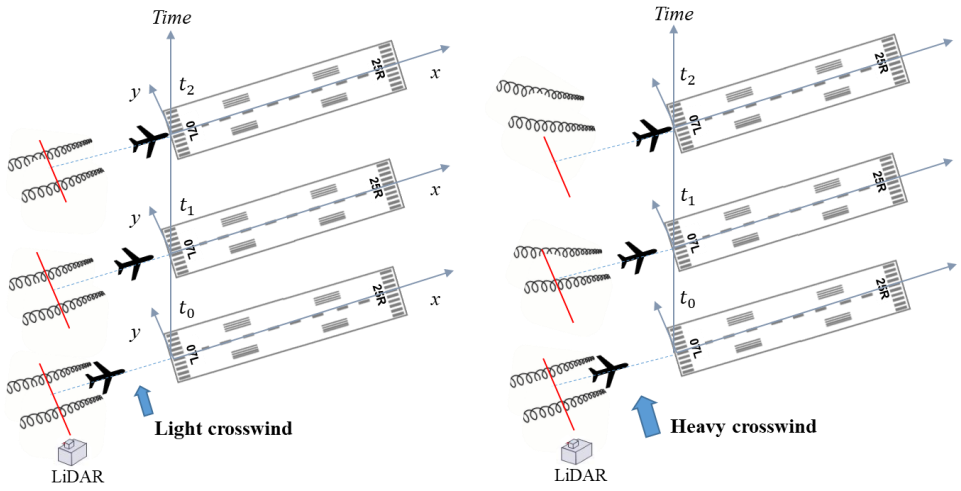

Figure 3-1. The movement of wake vortices under crosswinds. (Left: vortex sink under light crosswinds. Right: significant lateral transport of vortices with sink under strong crosswinds)

3.2.2. LiDAR implementation at HKIA

Four Leosphere Windcube200S LiDARs were installed in the Hong Kong International Airport for monitoring traffic in both directions of two runways, as shown in **Figure 3-2**. Each LiDAR executes the mode of range height indicator (RHI) scans that is perpendicular to the runway, at the scan rate of $5°/s$ and the scan repetition rate of approximately 10s. The three-dimensional setup of the RHI scan and the parameter definition of wake vortices in the Cartesian coordinate system is shown in **Figure 3-3**. The placements and characteristics of these LiDARs were optimised to capture the entirety of wake vortices and their decaying process, with the installation height at approximately 7 meters above the ground. The parameter settings are reported in **Table 3-1**. More in-depth information on LiDAR measurement at HKIA can be referred to (Hon et al., 2021).

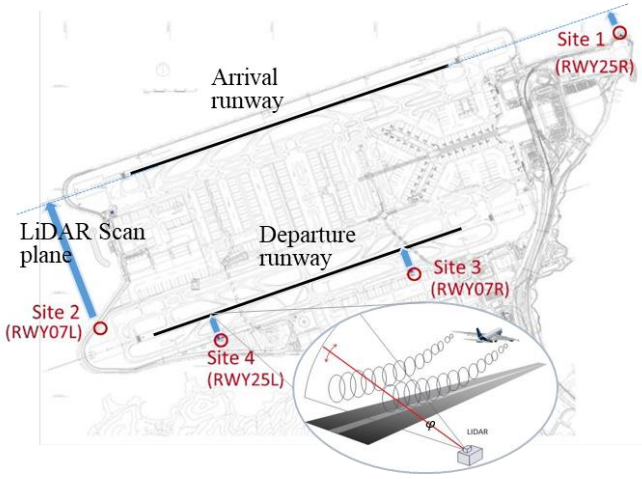

Figure 3-2. Locations of four LiDARs at HKIA.

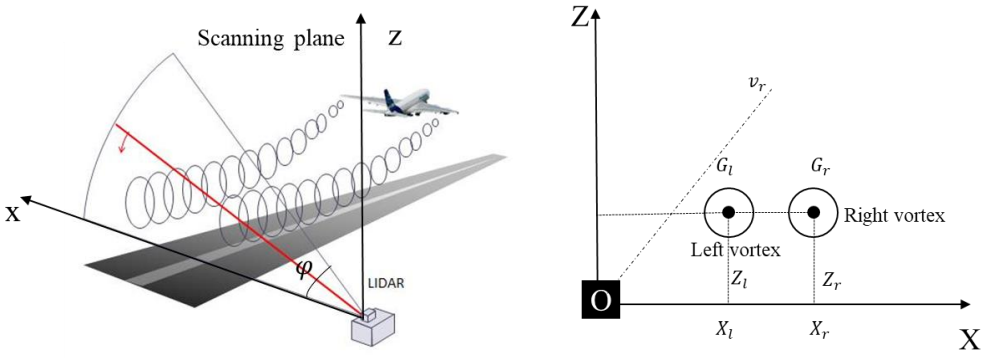

Figure 3-3. Scanning mode (left) and definition of the coordinate axis (right) of LiDAR instrument.

3.2.3. LiDAR processing algorithm

The processing algorithm for Windcube200S is designed by LEOSPHERE to capture vortex locations and, consequently, retrieve vortex strength. Initially, the algorithm verifies the status of vortex presence based on radial wind speeds calculated from the RHI scans. Next, the locations of vortex cores are roughly estimated using an image processing technique and are finely optimised. Vortex strength is further retrieved by fitting the Hallock-Burnham model (Burnham et al., 1982; Smalikho et al., 2015) on the Doppler spectra window that covers wake vortices. In addition to the generic parametric components of the Windcube200S processing algorithm (Smalikho et al.,

2015; Thobois et al., 2016), the positions and specific parameters of these LiDARs at HKIA are fine-tuned and calibrated specifically to reduce estimation error and assure data quality in all weather conditions and for as many aircraft types as possible. Furthermore, it has demonstrated the aircraft hit rate of 89%, overall mean error of 6% and 9.9% in wake span and initial wake strength measurement for two weeks (Hon et al., 2021).

Table 3-1. Parameter setting of LiDAR instrument.

LiDAR position	φ range(°	Radial range (m)	LOS beams	Wavelength (μm)	Pulse duration (ns)	Pulse repetition frequency (kHz)	Scanning rate (°/s)	Runway	Distance to Runway (m)
Site 1	0-50	80-865	786	1.54	200	20	5	25R (Landing)	275
Site 2B	0-5	1000-1785	786					07L (Landing)	1400
Site 3	0-36	80-865	786					07R (Take-off)	241
Site 4	0-36	80-865	786					25L (Take-off)	241

3.3. Methodology of two-stage wake vortex recognition and safety assessment

3.3.1. Overview of the methodology

Aircraft wake vortex detection is essential for ensuring safe separation between aircraft during the final approach. In this Chapter, a three-step data-driven approach is designed to recognise the locations and strength of aircraft wake vortices and to analyse their duration in the path of the final approach. **Figure 3-4** depicts the general

framework of the developed methodology. The first step is to map wake data with relevant flight information, visualise wake images from LiDAR data scanned during the final approach at HKIA, and clear the vortex data derived from the LiDAR processing algorithm. After pertaining data is extracted, a two-stage model framework comprised of two probabilistic convolutional neural networks is proposed. In the first stage, one CNN model is trained to locate vortex cores from the entire vortex images. In the second stage, the strength of wake vortices is captured from the other CNN model, utilising the most relevant image regions. This region of interest is derived from initially predicted vortex locations. Finally, the prediction reliability of the proposed model is clarified by visualising the significant image regions that positively contribute to model decisions. On the other hand, the predicted probabilistic vortex locations are then utilised to estimate the duration of wake presence in the path of the final approach. In addition, the relevance of vortex duration to wind conditions is also demonstrated to illustrate the potential of separation reduction in a dynamic flight environment in this context.

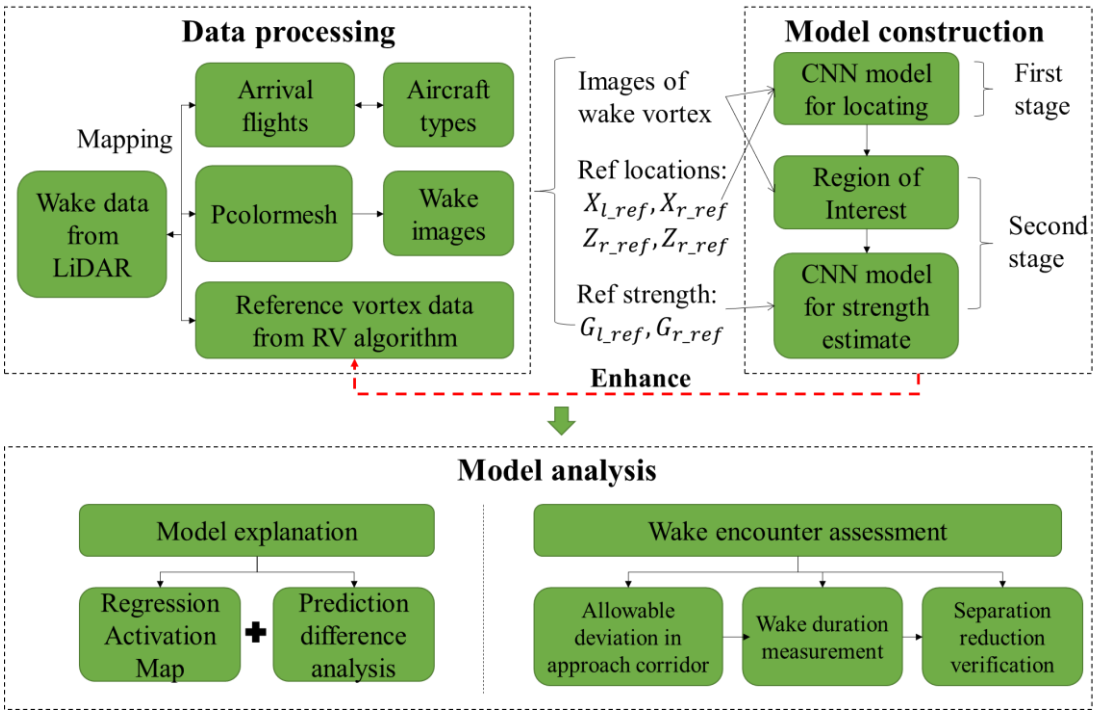

Figure 3-4. Flowchart of the proposed three-step methodology for identifying wake vortices and wake encounter assessment.

3.3.2. Deep learning models for wake vortex recognition

3.3.2.1. Convolutional neural network

Convolutional neural network derives features from input data using convolutional operations, including the convolutional layer and pooling layer, which are typically organised as modules. It provides several benefits, such as being connected locally, sharing weight and reducing dimension by down-sampling (Yamashita et al., 2018). The convolutional layer applies convolutional kernels to the input images to extract feature presentations and generate feature maps. Typically, zero padding is used to expand the input with a value of zero to adjust the size of feature maps so that more layers can be applied (Li et al., 2022; Yamashita et al., 2018). Stride defines the distance between positions of two consecutive sliding kernels to control the density of convolution (Li et al., 2022). The pooling layer with max pooling or average pooling operation will then simply execute down-sampling along the spatial dimensionality of the input data to further reduce parameter numbers. The fully connected layer serves the same role as that in other artificial networks to map the extracted features to the final categorical or regressive tasks.

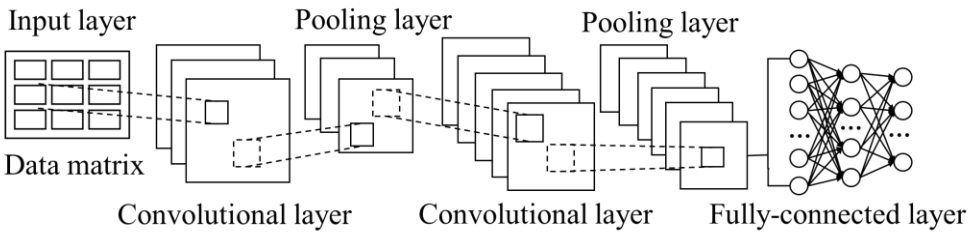

Figure 3-5. A general framework of convolutional neural network.

3.3.2.2. Object detection algorithms

The overall methodological framework for wake region detection and safety assessment is illustrated in **Figure 3-6**, including data processing, model construction, and model analysis. Data processing consists of two essential parts. The first is visualising the wake vortices in heatmaps, and the other is to label the box that covers the entire region of wake vortices to obtain the four coordinates of the box. For model construction, YOLO v5, one of the most popular model frameworks for object detection, is applied as a benchmark for our task. Furthermore, the loss function of YOLO v5 is modified and updated to conform to our performance specifications. Finally, the predicted box coordinates of wake regions are implemented for wake presence assessment.

The raw aircraft wake data utilised in this study comprises the radial wind velocities measured by the LiDARs installed at the entrances of the runways at Hong Kong International Airport. The LiDAR scans in the range height indicator (RHI) mode approximately every 10s at a scan rate of 5 °/s. The wind velocity data in polar coordinates was converted to the cartesian coordinate for visualisation and training convenience. Next, the aircraft wake vortices were visualised by heatmaps using the Pcolormesh. To achieve the wake region detection task, the ground truth boxes were labelled manually using the LabelImg toolbox. In total, 5432 wake images in the final approach phase were processed. Therefore, the obtained outputs are x_c, y_c, w, and h, where x_c and y_c represent the centres of the box in lateral and vertical directions. w and h denote the width and height of the labelled boxes. Notably, the boxes were labelled to encompass the entire region of the pairwise wake vortices; thus, each box was categorised into a single category of vortex pair.

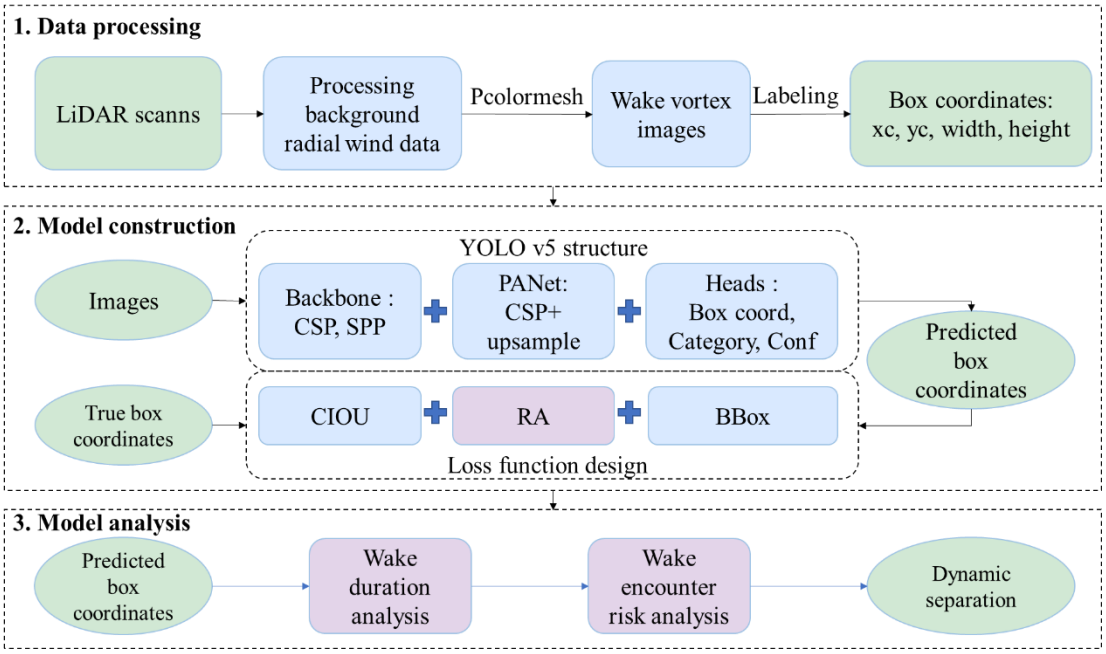

Figure 3-6. The framework of the proposed method for aircraft wake region detection and encounter analysis.

The mainstream models for object detection fall into two distinct categories: one-stage detection and second-stage detection. Popular algorithms belonging to the former category, including the YOLO networks, realise rapid object detection in images in a single forward pass of the network. In contrast, the second-stage algorithms, such as the Faster R-CNN (Ren et al., 2015) and Cascade R-CNN (Cai et al., 2018), require multiple passes in detection. In view of the portability and user-friendliness of the YOLO series, this study applies the YOLO v5 network as a benchmark for wake region detection.

(1) Structure of the YOLO v5 network

YOLO network comprises three primary components: the backbone, neck and heads. These components have undergone revisions since their inception in the initial version (Redmon et al., 2016), to v3 (Redmon et al., 2018) and v5 version (Ge et al., 2021). Compared to the former versions, the novelty of the YOLO v5 network exists mainly

in the structures of the backbone and neck. The integration of these components enables YOLO v5 to achieve high precision and speed, making it suitable for real-time detection of aircraft wake regions.

- The backbone module efficiently encodes the input image into a rich feature map, progressively downsamples the image and captures complex features at various scales. The cross-stage partial network (CSPDarknet53), in which a series of convolutional layers are employed, and spatial pyramid pooling (SPP) layers are applied in YOLO v5. Moreover, the focus layer is involved in the backbone of YOLO v5 to replace the first three layers in the v3 version to decrease memory utilisation.
- The neck module further processes and fuses these features to capture context and finer details, comprising modules of path aggregation network (PANet) and additional convolutional layers. PANet contains the feature pyramid network (FPN).
- The head of the YOLO v5 translates these features into meaningful object detection predictions, similar to the former versions. It includes convolutional layers that output the class probabilities, objectness scores and bounding box coordinates for each detected object.

(2) Loss function design and optimization

The loss function in object detection is a crucial component to guide the learning process, and it is a composite of the following individual loss terms.

- The bounding box regression loss, l_{box}. This term measures the accuracy of the predicted bounding boxes against the ground truth. It accounts for the shape, orientation, and overlap of the predicted and actual bounding boxes, thus driving

the model to improve the precision of object localisation. The intersection over union (IOU), as defined in Eq. (3-2), is initially applied to evaluate this loss, which outperforms the general metrics of mean square error. In addition, alternative metrics, such as complete intersection over union (CIOU) in Eq. (3-4) - Eq. (3-6), generalised intersection over union (GIOU), efficient IOU (EIOU) (Zhang et al., 2022), distance-IOU (DIOU), and soft-IOU (SIOU) in Eq. (3-11)-Eq. (3-14), are suggested to account for comprehensive situations based on the IOU.

- Objectness loss, l_{obj}. This metric evaluates the accuracy of the model in predicting the presence of an object within a bounding box. It typically uses binary cross-entropy to distinguish between boxes containing objects and those devoid of such objects, thereby enhancing the ability to discern relevant regions in the image.
- Classification loss, l_{cls}. The cross-entropy loss is also used in the predicted class probabilities to ensure the model accurately classifies the objects it detects, aligning the predicted classes with their corresponding ground truth labels.

Both the size and location of the bounding boxes matter for aircraft wake region detection tasks. Therefore, in addition to the IOU-related metric mentioned above, another component, *RA* in Eq. (3-6), is proposed in this study and integrated into the bounding box regression loss term, Eq. (3-7). This component constrains the relative size of the predicted box compared to the labelled box. Consequently, the total loss is calculated as follows. Therefore, taking the CIOU as a benchmark, the total loss is defined in l_{box}, as denoted in Eq. (3-8) (Chu et al., 2024).

$$IOU = \frac{area_{inter}}{area_{union}} \tag{3-2}$$

$$area_{union} = box_{area}^{gt} + box_{area}^{pred} - inter_{area} + 1e^{-6} \tag{3-3}$$

Where the constant value in $area_{union}$ is set to avoid division by zero and numerical instability, the superscript gt represents the ground truth, and $pred$ represents the prediction in model training.

$$CIOU = 1 - IOU + \frac{\rho^2(b,\, b^{gt})}{c^2} + \beta v \tag{3-4}$$

$$v = \frac{4}{\pi^2}\left(arctan\frac{w^{gt}}{h^{gt}}\right) - arctan\frac{w}{h})^2,\ \beta = \frac{v}{(1-IOU)+v} \tag{3-5}$$

$$RA = \frac{box_{area}^{gt}}{box_{area}^{pred}} \tag{3-6}$$

$$l_{box} = CIOU + c \cdot RA \tag{3-7}$$

$$loss = \lambda_1 \cdot l_{box} + \lambda_2 \cdot l_{obj} + \lambda_3 \cdot l_{cls} \tag{3-8}$$

Where c represents the weight of the RA term, λ_1, λ_2, and λ_3 represent the weight of these loss terms for the final loss.

(3) Model evaluation metrics

The evaluation metrics in object detection are primarily in the classification aspect, including the precision (P), recall (R) and mean average precision (mAP), and the mean of the average precision (AP) for each class. Given that mAP is the comprehensive evaluation index, it is utilised to implement it in our task, as formulated in Eq. (3-9).

$$\text{mAP} = \sum_{q=1}^{Q} \frac{aveP(q)}{Q} \tag{3-9}$$

where q represents the number of queries, and $aveP(q)$ denotes the average accuracy pertaining to a specific query.

Unlike object detection, which primarily classifies multiple objects in one image, the

prediction accuracy of box coordinates is considerably vital in wake detection. Therefore, the regressive metrics of boxes, typically the IOU and mean absolute error (MAE) of the box centres, as shown in Eq. (3-10), are also considered. Furthermore, the detection speed frames per second (FPS) of model inference is also evaluated.

$$\mathrm{MAE} = \frac{1}{\mathrm{N}} * \sum_{i=1}^{N} \left| y_{c,i}^{pred} - y_{c,i}^{gt} \right| \tag{3-10}$$

The definitions of the GIOU, EIOU, DIOU, and SIOU loss functions (Gevorgyan, 2022) are denoted in Eq. (3-11) – Eq. (3-14), respectively.

$$GIOU = 1 - IOU + \frac{|Cbackslash(b^{pred} \cup b^{gt})|}{|C|} \tag{3-11}$$

$$EIOU = 1 - IOU + \frac{\rho^2(b^{pred}, b^{gt})}{c^2} + \frac{\rho^2(w^{pred}, w^{gt})}{c_w^2} + \frac{\rho^2(h^{pred}, h^{gt})}{c_h^2} \tag{3-12}$$

$$DIOU = 1 - IOU + \frac{\rho^2(b^{pred}, b^{gt})}{c^2} \tag{3-13}$$

$$SIOU = 1 - IOU + \frac{\Delta + \Omega}{2} \tag{3-14}$$

Where $\Omega = \sum_{t=w,h}(1 - e^{-\omega_t})^{\theta}$, $\omega_w = \frac{|w^{pred} - w^{gt}|}{max(w^{pred}, w^{gt})}$, $\omega_h = \frac{|h^{pred} - h^{gt}|}{max(h^{pred}, h^{gt})}$, $\Delta = \sum_{t=x,y}(1 - e^{-\gamma\rho_t})$, where $\rho_x = \left(\frac{b_{cx}^{gt} - b_{cx}}{c_w}\right)^2$, $\rho_y = \left(\frac{b_{cy}^{gt} - b_{cy}}{c_h}\right)^2$

3.3.2.3. Transfer learning on pre-trained networks with fine-tuning

Fine-tuning on a pre-trained network is an efficient method to apply the pre-trained deep learning network from the large-scale datasets (classically in classification tasks) into small image datasets. The spatial structure of the features figured out by the pre-

trained network can successfully serve as a general component of the visual domain to be used in new scenarios, even if these new tasks refer to entirely different tasks. Two well-trained CNNs, VGGNet and ResNet models, are selected in this chapter. VGGNet comprises 5 sectors of convolution (2–3 convolution layers per section with a 3×3 kernel, with each section linked to the end of a 2×2 maximum pool layer to decrease the image size) (Simonyan et al., 2014). One of the key contributions of the ResNet model is the residual block developed by the shortcut connection to minimise the gradient vanishing problem without degradation, as the gradient can flow directly forward through shortcut connections (He et al., 2016; Li et al., 2022; Wan et al., 2018).

3.3.2.4. Probabilistic CNN model with Bayesian inference

The objective of the Bayesian approach is to infer the posterior distribution $p(\theta|X,Y)$ of the network parameters θ, where θ is typically described with a prior distribution $p(\theta)$ to indicate the prior belief over network weights. Next, a likelihood function $p(Y_i|X_i,\theta)$ is then established to model the probability of observing $\mathrm{Y_i}$ given X_i and θ. $p(\theta)$ is normally assumed as a Gaussian distribution $N(0,I)$ and bias vectors in the network are assumed to be a certain value for simplicity (Neal, 2012). Thus, the posterior distribution is able to be calculated with the below Bayesian theorem:

$$p(\widehat{\theta|X},Y) = \frac{\mathrm{p}\left(\widehat{\mathrm{Y}|\mathrm{X}},\theta\right)\mathrm{p}\left(\hat{\theta}\right)}{\mathrm{p}(\mathrm{Y}|\mathrm{X})} \tag{3-15}$$

Approximate inference techniques, for instance variational inference, are introduced to avoid the computational intractability of exact posterior distribution. The central concept of variational inference is to utilise a variational distribution $q(\theta)$ for approximating the true $p(\theta|X,Y)$ by minimizing the Kullback-Leibler (KL) Divergence between them. Gal et al. (2016) have proven that the Monte Carlo (MC) dropout has a similar effect in minimising KL divergence for approximating Bayesian

inference for broad deep neural models in a straightforward and easy approach. The term "dropout" represents the randomly elimination of units and their connections in the hidden layers of the network. By MC Dropout, the approximation to the full posterior distribution $p(\theta|X,Y)$ is obtained, with random samples generated from which to build the collection of model output. The probabilistic distribution of the model on new data x^* can therefore be generated by integrating over θ and estimated with MC samples, in which *K* is the number of MC samples:

$$p(y^*|x^*,X,Y) = \int p(y^*|x^*,\theta)p(\theta|X,Y)d\theta \approx \frac{1}{K}\sum_{n=1}^{K} p(y^*|x^*,\tilde{\theta}_k) \qquad (3\text{-}16)$$

From the foregoing, the MC Dropout can be applied to the above-mentioned CNN models to achieve the probabilistic distribution of prediction, and this CNN model with uncertainty estimation is called the probabilistic CNN model. In order to distinguish the CNN model with single-point outputs, the CNN model without uncertainty analysis is defined as the deterministic CNN model.

3.3.3. Explanation of convolutional neural network

In the context of the "black-box" characteristics of deep learning, the prediction transparency and confidence level of the neural network become crucial for its deployment in safety-critical wake separation systems. The transparency of networks can be considered from an explanatory and visual standpoint of model prediction. One component of visualising CNNs involves highlighting the "important" area of a given input image (Gan et al., 2015; Simonyan et al., 2013). Another visualisation technique synthesises images to maximally activate a network unit to visualise the overall model. Zhou et al. (2016) developed the Class Activation Mapping (CAM) technique to identify the discriminative regions on the raw input image under the image

classification-oriented CNN model, in which the global average pooling layer rather than the fully connected layers over feature maps was applied. Selvaraju et al. (2017) proposed a general Gradient-weighted CAM (Grad-CAM) to analyse feature maps with gradient signal, which can be applied to a substantially wider variety of CNN families, such as CNN models along with fully connected layers, CNNs with multi-modal inputs and structured outputs without that demand of architectural modifications or model re-training. This chapter applies both the feature analysis method and the Grad-CAM method in our regression task, with their methodological flowchart shown in **Figure 3-7**.

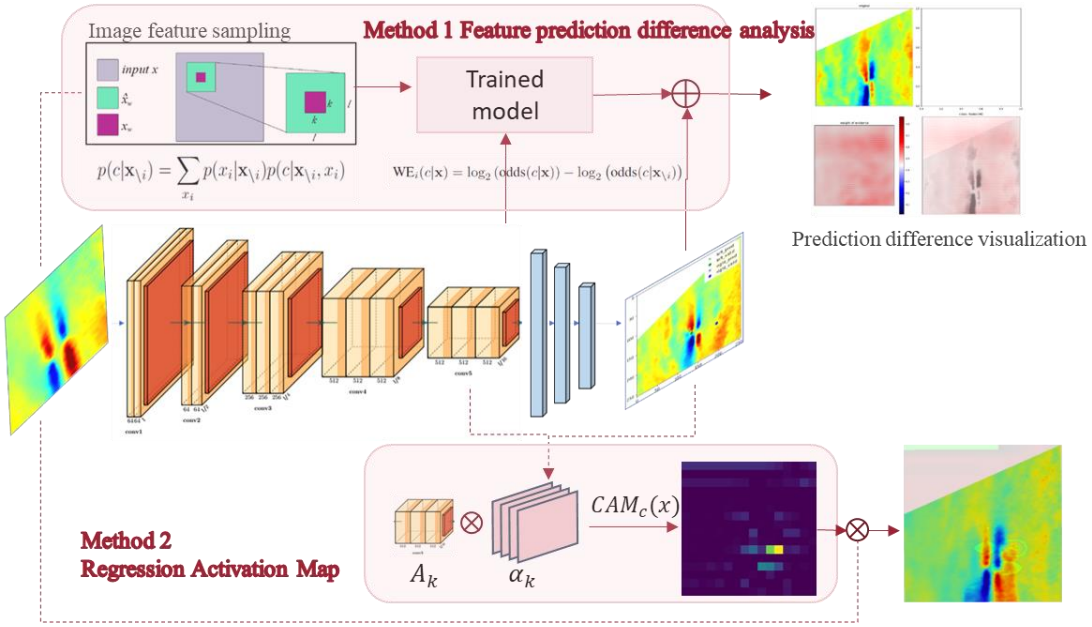

Figure 3-7. Feature analysis methods for model decision explanation.

(1) Grad-Regression Activation Map

The Grad-CAM technique (Selvaraju et al., 2017) is applied in our regression task of wake-vortex location and is called Grad-Regression Activate Map (Grad-RAM) in this chapter. Grad-RAM is simply the weighted sum of outputs in certain convolutional layers. These weights represent the connections between the outputs of the

convolutional layer and neurons in the output layer. In order to get the regression-discriminative localisation map Grad-RAM, $L^r_{Grad-RAM}$ of width u and height v for regressive output r, the gradient of the output to the feature map A^k of the convolutional layer is first computed, i. e. $\frac{\partial y^r}{\partial A^k}$. Next, the global average pooling is applied in gradients flowing back to get the neuron importance weights, α^r_k:

$$\alpha^r_k = \frac{1}{Z}\sum_i\sum_j \frac{\partial y^r}{\partial A^k_{ij}} \tag{3-17}$$

The weight α^r_k obtains the "importance" of feature map k with respect to the final output r. Then, a weighted sum above the activation maps is conducted, followed by a ReLU operation for capturing the area with a positive influence on output (Selvaraju et al., 2017).

$$L^r_{Grad-RAM} = \mathrm{ReLU}(\sum_k \alpha^r_k A^k) \tag{3-18}$$

(2) Prediction difference analysis of image features

The fundamental concept underlying prediction difference analysis is to estimate the relevance of feature x_i to model output by measuring the prediction disparity between $p(c|x)$ and $p(c|x_{\setminus i})$ in the absence of the feature is unknown (Robnik-Šikonja et al., 2008), where $x_{\setminus i}$ represents the input feature set without x_i. The prediction difference can be evaluated by the weight of evidence: $WE_i(c|x) = log_2\big(odds(c|x)\big) - log_2(odds\big(c\big|X_{\setminus i}\big))$, where $odds(c|x) = p(c|x)/(1-p(c|x))$.

3.3.4. Exploratory assessment of wake vortex duration in the final approach path for

dynamic separation

As stated previously, the movement of aircraft wake vortices is highly correlated with wind conditions. Strong winds may cause the aircraft wake vortices to dissipate rapidly. Therefore, the safe aircraft separation time under strong wind conditions has the potential to be reduced compared to currently defined static wake separation. Consequently, this section aims to provide one exploratory method for predicting the dynamic separation utilising the results of our proposed probabilistic CNN model, and demonstrate the effect of crosswind in the lateral movement of wake vortices in this process.

Specifically, when the crosswind is prevailing, the wake vortices generated by the leading aircraft will be generally blown away from the approach profile, with the movement direction dependent on the direction of the crosswind. The general way for determining safe flight separation time is to evaluate the hazard posed to the following aircraft when they encounter a certain level of wake vortex strength. However, due to the limited accuracy in vortex strength estimation, we propose an exploratory approach to assess safe separation by estimating vortex duration in the path of the final approach, using the extreme values of vortex locations forecasted by the probabilistic CNN model. Two main steps of this exploratory method are introduced as follows.

(1) Identify allowable aircraft path in the final approach

As the flight path in the final approach is quite standard and fixed following the requirement of the instrumental approach procedure, the allowable aircraft path in the LiDAR plane can be calculated first. **Figure 3-8** depicts the general instrumental landing procedure with the glideslope guidance and horizontal localiser at HKIA. Typically, aircraft approaches with a $3°$ glide path angle, a deviation tolerance of $\pm 0.7°$, and a horizontal deviation of $\pm 35°$ from the centreline within 10 nautical miles

away from the localiser. Based on the positions of the glideslope antenna and horizontal localiser, and the distances of LiDAR instruments to runway entries, the vertical and horizontal position allowance of aircraft in the LiDAR planes can be estimated, as shown in **Table 3-2**, in which the installation height of the LiDAR is also considered, assuming the landing point is 300m away from the runway end in computing the estimated allowable range of height in LiDAR scanning planes. Therefore, the duration of vortex presence in the above circumstances is evaluated upon the determination of standard approach profiles in LiDAR scan planes. The lateral and vertical boundaries of the approach profiles were loosened to achieve an initial vortex coverage of more than 80%.

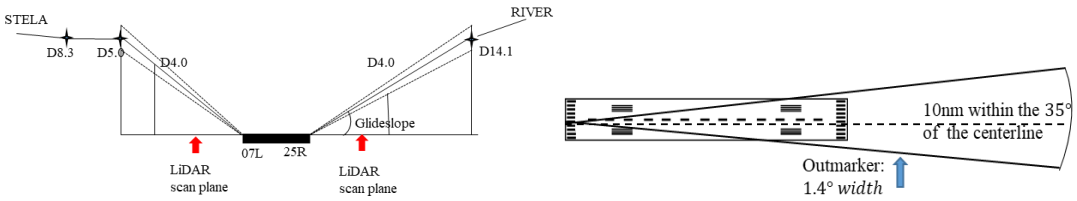

Figure 3-8. The instrument landing procedure of the north runway at HKIA (Left: Vertical profile of the instrumental landing; Right: Horizontal profile of the instrumental landing).

(2) Assess the duration of vortex presence in the approach profiles

After that, the probabilistic CNN model can then be used to determine the maximum and minimum values of vortex locations with a certain level of confidence in a wake sequence. Then, the duration of wake vortices in the two-dimensional flight profiles can be estimated based on the estimated position of vortex cores and the vortex radius related to aircraft weight. In addition, a certain safety margin is considered to enhance the safety and reliability of separation estimation. After the estimation, the relationship between the crosswind speed and the wake duration is analysed statistically to identify the foundations of dynamic wake separation. This exploratory result is expected to

serve as one reference for determining the final dynamic separation, and may therefore support the development of an online suggestion system of time-based aircraft separation. It can also serve as a supplementary tool for verifying dynamic flight separation time derived from other methods.

Table 3-2. The height and horizontal position range of aircraft at the LiDAR scanning plane.

Runway	LiDAR distance (m) to Runway (x profile)	LiDAR distance (m) to Runway (y profile)	Estimated allowable range of height (m) to ground	Estimated allowable range of height (m) in LiDAR plane	Estimated allowable range of horizontal position (m) in LiDAR plane
07L	1400	1116.31	56.84 - 91.40	49.84–84.40	$\pm$60.06
25R	275	1511.99	72.72 - 116.93	65.72–109.93	$\pm$64.90

3.4. Experiment and methods

3.4.1. Data processing

One-month LiDAR data in both Site 1 and Site 2B of arrival flights in May 2019 was selected for this research. The data from LiDAR is twofold: one is the radial wind velocity data obtained by LiDAR; the other is the data of wake vortices calculated by RV algorithm (height Z_{l_ref}, Z_{r_ref}, the lateral position deviation from the centreline $\Delta X_{l\_ref}, \Delta X_{r\_ref}$ of vortex cores, and the intensity of the vortex strength G_{l_ref}, G_{r_ref}). These two data sources are treated as inputs and training labels for the deep learning model, respectively. The radial wind velocity data were mapped to the Cartesian coordinate system to ensure the uniformity of data distribution and then plotted into heatmaps with Pcolormesh according to the timestamps of LiDAR scanning. **Figure 3-9** visualises the wake images of these two LiDARs in different meteorological conditions, where warm colour indicates positive velocities that radiate away from the LiDAR and cold colour represents negative velocities that radiate towards the LiDAR.

The theoretical estimated lateral position deviation was converted into the absolute lateral position of wake vortices relative to the LiDAR. The rationality of the transformation was validated by visual inspection of the reference locations in raw wake images, as the solid white dots are shown in **Figure 3-9**. Next, incomplete and anomalous LiDAR scans were removed, and the reference locations of the left and right wake vortex were cleaned to remove null data in both location and strength columns. Finally, 23511 LiDAR scans under a variety of meteorological conditions were selected and randomly divided into three datasets for model training, validation and testing in the proportion of 6:2:2.

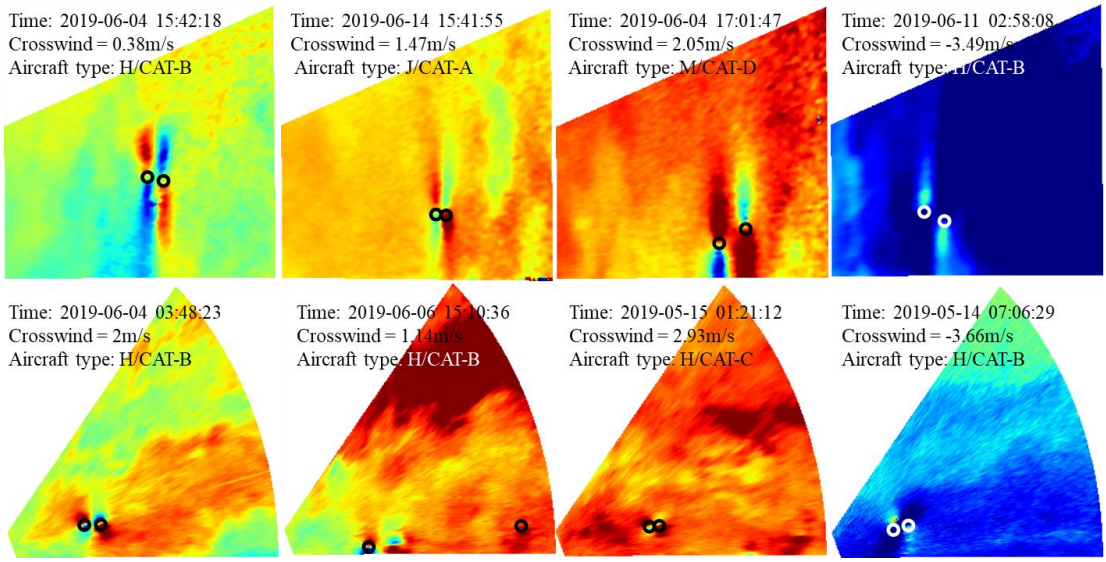

Figure 3-9. Visualisation of wake vortices with reference positions under several meteorological conditions.

3.4.2. Model configuration

(1) CNN models for wake location and strength estimation

The architecture of the proposed convolutional neural networks is listed in **Table 3-3**, including the input layer with images in 256×256×3 size, 5 convolutional modules (convolutional layer plus the max-pooling layer) and 3 fully-connected layers to match

final outputs in the task. The number of convolutional modules is determined after evaluating the model performance with 3-7 convolutional layers. Consequently, the same model structure is captured for both vortex locating and strength estimation, and the distinctions between models for these two tasks are the inputs and outputs (4-dimensional positions or 2-dimensional strength). The convolutional layers contain 64, 128, 256 and 512, 512 units with 3×3 kernel size and stride in size 1. The max-pooling layer contains a kernel size of 2×2 and a stride of 1. Batch Normalisation and dropout are applied after convolutional and pooling operations in the last three convolutional layers. Rectified linear units (ReLU) are used across all layers as the activation function. To quantify the uncertainty in network structure and parameters, MC dropout is performed by randomly dropping 10% to 20% units to estimate the Bayesian posterior distribution. For mini-batch training, the dropout is performed in smaller training networks.

(2) CNN-SVM and CNN-KNN models

Support Vector Machine and K-Nearest Neighbours (KNN) have advantages in nonlinear classification and regression of multiple variables. Unlike the SVM algorithm that finds the optimal hyperplane $f(w, x) = w \cdot x + b$ to separate outputs (Cortes et al., 1995), Support Vector Regression (SVR) identifies the optimal hyperplane to maximise the margin distance between the hyperplane and the nearest data points, while minimising the prediction error. It employs the $\varepsilon -$ insensitive loss function, where ε decides the margin of tolerance of prediction error. The kernel function improves the non-linear regression ability of SVR by mapping the input data to higher dimensional space (Awad et al., 2015). In the KNN algorithm, the predicted value of a point is derived by averaging the values of the *K* points closest to it, where "closest" can be

either in Euclidean distance or other distances.

Table 3-3. Structure of the proposed convolutional neural network for wake-vortex locating (Parameters in the convolutional layer are presented as "conv(kernel size)-(number of channels)". The ReLU activation function is omitted for concision.

Model layer	Parameter setting
Input	256×256 RGB image
Convolutional layer	Conv3-64
Max-pooling	2×2 Kernel
Convolutional layer	Conv3-128
Max-pooling	2×2 Kernel
Convolutional layer	Conv3-256
Batch Normalisation	-
Max-pooling	2×2 Kernel
Dropout	0.1-0.2
Convolutional layer	Conv3-512
Batch Normalisation	-
Max-pooling	2×2 Kernel
Dropout	0.1-0.2
Convolutional layer	Conv3-512
Batch Normalisation	-
Max-pooling	2×2 Kernel
Dropout	0.1-0.2
Flatten	-
Fully-connected layer	512
Dropout	0.1-0.2
Fully-connected layer	256
Fully-connected layer	128
Output layer	4

This chapter uses these two machine learning models as benchmarking models to compare their performance with pure CNN models. The proposed architectures of CNN-SVR and CNN-KNN are shown in **Figure 3-10**. The features of input images

were extracted from well-trained CNN convolutional structures. Next, Principal Component Analysis (PCA) was applied to reduce the dimension of the high-dimensional feature maps while maintaining the maximum amount of information. Finally, these low-dimensional features were fed into SVR and KNN models for task regression.

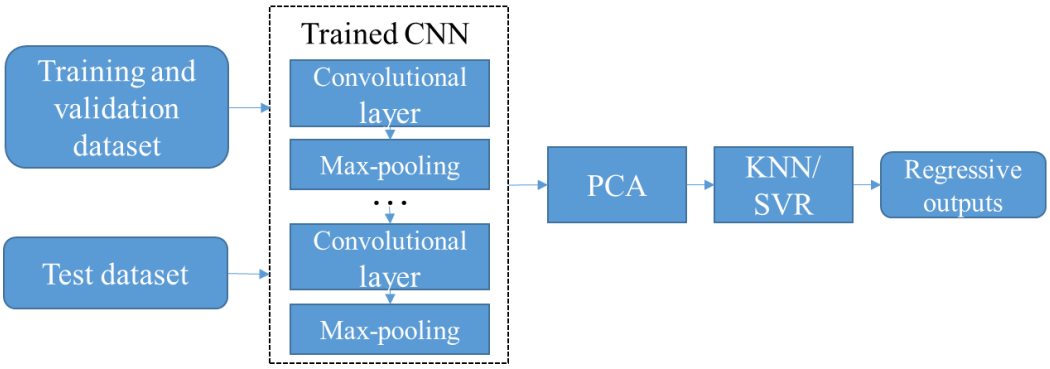

Figure 3-10. Architecture of proposed CNN-SVR and CNN-KNN model.

3.4.3. Model explanation

The Grad-RAM presented in Section 3.4 was applied in the final convolutional sector (the convolutional layer "*conv2d_4*" and the dropout layer "*max_pooling2d_4*") of the well-trained CNN models. These two layers are anticipated to provide the optimal compromise between the high-level concepts and details of the spatial features that are important for the regression outputs.

From the feature analysis perspective, we applied the conditional sampling technique with multivariate normal distribution proposed by (Zintgraf et al., 2017) to replace the feature patch rather than just a single pixel of the raw image to reduce the computational burden, and then simulated the prediction difference between the processed features and the raw images on the trained CNN model. In our regression task, the $odds(c|x)$ for the classification task was replaced directly with predicted outputs.

3.5. Computational results

This section discusses the computational results of the developed models in wake location and strength identification, illustrates their improved performance over three pre-trained CNN models and the benchmarking machine learning models, and presents the safety measurement of wake encounters in the approach corridor. All experiments in this chapter were conducted on a Windows 10 desktop with an Intel Core i7-12700K processor, NVIDIA GeForce RTX 3060Ti GPU (1.78 GHz), and DDR5 RAM with 32 GB. The models were implemented using Keras in Tensorflow 2.5.0.

Before model training, both input and output data were normalised using the MinMaxScaler method. Grid search was performed to tune the hyperparameters and relevant parameters of these two CNN models, such as the learning rate ([0.01, 0.001, 0.0005, 0.0001, 0.00005, 0.00001]), image size ([128, 256]), batch size ([16, 32, 64, 128, 256]) and size of ROI for strength estimation ([(20, 40), (30, 50), (40, 60)]). The early stop that monitors the validation loss was set to obtain the optimal set of hyperparameters, with conditions of minimum performance reduction of 0.0000001 in the patience of 100 epochs. The results of the grid search indicate that the minimum prediction error in wake locating occurs when the image size is 256, the batch size is 32, the Adam optimiser with a learning rate of 0.00005, and the minimum prediction error in strength estimation is under the combination of image size in 128, 20×40 cropped size of ROI, Adam optimiser with 0.0001 learning rate and batch size of 32.

The performance evaluation of these models is performed on the metrics of the mean absolute error (MAE) and the root mean square error (RMSE). In the probabilistic model, the mean value of prediction is used to calculate the MAE and RMSE. The detailed performance assessment of these CNN models and benchmarking models is demonstrated below.

3.5.1. Model performance comparison

3.5.1.1. Model performance in wake vortex locating

The performance of the proposed models was compared to benchmarking models in vortex locating, as reported in **Table 3-4**. In both the locating and strength estimation tasks, the proposed deterministic CNN model with single-point outputs and the probabilistic CNN model with prediction variance all exhibit superior performance with the lowest errors in terms of MAE and RMSE compared to other models. Conversely, the well-trained VGGNet demonstrates higher prediction errors, indicating that the training samples in this research are relatively small in comparison to the original task. Moreover, the complexity of the VGGNet makes it unsuitable for our specific tasks. Notably, our experiment reveals that the performance of ResNet models with residual blocks can be enhanced by increasing network layers, surpassing the performance of the VGG16. Furthermore, the KNN model is more suitable for this task compared to the SVR model when utilising the same feature inputs. The variables ΔD_L and ΔD_R describe the Euclidean distances between the predicted location and reference location of the pairwise vortex cores. In comparison to CNN models in (Wartha et al., 2022) with similar-sized inputs as our experiments, our CNN model reduces the Euclidean distance of the left and right vortexes by up to 26% and 30 %, respectively. Additionally, our proposed model predicts these four positional features in a single model, capturing the coupling relationships between pairwise vortices more efficiently than previous models. The authors adopted the CNN model framework proposed by Wartha et al., (2022) on HKIA dataset. The results may different from the original results report in the article. Readers may wish to refer to the original article.

Table 3-4. Performance comparison of the proposed CNN models with other machine learning models in vortex locating.

Model	MAE (m)						RMSE (m)			
	X_l	Z_l	ΔD_L	X_r	Z_r	ΔD_R	X_l	Z_l	X_r	Z_r
Deterministic CNN	11.57	3.58	12.11	12.29	3.72	12.84	26.66	7.59	29.52	8.17
Probabilistic CNN	12.40	4.45	13.17	12.43	4.12	13.10	26.49	8.19	29.77	7.95
VGG16	22.20	6.95	23.26	25.65	7.35	26.68	34.17	11.27	39.14	11.60
ResNet18	15.04	7.35	16.74	17.07	5.48	17.93	30.04	11.61	33.70	9.90
ResNet50	15.41	5.04	16.21	15.4	5.17	16.24	29.32	9.13	32.5	9.43
ConvLayer-KNN	20.75	6.33	21.69	20.10	6.06	20.99	41.43	11.96	44.01	11.08
ConvLayer-SVR	33.58	9.81	34.98	34.58	9.39	35.83	46.59	15.83	50.22	14.80
CNN model in (Wartha et al., 2022)	15.72	4.68	16.40	17.69	5.35	18.48	30.51	9.07	34.05	9.64

Note: the comparison with the existing work is primarily about model structure, under our computational hardware and data.

The proposed five-convolutional-sector CNN model demonstrates low prediction error, indicating its high accuracy in identifying the lateral positions and height of wake vortices from LiDAR scans. The result suggests that the predictions of the CNN model align closely with the reference positions of the theoretical LiDAR algorithm. Specifically, the low MAE shows the model's performance on average, and the low RMSE indicates the relatively small outliers or errors in the model's predictions. As depicted in the first row of **Figure 3-11**, the model performs exceptionally well in estimating both young coherent vortices with strong intensity and vortices that descend near the ground with weakened intensity. In addition to efficient regression based on the reference algorithm, this deep learning model also can rectify evident errors present in the reference data. The bottom images of **Figure 3-11** highlight noticeable errors in

the LiDAR locating algorithm in these scans, which can be further corrected by our CNN model. Through this revision strategy, we can anticipate improved accuracy in vortex locating through iterations. Furthermore, the integration of the physical reversion algorithm with the CNN model enhances decision accuracy and boosts confidence levels in wake-vortex locating.

In terms of computational performance, our trained CNN model achieves a prediction speed of 0.0255s per image using the aforementioned training environment. However, based on the processing time of the Windcube200S algorithm described in (Thobois et al., 2016), the computational speed of this physical algorithm reaches 0.7835s per image, under the conservative assumption of 15 scans in each wake sequence. Therefore, our data-driven approach demonstrates significant computational efficiency benefits.

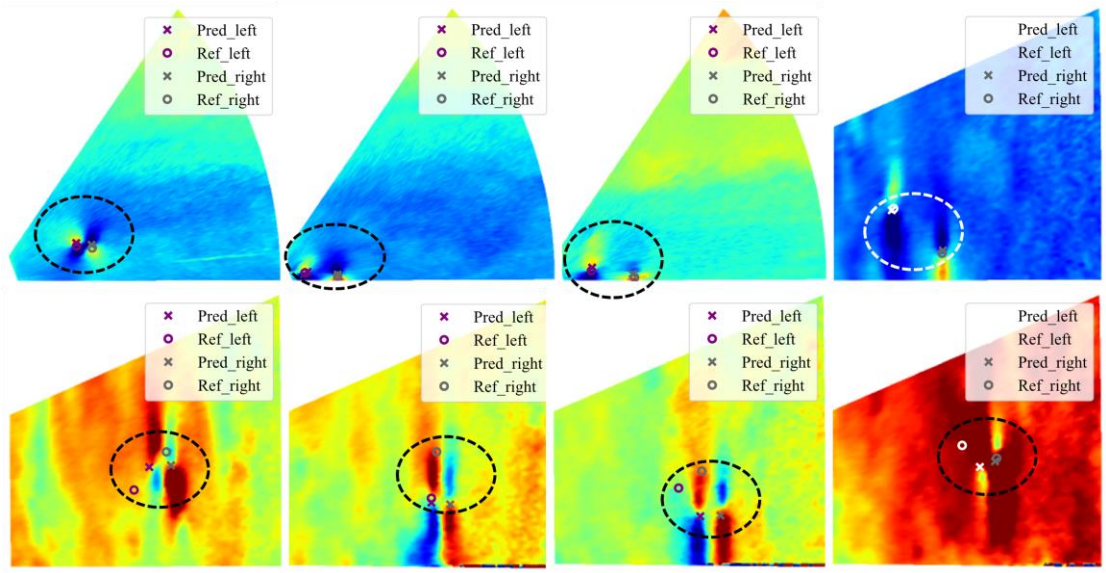

Figure 3-11. Visualisation of performance of wake vortex locating in the test dataset.

3.5.1.2. Model performance of wake region detection

The proposed models and the benchmarking models were trained in the Pytorch

environment using Adam optimiser. This was accomplished on Windows 10 with an Intel Core i7-12700K processor, the GPU of NVIDIA GeForce RTX 3060Ti and DDR5 RAM with 32GB. To obtain training, validation and test datasets, all 5432 images and relevant labelled boxes were randomly divided with a ratio of 6:2:2. The training with the best performance was configured with epochs of 300, batch size of 32, initial learning rate of 0.001 and cosine annealing learning rate decay, momentum and weight decay rates of 0.95 and 0.001, respectively. The gains for bounding box loss, object loss and class loss were maintained at 1, and the gain for the relative area (RA) was set to 0.01. Besides, the object confidence threshold was established at 0.25, and the IOU threshold was defined as 0.45 for model testing and inference. The hyperparameters were trained with the grid search.

Table 3-5 presents the computational performance of the YOLO v5 benchmarking model with various loss functions, including the loss function that we have proposed for this particular task. It indicates that box regression performance is enhanced when training on the large model with a greater number of parameters that have been pre-trained in COCO and other datasets, as opposed to the lightweight model that has been pre-trained. In contrast, the computational efficacy of the small model is considerably higher, as indicated by the FPS, that it can deduce nearly ten additional images within a single second. In addition, a comparison is made between the impact of various loss functions derived from IOU on the medium model, revealing that the fundamental loss functions are more suitable for our objective than the novel EIOU and Soft-IOU (SIOU) loss metrics. Furthermore, it is significant to highlight that by incorporating our proposed “relative box area” term into the box loss function, the model achieves the lowest MAE in both box centre and box area regression, as demonstrated in **Figure 3-12**, thus achieving both the goals of wake region regression and wake object

classification without incurring any additional computational burden.

Table 3-5. Test performance of the proposed algorithm in wake region detection.

YOLO v5 model	Loss function	mAP0.5	MAE			Computational speed (s)	FPS
			x_c	y_c	IOU		
Medium	IOU	99.6%	0.0218	0.0154	**0.7891**	0.0107	93
	GIOU	99.6%	0.0204	**0.0143**	0.7866	0.0104	96
	DIOU	99.5%	0.0194	0.0151	0.7837	0.0104	96
	CIOU	99.6%	0.0269	0.0155	0.7827	0.0104	96
	EIOU	99.5%	0.0314	0.0161	0.7567	0.0104	96
	SIOU	99.5%	0.0314	0.0158	0.7748	0.0108	92
	IOU+RA	99.6%	0.0304	0.01927	0.7681	**0.0099**	**101**
	CIOU+RA	99.5%	**0.0129**	**0.0135**	**0.8059**	0.0104	96
Small	CIOU	99.6%	**0.0177**	0.01493	**0.7942**	**0.0086**	**116**
Large	CIOU	99.6%	**0.0144**	**0.0141**	**0.7972**	0.0122	82

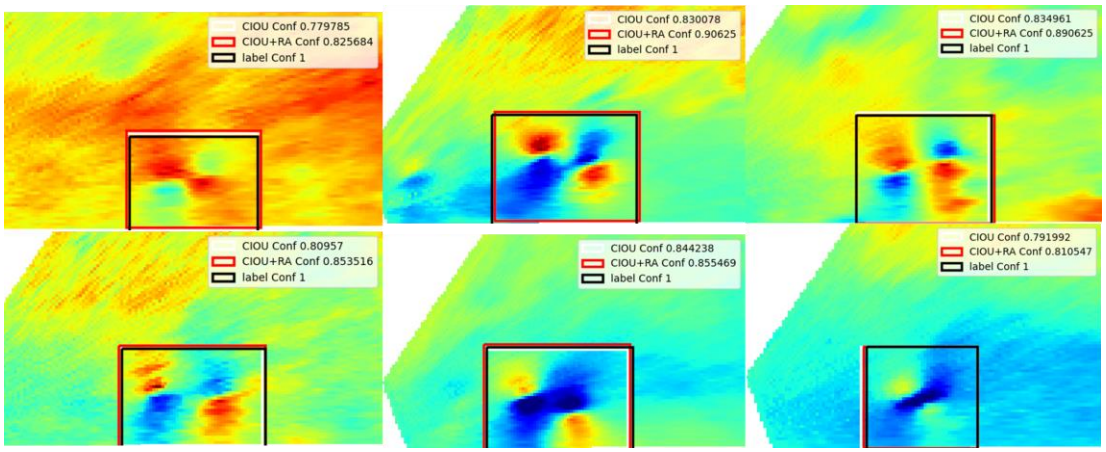

Figure 3-12. Visualisation of the performance of the proposed model compared to ground truth in wake region detection.

The refinement of the box regions in our proposed loss function is illustrated in **Figure 3-13**, where it is evident that the box areas are significantly larger in comparison to the CIOU loss function alone. Conf, as denoted in the label, refers to confidence in

box classification. With the larger box region detected with the updated loss function, the wake classification confidence is correspondingly enhanced. Hence, the inclusion of this supplementary loss term holds significant promise in improving the safety and reliability of wake region detection, which is critical for its application in wake region monitoring and encounter risk assessment.

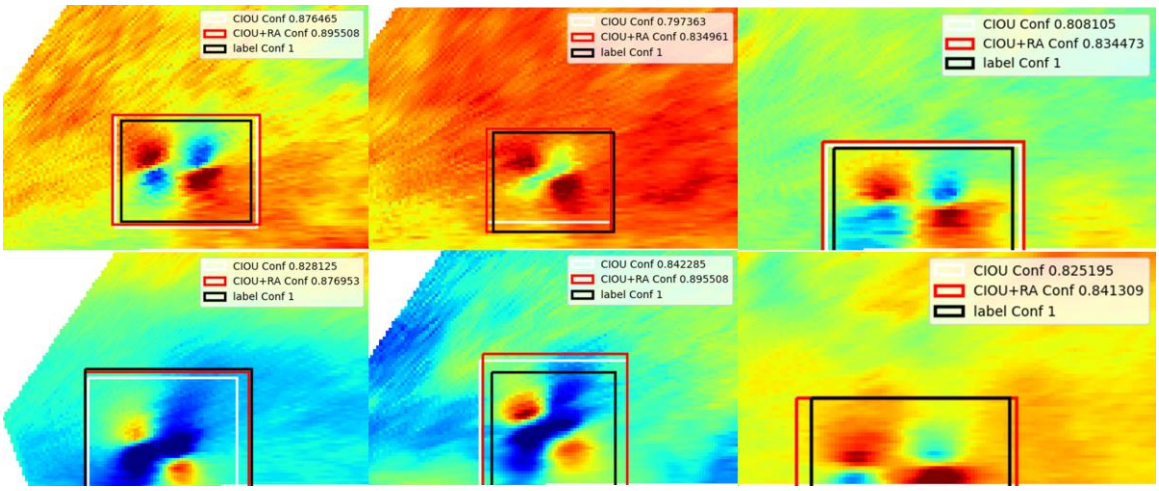

Figure 3-13. Comparison of the performance of the proposed loss function with benchmarks in wake region detection.

Drawing upon the aforementioned wake region detection and model performance verification, this sector explores its applicational potential in inferring the dynamic wake separation across different crosswind scenarios. Wind conditions at HKIA can demonstrate considerable variability (Hon et al., 2022), providing a challenging testing ground for the present study. As depicted in scenario 1, **Figure 3-14**, in a steady atmosphere with nearly no crosswind, the wake vortices will gradually descend with slight lateral diffusion, with the wake regions increasing. Consequently, based on the standard safe approach profiles illustrated in solid grey lines in **Figure 3-14**, the presence time of wake pairs in the approach path is observed to exceed 140 s. The dotted grey line in this figure represents the centreline of the runway. Indeed, according to the

wake separation of the present RECAT-EU standard, this circumstance describes the most severe wake encounter with the most protracted wake duration.

Nonetheless, in the presence of a strong crosswind in scenario 2, **Figure 3-15** suggests an evident lateral movement of wake vortices and a decrease in wake regions, resulting in a shorter duration of less than 60s along the approach path. Consequently, under these favourable wind conditions, the wake separation time may be diminished to the level of minimum radar separation or other constraints imposed on runways.

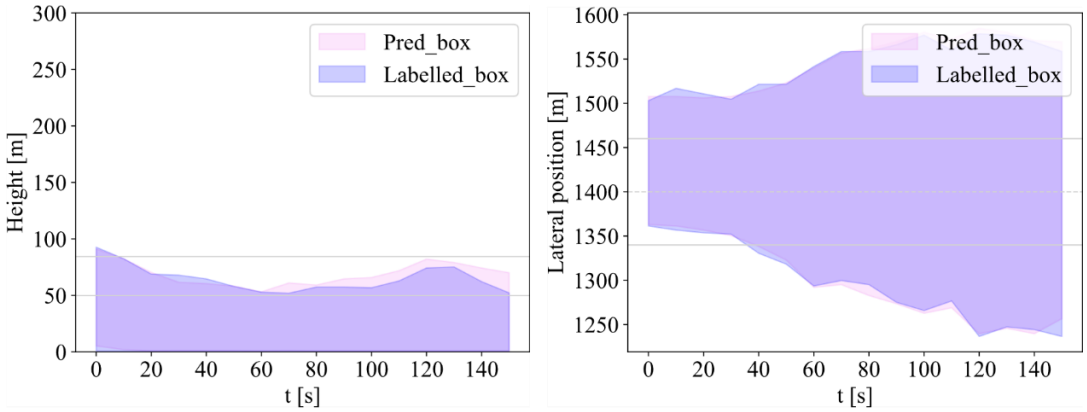

(a) Height of wake region (b) Lateral position of wake region

Figure 3-14. Visualisation of the wake region detection of the A320 aircraft in the approach path to runway 07L under a mean absolute crosswind of 0.11 m/s (Scenario 1, Time: 2019/06/04 15:42:18-15:44:38).

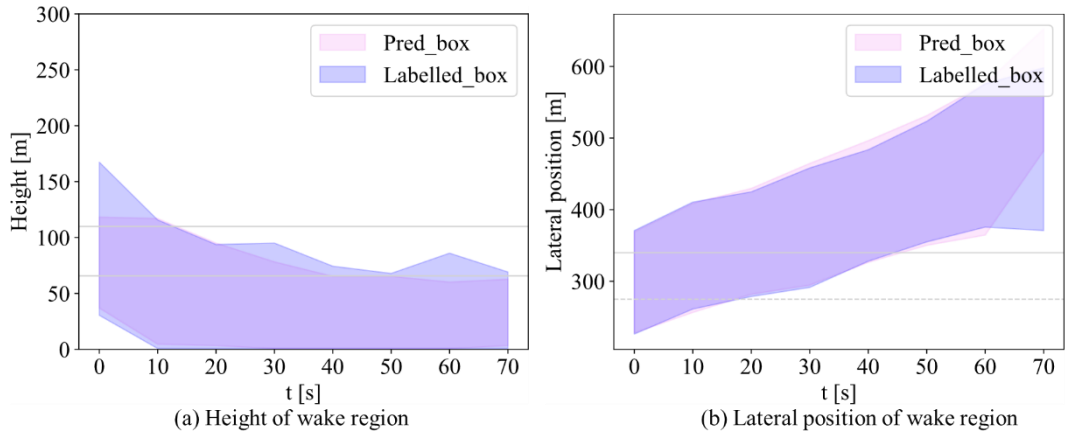

(a) Height of wake region (b) Lateral position of wake region

Figure 3-15. Visualisation of the wake region detection of the A320 aircraft in the final

approach to runway 25R under a mean absolute crosswind of 2.7 m/s (Scenario 2, Time: 2019/06/21 16:20:26-14:21:51).

The lateral transition of wake vortices under crosswind at 5-6 m/s scenario is shown in **Figure 3-16**. This indicates that the strong crosswind may further reduce the wake duration time to less than 30 s, resulting in a more streamlined and slenderer wake region. This verifies the effect of crosswind on wake separation reduction and the feasibility of experimentally determining the temporal wake separation time by the wake region detection. Overall, the labelled wake regions in these three figures are equivalent to or marginally smaller than the predicted regions. This further demonstrates that the YOLO v5 model, utilising our improved loss function, performs exceptionally well in this regard.

In **Figure 3-17**, the depiction of wake vortex movement within the two-dimensional LiDAR-scanning plane is discernible across three representative scenarios. Notably, a persistent trend is observed wherein wake vortices endure for an extended duration along the final approach path, characterised by prominently centralised wake regions throughout all temporal increments of their evolution (**Figure 3-17a**). However, the influence of robust crosswinds induces a rapid lateral displacement of the wake vortices towards either the left (**Figure 3-17c**) or right (**Figure 3-17b**) periphery of the final approach path, concomitant with a concurrent reduction in the spatial extent of the wake region.

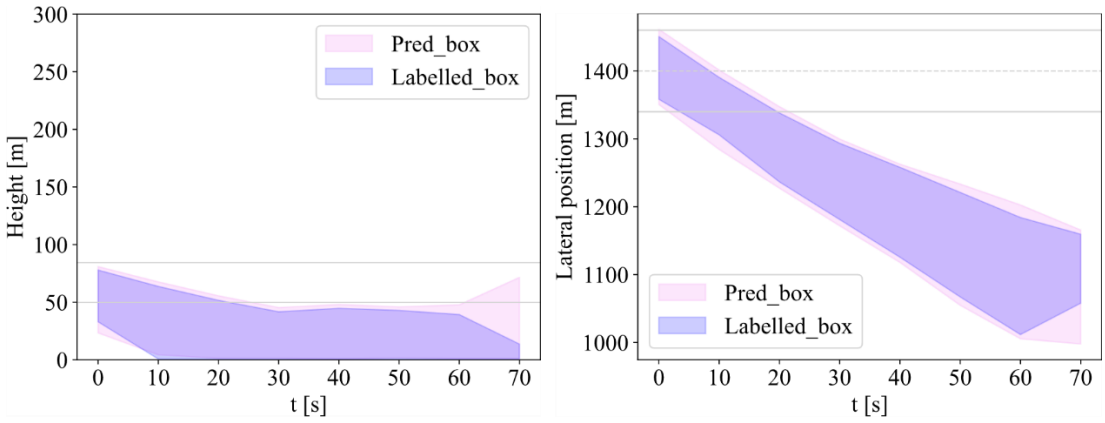

(a) Height of wake region (b) Lateral position of wake region

Figure 3-16. Visualisation of the wake region detection of A320 aircraft in the final approach to runway 07L under a mean absolute crosswind of 5.48m/s (Scenario 3, Time: 2019/08/28 02:23:21-02:24:26).

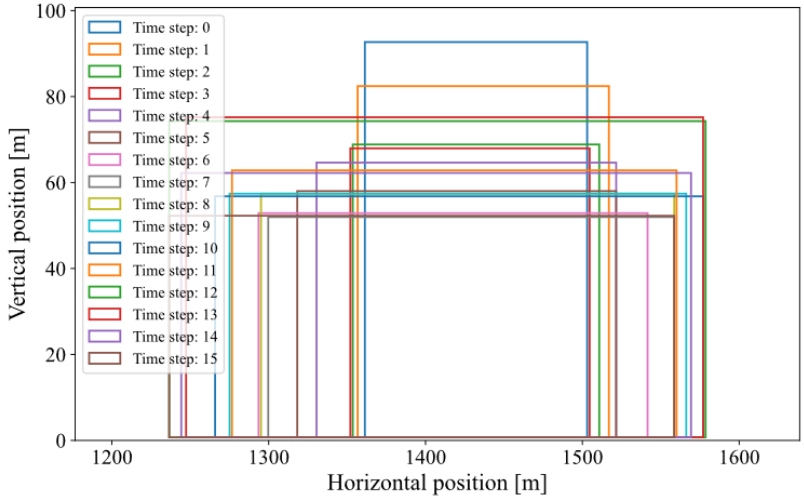

(a) Wake region movement in Scenario 1, Fig. 5.

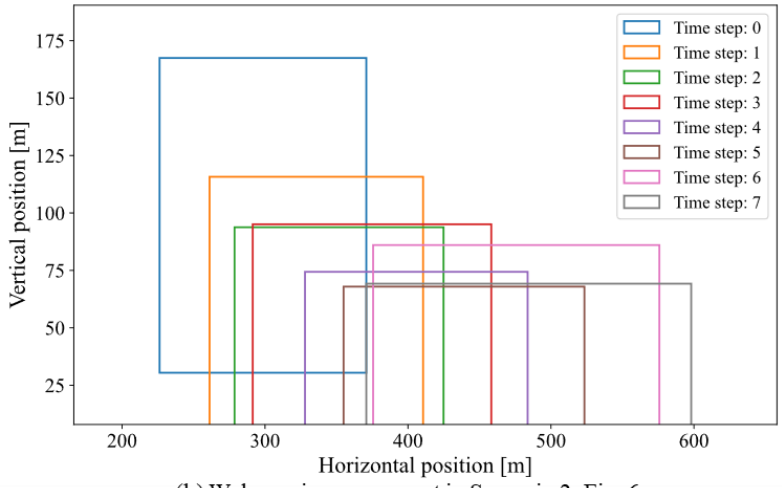

(b) Wake region movement in Scenario 2, Fig. 6.

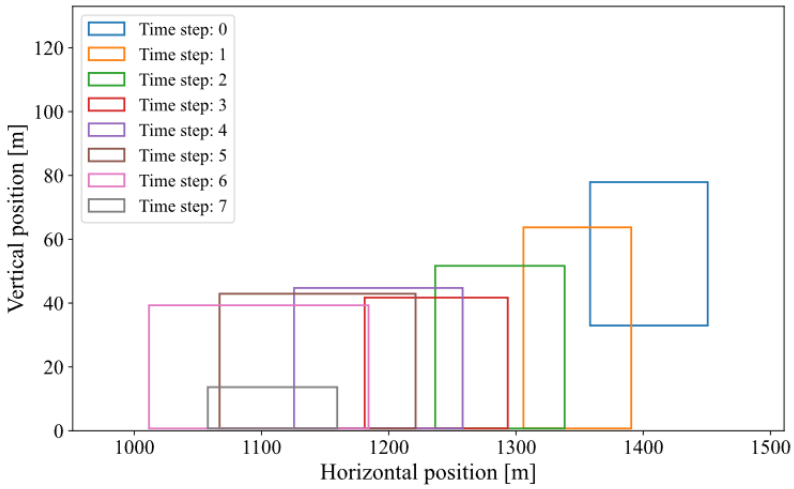

(c) Wake region movement in Scenario 3, Fig. 7.

Figure 3-17. The two-dimensional movement of wake region in the above three scenarios.

3.5.1.3. Model performance in strength estimation of vortex circulation

Table 3-6 demonstrates that the CNN model, when applied to raw images with ROI, achieves significantly higher prediction accuracy in strength estimation compared to other pre-trained CNN models. Notably, the CNN model trained on the entire raw images exhibits the largest errors in the MAE and RMSE, highlighting the efficiency and performance advantages of utilising ROI to refine specific zones for strength estimate. The ROI area for strength estimation is obtained by cropping relevant portions from raw images based on the predicted positions of pairwise wake vortices, as depicted in **Figure 3-18**. For instance, "X40" refers to 40 pixels between the left boundary of the ROI and the predicted lateral position of the left vortex, while "Z60" represents 60 pixels from the upper boundary of the ROI to the predicted height of the highest vortex. The right and lower boundaries of the ROI are defined similarly. Specifically, the influence of ROI size on strength estimation accuracy is presented in **Table 3-7**. The results indicate that an ROI size of "X20, Z40" is sufficient for capturing wake vortex circulation with minimal interference from background wind turbulence. It is worth

noting that the results in (Wartha et al., 2022) are similar to our deterministic CNN models without applying the ROI technique in the strength estimation of the vortices. However, our CNN model with region refinement achieves a significant 41% and 36% reduction in MSE compared to the reference study, revealing the performance enhancement of our model. It is worth mentioning that with more relevant information considered in the CNN model, such as the aircraft weight and flight speed, the atmospheric conditions, the performance of vortex strength estimation may be further improved.

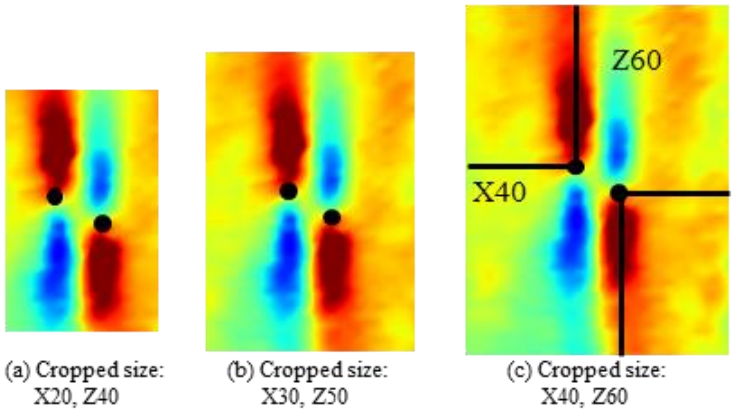

Figure 3-18. Size of the region of interest for vortex strength estimation.

Table 3-6. Performance comparison of CNN models with benchmarking models for vortex circulation intensity estimation.

Model		MAE (m^2/s)		RMSE (m^2/s)	
		G_l	G_r	G_l	G_r
Model with ROI	Deterministic CNN	32.56	34.53	46.43	48.86
	Probabilistic CNN	35.21	37.80	51.92	53.78
	VGG16	39.43	39.82	56.72	56.80
	ResNet18	39.24	42.21	56.19	58.97
	ResNet50	39.04	39.80	54.90	55.29
Deterministic CNN without ROI		50.36	50.77	78.49	78.48
CNN model in (Wartha et al., 2022)		55.31	52.97	77.26	77.21

Note: the comparison with the existing work is primarily about model structure, under our computational hardware and data.

Table 3-7. Performance comparison of ROI sizes for strength estimation.

Cropped size	MAE (m^2/s)		RMSE (m^2/s)	
	G_l	G_r	G_l	G_r
X20, Z40	32.56	34.53	46.43	48.86
X30, Z50	36.35	37.66	50.88	53.81
X40, Z60	35.45	37.53	51.23	53.41

3.5.2. Explanation of model decision with image feature analysis

We employed both Grad-RAM and prediction difference analysis on input images to investigate which part of the entire image contributes most to the final regression. As shown in **Figure 3-19**, for figures with high prediction accuracy, this region is mainly concentrated along the dividing line between the upper and lower velocities of the pairwise vortices, which confirms that the trained model operates as expected. However, for images with slightly larger prediction errors, the prediction results are influenced by a wider range of features. This can be explained from two aspects: first, the shape of the wake turbulence indicates that the entire wake-influenced slender region is highly related to the predicted output. That is also the reason that the vertical profile experiences larger prediction uncertainty than the horizontal profile. Second, it is unavoidable that the background turbulence may influence prediction, leading the model to conclude that some regions of background turbulence are also associated with prediction, and the more dispersed the background turbulence, the greater the effect. Given the background turbulence of LiDAR scanning in 25R exerts a bigger influence on the model estimation, it is possible to explain the instances that it has significantly higher prediction uncertainty, particularly in the vertical profile compared to LiDAR scans in 07L. In addition, the growth of the feature is depicted in the activation maps

of the penultimate and the final convolutional sector of the CNN model, as shown in **Figure 3-20**.

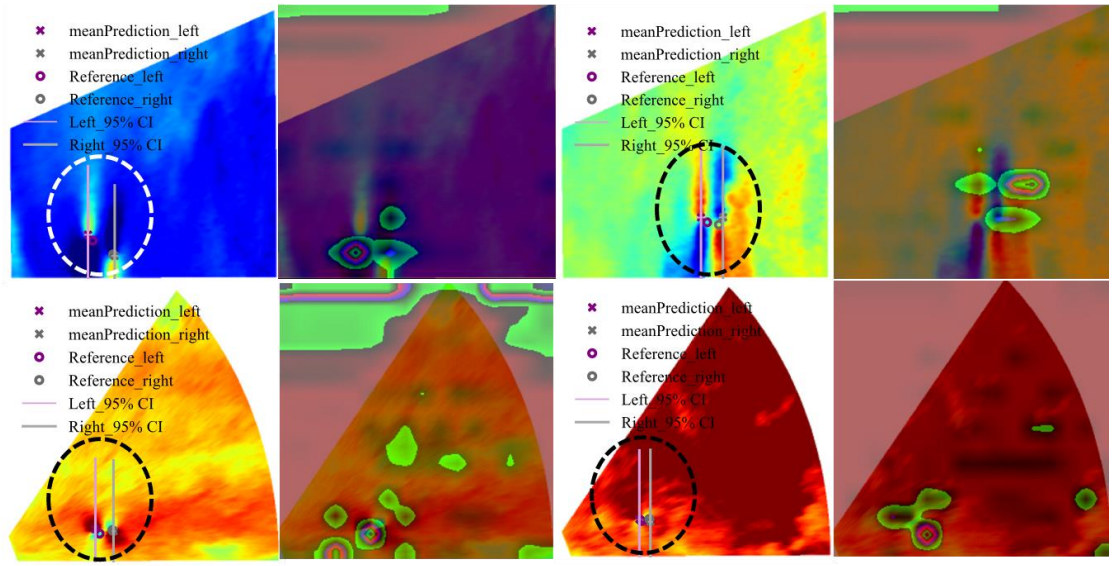

Figure 3-19. Visualisation of the activation maps on the final convolutional layer in the pairwise wake-vortex locating of the test dataset.

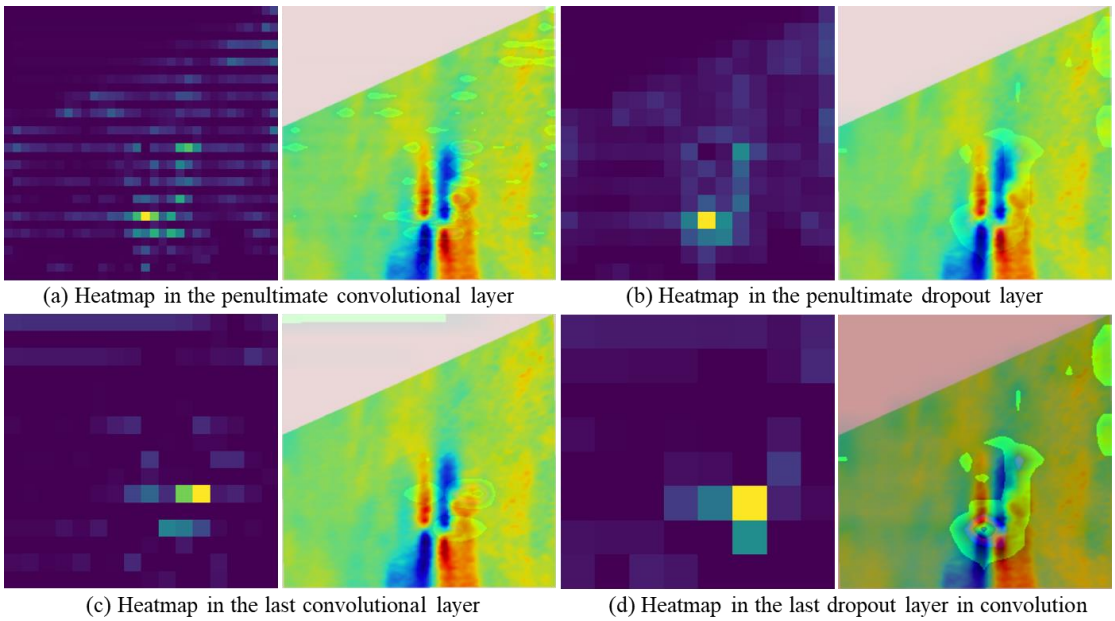

(a) Heatmap in the penultimate convolutional layer

(b) Heatmap in the penultimate dropout layer

(c) Heatmap in the last convolutional layer

(d) Heatmap in the last dropout layer in convolution

Figure 3-20. The activation maps in the penultimate and last convolutional layer of LiDAR image in 2019-05-22 00:22:50.

The comparison of feature importance analysis of Grad-CAM and PDA is shown in **Figure 3-21**. In conditional sampling, the PDA is performed with a sampling window size of 8 and a padding size of 2. The red pixels in the lower figures imply the prediction difference under patch marginalisation, and the darker the colour, the higher the predicted disparity. The relevance between the blank area of LiDAR scans and prediction can be seen in both methods, with both the region of wake turbulence and the significant background wind turbulence captured. As the Grad-RAM approach only preserves the most significant activation, whereas the PDA algorithm generates a saliency map of all prediction differences, it is evident that the relevant region of the input image is significantly larger in the PDA algorithm.

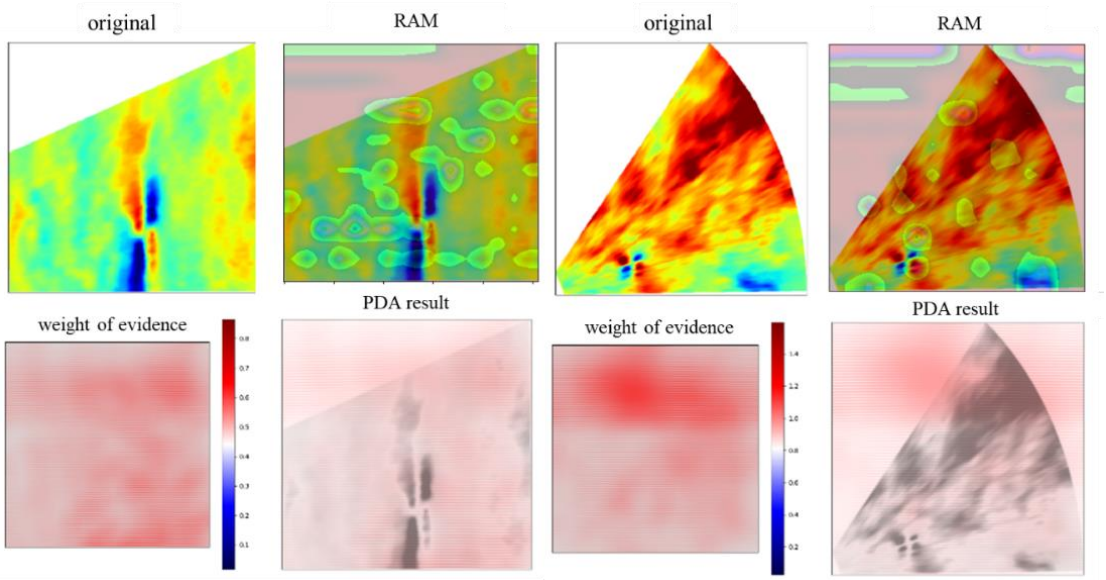

Figure 3-21. Comparison of Grad-RAM with prediction difference analysis of image features.

3.5.3. Exploratory results of vortex duration estimation for achieving temporal wake separation

This section discusses the exploratory results of vortex duration estimation based on the predicted vortex locations from the probabilistic CNN model. Next, the estimated duration is compared to current wake separation standards to analyse the potential of

separation reduction. Finally, the relationship between the deviation in wake duration and the leading factor, crosswind speed, is statistically discussed to demonstrate its managerial implications in runway operations.

Figure 3-22 to **Figure 3-24** illustrate the estimated vortex locations in three scenarios from the probabilistic CNN model. In addition to the mean values of locations, the prediction variance with one standard deviation, which shows a 95 % confidence level, is also captured from this model and represented using the shaded areas in light purple and pink. The boundaries of the wake vortex region for each aircraft weight category, are also estimated based on positions of wake cores and a safety margin, as illustrated in the light grey areas. Based on the final results of wake boundaries and the allowable approach profiles depicted with solid light grey lines, the duration of wake vortices in the approach profiles can be inferred. The dash-dot line in these figures represents the runway centreline.

As shown in **Figure 3-22** when the background wind is weak, the continuous descent of the wake vortices, accompanied by slow lateral diffusion, results in its presence in the approach path for over 100 s after its generation. Both the vertical profile (a) and horizontal profile (b) of the approach path exhibit significant probabilities of wake existence. While for **Figure 3-23** and **Figure 3-24** with crosswind exceeding 2 m/s, the wake vortices can be blown out of the path in the final approach in rapid lateral speed, which leads to considerable time saving in wake durations.

Consequently, the predicted wake durations can be compared to the current separation standard to catch the potential of wake separation reduction under favourable crosswinds. The distance-based RECAT-EU standard, as shown in the Appendix, is transferred to the time-based approach separation (TBS) (EUROCONTROL, 2020; NATS, 2015), considering the average approach speed for aircraft in each wake

category. Next, **Table 3-8** shows the computational process of allowable separation time reduction of the above three wake scenarios, with the leading aircraft in the upper medium category (CAT_D) and various levels of crosswinds. The comparison is based on the assumption of 130 knots average approach speed for the following light aircraft in CAT_F (Kolos-Lakatos, 2017). The positive crosswind values indicate lateral wind moving away from the LiDAR to one side of the runway, while the negative values represent crosswind moving to the other side.

The results in the first row of **Table 3-8** demonstrate that, with almost no crosswind, the wake duration predicted based on our CNN model reaches over 80s, which experiences the worst-case scenario and complies with the regulatory requirement. The second and last rows show that the duration of wake vortices in the approach path can be continuously reduced below 60s as the crosswind strength increases, with larger crosswinds resulting in a smaller wake duration. When the wake duration reduces below the level of other factors that limit runway separation, such as runway occupational time and the minimum radar separation (2.5 NM or 62.9s in this context), consequently, a separation time reduction of around 13s from raw static wake separation time to such as the minimum radar separation can be achieved in this situation. In addition, due to factors, such as the minimum radar separation, a higher degree of wake duration decrease does not further reduce the wake separation time.

Table 3-8. The potential of wake separation reduction in comparison with RECAT separation standard.

Wake scenarios	Leading aircraft (Aircraft category)	Average approach speed of the follower	Average crosswind	Minimum DBS in RECAT	Minimum TBS in RECAT	Wake duration predicted in this study	**Allowable wake separation reduction**
Figure 3-22	A320 (CAT_D)	130 knots	0.11 m/s	3 NM	82.1s	Over 100s/ 3.61 NM	**0s**
Figure 3-23	A320 (CAT_D)	130 knots	2.70 m/s	3 NM	82.15s	40s/ 1.44 NM	**12.95s**
Figure 3-24	B737 (CAT_D)	130 knots	-5.48 m/s	3 NM	82.15s	25s/ 0.9 NM	**12.95s**

Note: DBS refers to the distance-based separation, TBS represents the time-based separation, and NM refers to the nautical mile.

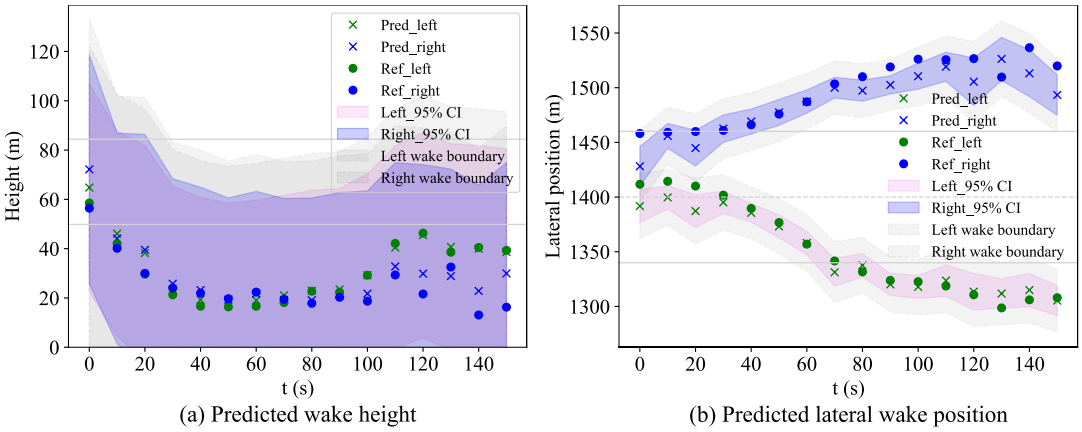

(a) Predicted wake height (b) Predicted lateral wake position

Figure 3-22. Visualisation of the wake existence situation in the approach path (Runway: 07L; Mean crosswind: 0.11m/s; Time:2019/06/04 15:42:18-15:44:38; Leading aircraft: A320).

From the statistical analysis perspective, the magnitude of the crosswind directly correlates with separation reduction, particularly for situations of small aircraft following heavy aircraft. Therefore, the impact of crosswind on aircraft separation time and lateral movement speed of wake vortices can be investigated for further implementation in runway scheduling, as shown in **Figure 3-25** and **Figure 3-26**. In

these two figures, the wake duration in final approach path is calculated based on the results from the probabilistic CNN model for vortex locating. A dataset consisting of 4298 wake vortex sequences from leading flights, encompassing aircrafts in CAT_A to CAT_E categories, were analysed. Among these sequences, the separation time of 2128 flights are expected to be reduced compare to their actual separation time from the following flights.

Figure 3-25 depicts the functional relationship between the separation time predicted by our proposed CNN model and the crosswind speeds in the LiDAR scanning planes. The horizontal lines in each column represent the upper limit, upper quartile (upper line of the colour-filled box), median value (black line inside the box), lower quartile (lower line of the box) and lower limit of the separation time for a certain aircraft weight category. Within the 0-2 crosswind speed class, the separation time range from 20s to 180s with respect to the aircraft category, especially for CAT_A and CAT_B. The median values of separation time decrease rapidly with the increase of crosswind speed, and the upper quartiles for all considered aircraft categories fall below 60s when the crosswind speed exceeds 3 m/s. However, the outliers for CAT_B and CAT_D under crosswinds of 3-4 m/s are still reaching a cut-off at 100s. The median separation time remains under 20s under crosswind over 6 m/s.

Figure 3-26 presents a similar analysis, depicting the dependencies of crosswind on the lateral movement speed of pairwise vortex cores. As the crosswind speed increases, the lateral movement of vortices accelerates. The median lateral speed remains below 2 m/s in the worst-case scenario with a crosswind speed of 0-1 m/s, while the median lateral speed reaches over 4 m/s when crosswinds exceed 4 m/s. In addition, for a certain crosswind level, another evident trend is that the lateral wake

speed will be larger for light aircraft. The rapid increase of the median lateral speed for CAT_C under crosswind of 6-7 m/s is due to the small amount of data.

It is worth to mention that the motion of aircraft wake vortices is a complex dynamic problem influenced by multiple external factors. Due to the limited predictability of vortex strength, the preceding analysis of separation time in this study is predicted based on the presence of wake vortices in the standard approach profiles of the instrument approach procedure, and the assumption of prevalent crosswinds. In addition, although the strength crosswind may reduce wake separation below 60s, the decision of the final dynamic separation time must also consider several other factors, such as the minimum radar separation, as the instanced time with the dotted line in **Figure 3-25**, and situation of wake vortex encounter for the following aircraft. Furthermore, additional data is required to support analysis of wake separation in other wind conditions, such as the prevailing headwind or wind shear, and wake separation in abnormal flight, such as go around and in other approach procedures, such as the visual approach.

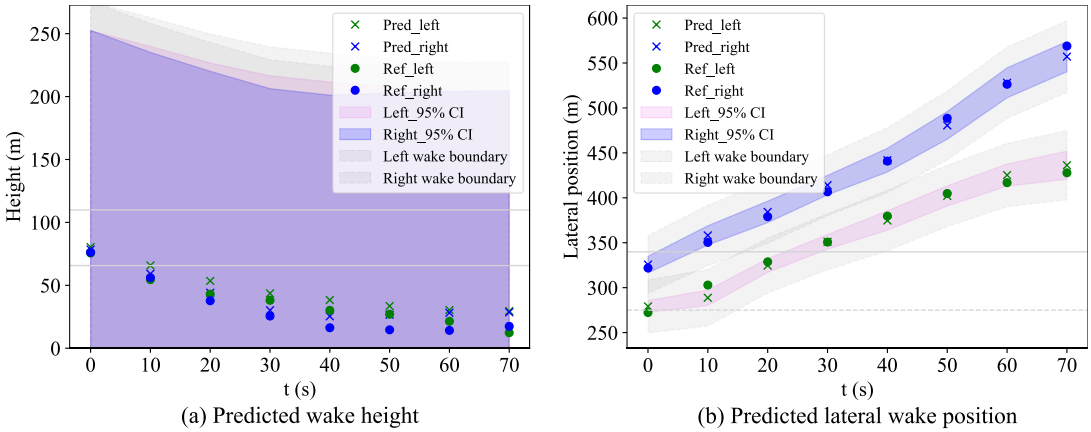

(a) Predicted wake height (b) Predicted lateral wake position

Figure 3-23. Visualisation of the wake existence situation in the path of the final approach (Runway: 25R; Mean crosswind: 2.70 m/s; Time: 2019/06/21 16:20:26-14:21:51; Leading aircraft: A320).

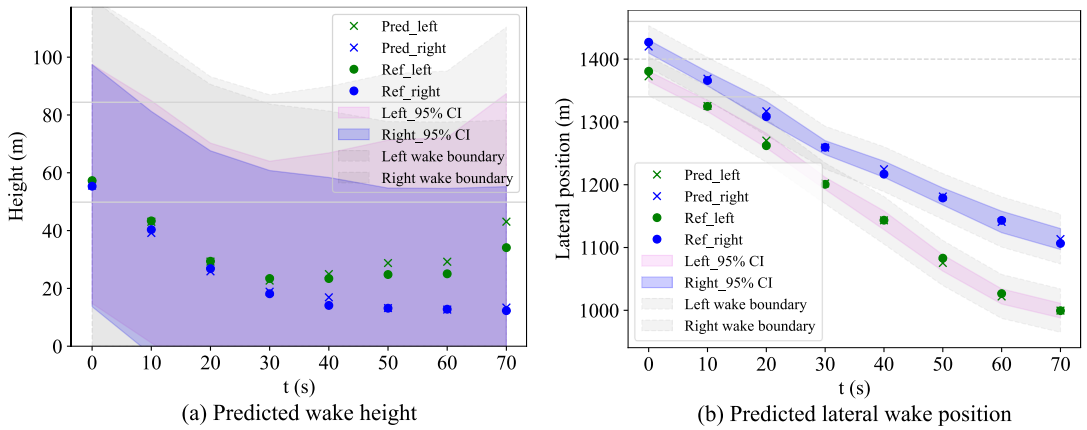

(a) Predicted wake height (b) Predicted lateral wake position

Figure 3-24. Visualisation of the wake existence situation in the path of the final approach (Runway: 07L; Mean crosswind: -5.48m/s; Time: 2019/08/28 02:23:21-02:24:26; Leading aircraft: B737).

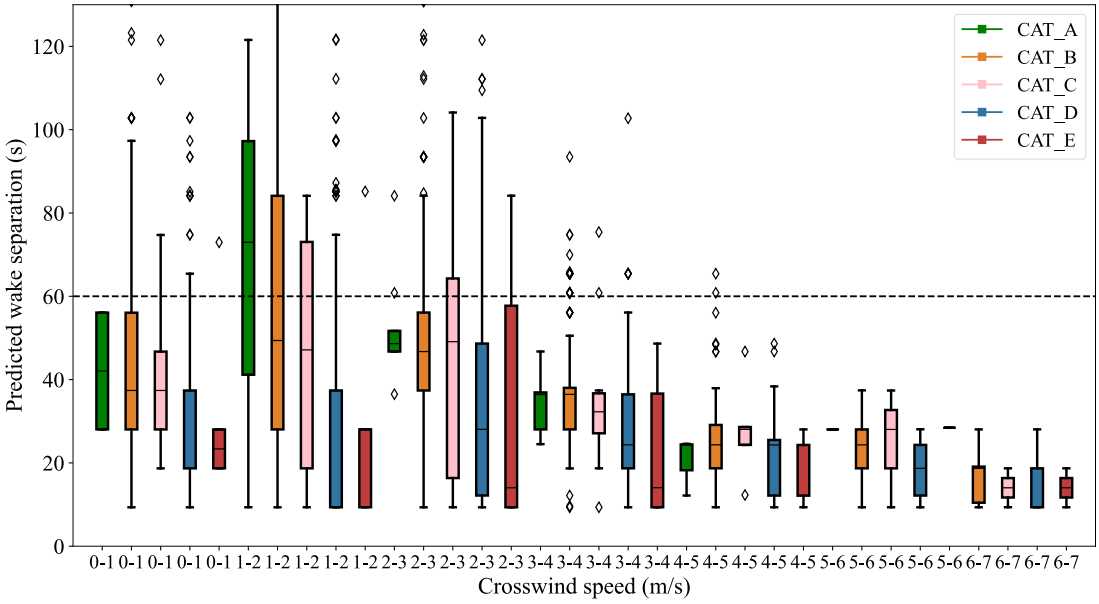

Figure 3-25. The allowable wake separation time predicted by the proposed CNN model under crosswind in certain levels.

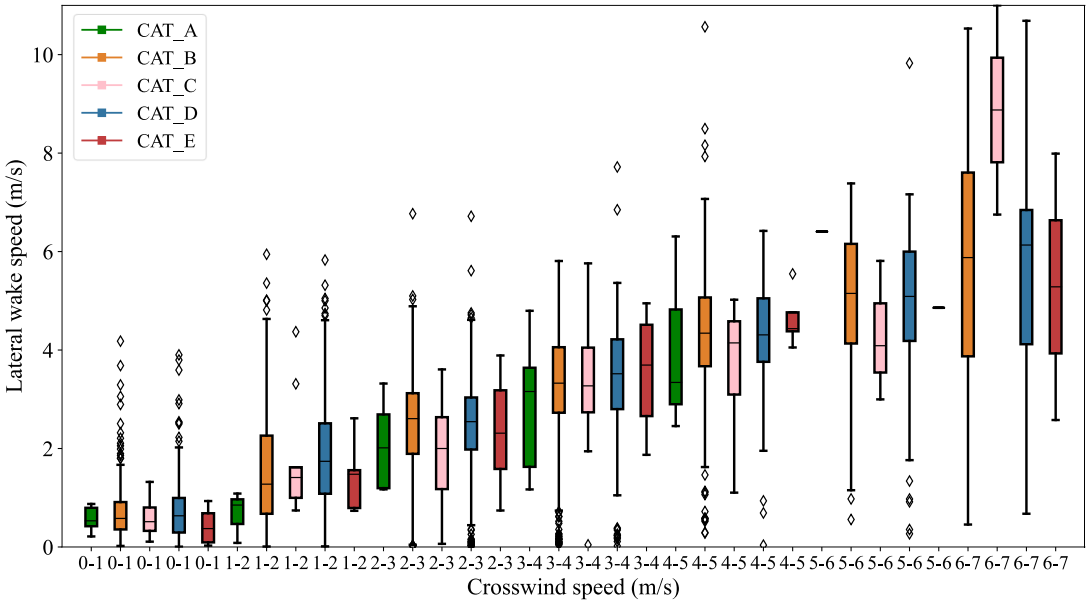

Figure 3-26. Lateral movement speed of the pairwise wake vortex under crosswind in certain levels.

3.6. Concluding remarks

3.6.1. Conclusion

This study establishes a two-stage probabilistic deep learning-based framework for location and strength estimation of aircraft wake vortices, and assesses its duration in the final approach path using LiDAR wake images at the Hong Kong International Airport. The first step is to perform data processing to visualise wake turbulence and map wake data to flight information. Next, the two-stage framework with two probabilistic convolutional neural networks is developed for wake vortex recognition. The first stage is for vortex locating, while the other involves estimation of the vortex strength using the refined region captured from the raw entire image based on vortex locating. In the third step, the situation of vortex existence in the vertical and horizontal profile of the flight path in the final approach is analysed based on the estimation of probabilistic vortex positions and measured with the safety metric of occupational time,

and the prediction uncertainty of the convolutional neural networks is analysed using model explanation techniques.

Several noteworthy contributions are made by the proposed methodology to aircraft wake vortex detection and quantifying aircraft separation. The novel data-driven deep learning models obtain improved prediction accuracy and computational speed compared to prior research based on high-dimensional feature analysis from wake images. In addition, the probabilistic prediction model provides an efficient and reliable method for visualising and analysing the duration of wake existence in the final approach path, considering meteorological conditions and aircraft types, which demonstrates the great potential of dynamical separation reduction in comparison to the updated standard of RECAT-EU. Finally, the model explanation with probabilistic estimation improves the trustworthiness and transparency of the convolutional neural networks. The methodology and results in this section can facilitate the development of the near real-time monitoring system of aircraft wake turbulence, and the advice system for dynamic aircraft separation in the final approach phase.

3.6.2. Managerial implications

Safety is one top priority in air traffic operations. The identification of aircraft wake vortices and assessment of their duration in the final approach path builds the foundation of quantifying the minimum aircraft separation to achieve both traffic optimisation resilience and flight safety. The managerial implications of this research are mainly in four aspects:

(1) The two-stage fast-time wake vortex recognition framework via deep learning achieves both high estimation precision and computational speed. It can facilitate the onboard and near real-time wake vortex monitoring. Furthermore,

the methods of probabilistic estimation and decision interpretation of the proposed deep learning models can improve their reliability and transparency in decision-making, facilitating their implementation in safety-critical wake vortex monitoring and prediction systems to reduce the workload of air traffic controllers in traffic guidance.

(2) This study demonstrates great potential and technical feasibility for reducing approach separation under certain wind conditions, aligned with the latest RECAT-EU standard. The statistical analysis of temporal wake separation in relation to crosswinds, presented in this study, allows for the establishment of time-based wake separation references applicable to future crosswind conditions within the next half to one hour. These references can effectively serve as constraints when addressing runway sequencing and scheduling challenges. This is crucial for large and busy airports with heavy traffic volume that cannot increase capacity by building new runways, to boost airport capacity and throughputs from the airport operator side.

(3) By accurately tracking the movement of wake vortices and implementing separation reduction between aircraft in real-time, airlines can minimise delays caused by spacing requirements and reduce fuel consumption, which leads to cost savings and improvement of their on-time performance, and support more efficient flight scheduling in both the short and long period of time.

Chapter 4. Data-driven aircraft wake vortex evolution prediction and safety assessment of separation minima reduction

Following the vortex recognition and feature analysis in Chapter 3, which is the fundamental step, research regarding predicting the decay and evolution process of wake vortices will be presented in Chapter 4. Although the dynamics of aircraft wake vortex have been studied over two decades, the research technique mainly focuses on numerical simulation with CFD and physical modelling. With the development of LiDAR detecting and computer techniques, machine learning models show great applicational potential. This chapter aims to research the potential of applying deep learning models to realise fast-time and real-time wake vortex decay prediction. This chapter develops the encoder and decoder recurrent neural network for predicting future wake vortex position and strength based on massive historical vortex data from the LiDAR processing algorithm. The online and near-real-time prediction methodology is also proposed by integrating the wake recognition model developed in Chapter 3. The results show that the proposed models achieve significantly high performance in both short-term and long-term wake decay prediction. Furthermore, the integration of wake recognition and decay prediction is applicable from both computational speed and forecasting accuracy aspects. This study indicates a considerable applicational value for building the online wake vortex monitoring and separation advisor system and builds the conditions for intelligent runway scheduling to improve traffic flow efficiency and runway throughputs.

4.1. Introduction

4.1.1. Research context

The aircraft re-categorisation concept proposed by the European Union Aviation Safety Agency (EASA) (EUROCONTROL, 2018a) and the Federal Aviation Administration (FAA, 2016) refines aircraft maximum take-off weight from four groups defined by International Civil Aviation Organisation (ICAO) to six categories to further reduce separation for certain aircraft pairs. Holzäpfel et al. (2021) verified that the aircraft separation under RECAT standard can be further reduced to minimum radar separation for a certain number of landings under favourable wind conditions, from the physical wake prediction perspective using one-year aircraft pairwise approaching separations in the Vienna International Airport.

From the perspective of wake generation and evolution, the weight of an aircraft has a strong relationship with the initial intensity of vortex circulation, and meteorology, particularly wind, plays a significant role in vortex movement in the air. Therefore, research on dynamic time-based wake separation in relation to pairwise aircraft and meteorology has extensive applicational value to unlock the potential of runway efficiency improvements, which is the current research focus worldwide in the air traffic management area.

Novel emerging machine learning models that are data-driven are suitable for wake vortex recognition and prediction. Deep learning techniques, such as convolutional neural networks, are adept at analysing features of LiDAR data in image format. A identification method for the existence of wake vortices using a Support Vector Machine is proposed (Pan et al., 2020), with LiDAR radial wind data, and meteorological parameters (temperature and air pressure). Shen et al. (2023) employed the object detection algorithms (R-CNN and YOLOv5 networks) for vortex

identification. Their proposed model can identify both a single vortex pair and the case of two vortex pairs superposed. These researches aim for qualitative vortex identification, rather than quantitative recognition of vortex locations and intensity. Although Wartha et al. (2022) utilised convolutional neural networks for vortex locating and strength estimation at the Vienna International Airport, each of their networks is only capable of estimating one positional or intensity-related parameter of a vortex pair. This could disregard the coupling relationship between pairwise vortices. Furthermore, few studies utilise novel data-driven models to predict the transport and decay process of aircraft wake vortices. The application of time series prediction models in flight trajectory prediction for air traffic operations, such as the individual LSTM, GNN, and the hybrid deep learning models (ConvLSTM) results in a considerable performance boost. In fact, the recurrent neural networks and models that can handle the temporal dependencies of data in time series are also appropriate for predicting the wake vortex evolution process and deserve to be developed.

4.1.2. Research gaps and contributions

From the foregoing, it is evident that the data-driven wake vortex prediction has great benefits in time saving and consideration of both qualitative and quantitative factors affecting the evolution of wake vortex. However, existing research focuses primarily on qualitative tasks, such as wake vortex existence recognition and classification of vortex strength level. Few studies have considered machine learning-based regression of positional and strength features of wake vortices, which is essential for proactive runway scheduling.

Implementing more efficient departure and arrival operations can boost runway throughput at airports with limited capacity. Consequently, based on the quantitative

aircraft wake recognition studies in Chapter 3, this research aims to develop an online and real-time wake vortex prediction and safety monitoring framework via deep learning and operational LiDAR techniques. The proposed methodology will facilitate the development of time-based separation indicators for the final approach, improve the runway throughput capacity as a result of reduced, optimised separations while maintaining safety under runway scheduling, and further result in fewer separation violations and missed approaches, and reduce the ATCOs' workload despite the fact that more aircraft per hour they will manage. The contributions of this study are threefold:

1. In terms of the overall methodology, we develop a model fusion strategy to enable online spatiotemporal vortex feature recognition and future evolution projection. The hybrid deep learning framework includes two parts: a two-stage Deep Convolutional Neural Network (DCNN) framework that is adept at capturing spatial features of vortex locations and strength; and Attention-based Temporal Convolutional Network (ATCN) models that are ideal for forecasting the long-term temporal dependencies in vortex transport and decay.
2. For model performance validation, the efficiency of the proposed ATCN models and hybrid DCNN-ATCN strategy is assessed using real flight data and wake data at the Hong Kong International Airport, encompassing several scenarios of background turbulence. This model fusion reveals superior performance compared to benchmarking methods.
3. In vortex duration assessment, both aleatoric uncertainty and epistemic uncertainty of the proposed model for predicting vortex location are characterised by Gaussian distribution. The dynamic separation minima regarding crosswinds are determined by the presence of vortices in the

approach profiles and verified from several aspects. Our preliminary results of dynamic separation minima show compliance with the current RECAT-EU standard, and also indicate the effect of strong crosswinds on separation reduction.

4.2. Preliminaries

4.2.1. Aleatoric and epistemic uncertainty estimation

When constructing a prediction model from input x to output y using a training set of finite size, both aleatoric uncertainty and epistemic uncertainty must be considered. Aleatoric uncertainty, which is related to the inherent noise or randomness in the data, is determined by the quality of the dataset and the nature of the prediction task. This uncertainty cannot be reduced as the size of the training dataset increases. Epistemic uncertainty resulting from model training process and knowledge. This uncertainty arises as a result of limited training data, model architecture or insufficient knowledge about the underlying data distribution, and it can be reduced by adding more data or enhancing models.

The Bayesian neural network is capable of handling both aleatoric uncertainty and epistemic uncertainty. The aleatoric uncertainty in the data can be incorporated by permitting the model to output probability distributions instead of deterministic point predictions. BNNs address epistemic uncertainty by utilising Bayesian inference techniques. Methods such as variant inference and Monte Carlo Dropout are used to approximate a posterior distribution over weights of the network that is consistent with the training data and prior knowledge.

Consider a standard neural network with weight and bias parameters denoted as Θ. Given the training data $D = \{(x_1, y_1), (x_2, y_2), \dots, (x_n, y_n)\}$, where x_i represents

input sample, y_i is corresponding target output, and $f(x_i, \Theta)$ represents the network.

To model the aleatoric uncertainty, a likelihood function that captures the noise or variability in the data is introduced. Assuming Gaussian noise in the data, the likelihood function is given as:

$$p(y|x, \Theta) = N(y|f(x, \Theta), \sigma^2) \tag{4-1}$$

where $N(y|f(x, \Theta), \sigma^2)$ represents the Gaussian distribution with mean model output $f(x, \Theta)$ and variance σ^2.

For epistemic uncertainty, a prior distribution over the parameters Θ is specified first to represent initial beliefs before updating them based on the observed data. Generally, a simple prior, such as a Gaussian distribution is used:

$$p(\Theta) = N(\Theta|\mu_0, \epsilon_0) \tag{4-2}$$

Based on the Bayesian inference theorem, the posterior distribution of the parameters Θ given the observed data D can be calculated as

$$p(\Theta|D) = \frac{p(D|\Theta) * P(\Theta)}{p(D)} \tag{4-3}$$

where $p(D|\Theta)$ is the likelihood function, $P(\Theta)$ is the prior, and $p(D)$ is the marginal likelihood and is calculated by integrating the product of the likelihood and the prior over all possible values of Θ. $p(D) = \int P(d|\Theta) * p(\Theta) d\Theta$.

As the above posterior distribution is too complex to solve, approximate methods such as variational inference and Monte Carlo methods are utilised to sample from the posterior distribution. The central concept of variational inference is to utilise a variational distribution $q(\Theta)$ for approximating the true $p(\Theta|X, Y)$ by minimising the Kullback-Leibler (KL) Divergence between them. Monte Carlo Dropout is one

popular technique used in Bayesian neural networks that has been proven with a similar effect in minimizing KL divergence to approximate the posterior distribution (Gal et al., 2016). After the inference, outputs can be made by averaging the predictions from multiple dropout samples. The probabilistic distribution of the model on new data x^* can therefore be generated by integrating over θ and estimated with MC samples, in which *K* is the number of MC samples:

$$p(y^*|x^*, X, Y) = \int p(y^*|x^*, \Theta)p(\Theta|X, Y)d\Theta \approx \frac{1}{K}\sum_{n=1}^{K} p(y^*|x^*, \widetilde{\Theta}_k) \quad (4\text{-}4)$$

Based on the above analysis, the total predictive uncertainty $V(y|x)$ can be computed by integrating these two kinds of uncertainties:

$$\mathrm{V(y|x)} = V(E[y|x, \Theta]) + E[V(y|x, \Theta)] \quad (4\text{-}5)$$

where $E[y|x, \Theta]$ denotes the $f(x, \Theta)$. $V(E[y|x, \Theta])$ is the variance of the predicted means of the Bayesian model and represents the epistemic uncertainty. The average of the model's predicted variance $E[V(y|x, \Theta)]$ under input and model parameters, is the aleatoric uncertainty, and can be denoted as $E[s^2(x, \Theta)]$.

Therefore, this ensemble approach utilises probabilistic modelling of both the aleatoric and epistemic uncertainty to provide comprehensive uncertainty estimates of the predictions.

4.2.2. Recurrent neural networks

RNN is a type of neural network that introduces feedback loops to process sequential data. The key idea is to share weights across time steps, which enables the network to maintain hidden state information and capture temporal dependencies in the data. The

forward pass in an RNN for each timestep t can be represented as $h_t = f(W * x_t + U * h_{t-1} + b)$, where x_t is the input at this timestep, h_t is the hidden state for this timestep and becomes the hidden state for the next timestep, h_{t-1} is the hidden output from the previous timestep, W, U, b are model parameters.

To address the vanishing gradient problem and capture long-term dependencies more effectively, LSTM (Hochreiter et al., 1997) and GRU (Chung et al., 2014) networks are specialised. The memory cells and gating mechanisms in the forget gate can control the flow of information through the cell, enabling LSTM to store and retrieve information over long periods, thereby making it effective in capturing long-term dependencies in sequences. The LSTM cell at timestep t can be denoted as

$$i_t = \sigma(W_i[h_{t-1}, x_t]) + b_i \quad (4\text{-}6)$$

$$f_t = \sigma(W_f[h_{t-1}, x_t]) + b_f \quad (4\text{-}7)$$

$$o_t = \sigma(W_o[h_{t-1}, x_t]) + b_o \quad (4\text{-}8)$$

$$g_t = tanh(W_g[h_{t-1}, x_t]) + b_g \quad (4\text{-}9)$$

$$c_t = f_t c_{t-1} + i_t g_t \quad (4\text{-}10)$$

$$h_t = o_t tanh(c_t) \quad (4\text{-}11)$$

Where x_t is the input at timestep t, h_t is the output at timestep t, c_t is the cell state at timestamp t, i_t, f_t and o_t are the input, forget and output gate activations, respectively. g_t is the candidate cell state, the information to be added to the cell state, W_i, W_f and W_o denote the learnable weight metrics, b_i, b_f and b_o denote the learnable bias vectors, and σ and tanh are the sigmoid and hyperbolic tangent functions.

GRU also has gating units for control of the information flow but without separate memory cells, making it computationally more efficient and easier to train. Update and

reset gate components determine how much of the previous hidden state will be retained and used for computing the candidate hidden state, respectively. The activation of a GRU cell at timestamp t can be denoted as

$$h_t = (1 - z_t)h_{t-1} + z_t\tilde{h}_t \quad (4\text{-}12)$$

$$\tilde{h}_t = tanh(W_h[r_t h_{t-1}, x_t]) + b_h \quad (4\text{-}13)$$

$$r_t = \sigma(W_r[h_{t-1}, x_t]) + b_r \quad (4\text{-}14)$$

$$z_t = \sigma(W_z[h_{t-1}, x_t]) + b_z \quad (4\text{-}15)$$

where z_t is the update gate that controls how much of the past hidden state h_{t-1} to keep. $\tilde{h}_t$ is the candidate hidden state and computed based on the input and reset gate r_t. x_t is the input at timestep t.

4.3. Research methodology

4.3.1. Overview of the methodology

This research aims to develop an integrated deep-learning strategy that can be used to recognise wake vortices in real-time, anticipate vortex decay and estimate separation minima. This will be achieved by utilising historical wake vortex data derived from the LiDAR technique at HKIA. The wake vortex recognition process involves quantifying vortex position and determining vortex strength based on LiDAR vortex images. The prediction of wake vortex evolution and decay provides insights into the future position and strength of vortices by utilising initial vortex data.

Figure 4-1 depicts the methodological flowchart of this study with four primary stages. Firstly, the wake sequences are segmented with relevant flight information (flight speed, heading, aircraft type) from ADS-B mapped and the ambient wind conditions considered. In the offline model training phase, the DCNN model for vortex recognition from LiDAR scans and Bayesian models (attention-based TCNs and RNNs)

for predicting vortex evolution are built and trained. Subsequently, the trained DCNN and ATCN models are integrated and applied in real-time scenarios, in which the recognised vortex positions and strength in the initial three timesteps from DCNN are fed into the Bayesian attention-based TCN and RNN models for predicting vortex decay. The ultimate phase evaluates the dynamic minimum in aircraft separation concerning wind conditions in the final approach based on vortex duration analysis. In addition, feature importance analysis is employed to elucidate the model decision process, thereby bolstering the credibility of the deep learning model. The subsequent subsections will explain the model architectures and strategies pertaining to each component.

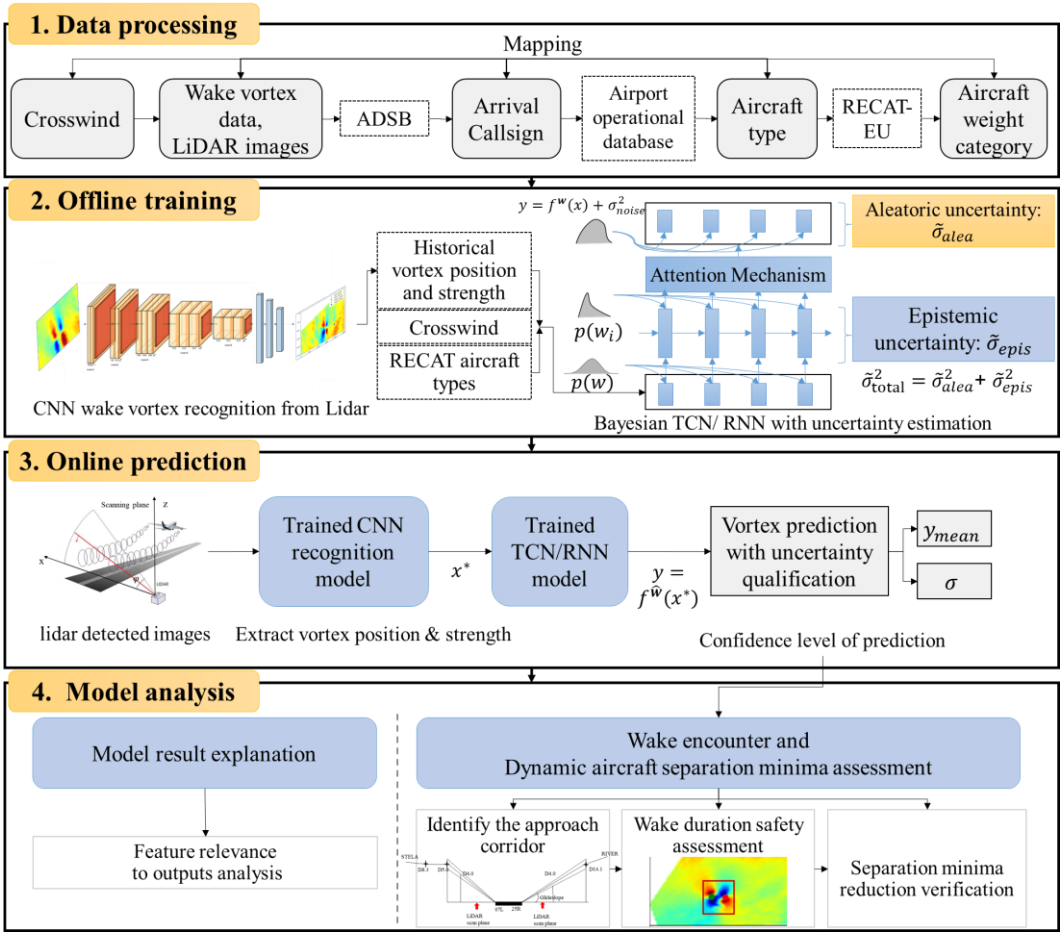

Figure 4-1. Flowchart of the methodology for dynamic aircraft wake vortex recognition and evolution prediction.

4.3.2. Data processing

The data derived from LiDAR for each scan contains two parts: the radial wind velocities, and values derived from the LiDAR processing algorithm (two-dimensional vortex locations relative to runway centrelines and height of LiDAR, and vortex intensity). The radial wind data are converted into heatmaps to visualise the whole vortex scope, where warm and cold colours indicate the positive and negative velocities relative to LiDAR, respectively. The relative positional deviations were converted into absolute values that are relative to LiDARs. Furthermore, the sequential vortex data with discontinuous scanning in time series and null values in each time step are removed, and these successive vortex scan data were segmented according to the characteristics of the initial and final wake vortices. In a stable ambient atmosphere, the wake vortices generated by heavy aircraft can persist for a dozen scans of LiDAR, lasting for several minutes. In the wake vortex series with more than 12 timesteps, a large proportion is caused by the superposition of two wake vortices caused by the error in the automatic segmentation of wake vortices. Therefore, to ensure the accuracy of wake vortex forecasting, vortex sequences with a duration time of less than 4 timesteps and over 12 timesteps are removed.

In addition to the wake vortex data, crosswind speed from the background turbulence is also considered as the main ambient feature. The crosswind values are averages on each LiDAR scan plane, with the same time interval as the LiDAR scan. Furthermore, the flight information (approaching speed and aircraft type) of the final approach from the ADS-B is also cleaned and mapped with each wake sector according to timestamps and three-dimensional positions when the flight approaches the LiDAR scan plane. To coordinate with the latest aircraft weight classification standard, the aircraft types

extracted for each wake sequence are mapped to the weight categories in RECAT-EU.

To summarise, for the historical vortex data of a flight denoted as $X = \{x_1, x_2, \ldots, x_n\}$, x_i represents features in timestep i, the input features for training the DCNN model and the time-series prediction model, as well as their respective outputs, are listed in **Table 4-1**. To improve prediction accuracy and utility, the length of the historical feature window is defined as three timesteps ($t_0 - t_2$) for predicting targets in future timesteps. For LiDARs in Site 1 and Site 2, the time intervals in each timestep are approximately 12s and 9s, respectively.

4.3.3. Model construction and evaluation

4.3.3.1. Attention-based TCN models

After the relevant aircraft wake vortex features and atmosphere features are derived, we proposed the novel one-dimensional dilated convolutional operations with an attention mechanism for efficient and high-performance sequential vortex feature prediction. The overall methodological framework of the proposed models is illustrated in **Figure 4-2**. Remarkably, two remarkable attention-based TCN models are proposed, which consist of three main modules: dilated convolutional residual block and multi-head attention module or Convolutional Block Attention Module (CBAM). To distinguish between the simple TCN model and the attention-based TCN models, the TCN model with multi-head attention mechanism is named multi-head attention-TCN (ATCN in following experiments), and the model with CBAM module is called the CBAM-TCN.

Table 4-1. Inputs and outputs of the DCNN model for vortex recognition and TCN models for vortex sequential prediction.

Model	Input/output	Feature variables	Description	Unit
CNN model	Inputs	Wake images	Images of LiDAR scans in the first three timesteps	-
	Outputs	$\widehat{X_l}^{(t_0-t_2)}$, $\widehat{X_r}^{(t_0-t_2)}$	Predicted lateral positions of vortex cores in the first three timesteps	m
		$\widehat{Z_l}^{(t_0-t_2)}$, $\widehat{Z_r}^{(t_0-t_2)}$	Predicted vertical positions of vortex cores in the first three timesteps	m
		$\widehat{G_l}^{(t_0-t_2)}$, $\widehat{G_r}^{(t_0-t_2)}$	Predicted strength in the first three timesteps	m^2/s
TCN models	Inputs	${X_l}^{(t_0-t_2)}$, ${X_r}^{(t_0-t_2)}$	Reference lateral positions in the first three timesteps	m
		${Z_l}^{(t_0-t_2)}$, ${Z_r}^{(t_0-t_2)}$	Reference vertical positions in the first three timesteps	m
		${G_l}^{(t_0-t_2)}$, ${G_r}^{(t_0-t_2)}$	Reference strength in the first three timesteps	m^2/s
		${v_{lat}}^{(t_0-t_2)}$	Average crosswind in the first three timesteps	m/s
		RECAT	The recategorised aircraft weight category in consistent with RECAT-EU	-
	Outputs	$\widehat{X_l}^{(t_3-)}$, $\widehat{X_r}^{(t_3-)}$	Predicted lateral positions in future timesteps	m
		$\widehat{Z_l}^{(t_3-)}$, $\widehat{Z_r}^{(t_3-)}$	Predicted vertical positions in future timesteps	m
		$\widehat{G_l}^{(t_3-)}$, $\widehat{G_r}^{(t_3-)}$	Predicted strength in future timesteps	m^2/s

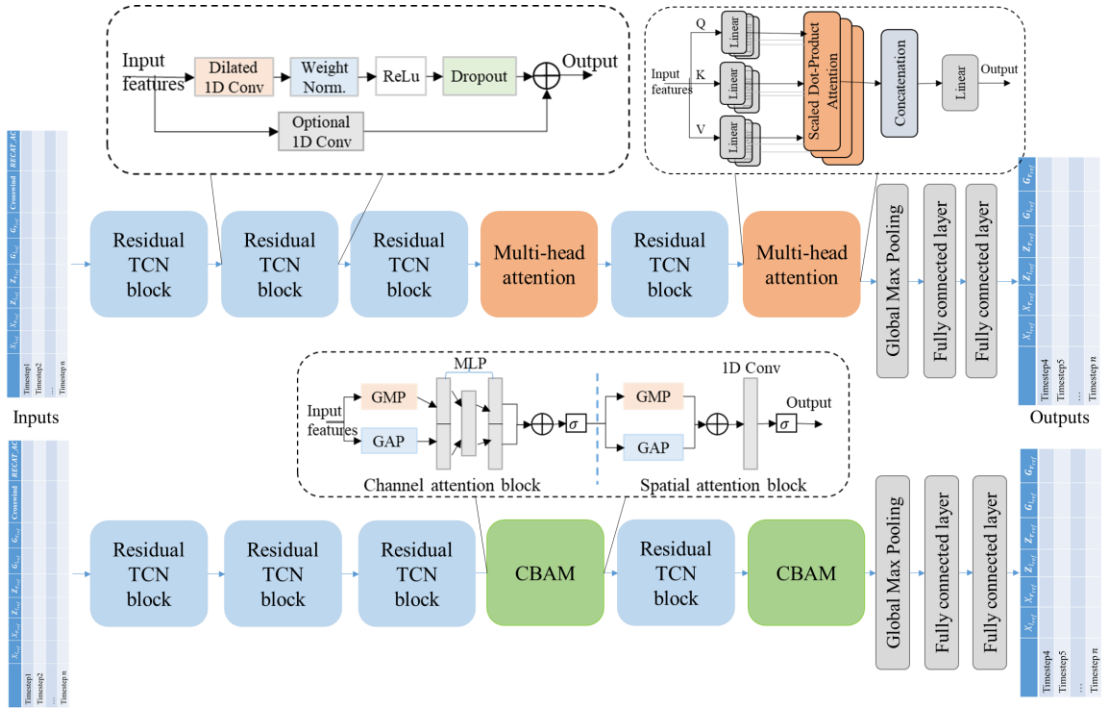

Figure 4-2. Overall methodological framework of proposed attention-based TCN models for vortex decay projection.

(1) Residual temporal neural network

The Temporal Convolutional Network (TCN) was first proposed by (Lea et al., 2016) for video-based action segmentation. It utilises one-dimensional causal convolutions with dilations to capture long-range temporal dependencies and patterns in the input sequences without recurrent connections. The parallelism convolutions achieve great computational efficiency compared to traditional recurrent neural networks. The dilated convolutions allow the receptive field of the network to grow exponentially with the number of layers and manipulate how many positions the convolutional kernel skips, as shown in **Figure 4-3**. By stacking multiple dilated convolutions with appropriate dilation rates and utilising non-linear activation functions, TCN can capture complex temporal patterns and long-term dependencies in the input sequence efficiently.

The dilation rate determines the rate of dilation. For a one-dimensional sequence data X with a timespan of l, $X = \{x_1, \dots, x_t, \dots, x_l\}, x_i \in R^n$ and a filter $f: \{0, \dots, k-1\}$,

$k \in R$, the dilated convolution F on sequence element x_t can be denoted as

$$F(x_t) = (X_{*d}\, f)(t) = \sum_{i=0}^{k-1} f(i) \cdot X_{t-d \cdot i} \tag{4-16}$$

Where d denotes the dilation factor, k represents the kernel size, and $s - d \cdot i$ is the direction of the past. Therefore, dilation is a means of adding a fixed step between each pair of adjacent filter inputs. A dilated convolution becomes a regular one when $d = 1$. The output of the dilated convolution is: $\tilde{X} = (F(x_1), F(x_2), \ldots, F(x_l))$.

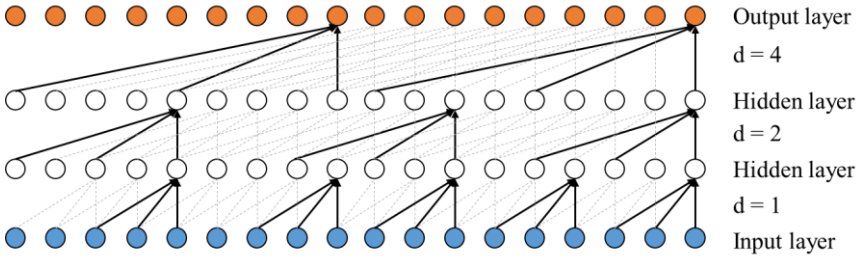

Figure 4-3. Graphical representation of dilated convolutions with dilation factors d=1,2,4 and filter size of 3.

After the dilated convolution, the weighted normalisation and dropout will be applied to the extracted features $\tilde{X}$, with the output denoted as $H(\tilde{X})$. Finally, the summation of operated outputs and the initial input, denoted as $G(x)$, can be formulated as $H(\tilde{X}) + X$, and will be taken as input for the subsequent residual module or attention module.

(2) Multi-head self-attention mechanism

To further improve the ability of long-term temporal dependencies, the multi-head self-attention mechanism is added after the final two residual convolutional blocks for capturing the most critical information and relationship of the elements in the feature space, thus further enhancing model performance and general ability. Specifically, for the sequence of embeddings (*G(x)*), three linear projections will be operated to obtain

the query (Q), key (K) and value (V) vectors for each token in the sequence. Then, for each position in the input sequence, the attention is denoted as

$$Attention(Q, K, V) = softmax(\frac{QK^T}{\sqrt{d_k}})V \quad (4\text{-}17)$$

Furthermore, in multi-head attention, the above attention layers, or heads, will be performed in parallel for k times, concatenated and then projected to get the final output.

$$head_i = Attention(Q_i, K_i, V_i)\ i = 1,2, \ldots . k \quad (4\text{-}18)$$

$$MultiHead_{output} = Concat(head_1, head_2, \ldots head_k)W_o \quad (4\text{-}19)$$

Where W_o is the learned matrix of the model parameter.

(3) Convolutional block attention module

Another solution for attention is the convolutional block attention module, which is an innovative architecture component designed to enhance the capabilities of convolutional networks. It sequentially combines both channel and spatial attention mechanisms to enrich the feature representations, allowing the network to focus on the most relevant regions (Woo et al., 2018). Specifically, to capture the channel-wise attention after one-dimensional convolutions in our model, the average pooling and max pooling are employed in parallel to learn the distinctive object features, F^c_{avg} and $F^c{}_{max}$, respectively. Next, each descriptor is forwarded to a shared multi-layer perceptron, and then their results are merged using element-wise summation and operated with a sigmoid function to get the one-dimensional channel-wise attention map $M_C(F)$.

$$M_C(F) = \sigma(W_1\left(W_0\left(F^C_{avg}\right)\right) + W_1\left(W_0(F^C_{max})\right)) \quad (4\text{-}20)$$

Where W_0, W_1 denotes the weights of MLP layers, and σ is the sigmoid function.

In addition, to identify where the two-dimensional feature map matters, the one-dimensional spatial attention map in this study ($M_s(F)$) is generated across the channel, by one convolutional layer over the concatenated average-pooled and max-pooled features.

$$M_s(F) = \sigma\left(f^2\left(\left[F_{avg}^C, F_{avg}^C\right]\right)\right) \tag{4-21}$$

Where f^2 represents the one-dimensional filter with a size of 2, and σ denotes the sigmoid function.

4.3.3.2. Model fusion strategy

The aforementioned DCNN models are adept at data mining from wake vortex images, indicating their suitability for vortex monitoring in near real-time. However, to support advanced runway operations, it is anticipated that the future duration of vortices will be estimated when only the initial vortex images are captured by LiDAR. Therefore, the fusion of DCNN and ATCN is proposed to integrate the advantages of these two models in both capturing spatial features and identifying temporal dependencies, thereby achieving both superior performance and long-term prediction capability in vortex recognition and evolution prediction.

4.3.4. Model explanation via feature analysis

Explainable AI (XAI) has emerged as a crucial area that aims to address the black-box nature of complex machine learning models by providing human-interpretable explanations of model predictions. This is particularly important when applying machine learning techniques in safety-critical flight separation suggestion systems. Some tools and methods have been proposed to enhance model transparency and interpretability, such as Local Interpretable Model-agnostic Explanations (LIME),

Shapley Additive exPlanations (SHAP), Layer-wise Relevance Propagation (LRP), and Gradient-weighted Class Activation Mapping (Grad-CAM). LIME approximates the behaviour of black-box models through local interpretable models, enabling the explanation of individual predictions. SHAP leverages cooperative game theory to attribute features importance and offers a unified framework for global and local interpretability. Grad-CAM visualises significant regions in images for convolutional neural networks.

For interpretation of the tasks of forecasting sequential wake vortex data and enhancing our understanding and confidence in the model decision-making process, the SHAP model is applied in this research for local explanation using the additive feature attribution method. The Shapley values of a feature represent the average contribution of that feature across all possible combinations of features (Lundberg et al., 2017). Let $F(\cdot)$ represents the trained TCN or LSTM models, while $G(\cdot)$ represents the explanation model. The input for the explanation model, which is the simplified wake feature input x', is mapped with original input by function $x = h_x(x')$. The explanation expects $G(z') \approx F\left(h_x(z')\right)$ when $z' \approx x'$. Next, the explanation model for additive feature attribution approach is in the format of a linear function of binary variables.

$$G(z') = \phi_0 + \sum_{i=1}^{M} \phi_i z_i' \tag{4-22}$$

Where $\mathrm{z}' \in \{0,1\}^{\mathrm{M}}$, M is the feature number, ϕ_i is the contribution of feature *i* and is allocated by their marginal contribution, and $\phi_i \in R$.

The kernel explainer which employs a weighted sampling approach to estimate Shapley values is used in this study for interpreting the trained deep learning models. For the three-timestep window with eight features per timestep, the contribution of a

total of 24 features about vortex positions, strength, crosswind and aircraft types to each positional output or strength estimation is analysed.

4.3.5. Exploratory evaluation of wake presence in the final approach path towards dynamic wake separation

As wind conditions play a leading role in the descent and transport of wake vortices, strong winds and unstable atmospheric turbulence may expedite the decay, blowing vortices away from runway centrelines to the left or right side. If so, the wake separation may be reduced in these instances. Therefore, based on the above probabilistic and reliable vortex evolution prediction under the developed models, the potential of aircraft separation minima reduction can be verified through duration assessment of vortex presence.

The duration of vortex presence in the above circumstances is evaluated upon the determination of standard approach profiles in LiDAR scan planes. In addition to the allowable approach paths calculated for instrument landing rules in (Chu et al., 2024), the lateral and vertical boundaries of the approach profiles were loosened to achieve an initial vortex coverage of more than 80%, as shown in **Table 4-2**.

Notably, the above approach profiles are defined for flights at low altitudes and under steady wind conditions. In the presence of wake vortices in the approach corridor at all times (typically in a stable atmosphere or with weak crosswinds), further separation reduction must be evaluated in light of the wake encounter risk, which requires consideration of vortex intensity and following aircraft (Visscher et al., 2016). As the performance of vortex strength estimation is quite worse than vortex location prediction, the separation reduction is illustrated only in terms of the cleanliness of the approach profiles, encompassing the following two aspects:

(1) Get the positional boundaries of the two-dimensional vortex cores with a 95% confidence level through the probabilistic TCN model with the best performance.

(2) Determine the last timestep that the entire wake pair is outside of the approach profiles, either laterally or vertically, considering also the regions of wake turbulence and a safety margin. Therefore, separation reduction evaluated in this study occurs exclusively when the anticipated wake duration is shorter than the lifecycle of the wake as detected by the LiDAR.

Table 4-2. The height and horizontal position range of aircraft at the LiDAR scanning plane.

Runway	LiDAR distance (m) to Runway (x profile)	LiDAR distance (m) to Runway (y profile)	Estimated allowable range of height (m) to ground	Estimated allowable range of height (m) in LiDAR plane	Estimated allowable range of horizontal position (m) in LiDAR plane	Coverage percentage of initial wake vortices
07L	1400	1116.31	56.84 - 91.40	35 - 84.40	±120	96%
25R	275	1511.99	72.72 - 116.93	50 - 109.93	±120	81.69%

4.4. Numerical study

This section presents the training configuration of the two-stage DCNN model and the attention-based TCN models, and illustrates the performance of proposed models in location and strength projection of aircraft wake vortices at HKIA. Furthermore, we also verify the applicability of the developed model in exploring the dynamic flight separation minima under vortex duration analysis.

4.4.1. Model training and evaluation configuration

A total of 17254 wake vortex sequences from arrival flights at HKIA, consisting of 108377 timesteps from June to October 2019, were captured by LiDARs Site 1 and Site 2, and then processed for this study. As the evolution of wake vortices is forecasted through time series analysis in this study, all processed historical wake sequences were split into training, validation and test datasets randomly by sequence flags in the proportion of 6:2:2. This guarantees the ability to acquire knowledge of wake vortices generated by various aircraft types and background atmospheres. The short-term prediction described in this study represents a single-timestep forecast for roughly 10s. The term "long-term prediction" refers to a series of forecasts in the next several steps that, dependent on the vortex lifespan detected by LiDAR, may last for one to two minutes.

All experiments in this research were conducted on the same hardware environment as in Chapter 3. Before model training, input and output data were normalised using the MinMaxScaler. Grid search was performed to tune the hyperparameters and relevant parameters of these models, such as the batch size and model layers. The training process employs the Adam Optimiser and has a decayed learning rate of 0.95 in every 30 epochs. The DCNN models perform under 500 epochs, and the attention-based TCN models run under 1000 epochs. The early stopping technique is applied to identify model parameters with the best performance.

The four residual temporal convolutional modules in the proposed TCN models are comprised of one-dimensional causal dilated convolutional layers with dilation rates of 0, 2, 4 and 8, respectively, and 64 filters with a kernel size of 2 in each layer. The dropout rate in these modules is 0.2.

The multi-head attention mechanism in this model is defined under 16 heads and a total 64 neurons of the dense layer for linear projection of Q, K, V vectors. The channel attention in the CBAM module is constructed under one dense layer with 32 neurons and activation function of Rectified Linear Units, and another dense layer with 64 neurons for vector reshaping.

In the decoder part of the model, the global max-pooling layer extracts the most salient features across the temporal dimension and reduces the output to a fixed-size representation, followed by one dense layer with 128 neurons and another dense layer that produces the output. For wake decay prediction, the LSTM model and GRU model are taken as benchmarks. These two models contain two layers with 64 and 32 neurons with a dropout rate of 0.2.

Both the Mean Absolute Error (MAE) and Root Mean Square Error (RMSE) metrics are used for model performance evaluation, with their formulas as below:

$$MAE = \frac{1}{n}\sum_{i=1}^{n}|y_i - \hat{y}_i| \tag{4-23}$$

$$RMSE = \sqrt{\frac{1}{n}\sum_{i=1}^{n}(y_i - \hat{y}_i)^2} \tag{4-24}$$

where n is the number of data points in the dataset, y_i is the vector of true target values, and $\hat{y}_i$ is the vector of predicted values.

4.4.2. Model performance assessment

Under the same experimental conditions and test dataset, the performance of the proposed attention-based TCN models is compared to that of benchmarking models. This comparison encompasses the short-term prediction performance on a single test

dataset and the average performance under 5-fold cross-validation, the performance of long-term prediction and the model hybrid.

Performance of ATCN models in short-term prediction horizon: Table 4-3 demonstrates the superior performance of the proposed two attention-based TCN models, especially the TCN model with a multi-head attention mechanism, compared to the pure TCN model and two typical recurrent neural networks. The dilation convolutions exhibit a broader range of temporal dependencies, with efficient utilisation of features in the time window. Moreover, the attention mechanism further improves the feature mining process. Specifically, the multi-head attention-based TCN model achieves nearly 68% and 70% MAE reduction in X_l and X_r prediction, compared to GRU and LSTM, respectively. To achieve a comprehensive assessment of model generalisation performance and avoid the variance associated with single-fold validation, we also applied the 5-fold cross-validation to evaluate the average performance of these models across five partitions in **Table 4-4**. It also indicates the best performance of the ATCN models in lateral position prediction despite a decline in performance gains. Nevertheless, the performance improvement of strength estimation in ATCN and CBAM-TCN models is not as significant as the location estimation, as vortex circulation is more challenging to identify, thus resulting in more significant errors in the initial measurement.

In essence, this improvement can be demonstrated through feature relevance visualisation with SHAP values (Lundberg et al., 2017) by providing insights into how different features impact the prediction outcomes. The positive SHAP values indicate that the corresponding feature has a positive impact on increasing the prediction value, while negative values indicate the opposite. In **Figure 4-4** and **Figure 4-5**, for each location output, the left figure represents the influence of each feature on the output for

a specific individual input sample. They provide detailed insight into how historical locations and other features in the input impact prediction for this sample. Nonetheless, the right figure, which is the summary plot, intuitively shows the importance ranking of all features in the overall test dataset, as well as the impact of each feature on the prediction.

Figure 4-4 demonstrates that the most relevant vortex features for future location prediction in the ATCN model span all timesteps in the input feature window (8×3 dimensions with 8 features in three timesteps), while the LSTM model depends primarily on input in the first timestep and achieves the worst prediction performance, as depicted in **Figure 4-5**. More specifically, the features of lateral positions in the first three timesteps not only lead the forecast of their future values but also more intriguingly, play a leading role in future vortex height prediction. In addition, the decay of strength also correlates strongly with vortex height reduction, which reveals the coupling relationship between the horizontal and vertical positions of the vortex pair.

The above results can also be interpreted in relation to vortex physics despite the learning process being different from the mechanism of vortex physics. The dynamics of wake vortices involve not only instantaneous positions but also historical information (the increment of lateral positions or lateral movement speed) for future vortex position prediction. Furthermore, changes in lateral positions can impact vortex height, indicating a coupling between horizontal and vertical positions in vortex evolution. The strong correlation between strength decay and vortex height reduction also aligns with known vortex physics principles. As a vortex weakens over time (due to diffusion or other factors), its height tends to decrease, reflecting the energy dissipation and spreading characteristics of wake vortices.

Table 4-3. Test performance comparison of the proposed models for short-term vortex position and strength prediction.

Deterministic model	Vortex location estimation								Vortex strength estimation			
	MAE (m)				RMSE (m)				MAE (m^2/s)		RMSE (m^2/s)	
	X_l	Z_l	X_r	Z_r	X_l	Z_l	X_r	Z_r	G_l	G_r	G_l	G_r
ATCN	**8.32**	**4.48**	**8.72**	**4.47**	**11.68**	**6.53**	**12.36**	**6.59**	**48.86**	**49.06**	**66.74**	**65.03**
CBAM-TCN	**10.45**	**4.52**	**9.93**	**4.52**	**13.58**	**6.57**	**13.28**	**6.64**	49.07	**49.16**	67.08	65.66
TCN	11.37	4.58	11.12	4.64	15.35	6.58	15.01	6.57	**48.95**	49.17	**66.78**	**65.42**
GRU	27.75	9.61	27.19	9.82	36.24	13.12	35.50	13.64	50.11	50.38	67.48	66.12
LSTM	28.44	9.35	28.10	9.65	38.33	13.49	36.14	14.41	70.44	69.56	88.82	86.63

Table 4-4. 5-fold cross-validation of the proposed models in wake vortex location estimation.

Deterministic model	Vortex location estimation							
	MAE (m)				RMSE (m)			
	X_l	Z_l	X_r	Z_r	X_l	Z_l	X_r	Z_r
ATCN	**11.724**	**4.54**	**11.406**	**4.584**	**15.226**	**6.642**	**14.98**	**6.61**
CBAM-TCN	**13.712**	5.476	**12.294**	**5.118**	**17.678**	8.602	**16.178**	7.508
TCN	20.752	**4.616**	23.956	4.64	26.342	**6.682**	29.932	**6.662**
GRU	31.716	9.506	30.948	9.88	39.876	12.826	40.512	13.4
LSTM	34.918	9.738	36.174	10	46.022	12.942	46.91	13.472

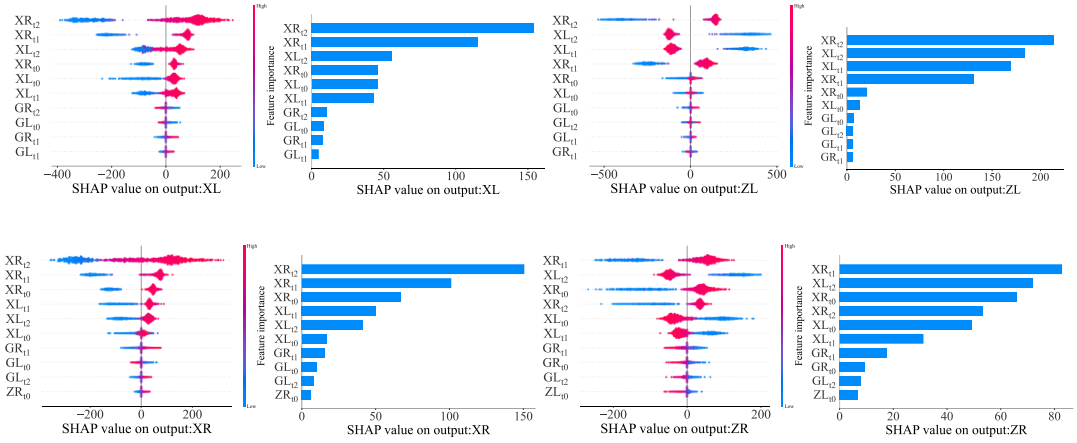

Figure 4-4. Relevance of features to outputs of the multi-head attention-based TCN model based on the SHAP kernel explainer.

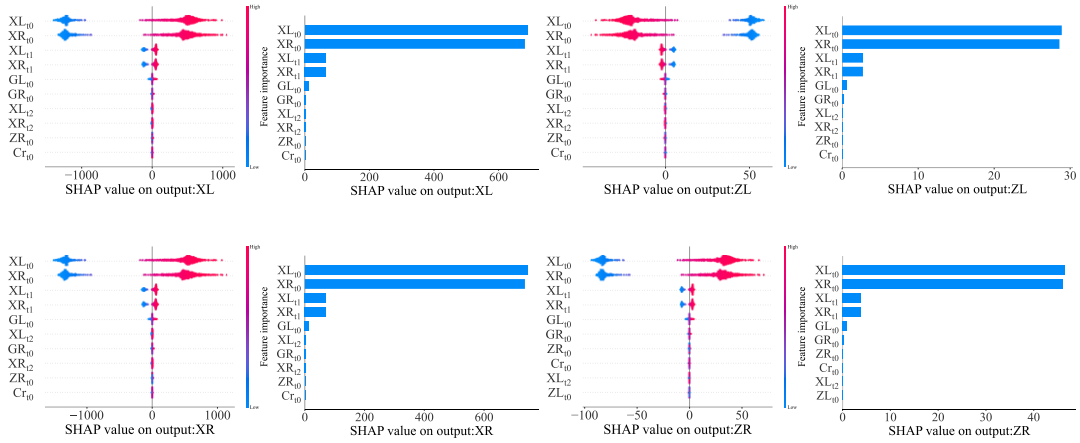

Figure 4-5. Relevance of features to outputs of the LSTM model based on the SHAP kernel explainer.

The performance of the ATCN model in long-term prediction horizon: **Table 4-5** verifies the online and long-term prediction ability of the attention-based TCN models trained offline. As vortex location prediction is more accurate than intensity estimation, it is more reliable and usable for runway operations. Therefore, wake locations are the focus of research on long-term decay prediction and hybrid models for online prediction. The overall MAEs of the ATCN model in long-term lateral location projection are similar to those of the pure TCN model, and are reduced by around 40% when compared to GRU and LSTM. Moreover, although **Figure 4-6** suggests that prediction errors may increase as the length of the vortex sequence increases, the ATCN model achieves considerable low-level MAE in the lateral position, specifically approximately 37% and 45% less than GRU and LSTM, respectively, for vortex sequences consisting of 9 -12 timesteps. It is worth mentioning that the long-term prediction in this study is conducted on wake sequences with no more than 12 timesteps to guarantee the quality of wake segmentation. Additional detailed analyses can be performed to investigate vortex behaviour in the second stage with consideration of the ground effect when high-quality and long-lifetime wake sequences are available.

Table 4-5. Long-term prediction performance of the proposed models in test dataset under different vortex lengths.

Deterministic Model	Number of wake seq.	Seq. length (time steps)	MAE				RMSE			
			X_l	Z_l	X_r	Z_r	X_l	Z_l	X_r	Z_r
ATCN with roll prediction	1575	4 - 12	17.07	6.49	18.98	6.70	27.09	9.43	30.29	10.91
	567	4 – 6	**10.73**	6.10	**11.27**	**6.38**	**15.11**	8.67	**15.61**	**9.33**
	592	6 - 9	15.33	**6.01**	16.57	**6.22**	23.04	**8.30**	24.96	9.49
	416	9 – 12	19.75	6.97	21.79	6.93	30.37	10.16	34.00	9.84
TCN with roll prediction	1575	4 - 12	16.35	6.29	16.53	6.58	23.54	9.02	24.11	9.75
	567	4 – 6	**12.16**	5.99	**12.35**	6.45	**16.99**	8.65	16.97	**9.34**
	592	6 - 9	15.35	**5.96**	15.78	6.33	22.12	**8.29**	22.74	9.54
	416	9 – 12	18.32	6.63	18.30	6.81	26.08	9.65	26.72	10.02
CBAM-TCN with roll prediction	1575	4 - 12	24.92	6.62	21.98	6.97	35.6	9.57	31.84	10.48
	567	4 – 6	13.88	6.12	12.85	6.46	18.58	8.75	**16.90**	9.56
	592	6 - 9	20.03	6.12	19.57	6.41	27.40	8.47	26.96	9.63
	416	9 – 12	30.30	6.90	26.73	7.28	42.83	9.79	38.60	10.27
GRU with roll prediction	1575	4 - 12	29.02	9.50	29.54	9.70	38.56	13.01	40.29	13.51
	567	4 – 6	27.09	9.67	25.63	9.55	34.82	13.12	34.71	13.06
	592	6 - 9	30.29	11.33	25.37	11.62	36.91	15.15	31.66	16.17
	416	9 – 12	31.16	9.34	29.17	9.57	40.95	12.83	39.42	13.26
LSTM with roll prediction	1575	4 - 12	31.16	9.36	29.01	9.65	42.34	13.49	37.53	14.41
	567	4 – 6	24.55	11.99	27.31	11.07	30.20	16.20	33.09	16.53
	592	6 - 9	26.95	8.92	27.96	9.16	35.10	11.89	36.37	11.92
	416	9 – 12	37.04	8.95	30.50	9.66	50.76	13.96	39.80	15.74

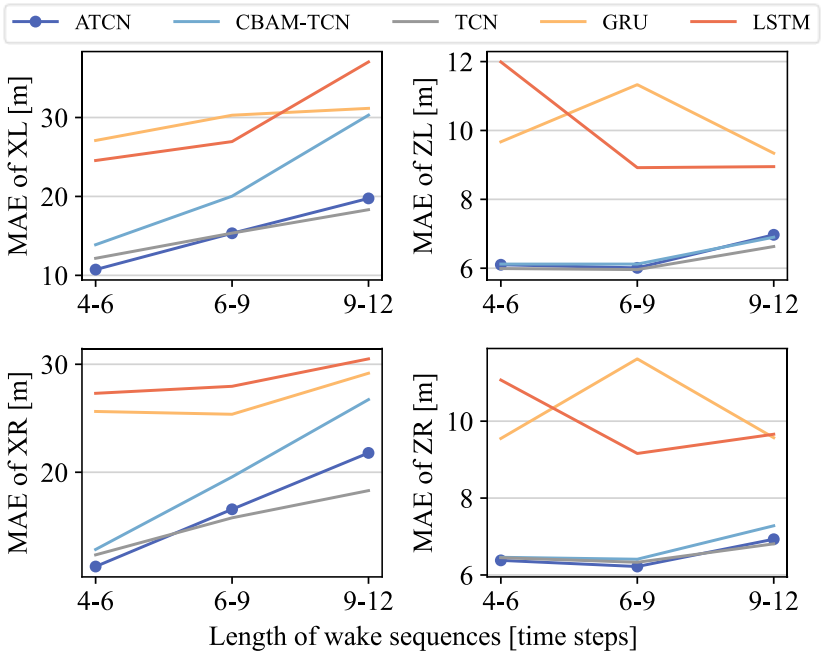

Figure 4-6. Performance comparison of proposed models and benchmarking models based on the same test dataset with different wake sequence lengths.

As model performance at high crosswinds is crucial for further separation assessment, we also analysed model performance under different levels of crosswind speeds. Wake sequences from January to April 2019 were incorporated into the above test dataset for evaluating crosswinds. **Figure 4-7** demonstrates model performance comparison under 800, 800, 800, and 569 wake sequences with absolute crosswinds of 0-2, 2-4, 4-6, and 6-8 m/s, respectively. These data are independent of the above training and validation datasets. The quantity of wake sequences under absolute crosswinds exceeding 8 m/s is small and is therefore disregarded. The results show an evident trend of MAE reduction with the increase of crosswind speeds for all models. Notably, the ATCN model exhibits a superior performance, leading credibility to its application in separation suggestion.

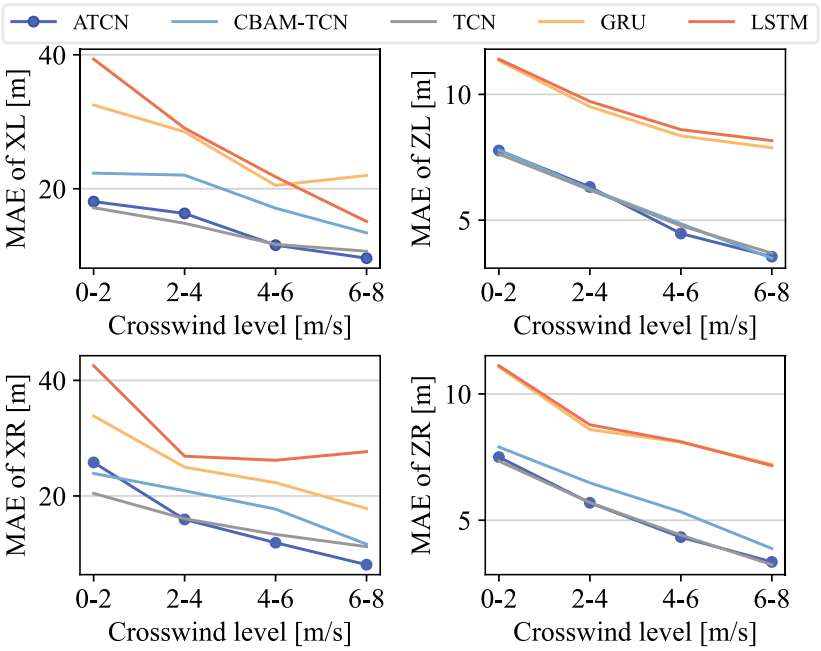

Figure 4-7. Performance comparison of proposed models and benchmarking models based on the same test dataset under different levels of crosswinds.

The performance of model fusion strategy for both vortex recognition and future prediction: **Table 4-6** shows the results of model fusion for online wake vortex prediction with initial vortex data captured from DCNN models. With the highly accurate vortex locations and intensity estimated by DCNNs, the ATCN model and the TCN model obtain over 27% and 11% performance enhancement in the long-term prediction of X_l and X_r, compared to the other benchmarks. Nonetheless, the CBAM-TCN model achieves a worse performance with more computational time. Notably, wake sequences with lengths of more than 9 timesteps have an approximately 15% additional MAE reduction compared with the results from the shorter sequences in the CNN-TCN fusion strategy. One reason behind this is the superior recognition accuracy of the DCNN model on initial vortex images generated in a more stable atmosphere, which thus lasts for a long time. In addition, the computational speed of the long-lifetime vortex sequences gets to an average of 7.76s per sequence, which provides

strong preconditions for near real-time and online vortex monitoring and flight separation suggestion, thereby supporting efficient runway operational decisions.

Table 4-6. Performance of CNN-TCN/LSTM/GRU models in long-term prediction of vortex evolution based on wake recognition for real flight scenarios.

Deterministic Model	Number of wake seq.	Seq. length (time steps)	MAE (m)				RMSE (m)				Computation time (min)
			X_l	Z_l	X_r	Z_r	X_l	Z_l	X_r	Z_r	
CNN-TCN	100	4-12	**20.99**	**7.05**	**22.52**	**6.99**	**29.07**	**9.65**	**34.31**	**9.49**	21.14
	904	9-12	**17.73**	**8.18**	**17.10**	8.27	**26.54**	11.78	**25.65**	12.27	117.07
CNN-ATCN	100	4-12	22.70	7.45	24.76	**6.45**	36.50	10.05	41.04	**8.95**	22.53
CBAM-TCN	100	4-12	25.81	6.91	25.89	6.71	35.72	**9.52**	39.77	9.41	34.96
CNN-GRU	100	4-12	33.81	8.93	31.23	9.09	42.37	11.16	43.56	11.45	20.80
CNN-LSTM	100	4-12	31.28	10.64	29.10	10.50	40.18	17.93	37.72	16.17	21.14

Following are three typical wake sequences lasting for 7, 9 and 12 timesteps in absolute crosswinds of 0.23, 2.08 and 5.9 m/s, respectively. The results of vortex recognition and evolution prediction from our proposed hybrid CNN-ATCN model are visualised accordingly. For wake vortices generated in a stable atmosphere and lasting for a long time, as depicted in **Figure 4-8** and **Figure 4-9**, the rapid vortex decay and sink in the first stage are evident with high prediction accuracy (timestep 4-8), while the second phase, starting from the 9th timestep, achieves increased errors, especially for the lateral position. The green and blue colours in the figure indicate the left and right vortex. The solid dot, "+" and "x" markers represent the ground truth of location, and the predicted results of CNN and ATCN models, respectively. Furthermore, both the aleatoric uncertainty and total uncertainty considering epistemic uncertainty in 95% confidence interval are visualised in pink and blue colour with dot-dash lines. The grey area represents the region of wake vortices with consideration of vortex radius that relates to the aircraft wingspan. The dotted lines in **Figure 4-8** represent the allowable

approach profiles. Given the perpetual presence of a wake vortex within this profile, separation reduction in this scenario is not feasible.

Figure 4-10 and **Figure 4-12** indicate that even for wake pairs generated under unstable background turbulence (**Figure 4-11**), the prediction of vortex transport and descent in the short term also achieves high accuracy. Although the long-term prediction of vortex cores is not so accurate, the consideration of positional uncertainty and a safety margin in the wake region improves reliability. Moreover, there is a remarkable and rapid lateral movement of the whole wake pair till they move outside of either the left or the right of the approach profile. The strong crosswind blows the wake pair laterally, as illustrated in **Figure 4-12**(c), which results in a clean approach profile.

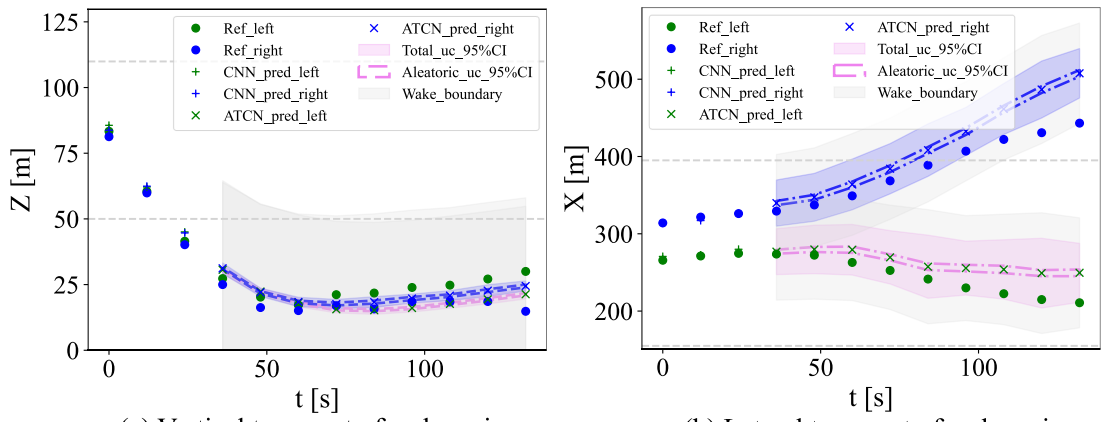

(a) Vertical transport of wake pair (b) Lateral transport of wake pair

Figure 4-8. Visualisation of the long-term prediction results of the CNN-ATCN model for a vortex sequence generated by aircraft in the CAT-B category under mean crosswind of 0.23 m/s during 2019/08/16 17:34:04 – 17:36:18.

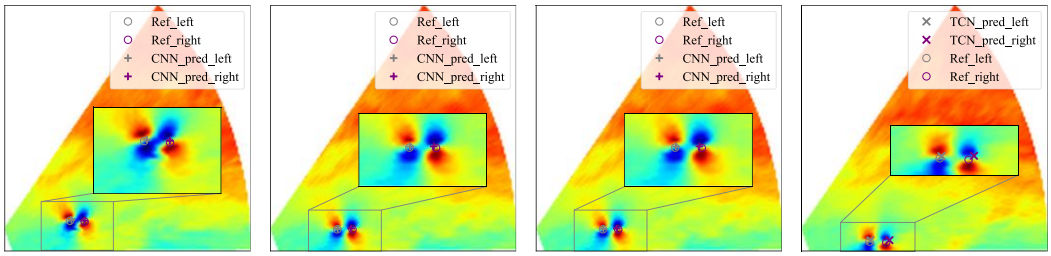

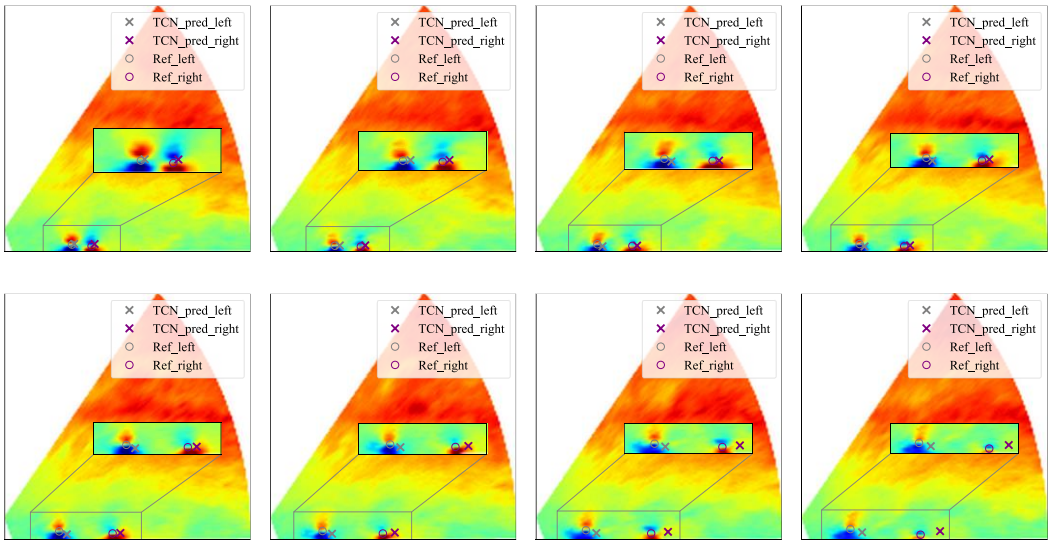

Figure 4-9. Visualisation of the predicted results of **Figure 4-5** in LiDAR wake images.

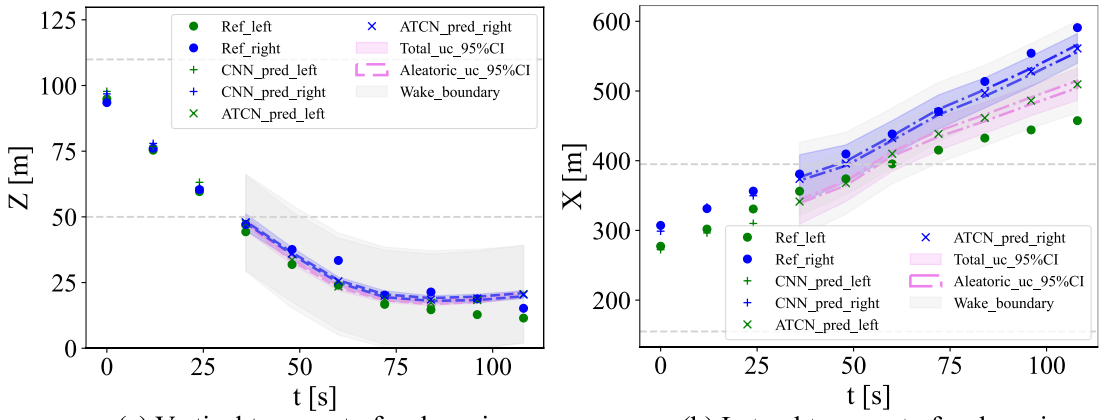

(a) Vertical transport of wake pair (b) Lateral transport of wake pair

Figure 4-10. Visualisation of the long-term prediction results of the CNN-ATCN model of a vortex sequence generated by aircraft in the CAT-B category under mean crosswind of 2.08 m/s during 2019/07/14 15:08:55 – 15:10:45.

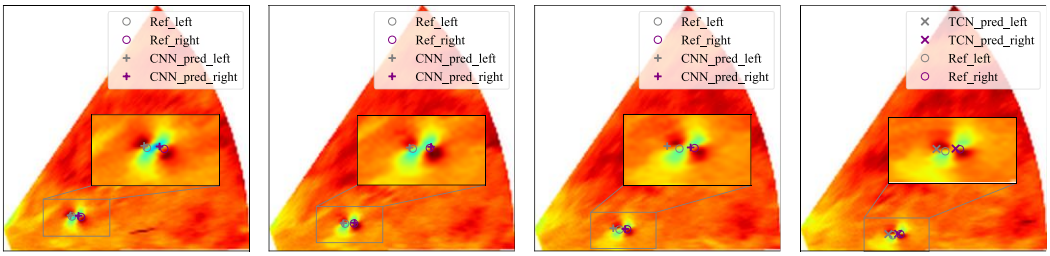

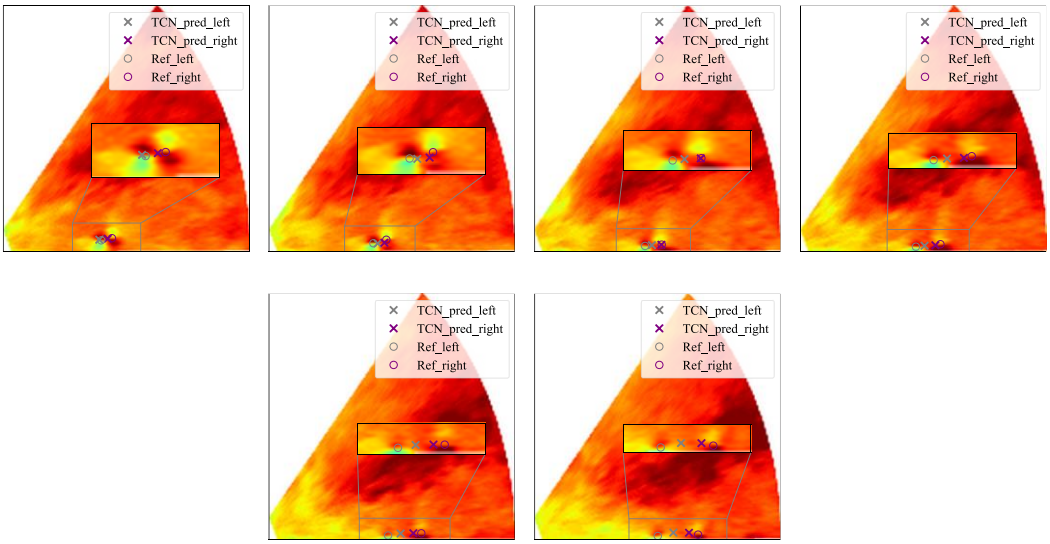

Figure 4-11. Visualisation of the predicted results of **Figure4-7** in LiDAR wake images.

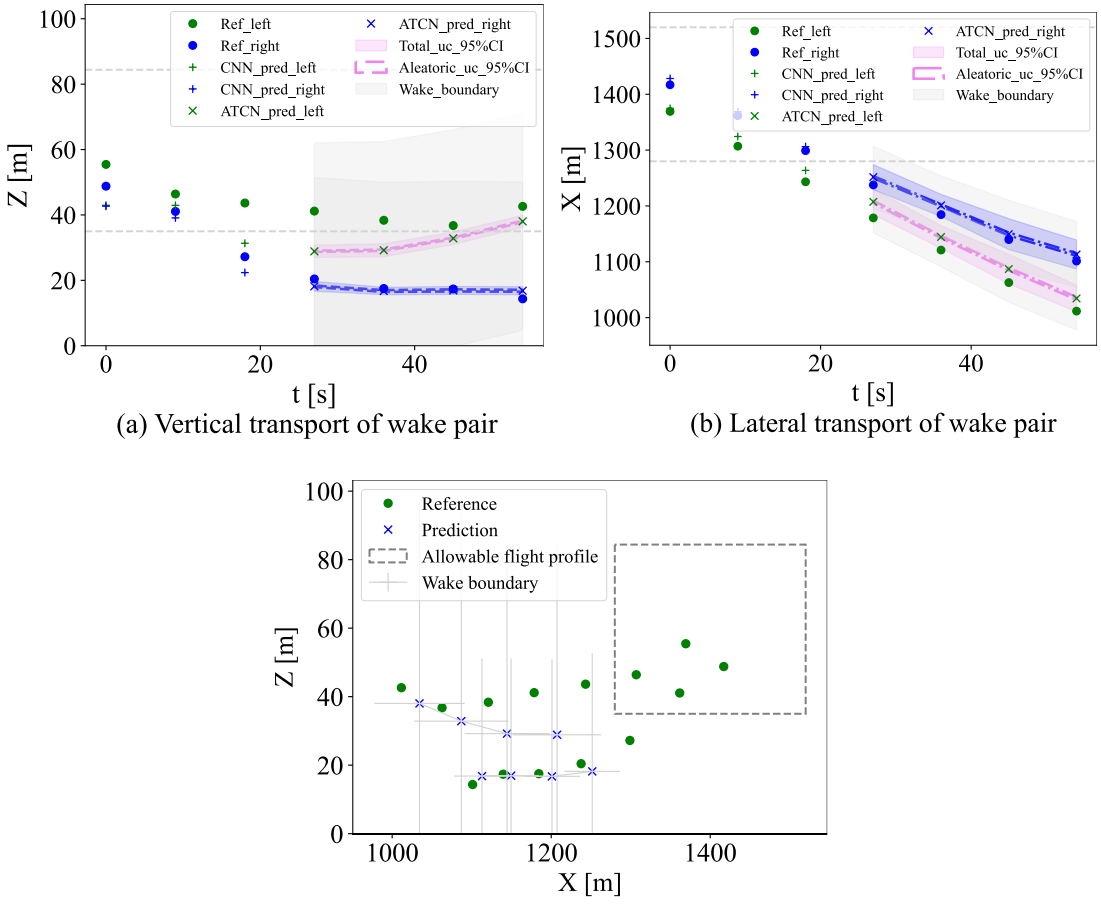

(a) Vertical transport of wake pair

(b) Lateral transport of wake pair

(c) Transport of wake pair in LiDAR scan plane

Figure 4-12. Visualisation of the long-term prediction results of the CNN-ATCN model of a vortex sequence generated by aircraft in the CAT-D category in a mean crosswind of – 5.9 m/s

during 2019/09/20 23:45:25 – 23:46:21.

4.4.3. Exploratory evaluation of aircraft separation minima reduction in the final approach

The above probabilistic ATCN model with long-term prediction ability is expected to provide reliable vortex locations to further support dynamic flight separation. For the above three scenarios of probabilistic long-term vortex prediction under different levels of crosswinds, the wake separation and separation reduction compared to the RECAT-EU standard are demonstrated in **Table 4-7**. The separation is evaluated under minimum radar separation of 3 nautical miles and an average approach speed of 140 knots. It indicates that a strong crosswind of 5.9 m/s is able to reduce wake separation generated by aircraft in CAT-B to under 60s, consequently reducing the approach separation for following aircraft in CAT-C and CAT-D to the minimum radar separation (MRS) by 25.9s when compared to the separation in RECAT-EU standard. The second row shows that the separation reduction is more significant for lighter aircraft.

In addition, the vortex durations on the approach profiles were analysed statistically on the test dataset and wake sequences from January to April 2019, involving a total of 12091 sequences and 2744 vortex sequences with mapped aircraft weight categories that are independent of the training dataset. **Figure 4-13** illustrates the transport of wake sequences in the test dataset under different levels of crosswinds, in which the colour represents the crosswind speed with directions, and the direction of the arrow indicates an increase in the timestep in the wake sequence. It is evident that the strong crosswinds are capable of removing entire wake pairs from the approach profiles at both runway entrances. Although the wake vortices may rebound with the increase in height, the lateral vortex movement is able to make the approach profile clear. The enlarged area shows that a large proportion of wake pairs with large lateral movement speeds are

generated by aircraft in CAT-B and CAT-D categories, which provides evidence of separation reduction for heavy aircraft.

Table 4-8 lists the proportion of flights with potential separation reduction relative to the entire wake lifetime for each aircraft category. The number of flights whose wake separation could be shortened accounts for 27.33% of the total. In addition, 91.06% of flight separation reduction is generated when the absolute crosswind speed is over 2.5 m/s, indicating the effects of crosswind in lateral vortex transport. It is noteworthy to remark that when taking wake encounter risk analysis into consideration for determining the separation reduction, the proportion of flights with wake separation reduction may be further increased, especially for those under a mean absolute crosswind of 0-3 m/s.

More specifically, **Figure 4-14** illustrates the predicted wake separation for flights in each aircraft category. The trend towards a shorter separation interval (the greatest separation) is evident as aircraft weight decreases. The separation time under an absolute crosswind of 0-3 m/s, which also represents the worst-case wake encounter, is also compatible with the current RECAT-EU standard. Nonetheless, when the absolute mean crosswind is over 5 m/s, the mean duration time of wake vortices on the approach profiles for all aircraft may be reduced to under 60s. It is worth mentioning that for wake pairs that always last in the approach profiles, the wake separation is taken as no reduction and as the same as their lifetime detected by the LiDAR, lacking consideration of wake encounter and its effect on separation reduction. Furthermore, the wake sequences over 12 timesteps are neglected. These may lead to an underestimation of the boundary values of the blue boxes in crosswind 0-3 m/s. More importantly, the actual flight separation will be the maximum between the predicted wake separation and the minimum radar separation, although the wake separation may

be reduced to below 60s.

Figure 4-15 reveals wake separation reduction from the perspective of the proportion of aircraft numbers in each separation interval period. The time intervals in the x-axis represent the real duration of wake pairs with both vortices measured by LiDAR for the "Measurement" legend, while for the "Prediction" legend, they mean the predicted wake separation time by the DCNN-ATCN model. **Figure 4-15**(a) reveals that separation can be reduced for 21% of wake vortices with a lifetime of at least 60–100s to less than 60s, and even below 40s. Moreover, **Figure 4-15**(b) shows that under a stable atmosphere (mean absolute crosswind of 0-3 m/s), the proportions of detected wake lifetime and predicted separation time in all time intervals are almost overlapped. These proportions peak between 80-100s, indicating no evident separation reduction. Conversely, for a large proportion of wake pairs generated under an absolute crosswind of 3-6 m/s with a lifetime of 60-80s, their predicted wake separation time can be reduced to below 60s, with the most significant proportion in the time interval of 40-60s. Although the measured lifetime or predicted separation time may be under 60s, the actual flight separation should be the maximum between predicted wake separation and the minimum radar separation.

Table 4-7. Scenarios of wake transport with dynamic separation reduction compared to the RECAT-EU standard.

Wake scenarios	Leading aircraft (Aircraft category)	Average approach speed	Average crosswind	Follower aircraft	Minimum DBS in RECAT	Minimum TBS in RECAT	Predicted wake duration	Minimum radar separation	Separation reduction
Figure 4-8	A359 (B)	140 knots	0.23 m/s	CAT-D	4 NM	102.9s	Over 120s	3 NM/ 77s	0
Figure 4-10	A320 (D)	140 knots	2.08 m/s	CAT-F	5 NM	128.6s	70s / 2.33 NM	3 NM/ 77s	51.6s
Figure 4-12	A330 (B)	140 knots	-5.9 m/s	CAT-D	4 NM	102.9s	35s / 1.17 NM	3 NM/ 77s	25.9s

Note: DBS refers to the distance-based separation, TBS represents the time-based separation, and NM refers to the nautical mile.

Table 4-8. The proportion of flights with separation reduction under each aircraft weight category based on the long-term vortex location prediction.

Aircraft weight categories	Proportion of flights with separation reduction	Proportion of flights under absolute crosswind over 2.5m/s of the separation reduced flights
CAT_A	34.48%	**100%**
CAT_B	23.6%	99.22%
CAT_C	22.95%	92.85%
CAT_D	**33.13%**	81.46%
CAT_E	**40%**	**83.33%**
Total flights	27.33%	91.06%

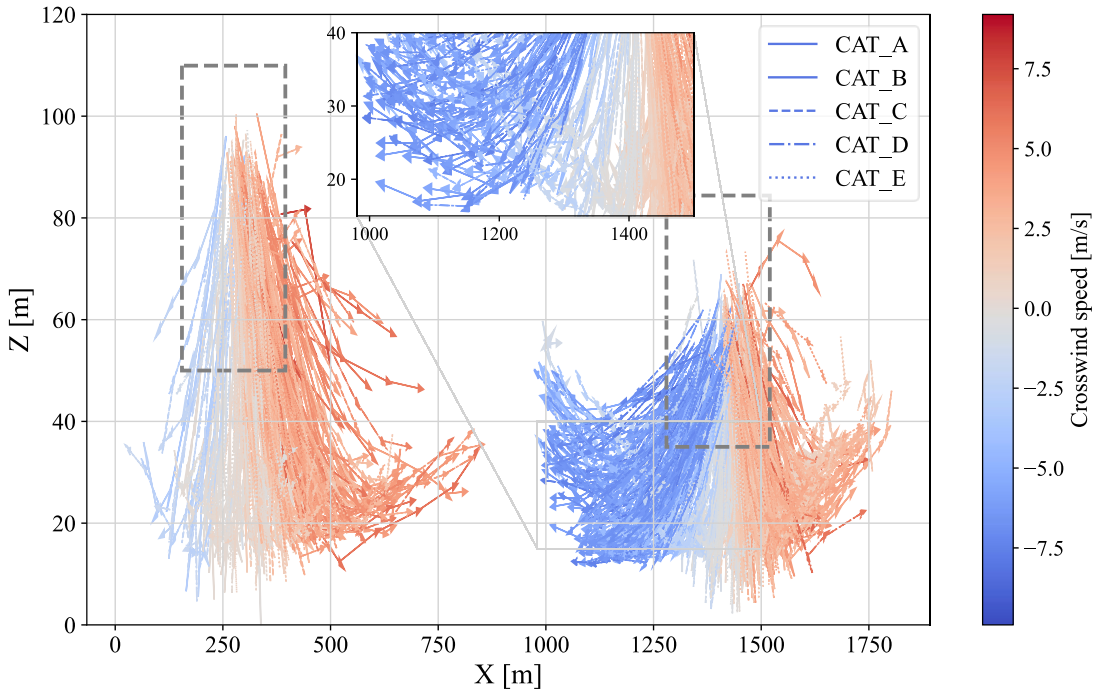

Figure 4-13. Predicted transport of wake pairs in the test dataset under different mean crosswinds at Runway 25R and 07L.

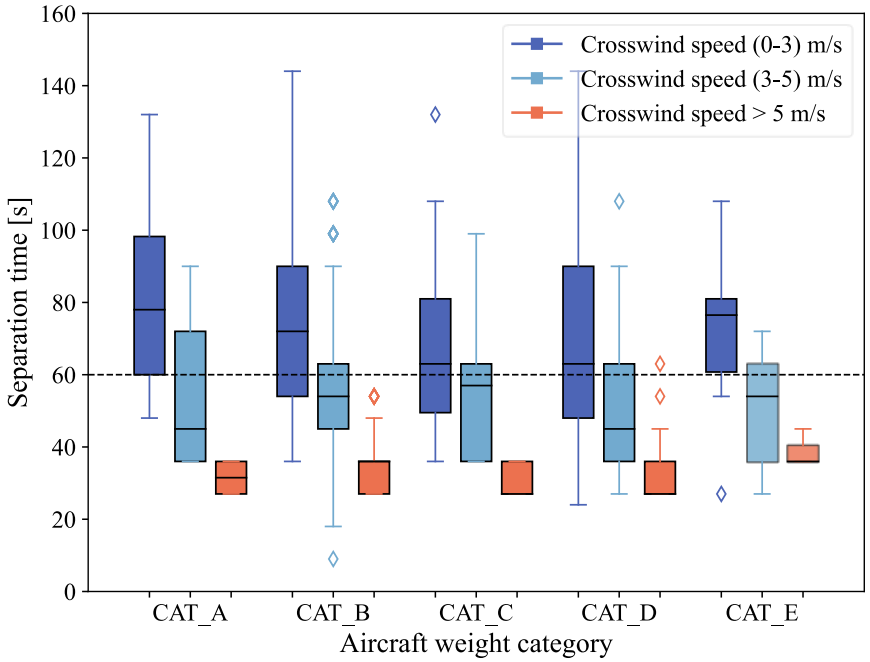

Figure 4-14. Predicted wake separation minima under each aircraft weight category and different levels of mean absolute crosswinds.

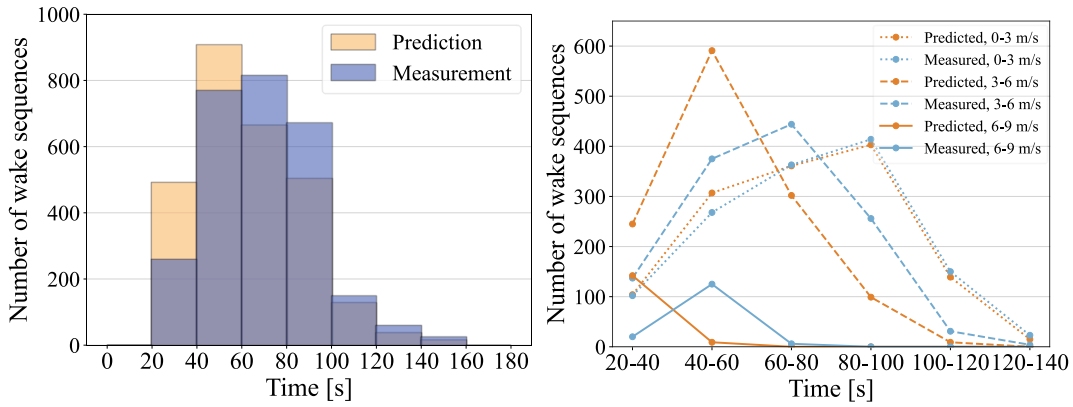

(a) Total sequence number (b) Sequence number by crosswind level

Figure 4-15. The total number of wake sequences and wake sequences under different levels of mean absolute crosswinds by the time interval of LiDAR measured lifetime or predicted separation time.

4.5. Discussion

The present study demonstrated the performance of hybrid deep learning approaches in aircraft wake vortex feature mining, and the influence of crosswind in dynamic separation time in the final approach. In addition to the superior performance enhancement analysed previously, the managerial implementations of the proposed models and future work will be discussed in this section.

4.5.1. Managerial implementations

This section presents the fast-time data-driven methodology for dynamic flight separation suggestion in the final approach through near real-time aircraft wake vortex recognition and evolution prediction, using a hybrid deep learning framework. This research will foster more efficient and intelligent runway scheduling without sacrificing flight safety. The managerial implications of this research are described from three aspects:

(1) **Support the development of wake vortex analysis models.** This section

presents a hybrid deep learning framework for onboard aircraft wake vortex recognition and evolution prediction, with considerable prediction accuracy and computation speed achieved. This will support the online monitoring of the vortex state and lifetime. Furthermore, this data-driven methodology can be ensembled with physical-based vortex modelling and simulation methods to enhance vortex prediction performance.

(2) **Support the construction of dynamic flight separation system.** The potential of flight separation reduction is assessed based on the probabilistic results of vortex location prediction under vortex duration estimation. This exploratory flight separation evaluation with reliability analysis using data in real operational scenarios provides a promising idea for safety regulators in developing the time-based dynamic fight separation minima.

(3) **Improve runway operational efficiency and on-time performance.** The proposed wake prediction models may not directly support the advanced runway sequencing due to their limited prediction time horizon, but they may be applied to runway re-scheduling in near real-time situations. Next, the statistical analysis of flight separation reduction based on flight safety will benefit runway throughput and operational efficiency increase, especially during peak periods under optimisation of the traffic mix. For a specific arrival or departure sequence, the reduced flight separation also permits a reduction in the total flight time. This may provide air traffic controllers with additional flexibility in managing traffic. Furthermore, it will also allow for a more expeditious recovery from adverse weather or emergent situations, thereby reducing overall delays.

4.5.2. Results interpretation and future work

The evaluation of dynamic wake separation in this study is an exploratory attempt, despite the above reliability-improvement strategies to guarantee credibility. The potential and range of separation reduction are evaluated under the instrument landing procedure and approach profiles only in the LiDAR scan planes at the runway entrances. Furthermore, the background atmosphere conditions, which are a crucial factor in vortex transport, are considered in only the lateral direction and in a steady status in the entire vortex decay process. Due to the limitation of LiDAR's number, the crosswinds along the flight direction are also assumed to be the same and prevailing. Therefore, for situations of noticeable wind shear, headwind and dynamic crosswind along the flight direction, and other flight procedures, the duration time of aircraft wake vortices in the entire approach profiles, including the high airspace, deserves to be further optimised with additional data support. Furthermore, with more accurate wake strength estimation available, the separation reduction can also be verified from the perspective of wake encounter risk analysis for the wake pair always staying in the approach corridor.

Next, the ATCN and CNN-ATCN models proposed in this research can only be implemented to predict future wake evolution at the minute level when the initial three-timestep wake features are known. These models may support the near real-time runway re-scheduling. Nonetheless, to achieve more advanced runway sequencing hours in advance and under dynamic wake separation, the transport and duration of wake vortices in the approach path should be forecasted in a longer time horizon considering four-dimensional flight trajectory and dynamic wind prediction.

Finally, this study proposes a data-driven deep-learning approach for forecasting the decay and transport of aircraft wake vortices. Although it indicates a considerable good fit with the LiDAR processing algorithm, other physical models and the CFD

simulation can be used to verify or support the development of the deep learning approach and provide a more comprehensive analysis. It is also worth investigating methods to improve the generalisation of the model for handling complex situations where the LiDAR processing algorithm may fail.

4.6. Concluding remarks

Overall, a new data-driven fusion framework of deep learning is proposed for aircraft wake vortex recognition and decay prediction, which provides a promising solution for wake vortex monitoring and duration assessment. In the offline stage, the two-stage deep convolutional networks that permit prompt and accurate identification of vortex locations and strength from wake vortex images are utilised for initial vortex recognition. Furthermore, we propose the probabilistic attention-based TCN models for vortex transport and decay forecasts, using historical spatiotemporal vortex data. Next, the DCNN and the ATCN model are integrated in sequence to realise online vortex recognition and future evolution prediction, combining the benefits of spatial feature analysis and temporal dependency identification. Finally, based on the predicted vortex locations with a high confidence level and duration assessment of vortex presence in the final approach profiles, the potential of dynamic flight separation minima is tentatively inferred for flights with aircraft in each weight category and under crosswind conditions.

As revealed in the performance indicators MAE and RMSE, the fusion of DCNN together with ATCN for forecasting aircraft wake vortices appears to be a promising solution. In addition, it provides a comprehensive view of spatial and temporal characteristics of current and future vortex locations. Moreover, the proposed ATCN model outperforms specific state-of-the-art models substantially, especially for

predicting the long-term movement of wake vortices. This framework achieves both outstanding prediction performance and low computational time. More importantly, the hybrid probabilistic models verify the potential of dynamic flight separation under crosswinds from several aspects.

Therefore, the benefit of fusing deep convolutional networks and attention-based temporal convolutional networks manifests in three forms. It facilitates online and real-time aircraft wake vortex monitoring and duration evaluation. Next, it also supports the development of the dynamic flight separation system. Finally, the dynamic separation time indicated over this framework also facilitates runway rescheduling and near real-time scheduling for improving runway operational capacity and efficiency.

Chapter 5. Runway capacity improvement under smart prediction-then-optimise methodology with dynamic wake separation prediction

The previous chapters have explored the foundations of dynamic wake separation through advanced deep-learning techniques, focusing on recognising and predicting wake vortex characteristics and their spatial-temporal evolution. Building upon these advancements, this chapter transitions from wake turbulence prediction to its practical implementation within runway capacity optimisation. Dynamic wake separation, as a flexible and adaptive approach, offers the potential to significantly improve runway throughput by reducing the conservatism inherent in traditional static separation standards. This chapter focuses on quantifying the impact of dynamic wake separation on runway capacity, investigating both theoretical and operational perspectives and comparing its performance under traditional FCFS scheduling and advanced optimisation strategies. Through a detailed runway sequencing and scheduling model, combined with dynamic separation matrices, the study evaluates the extent to which time-based and weather-responsive separation can unlock additional runway capacity and enhance runway utilisation without compromising safety during periods of high traffic density. This transition underscores the importance of bridging wake turbulence research with operational decision-making tools to balance efficiency and safety in runway operations.

5.1. Introduction

5.1.1. Research context

The terminal flight zone and the final approach region are two main areas that require

efficient traffic dispatch. Otherwise, misleading traffic planning may lead to unsafe flight conflicts or continuous and extensive traffic delays. The concern regarding congestion has escalated at significant international terminals in the United States, Europe and Asia. The primary cause of this phenomenon is the ongoing rise in air travel demand, which starkly contrasts the limited capacity to expand airport infrastructure, such as cargo terminals, passenger amenities, and runways. Consequently, it is imperative to take proactive measures, including investigating alternative capacity management strategies (Ikli et al., 2021) and aligning airline schedules with current airport capacity during the initial planning phases. These measures aim to alleviate congestion and reduce delays by optimising the utilisation of existing infrastructure, addressing demand-side challenges, and concurrently investigating initiatives to improve runway operational capacity to surmount supply-side constraints.

Runway operations are the primary impediment to airport capacity, as they are impeded by various operational constraints. Conservative distance-based aircraft separation, which is regulated to prevent aircraft conflicts and wake turbulence (ICAO, 2023), is one aspect that warrants attention. The separation minima in miles-in-trail are initially released for aircraft sequencing (Kopardekar et al., 2003). Nevertheless, such static separation management assumes the worst-case scenarios of wake encounters and may restrict the rate of aircraft throughputs in a particular time period in a sub-airspace, which results in delays and cascading delay propagation under severe weather or other uncertain situations. Diana (2015a) investigated the positive influence of implementing the RECAT separation standard in departure throughputs, utilising the Markov regime-switching model. The peak hour runway capacity in Paris Charles de Gaulle Airport has been shown to increase by 2-4 flights under RECAT separation (EUROCONTROL, 2018b). Li et al. (2021) simulated the benefits of fuel saving, especially for aircraft in

light and medium weight categories, under separation reduction in the oceanic airspace with satellite-based technologies.

5.1.2. Research gaps and objectives

There are also existing research studies concentrating on runway separation. Nevertheless, most of them concentrate on runway operational separation, which is regulated by air traffic controllers by margins exceeding the minimum aircraft wake separation (Gu et al., 2022; Pang et al., 2024). In addition, the static ICAO separation standards were implemented in the existing research on runway scheduling, whether for the single runway landing problem (Balakrishnan et al., 2010; Ng et al., 2017) or the multiple runways with the departure in modelling (Lieder et al., 2016; Malik et al., 2016; Pohl et al., 2021). Based on the authors' knowledge, there are few studies about separation reduction from the aircraft wake analysis perspective, and only a few attempts to integrate dynamic separation with runway operational optimisation.

Therefore, this research aims to investigate the impact of dynamic wake separation on runway capacity, focusing on both theoretical and operational aspects. By integrating advanced deep learning techniques for wake turbulence prediction with practical runway sequencing and scheduling models, the research examines the potential of dynamic separation matrices to reduce conservatism in static standards like RECAT-EU. Additionally, the study compares the performance of traditional FCFS scheduling with optimised scheduling strategies under dynamic wake separation. The goal is to develop a comprehensive framework for evaluating the effects of time-based and crosswind-responsive separation on total arrival times, flight delays, and overall runway efficiency in real-world operational scenarios, using Hong Kong International Airport as a case study. The contributions of this research are threefold:

(1) Advancement in wake separation techniques. This research introduces a dynamic wake separation model that leverages crosswind conditions and pairing characteristics to reduce separation intervals. The study demonstrates how dynamic adjustments can increase runway throughput, particularly under strong crosswind conditions, by achieving separation reductions tailored to aircraft categories in dynamic winds.

(2) Operational scheduling optimisations. By integrating optimisation algorithms for real-time runway sequencing and scheduling, the research achieves significant improvements over traditional FCFS strategies. Optimising scheduling under dynamic separation matrices reduces total arrival times and enhances operational flexibility, providing a viable alternative to static standards.

(3) Balanced decision-making for runway utilisation with enhanced theoretical and operational capacity. The research provides a dual-perspective runway capacity analysis by evaluating theoretical maximum capacity and real-world operational limitations. This comprehensive approach offers a deeper understanding of how dynamic wake separation influences runway performance under varying traffic and weather conditions, aiding in developing more resilient air traffic management strategies.

5.2. Methodology

5.2.1. Problem description

As aircraft take off and land, they generate wake vortices that can pose a risk to the following aircraft, necessitating specific separation distances to ensure safety. This dynamic nature of wake turbulence, which varies based on aircraft type, weight, and

environmental conditions, complicates the task of optimising runway operations. The 10-month arrival data at HKIA from 2019 January to October in **Figure 5-1** shows that the heavy traffic periods at HKIA are usually from 10:00 to 22:00, with the maximum number of arrivals reaching 30 to 35, and the historical Meteorological Aerodrome Report (METAR) data demonstrates high-frequency strong crosswinds above runways, which reveals the promising potential of implementing dynamic wake separation at this airport. In July, nearly 10 days of each peak hour experience a crosswind of over 3 m/s, and roughly half of a month experience an average crosswind of over 3 m/s.

Consequently, in this context, this section develops a comprehensive methodological strategy that is robust and flexible, allowing for real-time runway sequencing and scheduling while accommodating the variability of wake separation requirements with intelligent predictive modelling.

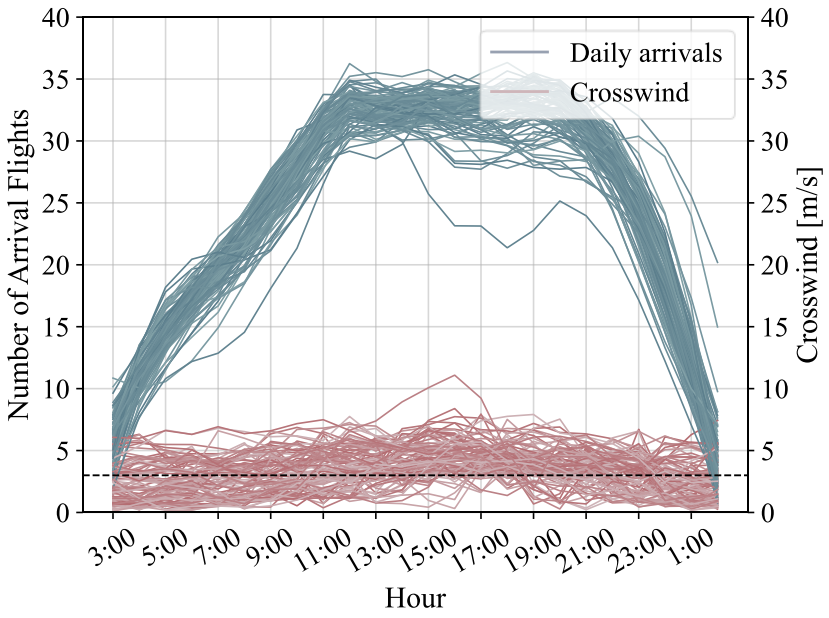

Figure 5-1. Arrival flight number by hour and daily crosswind at HKIA for peak traffic hours from January to October 2019.

5.2.2. Wake prediction model

Aircraft wake turbulence represents a multifaceted phenomenon, with its generation and movement predominantly influenced by aircraft configuration and flight performance, prevailing meteorological factors, and ground effects (Breitsamter, 2011). The initial attributes of the vortices, encompassing their spatial position and intensity, are determined by the aircraft's operational parameters, including weight, wingspan, lift distribution, and flight speed (Hallock et al., 2018). The subsequent evolution and dissipation of these vortices are markedly influenced by atmospheric elements, such as wind patterns and velocities, instances of wind shear, and the presence of atmospheric turbulence.

To accurately model wake dynamics, we incorporate a comprehensive range of wake-related features. These include wake positions and intensity obtained from LiDAR-derived radial wind data and aircraft performance parameters such as flight speed and weight categories defined by RECAT-EU standards. Additionally, METAR data are up-sampled to maintain consistent temporal alignment with wake data. Crosswind is a critical factor influencing wake presence during the final approach (Chu et al., 2024; Holzäpfel et al., 2021). We fuse crosswind measurements from both METAR and LiDAR to enhance the reliability of wind forecasts. Notably, headwinds are known to accelerate wake dissipation, whereas tailwinds have the opposite effect; thus, headwinds are also included as an input feature. Furthermore, we consider various meteorological factors, including temperature, humidity, and cloud conditions.

We have developed two kinds of deep learning models for dynamic wake prediction: the TCN model (Lea et al., 2016) and the MLP neural network, as depicted in **Figure 5-2**. All the above features can be denoted as X, and $t_0, t_1 \ldots, t_l$ represent the input

features in $0, 1 \ldots l$ time steps. l represents the last time horizon of the lifetime of a wake pair. The wake separation measured by wake presence in the standard approach path is labelled as y_{sep}.

The temporal convolution neural networks are adept at processing sequential data by capturing long-range dependencies through casual convolutions, making them well-suited for time series prediction tasks. We apply the structure of the TCN model developed in our previous work (Chu et al., 2024). These dilated causal convolutions enable the network to preserve the temporal order of input features while expanding the receptive field without the need for additional parameters. Notably, our current work differs from the previous study in the duration of the time window used for both current features and future forecasts. Conversely, the fundamental feed-forward neural network is designed to regress wake separation directly. The distinctions between these two models are summarised in **Table 5-1**. The TCN model predicts future 2D positions and the intensity of pairwise wake vortices over time, subsequently forecasting the required separation time for trailing aircraft. In contrast, the MLP model directly estimates the wake separation time using only initial wake features and other relevant features.

In addition to the above benchmarking models, we also utilised the transformer model for wake evolution prediction based on the initial wake information with a fixed input window size of 1 and 18 feature columns, combining the advantages of LSTM in feature embeddings. The transformer model is composed of an encoder and a decoder (Vaswani et al., 2017). The input layer accepts a three-dimensional tensor, including the temporal attributes and features of the input sequences. A masking layer is applied to ignore padded values in the sequence. The model proposed in this paper begins with a learnable positional encoding implemented using an LSTM layer with 16 units, which captures sequential dependencies and encodes positional information into the feature

embeddings. The encoder consists of two multi-head attention layers with 8 attention heads. The outputs are then combined with the positional encoding using residual connections, followed by layer normalisation to ensure numerical stability. The feed-forward networks with two dense layers and dropout regularisation are applied throughout the encoder to prevent overfitting. After the encoder, the output sequence is aggregated through a global average pooling layer, reducing the temporal dimension. The resulting feature vector is passed through a dense layer, followed by a final output layer to produce the model's predictions.

In addition to the dynamic wake separation predicted by the aforementioned deep learning models, we also propose two wake separation matrices informed by the 6×6 dimensional wake separation matrix of RECAT-EU (Chu et al., 2024), incorporating the effects of winds. Given that crosswinds are prevalent at HKIA and influence both the descent and lateral movement of wake pairs, we decouple the crosswind and headwind effects. For illustrative purposes, we focus on crosswinds to demonstrate their impact on wake separation. The values in these two crosswind-related wake separation matrices are verified against historical wake encounters for arrival flights from January to October 2019 (as shown in **Figure 5-3**), alongside our previous findings (Chu et al., 2024).

Table 5-1. Input and output features of the Transformer model, TCN model and MLP model for wake evolution and separation prediction.

Model	Input/output	Feature variables	Descriptions
Transformer/ TCN	Inputs	$X_l^{(t_0-t_{l-1})}, Z_l^{(t_0-t_{l-1})}, X_r^{(t_0-t_{l-1})}, Z_r^{(t_0-t_{l-1})},$ $G_l^{(t_0-t_{l-1})}, G_r^{(t_0-t_{l-1})}$	Wake data of leading aircraft i
		Cat^i, FS^i, TA^i	Flight performance data of leading aircraft i
		$u^{(t_0-t_{l-1})}, v^{(t_0-t_{l-1})}, Vis^{(t_0-t_{l-1})}, Tem^{(t_0-t_{l-1})},$ $Hum^{(t_0-t_{l-1})}, Dew^{(t_0-t_{l-1})}, Pres^{(t_0-t_{l-1})},$ $FEW^{(t_0-t_{l-1})}, SCT^{(t_0-t_{l-1})}$	METAR data in t_0 timestep
	Outputs	$X_l^{(t_1-t_l)}, Z_l^{(t_1-t_l)}, X_r^{(t_1-t_l)}, Z_r^{(t_1-t_l)},$ $G_l^{(t_1-t_l)}, G_r^{(t_1-t_l)}$	Future wake features of aircraft i in $t_1 - t_l$ timesteps
MLP	Inputs	$X_l^{t_0}, Z_l^{t_0}, X_r^{t_0}, Z_r^{t_0}, G_l^{t_0}, G_r^{t_0}$	Wake data of leading aircraft i
		Cat^i, FS^i, TA^i	Flight performance data of leading aircraft i
		$u^{t_0}, v^{t_0}, Vis^{t_0}, Tem^{t_0}, Hum^{t_0}, Dew^{t_0},$ $Pres^{t_0}, FEW^{t_0}, SCT^{t_0}$	METAR data in t_0 timestep
	Outputs	$\hat{y}_{sep}^i$	Dynamic wake separation of leading aircraft i

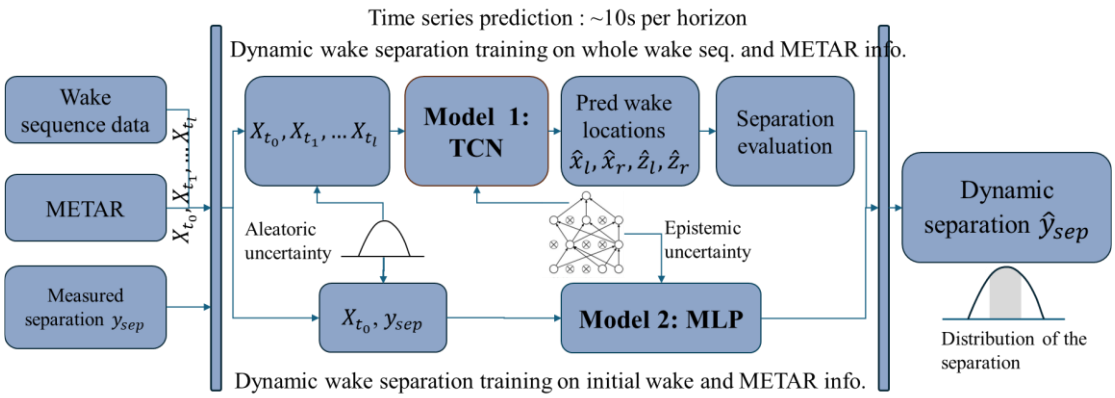

Figure 5-2. Two kinds of deep learning models for aircraft wake evolution and dynamic separation prediction.

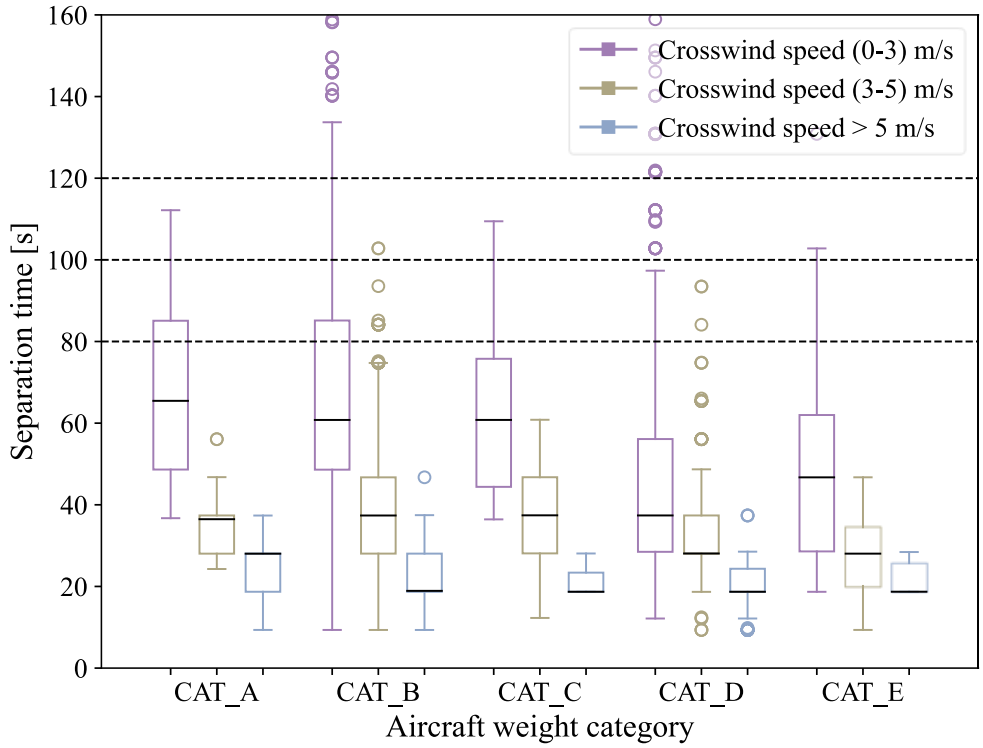

Figure 5-3. Relationships between wake separation and crosswind for all aircraft categories were measured based on detected wake vortices from January 2019 to October 2019.

Table 5-2 delineates the light-wind separation matrix (LW) applicable when crosswind speeds range from 3 to 5 m/s. This matrix introduces a nuanced separation reduction compared to the RECAT-EU standard, referred to as REGULAR in this research. Under the LW matrix, the separation time for aircraft classified as CAT_D and CA_E is adjusted to 120s when trailing aircraft from CAT_A or CAT_B. Furthermore, when following CAT_C aircraft, these separation times can be reduced to 100s or be minimised to the minimum values between the 80s and the minimum radar separation. For CAT_E aircraft specifically, the separation time can be minimised to 100 seconds when the preceding aircraft is categorised as CAT_D.

Conversely, **Figure 5-3** indicates that the separation matrix for crosswinds exceeding 5 m/s, designated as SW, permits the reduction to the minimum radar separation. It is important to note that these separation matrices assume stable, large-scale prevailing

crosswind conditions and are conservative as they apply to the entire wake turbulence region outside the flight approach path. Both headwind and vertical wind factors are relevant to horizontal wake length and vertical wake descent, underscoring the need for a holistic approach to determine wake presence at the final approach accurately.

For the predicted wake separations and the two wind-specific separation matrices, additional operational buffers have been established for both the open case in which the following aircraft is slower than the leading and the closed case in which the opposite is slower. In addition, final separations on the runway are subject to additional constraints, including Runway Occupancy Time (ROT) and Minimum Radar Separation (MRS). Consequently, the separation time t_{sep} is defined as the minimum value of these operational factors:

$$t_{sep} = min(t_{wake}, t_{ROT}, t_{MRS}) \quad (5\text{-}1)$$

Table 5-2. Dynamic wake separation matrix under light crosswind (LW-DWS, 3-5m/s).

	CAT_A	CAT_B	CAT_C	CAT_D	CAT_E
CAT_A	MRS	MRS	120s	120s	120s
CAT_B	MRS	MRS	MRS	120s	120s
CAT_C	MRS	MRS	MRS	100s	100s
CAT_D	MRS	MRS	MRS	MRS	100s
CAT_E	MRS	MRS	MRS	min(80s, MRS)	min(80s, MRS)

MRS: minimum radar separation. 3 nautical miles for CAT_(A, B), 2.5 nautical miles for CAT_(C,D,E).

5.2.3. Runway sequencing and scheduling model

The runway approach sequencing and scheduling problem (RSSP) involves determining the order in which aircraft should land and their specific landing time. Before the three-runway system, there are two independent runways for departure and

landing separately at Hong Kong International Airport. As the arrival phase is much more complex and dangerous than departure, we consider single-runway approach optimisation at HKIA utilising historical arrival data in this study.

5.2.3.1. Decision variables and objectives

The Nomenclature of this model is listed in **Table 5-3**. The single runway sequencing and scheduling problem in this research is defined on an aircraft set F in a time horizon. The decision variables include aircraft adjacent order y_{ij}, where

$$y_{ij} = \begin{cases} 1 \ i \text{ precedes } j, i, j \in F, \text{but } i \neq j, \\ 0 \ i \text{ not precedes } j. \end{cases} \quad (5\text{-}2)$$

y_{ij} take value 1 when aircraft $i \in F$ is precedes aircraft $j \in F \backslash \{i\}$ in the runway sequence. The aircraft landing time $t_i, i \in F$ is another decision variable. The runway sequence begins with a dummy starting aircraft s and finishes with a dummy ending aircraft e. A separation time S_{ij} is required to ensure safety when aircraft $i \in F$ and aircraft $j \in F \backslash \{i\}$ use the runway consecutively. For each aircraft $i \in F$ the earliest possible landing time of each aircraft $i \in F$ is E_i and the latest possible landing time is L_i. Aircraft $i \in F$ should be scheduled within its time window $[E_i, L_i]$, which implies that the landing time or take-off time t_i should be greater than E_i and no later than L_i.

Runway efficiency is one of the most important objectives in runway operations. Thus, minimising the total arrival time (Makespan) for all aircraft is taken as the objective. The total arrival time is defined as the deviation between the maximum arrival time z and the minimum arrival time r, with the total delay time included to make sure arrival equality from airlines' perspectives.

$$L = \min(W_1 * (z - r) + W_2 * \sum_{i=1}^{F} d_i) \quad (5\text{-}3)$$

Table 5-3. Nomenclature and descriptions.

Sets	Description
F	Set of actual aircrafts
Parameters	Explanations
S_{ij}	Separation time required between consecutive aircraft i and j
E_i	Earliest possible landing time of aircraft i
L_i	Latest possible landing time of aircraft i
W_1	Weight of Makespan
W_2	Weight of total delay time
K	Constraint of the maximum position shifting for each aircraft
IP_i	Initial position of aircraft i
Decision variables	Explanations
y_{ij}	1, if aircraft i precedes aircraft j; 0, otherwise
t_i	Landing time of aircraft i
z	Makespan, the maximum arrival time
r	Minimum arrival time
d_i	Delay time of aircraft i
Pos_i	Order index in the arrival sequence of aircraft i

5.2.3.2. Constraints

Table 5-4 defines the constraints regarding this ASSP model. Constraints (5-4) ensure each aircraft is within the runway sequence. Constraints (5-5) and (5-6) guarantee that the runway sequence starts with a dummy starting aircraft s and ends with a dummy ending aircraft e. Constraints (5-7) maintain the flow conservation of each runway sequence. Constraints (5-8) require that the landing time of the aircraft i should be within its time window. Constraints (5-9) ensure the separation time between two aircraft that land consecutively. Constraints (5-12) determine the delay time of each

aircraft. Constraints (5-13) define the domain of decision variables. W_1 and W_2 indicate the trade-off between Makespan and delay time. Eq. (5-15) constraints the maximum position shifting of each aircraft compared to their initial position in the estimated sequence. Eq. (5-16) makes sure that the position for each aircraft is unique, and Eq. (5-17) constraints the positions of two closely adjacent aircraft. Eq. (5-17) defines the minimum arrival time of this aircraft sequence.

The above constraints also apply to the objective of minimising only the total delay time. To minimise only the Makespan, in addition to the constraints from Eq. (5-4) to Eq. (5-11), the Makespan should be a positive real number and the determination of the Makespan is also required to be defined, $z \geq t_i, \quad \forall i \in F$.

Table 5-4. Overall constraints and special constraints for each element in the objective function.

$$\sum_{j \in F \cup \{e\}} y_{ij} = 1, \quad \forall i \in F, \tag{5-4}$$

$$\sum_{j \in F} y_{sj} = 1, \tag{5-5}$$

$$\sum_{i \in F} y_{ie} = 1, \tag{5-6}$$

$$\sum_{j \in F \cup \{s\}} y_{ji} = \sum_{j \in F \cup \{e\}} y_{ij}, \quad \forall i \in F, \tag{5-7}$$

$$E_i \leq t_i \leq L_i, \quad \forall i \in F, \tag{5-8}$$

$$t_i + S_{ij} - t_j \leq M\left(1 - y_{ij}\right), \quad \forall i \in F, \forall j \in F, i \neq j, \tag{5-9}$$

$$y_{ij} \in \{0,1\}, \quad \forall i \in F \cup \{s\}, \forall j \in F \cup \{e\}, i \neq j, \tag{5-10}$$

$$t_i \in \mathbb{R}^+, \quad \forall i \in F, \tag{5-11}$$

$$d_i \geq t_i - E_i, \quad \forall i \in F, \tag{5-12}$$

$$d_i \in \mathbb{R}^+, \quad \forall i \in F, \tag{5-13}$$

$$z \geq t_i, \quad \forall i \in F, \tag{5-14}$$

$$IP_i - K \leq Pos_i \leq IP_i + K, \quad \forall i \in F, \tag{5-15}$$

$$Pos_i \neq Pos_j, \forall i \in F, \forall j \in F, i \neq j, \tag{5-16}$$

$$Pos_j \geq Pos_i + 1 - M * \left(1 - y_{ij}\right), \tag{5-17}$$

$$r \leq t_i, \forall i \in F. \tag{5-18}$$

5.3. Experiment setting

5.3.1. Data preparation

The actual historical arrival time of these flights was kept as a benchmark for arrival flight optimisation under dynamic separation prediction. As shown in **Figure 5-4**, the aircraft landing at HKIA in February 2019 is mainly in CAT_B and CAT_D, with almost no light aircraft.

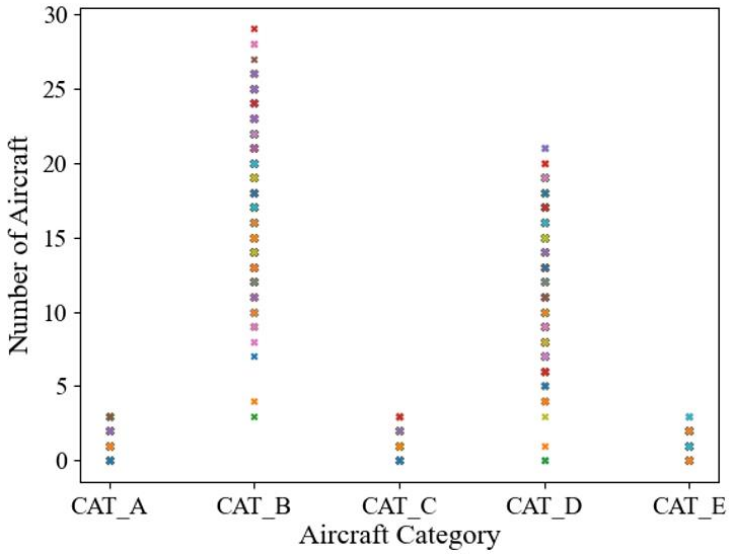

Figure 5-4. Landing aircraft number at HKIA in February 2019.

5.3.2. Model training configuration

This study utilised four months of aircraft wake vortex data detected by LiDARs at HKIA, resulting in 10,212 wake sequences from arrival flights after data cleaning. Wake separation time was derived from the wake presence during the entire evolution process on the final approach path. The evolution of a wake pair is represented by a time series of its location and strength, with time steps of approximately 12s and 9s for LiDARs at the entrances of runways 25R and 07L, respectively. Additionally, METAR data, updated every half hour, were incorporated as features for wake separation

prediction. These include wind direction, speed, temperature, visibility, and other weather phenomena.

To prevent overfitting, dropout regularisation was employed. A grid search was conducted to optimise hyperparameters for both models, including neuron count, kernel size, learning rate, and batch size. Model performance was assessed using the Mean Absolute Error (MAE) and the Root Mean Square Error (RMSE). The results indicate that the TCN model achieved optimal performance with a learning rate of 0.0001 and a batch size of 256, while the MLP model performed best with a learning rate of 0.0005 and the same batch size. 60% of the datasets were randomly selected for model training, with the remaining data equally divided into validation and test datasets. The training was conducted over 1000 epochs.

The RSSP model is built and solved in Gurobi, which is a leading commercial optimisation solver widely used for solving complex mathematical optimisation problems. It integrates the heuristic method and the Branch and Bound algorithm to solve the MILP problems. The heuristic method provides good and feasible solutions early in the process and guides the search. The branch and bound algorithm systematically explores branches of a tree where each node represents a subproblem, solves linear relaxations of the subproblems, and uses bounds to prune branches that cannot lead to an optimal solution. The allowable arrival time window for each flight is defined to be 20 minutes before and after the estimated arrival time at most.

5.4. Numerical results

5.4.1. Wake separation prediction performance

Table 5-5 compares the performance of the proposed Transformer model against two baseline models, the TCN model and the MLP model for predicting wake positional

attributes and wake separation. The performance is evaluated using MAE and RMSE across different feature sets. With the inclusion of weather features (Wake, flight information and weather), the Transformer model achieves the best performance in wake separation prediction across all metrics, with 22.34% improvement in MAE and 13.75% improvement in RMSE compared to the TCN model. When only considering the wake and flight information in the feature set, the Transformer model outperforms the TCN model with a 56.6% improvement in MAE and a 51.87% improvement in RMSE, highlighting its ability to capture wake separation dynamics even in the absence of weather data. Furthermore, compared to the MLP model, the Transformer model achieves substantial gains with a 68.91% improvement in MAE for wake separation prediction. These results emphasise the superior capability of the proposed Transformer model in modelling complex temporal dependencies and effectively utilising additional weather data, leading to more accurate and reliable predictions in wake attribute and separation modelling.

It is worth mentioning that the wake location prediction achieved by these deep learning models is more significant than that observed in wake separation prediction. This disparity arises primarily due to the conservative approach used in measuring wake separation to improve flight safety.

5.4.2. Performance of theoretical runway capacity under dynamic wake separation

The runway capacity can be defined from theoretical (Hockaday et al., 1974) and operational aspects (Farhadi et al., 2014). Theoretical runway capacity refers to the maximum number of aircraft movements a runway can handle under ideal conditions of perfect efficiency and no delays or interruptions. It is calculated based on factors such as runway configuration and aircraft performance. On the other hand, operational

runway capacity represents the actual number of aircraft movements a runway can accommodate in real-world conditions, reflecting practical limitations and inefficiencies considering factors such as air traffic control strategies, operational constraints, traffic demand and weather situations. This research investigates the effect of dynamic wake separation on both the theoretical and operational capacity of the single-runway arrival at HKIA.

Table 5-5. Performance of proposed models in wake attributes prediction and wake separation prediction.

Probabilistic wake prediction model	Features	MAE(m)				MAE(s)	RMSE(m)				RMSE(s)
		X_l	Z_l	X_r	Z_r	Separation	X_l	Z_l	X_r	Z_r	Separation
Transformer	Wake and flight info. + weather	20.81	7.64	22.45	7.69	6.85	31.54	10.55	33.62	10.78	12.36
	Wake, flight info.	49.48	7.93	47.96	7.62	8.15	74.77	10.83	71.30	10.71	13.97
Probabilistic TCN model	Wake and flight info. + weather	23.48	7.52	22.45	8.23	8.82	33.87	10.09	33.73	11.05	14.33
	Wake, flight info.	52.42	7.84	54.70	7.57	18.80	82.62	10.90	83.82	10.55	29.02
Probabilistic MLP	Wake and flight info. + weather	-	-	-	-	22.04	-	-	-	-	29.71
	Wake, flight info.	-	-	-	-	23.52	-	-	-	-	31.46

Theoretical arrival capacity at a single runway refers to the maximum number of aircraft that can land on the runway per hour at the minimum interval between successive landings. This interval depends on several factors, including the proportion of pairs of landings between different aircraft types P_{ij}, their wake separation $t_{wake_{ij}}$, flight speed V_i, V_j and the ROT of the leading aircraft. Based on the pairing situations of historical landing aircraft at HKIA, as depicted in **Figure 5-5** and **Table 5-6**, the results of theoretical arrival capacity under different levels of wake separation reduction can be referred to in **Table 5-7**. **Figure 5-5** shows that the most frequent arrival pairs exist between aircraft in CAT_B and CAT_D. The highest pairing frequency is in (CAT_B, CAT_B) with 35.73%, which means both the leading and following aircraft are in the CAT_B category. Furthermore, there is over 50% probability that the aircraft in CAT_D follows the aircraft in CAT_B. The low efficiency of this scheduling by the ATCOs is evident as a larger separation time is required compared to that when aircraft in CAT_D leads.

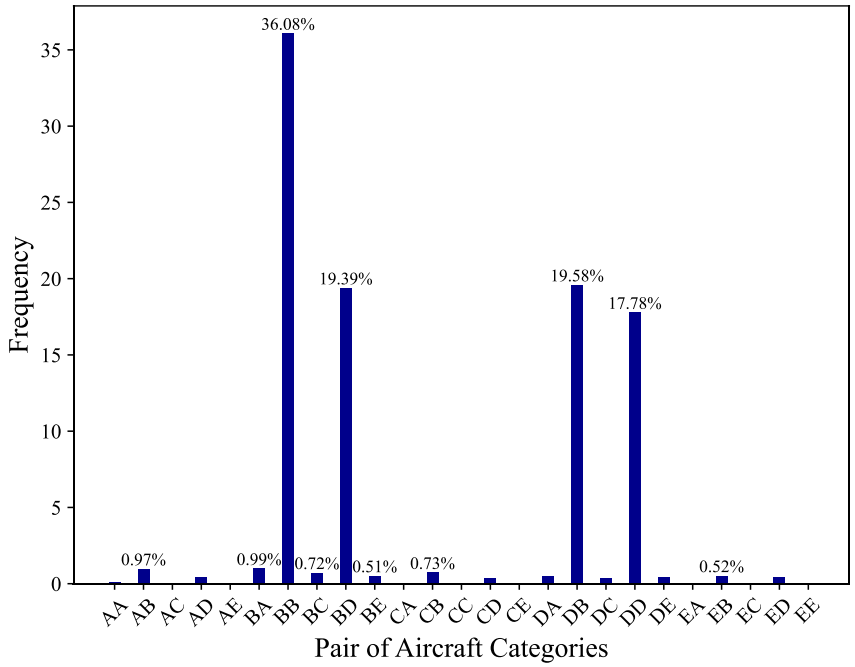

Figure 5-5. Probability of landing aircraft pairs at HKIA from 11:00-21:00 in February 2019.

Table 5-6. The probability of the occurrence of various aircraft combinations at the HKIA.

	CAT_A	CAT_B	CAT_C	CAT_D	CAT_E
CAT_A	0.0872%	0.97%	0.042%	0.427%	0.0312%
CAT_B	0.985%	**36.00%**	0.719%	**19.3%**	0.511%
CAT_C	0.0026%	0.726%	0.00134%	0.357%	0.000714%
CAT_D	0.499%	**19.50%**	0.356%	**17.7%**	0.423%
CAT_E	0.0182%	0.517%	0.000907%	0.440%	0.000208%

Table 5-7. Theoretical runway capacity at the HKIA under aircraft wake separation reduction.

Capacity	Arrival in a single runway
Separation of RECAT-EU	44.74
Separation matrix under crosswind of 3-5 m/s	44.92
Separation matrix under crosswind of over 5 m/s	47.08

5.4.3. Performance of dynamic wake separation under FCFS strategy

FCFS is a fundamental and straightforward principle used in runway scheduling for air traffic controllers to manage the sequence of aircraft arrivals and departures. Under this system, aircraft are processed equally by the order they arrive at the initial approach fix (IAF). However, it may lead to strong delays in peak hours, especially if a slower aircraft arrives first, causing subsequent aircraft to wait longer than necessary. The near real-time arrival sequencing and scheduling based on optimisation algorithms can contribute to more efficient and flexible landings and reduce wait times at busy airports. Therefore, both the FCFS and the RSSP scenarios under aircraft wake separation reduction are considered in this section in comparison with the static wake separation standards to analyse runway operational capacity.

The results presented in **Table 5-8** highlight the impact of dynamic wake separation (DWS) on total arrival time in the FCFS strategy under various wind conditions. The

separation for each aircraft under DWS is dynamically determined based on the crosswind speed levels within an estimated arrival time window of 6 minutes. Firstly, under FCFS sequencing managed by ATCOs, incorporating weather-related wake separation, particularly DWS, significantly decreases overall arrival time. Across the scenarios, DWS shows the greatest improvement, with reductions of up to 19.79% in Scenario 1 compared to the static RECAT-EU standard. This underscores the potential of adaptive wake separation to optimise runway throughput under dynamic wind conditions. Secondly, the improvements observed in the last two columns for Scenarios 2 and 4 are similar, with both showing strong reductions in total arrival time (18.81% and 13.10% for the three-level separation matrix, and 19.53% and 14.95% for DWS, respectively). This similarity is attributed to the highest crosswind levels in these scenarios, which enable both the three-level separation matrix and DWS to achieve the minimum allowable wake separation. This adaptive approach ensures that separation standards are tailored to the prevailing wind conditions during the arrival window, allowing for more efficient runway operations while maintaining safety.

5.4.4. Performance of dynamic wake separation in large-scale runway scheduling

Table 5-9 highlights the effectiveness of the runway sequencing and scheduling process in further improving total arrival time compared to the FCFS strategy employed by ATCOs. The time limit in the optimisation process is set to ensure a feasible solution rather than achieving an optimal one due to the computational burden of the scheduling objective. The arrival time range for each aircraft is restricted to a [-20, 20] minute window around the planned arrival time, balancing computational efficiency with practical feasibility while still yielding significant improvements in runway throughput.

Table 5-8. Scenario analysis of total arrival time under different separation matrices in the First-Come-First-Serve strategy.

Scenarios	Time horizon in peak hour	Aircraft number	Total arrival time (s)			
			Real arrival time	FCFS + RECAT-EU	FCFS + 3-level separation matrix	FCFS + DWS
1	20190105 14:01-15:01	34	3600	3302 (8.28%)	2987.3 (**17.02%**)	2887.5 (**19.79%**)
2	20190117 08:57-10:05	36	4080	3489.3 (14.48%)	3312.4 (18.81%)	3283.2 (19.53%)
3	20190224 15:02-16:00	33	3480	3210 (7.76%)	3118.8 (10.38%)	2969.7 (14.66%)
4	20190225 13:59-15:00	35	3660	3392.4 (7.31%)	3180.5 (13.10%)	3112.7 (14.95%)
5	20190529 14:01-15:00	33	3540	3399.8 (3.96%)	3143 (11.21%)	3034 (14.29%)
6	20190105 14:01-16:59	95	10680	9266.9 (13.24%)	8701.19 (18.52%)	8424.9 (21.13%)

Across all scenarios, RSSP strategies incorporating DWS demonstrate a significant reduction in total arrival time, with improvements exceeding 20% in several cases, particularly when no position shifting constraints are applied. For instance, in Scenario 1, RSSP with DWS achieves a 23.67% improvement, showcasing the benefits of optimised sequencing and scheduling. In addition, introducing position shifting constraints for each aircraft, such as when K=5 scenario, results in a slight increase in total arrival time. For example, in Scenario 5, the total arrival time increases marginally

from 2737s to 2767s when position shifting of maximum 5 is limited. This indicates a trade-off between flexibility in aircraft sequencing and achieving optimal arrival efficiency.

Table 5-9. Scenario analysis of total arrival time under different separation matrices with aircraft sequencing and scheduling.

Scenarios	Time horizon in peak hour	Aircraft number	Total arrival time (s)				
			Real arrival time	RSSP + RECAT-EU	RSSP + 3-level separation matrix	RSSP + DWS (K=N)	RSSP + DWS (K=5)
1	20190105 14:01-15:01	34	3600	3004 (16.56%)	2878.69 (20.04%)	2748 (**23.67%**)	2763.1 (23.25%)
2	20190117 08:57-10:05	36	4080	3323.6 (18.54%)	3278.1 (19.64%)	2939 (**28.00%**)	2942.3 (27.91%)
3	20190224 15:02-16:00	33	3480	2948.5 (15.27%)	2960 (14.94%)	2766.9 (20.49%)	2782.1 (20.06%)
4	20190225 13:59-15:00	35	3660	3148.2 (13.98%)	3096.8 (15.39%)	2919.7 (20.23%)	2928.3 (19.99%)
5	20190529 14:01-15:00	33	3540	2890 (18.36%)	2867.8 (18.98%)	2737.6 (**22.66%**)	2767.8 (21.81%)

5.4.5. Discussion

The findings from the above two tables have several limitations in implementing dynamic wake separation, particularly in operational scenarios. The development and application of weather-related wake separation matrices heavily rely on accurate and advanced wind forecasting at low altitudes above the runway. Wind conditions, such as

crosswinds, headwinds, and tailwinds, can vary significantly in direction and intensity due to localised atmospheric phenomena. This paper focuses on crosswind-prevailing situations as an example of dynamic wake separation, but the complexity of real-world wind variability underscores the need for more comprehensive meteorological modelling to enhance the reliability and robustness of these matrices.

Furthermore, we cannot deny that chasing efficiency in runway throughput may lead to increased flight delays, which is unexpected from the airlines' benefits perspective. While dynamic wake separation successfully reduces total arrival times, its impact on other critical performance metrics, such as flight delay and passenger connection times, has not been thoroughly investigated. Understanding these trade-offs is crucial for balancing operational efficiency with stakeholder priorities, including airline schedules and passenger satisfaction. Specifically, the macroscopic impact of dynamic wake separation in terminal approach traffic flow will be investigated in Chapter 6.

In addition, the proposed wake prediction model and dynamic separation matrices were tested using data from a single airport, Hong Kong International Airport. Verifying these methods at other airports with different traffic densities, runway configurations, and meteorological conditions is essential to validate their generalisability and scalability. This broader evaluation would ensure the applicability of the models to diverse operational environments and improve their utility in global air traffic management systems.

5.5. Conclusion

This study suggests a new approach to runway sequencing and scheduling that addresses the challenges associated with dynamic pairwise wake separation. This investigation aims to optimise airport operations and improve decision-making processes by utilising simulation-based techniques and machine learning. The findings

are anticipated to contribute to the body of knowledge in air traffic management and provide practical solutions for existing aviation challenges.

Overall, two deep-learning models are proposed to predict pairwise aircraft wake separation utilising historical LiDAR wake data and ADSB flight trajectory data at HKIA. The relationships between crosswinds and wake separation time for aircraft in each weight category are explored with the conservative separation reduction inferred. Further, two wake separation matrices with reduction under two levels of crosswinds are proposed based on the RECAT-EU standards. Finally, the runway operational efficiency of these three wake separation strategies is tested in both the FCFS principle and RSSP problem based on actual arrival information at HKIA. Both the improvements in theoretical arrival capacity and operational arrival throughputs of the arrival in a single runway are explored. The above work would contribute to improving runway throughputs and capacity and developing efficient, proactive runway scheduling methods, especially for high-density traffic scenarios in abnormal events.

Chapter 6. Integrated terminal traffic flow management and managerial effect under dynamic wake separation

The preceding chapters have progressively established the foundation for leveraging dynamic wake separation and its effect on runway capacity at a microscopic level, addressing single-runway sequencing and scheduling. By constructing and solving the runway scheduling model with dynamic separation matrices, the study demonstrated how adaptive wake separation could optimise runway throughput under both FCFS and advanced optimisation algorithms, particularly when compared to traditional static separation standards such as RECAT-EU.

Based on these insights, this chapter further expands the scope of analysis to a macroscopic level, exploring the broader implications of dynamic wake separation on terminal traffic flow management. Beyond single-runway optimisation, the final part of this thesis integrates the dynamic wake separation framework into a holistic approach for high-density airspace scenarios. The study evaluates the contributions of time-based wake separation to overall terminal traffic flow efficiency and assesses the scheduling burden of separation reduction in the final approach to terminal flight path control. By verifying the implementation of dynamic wake separation at the terminal-wide level, this chapter presents a comprehensive strategy for optimising air traffic management in congested terminal areas, providing actionable insights for air traffic controllers and airport managers in addressing future challenges in high-demand environments.

6.1. Introduction

The Terminal Manoeuvring Area and runway are vital elements of the air traffic

management system, significantly influencing airport throughput and operational efficiency. Given the continuous rise in air travel demand and alongside limited opportunities to expand runway configurations and infrastructure, improving capacity and efficiency and reducing congestion have become an imperative concern at major international airports for addressing demand-supply imbalance challenges. Consequently, it is crucial to implement proactive measures that include exploring alternative capacity management strategies (Ikli et al., 2021) and aligning airline schedules during the initial planning stages.

Time-based separation (TBS) supplants the traditional distance-based separations with temporal separations, thereby enabling greater adaptability to fluctuating weather conditions. The delay propagation of inefficient aircraft separation is investigated in (Louie et al., 2023). Morris et al. (2013) investigated the implementation of time-based separation under different levels of headwind and verified the separation using LiDAR wake data and wake encounter risk analysis. However, this kind of time-based separation is achieved by adjusting ground flight speeds and by referring to the distance-based RECAT-EU wake separation standard. Baren et al. (2016) also developed a data-driven model to forecast approach speed and time to fly, taking into account current headwind conditions and aircraft type by utilising radar and weather data. Nonetheless, the dynamic time-based separation is not analysed from the perspective of wake evolution under dynamic wind conditions.

As illustrated in Section 2.2, there are existing research studies concentrating on aircraft separation based on historical flight data. Visscher et al. (2018) applied the machine learning model to regress time-based pairwise operational separation with buffer based on one-year traffic data, aircraft types and local weather data. The operational separation, which is regulated by air traffic controllers by margins that

exceed the minimum aircraft wake separation and is affected by traffic conditions, is also investigated (Gu et al., 2022; Pang et al., 2024). However, the aircraft separation derived from historical flight data is conservative, with the operational buffer taken into consideration.

To the best of the authors' understanding, the existing studies concerning the reduction of separation standards through analysing aircraft wake characteristics are rather limited. Furthermore, few of them endeavour to integrate dynamic separation strategies with runway optimisation. According to the roadmap outlined in the SESAR wake project (Barbaresco et al., 2013), the development of weather-adaptive wake separation criteria and the implementation of pairwise wake separation are identified as natural progressions from traditional time-based separation, which warrant further academic and industrial research.

The physical-based wake estimation has not capitalised on the advantages offered by extensive historical data, resulting in limited simulations of real-world environments (Mutuel et al., 2014). Furthermore, the efficient approach towards weather-related dynamic wake separation in the final approach and its impact on the runway and airside operations and Air Traffic Controllers (ATCOs)' situational awareness and workload remain unclear. Therefore, this research is inspired to explore a synthetic solution for dynamic wake separation and its implementation in integrated terminal arrival control. The contributions of this study are as follows:

1. This research presents an integrated TMA arrival optimisation framework based on data-driven dynamic wake separation prediction. Two kinds of deep learning models are developed to infer dynamic wake separation time. Compared to the multiple-layer perception model, the temporal convolutional network achieves superior performance in separation interval inference based

on wake attributes forecasted in time series.

2. Based on the dynamic wake separation results, we propose the K-CPS-based SA algorithm for integrated flight arrival sequencing and arrival time optimisation from terminal airspace to the runway at HKIA. The K-CPS strategy avoids the greedy behaviour in local search to some extent and achieves reduced arrival time by changing the decision sequences with positional constraints.

3. The effect of weather-related and pairwise wake separation on terminal arrival control at HKIA is evaluated based on historical traffic data from several aspects, including operational capacity, flight delay and ATCOs' workload. The simulation results indicate that the dynamic wake separation in the final approach with time reduction may pose scheduling pressure to terminal airspace before the initial approach fix. Nonetheless, this problem can be solved by integrated traffic flow optimisation in extended TMA. The total arrival time can be reduced without evident flight delay and flight speed change. Furthermore, the runway arrival throughput can be continuously improved under the rolling horizon in comparison with traditional RECAT-EU separation.

4. The exploration of dynamic wake separation enriches existing studies on time-based aircraft separation. Furthermore, the proposed methodological framework utilising advanced dynamic wake prediction and separation assessment may be tailored based on traffic density and weather conditions, thereby providing an alternative solution of the decision support tool for automating and integrating runway scheduling with terminal traffic flow optimisation, and finally leading to an efficient, intelligent and streamlined air traffic management.

6.2. Problem description and modelling

This section develops a methodological strategy for scheduling arrival aircraft in TMA and runway jointly while also accommodating the variability of wake separation requirements with intelligent predictive modelling. **Figure 6-1** illustrates the overall methodological flowchart of this study, which consists of four parts. First, the historical arrival trajectory data at HKIA from ADS-B is processed. The entry waypoint, entry time and entry speed of each flight are picked to build the flight sets for consequent scheduling. Furthermore, the flight data with aircraft performance are utilised for wake separation time or wake decay prediction, along with the wake vortex data retrieved from radial wind data scanned by LiDAR, and the METAR data. Consequently, the predicted wake separation and the flight data are used to model the arrival problem in TMA, which is constructed as a graph based on the Standard Terminal Arrival Routes (STARs) at HKIA. Finally, the test scenarios of historical arrival flights are optimised under several operational constraints to achieve both flight safety without conflict and approach efficiency with minimum arrival time.

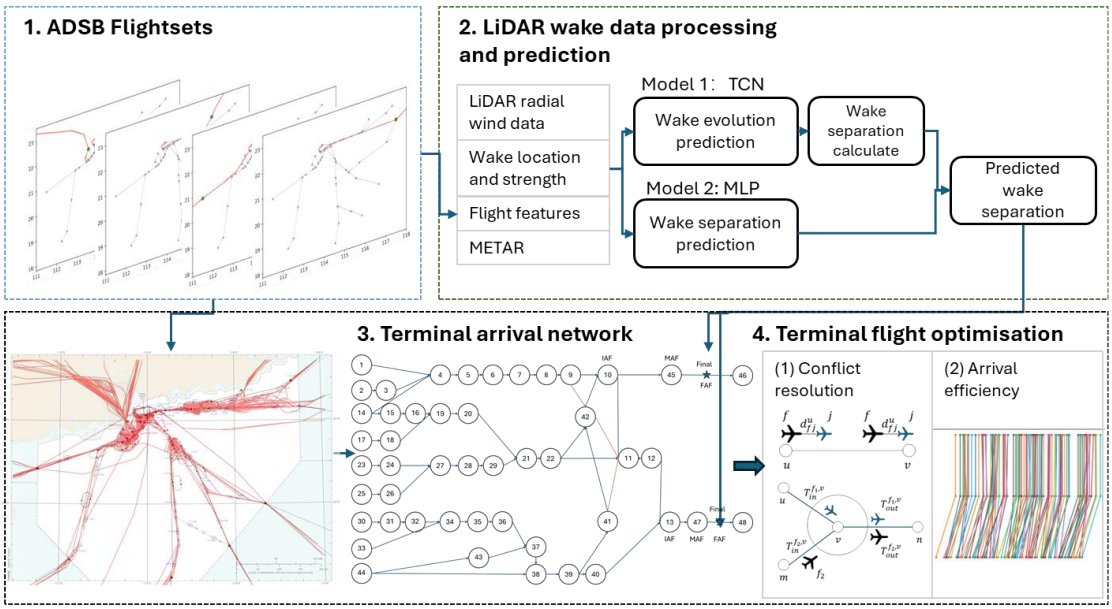

Figure 6-1. Methodological framework of integrated terminal arrival management under

dynamic wake separation prediction.

6.2.1. Network structure

In the context of terminal airspace management, aircraft approaching from multiple directions must be integrated and sequenced into a cohesive traffic flow. This integration adheres to the Standard Terminal Arrival Routes, which are pre-established flight paths that dictate altitude and speed in certain waypoints and serve as a reference for ATCOs when issuing scheduling directives. The STARs of HKIA are illustrated in **Figure 6-2**, featuring 9 entry waypoints at the boundaries of the terminal sector, oriented in various directions, 2 runway entrance points for the approach runway in the north, and 51 alternative paths. The STAR network is represented as a graph $G(N, L)$, where N denotes the set of waypoints that correspond to the routes defined by the STARs, and L is the set of links that represent the ensemble of direct connections between these waypoints, visualised as straight-line segments. To mitigate the accumulation of positional errors inherent in geographic coordinate systems and to simplify the calculation of distances, the spatial coordinates of all waypoints have been converted into a Cartesian Orthogonal Coordinate System.

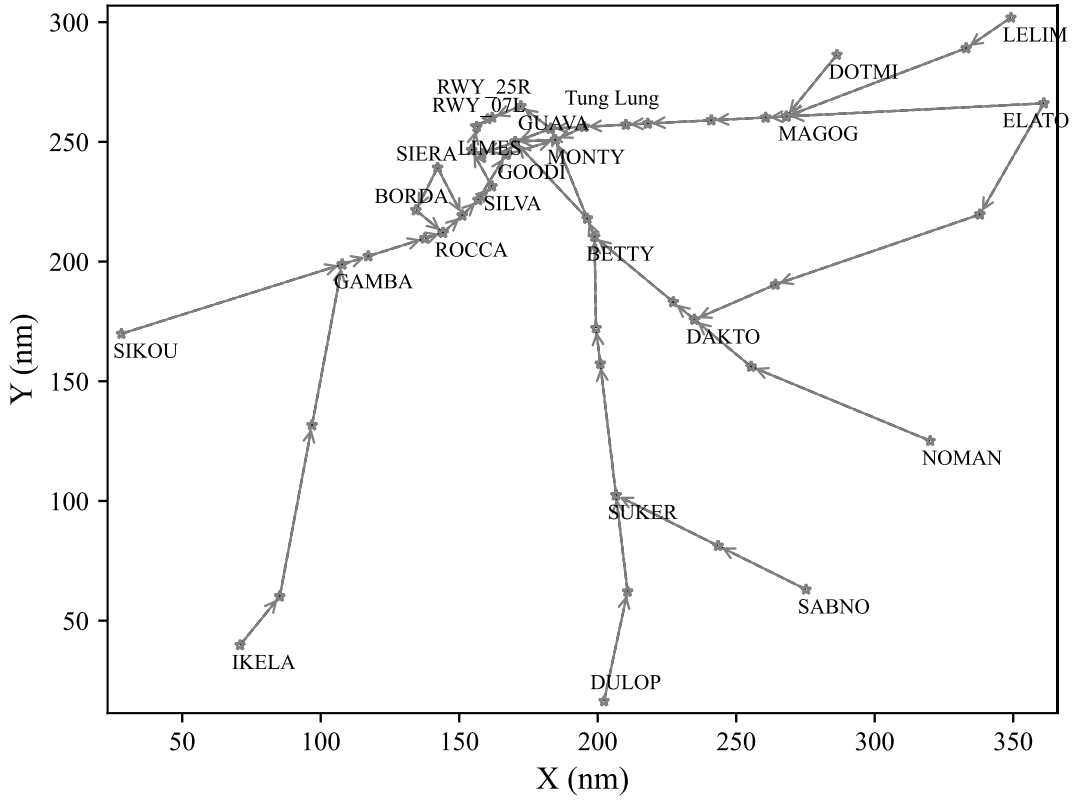

Figure 6-2. Standard terminal arrival route at the Hong Kong International Airport.

6.2.2. Problem modelling

6.2.2.1. Assumptions of the terminal traffic flow model

Before we model the terminal arrival problem, assumptions from several operational aspects are made:

- Wake separation: the predicted dynamic wake separation of the leading aircraft is assumed to be applicable to subsequent aircraft across all weight categories in stable, large-scale wind conditions above the runway. Additionally, the crosswind-related separation matrices proposed in this study suit atmospheres with prevailing and stable crosswinds.
- Network structure and paths: the network structure is deterministic, and any changes in the approach paths are unavailable within the decision horizon.

STARs are built in two-dimensional space, intentionally excluding flight levels to enhance computational efficiency.

- ATC operational regulation: flights approach in the TMA following the STARs. Any route changes out the scope of alternative paths, aeronautical holding, missed approaches and other ATC operations are not considered. The daily flights in peak hours are assumed to arrive at the same end of a single runway without a runway configuration switch.
- Flight performance on the paths: aircraft enter the TMA with fixed flight speeds and deterministic entry waypoint, and the aircraft approaches with a constant deceleration. Furthermore, the average flight speed on each link is considered in this model, with the speed constrained by ATC in STARs.
- Scheduling scale: the air traffic control is limited to approaching the terminal area without involving ground operations or cruise operations. However, aircraft may arrive at the entrywaypoints in a predefined time window. This is assumed to be realised by regulating speed in the cruise phase.

6.2.2.2. Decision variables

This research aims to schedule the arrival aircraft in the TMA under dynamic wake separation in the final approach. Therefore, the scheduling includes selecting the route for each aircraft entering the TMA and changing its flight speed to ensure flight safety and flow efficiency in the entire route until all aircraft reach the initial approach fix, and then merge to the final approach fix and arrive at the runway under the constraint of dynamic wake separation. Given a set of flight data F, for aircraft i, $i \in F$, the decision variables are in three types:

1. TMA entry time t_i. The entry time is predefined in a time slot $[t_i^o + \Delta T_{min}$,

$t_i^o + \Delta T_{max}]$, where ΔT_{min} and ΔT_{max} represent the maximum advance and delay compared to the planned entry time t_i^o, respectively. Further, a time-slot discrete variable $j, j \in Z$ is utilised to define the entry time, where $t_i = t_i^o + j \cdot \Delta T$ and ΔT is the time length adjusted by each step. The benchmarks of ΔT_{min} and ΔT_{max} are defined as 0 mins and 30 mins, respectively, and ΔT is set to be 5s. The impact of the entry time window in optimisation is also investigated in Section 6.4.

2. TMA entry speed v_i before the final approach. As the extended TMA depicted in **Figure 6-2** covers quite a large airspace, in order to simulate flight performance in TMA more realistically, the initial entry speed v_i^o of aircraft i is defined by fusing its historical entry speeds at the TMA boundary and the average flight speeds on alternative paths in the high-altitude airspace before the initial approach fix. Furthermore, v_i is also optimised discretely by the speed increment Δv_i, which can be defined as:

$$v_i \in V_f := \{v_i^o + j \cdot \Delta v_i | j \in Z, \Delta v_{i,min} \leq j \cdot \Delta v_i \leq \Delta v_{i,max}\} \qquad (6\text{-}2)$$

Where $\Delta v_{i,min}$ and $\Delta v_{i,max}$ are set to be $-0.1v_i^o$ and $0.2v_i^o$, respectively, and $\Delta v_i = 0.01v_i^o$.

3. Flight path p_i. When an aircraft enters from the fixed entry waypoint, its flight path is in a set of alternative paths P_i that relates to this entry waypoint and runway entrance threshold $p_i \in P_i$.

6.2.2.3. Constraints

The constraints for this terminal traffic flow optimisation problem are mainly in two

aspects: the conflict avoidance in the TMA network and the separation requirements in the final approach under dynamic wake separation. Conflicts regarding the nodes and links define flight unsafety in the STARs. The violation of minimum aircraft separation in the final approach also contributes to runway conflict.

- Node conflicts. When the flight routes of several aircraft are merged at one node, the separation violation must be avoided. The protected zones in the vicinity of nodes are defined to measure the node conflict. A conflict is identified when the latest exit time of the leading aircraft exceeds the earliest entry time of the following aircraft within the same detection zone. $N_{ij}^{n}(s)$ represents both the conflict number and conflict time proportion between aircraft pair i,j at node n.
- Link conflicts. For aircraft flying on the same link, the current aircraft and the leading aircraft must keep a safe separation distance and a fixed sequence when they are entering, exiting the link and flying on the link. We use the $L_{ij}^{l}(s)$ to define both the conflict number and conflict time percentage which reveals the conflict severity of the consequent aircraft i and j at link l.
- Separation constraints in the final approach. As discussed in Subsection 5.2.2, the aircraft separation s_{ij} in the final approach towards the runway is under constraints from several aspects. The conflict situation of the adjacent aircraft pair on runway r is defined as:

$$P_{ij}(s) = \begin{cases} 1, \text{if } 0 \le t_i^r(s) - t_j^r(s) < t_{ij} \\ 0, \text{otherwise} \end{cases} \quad (6\text{-}3)$$

- Earliest TMA entry time and runway arrival time in the rolling horizon. In the rolling horizon, the decisions of flights optimised in the last time horizon will

be frozen and serve as constraints for optimisation in the current time horizon. Specifically, the TMA entry time for flights under optimisation should be no less than the latest TMA entry time of each corresponding entry waypoint decided in the last horizon. Furthermore, the earliest runway arrival time on the current horizon should maintain a safe separation deviation with the largest arrival time in the last frozen flight set.

In conclusion, the total conflict regarding the decision vector s is:

$$A(s) = \sum_{i,j \in F, i \neq j} \left\{ \sum_{n \in C_n} N_{ij}^{n}(s) + \sum_{l \in C_l} L_{ij}^{l}(s) + \sum S_{ij}(s) \right\} \tag{6-4}$$

where C_n and C_l are the set of nodes and links at the STARs, respectively. In addition, the conflicts relating to separation are all manifested in time-based on flight speed.

6.2.2.4. Objectives

In this study, the conflicts are considered as a relaxation of optimisation criteria. The objective function L of this problem is thus a weighted sum of conflict situations at the TMA network and the total flight time relating to flight efficiency, which can be described as:

$$L(s) = \alpha \cdot A(s) + \beta \cdot B(s) \tag{6-5}$$

$$B(s) = \sum_{i \in F} t_i - n \cdot \min_{i=1}^{n} t_i^o \tag{6-6}$$

$A(s)$ represents the total number and extent of conflicts, and $B(s)$ defines the aggregate deviation of each aircraft's arrival time from the earliest reference arrival time.

In the rolling horizon framework, the reference arrival time is updated by the output in the last time horizon. α and β, respectively, indicate the weighting coefficients for the conflict term and the flight time term.

6.3. Methodologies

This section describes the research problem, which includes data acquisition, model development, and simulation-based optimisation to dynamically predict the separation of aircraft wake turbulence and optimise runway scheduling accordingly. The complexity of the large-scale operational problem increases with aircraft number. Given that aircraft landing scheduling is recognised as NP-hard (Beasley et al., 2000), heuristics and hybrid methods may provide more effective solutions than exact algorithms. This study introduces a time decomposition strategy paired with a simulated annealing algorithm to integrate terminal arrival flow management and runway scheduling, while accommodating dynamic wake separation requirements.

6.3.1.1. Simulated annealing

Simulated annealing models the thermal annealing process of metals by heating up and subsequently cooling them to achieve an optimal energy state (Laarhoven et al., 1987). The objective function in SA is minimised and analogous to this physical process. The heat-up phase investigates the solution space to identify the initial temperature T_0 that facilitates thorough and extensive exploration during the cooling phase. The cooling phase involves gradually lowering the temperature, which traps out of local minima and corresponds to a reduced likelihood of accepting inferior solutions while navigating the solution space.

At each temperature step, multiple iterations are performed to refine the solution. If

the objective of the newly generated solution is smaller or larger than the objective of the current solution with a probability $e^{\Delta Y/T}$ where ΔY is the difference in these two objectives, the current solution may be replaced by this randomly generated new solution in the neighbourhood. The decreased probability of objective value becomes smaller and smaller with temperature decreases, ultimately guiding the algorithm toward convergence at or near a global optimum.

6.3.1.2. K-Conditional position shift

In the SA algorithm used in (Ma et al., 2019), aircraft in the current time horizon are optimised based on a fixed sequence (0, 1, 2 ... aircraft number) of estimated arrival time. The optimisation sequence in this study is determined by the TMA entry sequence of aircraft in the flight set. In fact, this optimisation based on the First-Come-First-Served strategy makes it easy to get into greedy and local searches. Therefore, we proposed the K-CPS strategy to generate several alternative aircraft sequences with aircraft position constraints to avoid this challenge. In K-CPS, aircraft can only move forward or backward by a maximum of K positions within a given sequence. This constraint allows for the generation of multiple alternative sequences, as shown in the pseudo-code of **Table 6-1**, which decides the decision-making sequences among aircraft in the flight set and enables certain aircraft to be prioritised under the current solution context. Finally, the K-CPS sequence with the minimum objective value is picked to get the optimal performance.

Table 6-1. Pseudo-code of algorithm of K-CPS-based simulated annealing.

Initialisation:
number of transition under each temperature $nbTransition$; $Y_{cps\_min} = 10000000$;

sequences of aircraft indices for optimisation generated with CPS cps_seq_array;
alternative sequence number generated by CPS cps_seq_num;

Iterate aircraft sequence generated with K-CPS:

for row=0 to cps_seq_num do

$flightset\_indices = cps\_seq\_array[row]$

HeatUpLoop for one cps sequence:

Initialise:

initial temperature T = 0.01, temperature heat up rate α = 0.1;

$nbTransition = 1000$;

$index = 0; aircraft\_num; flightset\_array$

While acceptRate $\theta < 0.8$ do

acceptCount $\theta \leftarrow 0$

for $i = 0$ to $nbTransition$ do

aircraft $\leftarrow flightset\_array[flightset\_indices[index]]$

Evaluate current objective $X_1(aircraft), Y_1$

Select a new solution $X_2(aircraft)$ = generateNeighborhood(X_1)

Evaluate new objective, Y_2

Generate random number, λ

If $Y_1 > Y_2$ then

$X_1 = X_2$

$\theta++$

else if $\lambda < exp(Y_2 - Y_1)/T$

X_1 = X_2

$\theta++$

end if

index = (index+1) % $aircraft\_num$

end for

$\Theta = \theta / nbTransition$

$T = T \cdot (1 + \alpha)$

End while

$T_{init} = T$

Return T_{init}

CoolingLoop for one cps sequence:

Initialise:

initial temperature T = T_{init}; temperature cooling rate $\alpha = 0.999$;

$nbTransition = 1000$; initial solution $X_0, Y_{all\_min} = 10000000$; index=0; $aircraft\_num$

While $T > 0.0001 * T_{init}$

For $i = 0$ to $nbTransition$ do

Aircraft ← $flightset\_array[flightset\_indices[index]]$

Evaluate current objective $X_1(aircraft), Y_1$

Select a new solution $X_2(aircraft)$= generateNeighborhood(X_1)

Evaluate new objective, Y_2

Generate a random number λ

If $Y_1 > Y_2$ then

$X_1 = X_2$

else if $\lambda < exp(Y_2 - Y_1)/T$

X_1 = X_2

end if

index = (index+1) % $aircraft\_num$

if index=0 then

Calculate objective values of all aircraft, Y_{all}

If $Y_{all} < Y_{all\_min}$ then

$Y_{all\_min} = Y_{all}$

$T = T \cdot \alpha$

End while

Getting the minimum objectives:

If $Y_{all\_min} < Y_{cps\_min}$ then

$Y_{cps\_min} = Y_{all\_min}$

row ++

end while

Output best solution Y_{cps_min}

6.3.1.3. Time decomposition with sliding window

The time sliding-window decomposition approach tackles the initial problem by breaking it down into smaller sub-problems through the use of a sliding window. This technique reduces both the complexity of the problem and the associated computational load. It is a generic approach that can be adapted to various real-time operational problems.

As shown in **Figure 6-3** of a given long time interval $[T_{START}, T_{END}]$ that we intend

to optimise over, we can divide it into K sliding windows with a time length of L and a shift length of S. Further, the starting time t_s^k and end time t_e^k of the sliding window $k(k \in K)$ are $[T_{START} + KS, T_{START} + KS + L]$, respectively. For the sliding window k that is active, if the estimated earliest entry time or the estimated latest arrival time of a flight is in this window, then this flight is ongoing or active in this time horizon. The flight is finished if its latest arrival time is less than the start time of this horizon, and the flight is in the planning phase if its earliest entry time is larger than the end time of this window. In addition, the earliest arrival in this window should be larger than the latest arrival time of the finished flights, plus a deviation of separation time. Furthermore, the flight entry time for each entry waypoint in this window should also be larger than the optimised entry time of corresponding completed flights entering from the same entry waypoints. In addition, a time interval is assigned for the starting time and end time of each sliding window. The starting time interval is $[t_s^k - \Delta t_{min}, t_s^k + \Delta t_{max}]$, and the end time spreads in $[t_s^k - \Delta t_{min}, t_s^k + \Delta t_{max}]$.

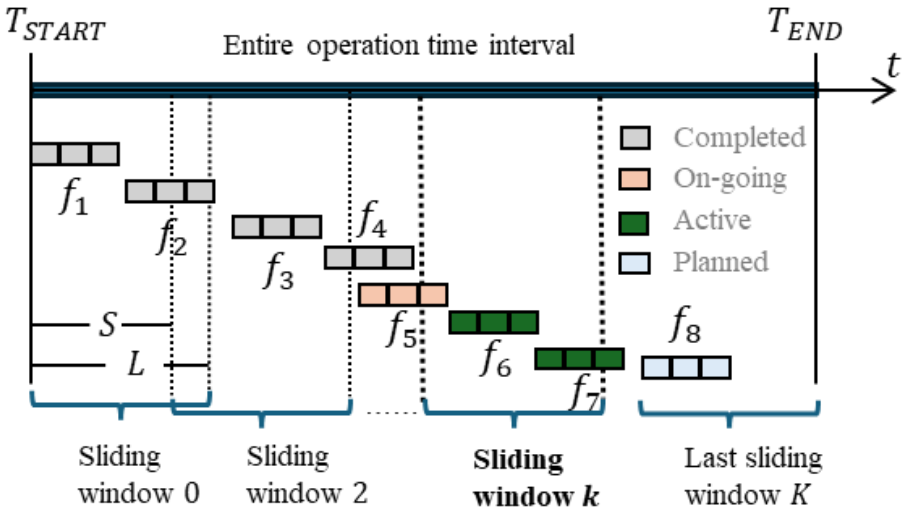

Figure 6-3. Rolling time horizon frame for long-term arrival optimisation.

6.4. Numerical experiments

6.4.1. Test instances and experimental setting

In addition to the wake separation model constructed in Section 5.2.2, this study also analyses historical arrival flight data from February 20, 2019, involving 384 flights at HKIA. At that time, the runway configuration comprises two independent runways for arrivals and departures, respectively. The analysis focuses on single-runway landing problems during peak hours to reduce scheduling complexity. As shown in **Table 6-2**, the majority of landings on this day are in categories CAT_B and CAT_D, with only 3% in categories CAT_A, CAT_C, and CAT_E. **Figure 6-4** illustrates the hourly arrival numbers for the day and highlights the strong crosswinds exceeding 3 m/s throughout the peak traffic period.

Table 6-2. Landing flight distribution by aircraft weight category in peak hours of 2019-02-20 at HKIA.

Aircraft weight category	Landing flight distribution
CAT_A	4 (1.04%)
CAT_B	216 (56.25%)
CAT_C	3 (0.78%)
CAT_D	156 (40.6%)
CAT_E	5 (1.3%)
Total	384

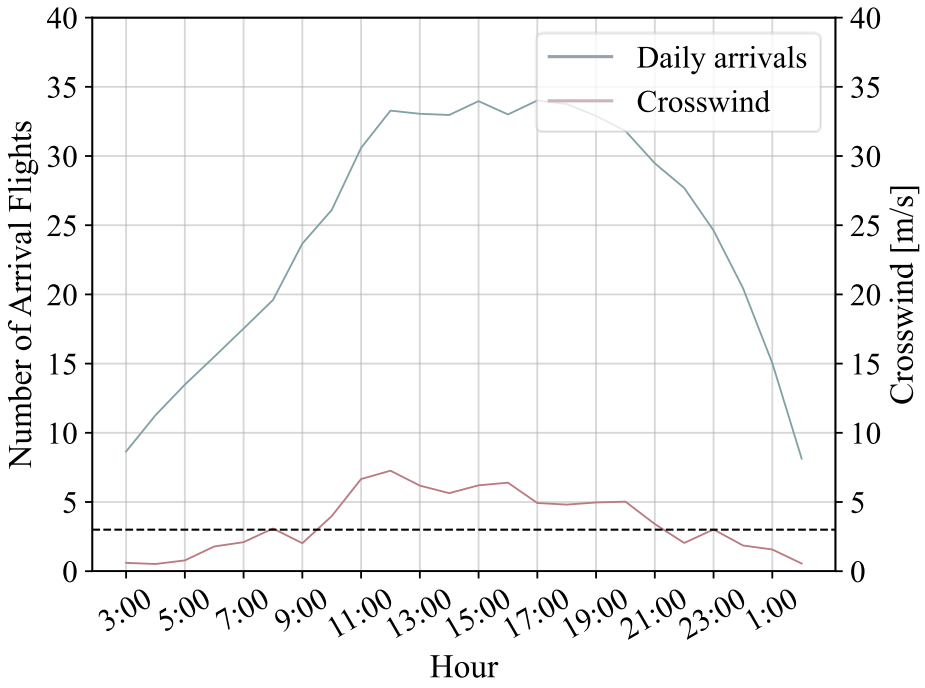

Figure 6-4. Arrival flight number by hour and daily METAR crosswind at HKIA on 2019-02-20.

The terminal air traffic flow model is implemented in Java and executed in the same hardware environment. All experiments in this study were performed using an Intel Core i7-12700K processor, an NVIDIA GeForce RTX 3060 Ti GPU (1.78 GHz), and 32 GB of DDR5 RAM. The deep learning models were developed and trained using Keras on TensorFlow 2.5.0. The TCN model consists of four residual 1D convolutional layers, in addition to the input and output layers, while the MLP model includes three hidden fully connected layers. The Gradient Boosting, K-Nearest Neighbors, and Decision Trees (DT) are benchmarking models. Notably, data from February 20, 2019, was reserved exclusively for the test dataset, without participating in the training and validation phases.

6.4.2. Wake prediction performance

Table 6-3 presents the performance of the proposed models in wake separation

prediction, contrasting them with three benchmark machine learning models. It highlights the superior performance of the MLP model compared to the benchmarks, particularly with an 11.48% reduction in MAE based on the DT model. Additionally, the TCN model, with its ability to capture temporal features, reduces the MAE and RMSE of wake separation time by nearly 50% compared to the MLP model. The results also show that predictions based only on wake and flight data are less accurate than those incorporating weather conditions, underscoring the influence of wind on wake movement and separation. Notably, the TCN model's performance in predicting wake location declines significantly without weather features. Nonetheless, this impact is less pronounced for separation time predictions, which is attributed to an additional margin added to the wake pair region, resulting in more conservative separation estimates.

Table 6-3. Performance of proposed models in wake attributes prediction and wake separation prediction.

Probabilistic wake prediction model	Features	MAE(m)				MAE(s)	RMSE(m)				RMSE(s)
		X_l	Z_l	X_r	Z_r	Separation	X_l	Z_l	X_r	Z_r	Separation
Probabilistic TCN model	Wake and flight info. + weather	23.48	7.52	22.45	8.23	8.82	33.87	10.09	33.73	11.05	14.33
	Wake, flight info.	52.42	7.84	54.70	7.57	18.80	82.62	10.90	83.82	10.55	29.02
Probabilistic MLP	Wake and flight info. + weather	-	-	-	-	22.04	-	-	-	-	29.71
	Wake, flight info.	-	-	-	-	23.52	-	-	-	-	31.46
Gradient Boosting	Wake and flight info. + weather	-	-	-	-	22.25	-	-	-	-	29.81
	Wake, flight info.	-	-	-	-	20.61	-	-	-	-	27.86
KNN	Wake and flight info. + weather	-	-	-	-	22.85	-	-	-	-	31.30
	Wake, flight info.	-	-	-	-	23.01	-	-	-	-	31.18
DT	Wake and flight info. + weather	-	-	-	-	24.90	-	-	-	-	34.95
	Wake, flight info.	-	-	-	-	24.48	-	-	-	-	34.45

6.4.3. Performance of 3-level wake separation matrices in single test cases

This subsection demonstrates the impact of reduced wake separation on terminal aircraft arrival management. The SA algorithm modelled in this study tackles the terminal arrival flow management problem by rapidly searching for high-quality solutions for TMA entry time, flight speed and entry route for each aircraft to achieve conflict-free and most time-saving flight operations. The weight ratios of conflict and total arrival time are tuned to avoid conflicts within the TMA while enhancing overall arrival performance for all test scenarios, as shown in **Figure 6-5**. As illustrated in **Table 6-4**, the hourly arrival performance derived under the above-mentioned two weather-related wake separation matrices (LW and SW for short) alongside the traditional RECAT-EU wake separation (denoted as REGULAR) are compared. In this analysis, the entry times of each aircraft are restricted to be no less than the estimated times and no more than 30 minutes later. Flight speed changes are limited to a range of -0.1 to 0.2 times the planned flight speed. Arrival performance metrics assessed include total arrival time and average flight delay, with the values in parentheses in the "Total arrival time" column indicating reductions relative to REGULAR separation. Additionally, the variations in decision variables such as average entry time delay, maximum speed changes, and the proportion of shortest routes selected based on corresponding entry waypoints are also examined.

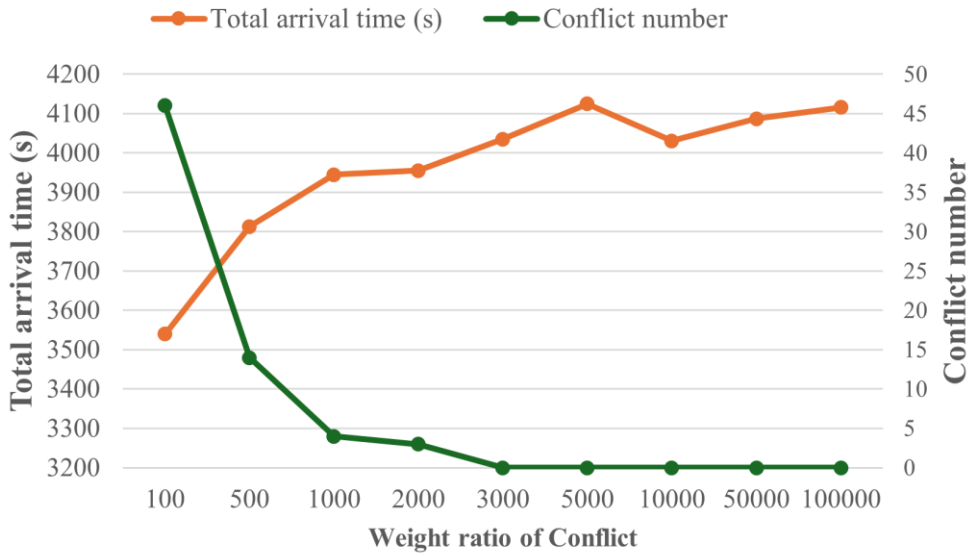

Figure 6-5. Trade-of between the weight of conflict and the weight of arrival time of Scenario 2 under regular RECAT-EU separation.

For the heavy traffic situation on February 20, 2019, the results reveal a prominent trend of total arrival time decrease when the wake separation is reduced from regular separation to separation under light and strong winds. Specifically, Scenario 7, which involves 30 arrival flights between 16:40 and 17:36, demonstrates the greatest reduction in total arrival time under strong-wind wake separation, achieving a 15.4% decrease compared to the standard RECAT-EU protocol. This improvement is primarily attributed to adjustments in flight speed and routing. Furthermore, although the average TMA entry time delay and length of flight route are reduced, the significant arrival efficiency improvement in this scenario occurred despite an average arrival time delay of 2 minutes. In contrast, other scenarios show less pronounced reductions in total arrival time, with only minor deviations in decision variables and average flight delay. This suggests a potential for enhancing runway operational efficiency while still accommodating the needs of other stakeholders.

Table 6-4. Simulation results of 3-level wake separation matrices under heavy traffic hours on February 20, 2019.

Scenarios/Time interval/ Aircraft number	Separation scenarios	Total arrival time (s)	Average flight delay (min)	Average entry time delay (min)	Maximum speed change	Shortest route percentage
1 10:12-11:15 (35)	REGULAR	4654	6.95	5.70	-0.51%	51.42%
	LW	4094 (12%)	6.82	3.44	-1.11%	40%
	SW	**4094 (12%)**	**4.70**	**3.28**	**-0.34%**	**51.42%**
2 11:00-12:01 (28)	REGULAR	4105	5.83	1.74	-0.78%	57.14%
	LW	4195	5.37	2.00	-0.71%	78.57%
	SW	4017 (2.2%)	4.52	0.63	-0.67%	60.71%
3 11:56-13:02 (38)	REGULAR	4305	7.28	4.56	-0.36%	71.05%
	LW	4286 (0.44%)	8.79	5.36	-0.44%	63.15%
	SW	4220 (1.97%)	6.14	4.10	-0.40%	62.16%
4 13:03-14:09 (33)	REGULAR	4599	8.34	5.52	-0.04%	50.28%
	LW	4389 (4.56%)	6.71	2.71	-0.06%	54.39%
	SW	**4334 (5.76%)**	**7.42**	**3.6**	**-0.07%**	**68.47%**
5 14:09-14:59 (28)	REGULAR	3449	7.18	6.11	-0.39%	39.28%
	LW	3451	6.66	5.38	-0.28%	67.85%
	SW	3451	6.48	4.48	-0.39%	67.85%
6 15:02-16:02 (28)	REGULAR	3721	4.95	2.98	-0.14%	71.42%
	LW	3719	5.34	1.12	-0.67%	60.71%

	SW	3631 (2.41%)	5.66	2.96	-0.64%	71.42%
7 16:40-17:36 (30)	REGULAR	3888	6.90	6.04	-0.13%	50%
	LW	3370 (13.32%)	8.95	6.33	-0.36%	43.33%
	SW	**3289 (15.4%)**	**8.91**	**5.34**	**-0.76%**	**56.67%**
8 17:40-18:44 (37)	REGULAR	4192	4.50	4.42	-0.54%	48.64%
	LW	4163 (0.69%)	5.22	3.65	-0.56%	51.35%
	SW	4124 (1.62%)	4.35	4.32	-0.27%	64.86%
9 19:11-21:16 (70)	REGULAR	7951	9.14	6.28	-0.2%	52.85%
	LW	7902 (0.61%)	9.58	5.68	-0.72%	58.57%
	SW	7845 (1.33%)	8.92	4.59	-0.48%	57.14%

Figure 6-6 presents the iteration of objectives for Scenarios 4 and 7 as temperature decreases. The initial temperature for the cooling-up phase is established following the heating process. As the temperature lowers, the objective values generally decrease across all three levels of wake separation, suggesting convergence toward an optimal solution. The observed fluctuations in the curves reflect the stochastic nature of the SA algorithm, which permits occasional uphill moves in the solution space to escape local optima. Interestingly, the optimisation of wake separation under light wind conditions starts with a temperature similar to that used in strong wind scenarios, but converges more slowly and often to less optimal solutions. Notably, the initial temperature in traditional wake separation contexts is significantly higher than those observed with reduced wake separation. Furthermore, the curve corresponding to the traditional RECAT-EU standard serves as a benchmark, revealing that the performance of the SA algorithm is poorest under conservative wake separation conditions regarding arrival time.

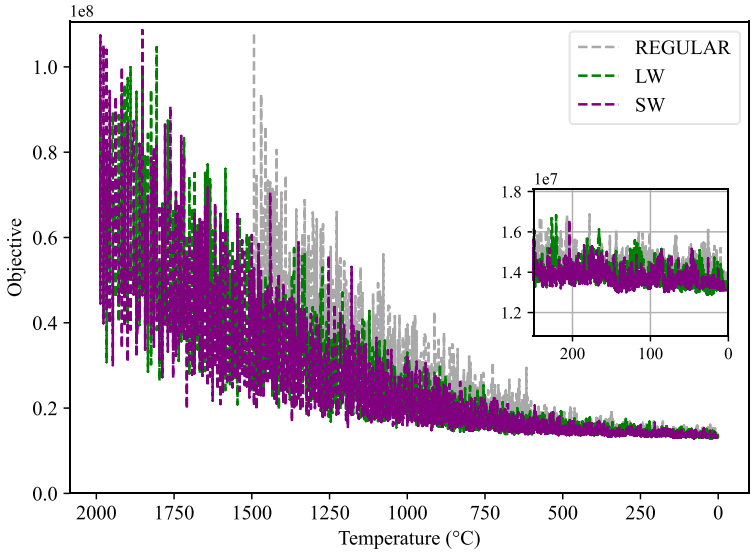

(a) Iteration of objective values in Scenario

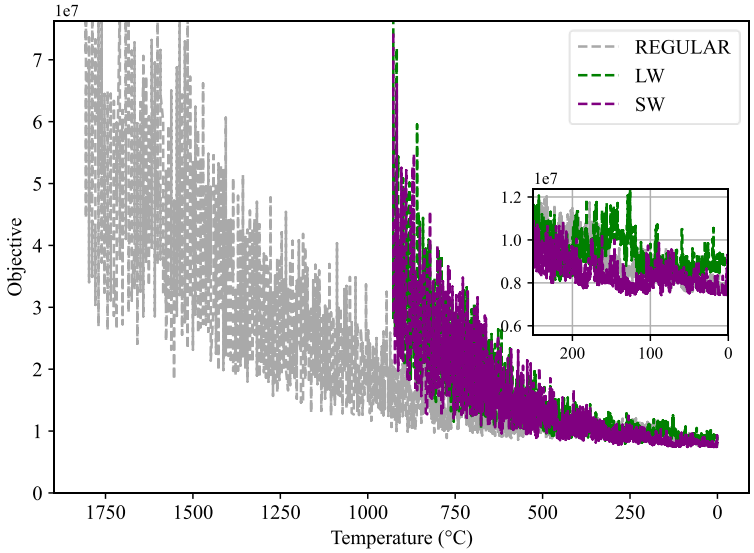

(b) Iteration of objective values in Scenario 7

Figure 6-6. Objective performance of Scenarios 4 and 7 in **Table 6-4** in the process of temperature decrease of the SA algorithm.

Figure 6-7 illustrates the converging process of the conflict situations, including the total conflict number and conflict on both nodes and links. Although the improvement of arrival time performance in Scenario 4 is less evident compared to Scenario 7, it exhibits a more consistent convergence pattern in conflict resolution. **Figure 6-8** depicts the deviations in decision variables across three levels of wake separation, highlighting the distinct control strategies employed in these scenarios to achieve superior arrival efficiency. The decisions of prominent flight speed decrease within the most wake separation reduction is made for both two scenarios to achieve both smaller total arrival time in **Table 6-4**. Furthermore, both scenarios result in reduced TMA entry delays, as shown in the first subplot of **Figure 6-8**, compared to the REGULAR wake separation. Nonetheless, it is noteworthy that the total length of optimised flight routes in Scenario 7, under strong-wind wake separation, is greater than that observed under the baseline RECAT-EU wake separation.

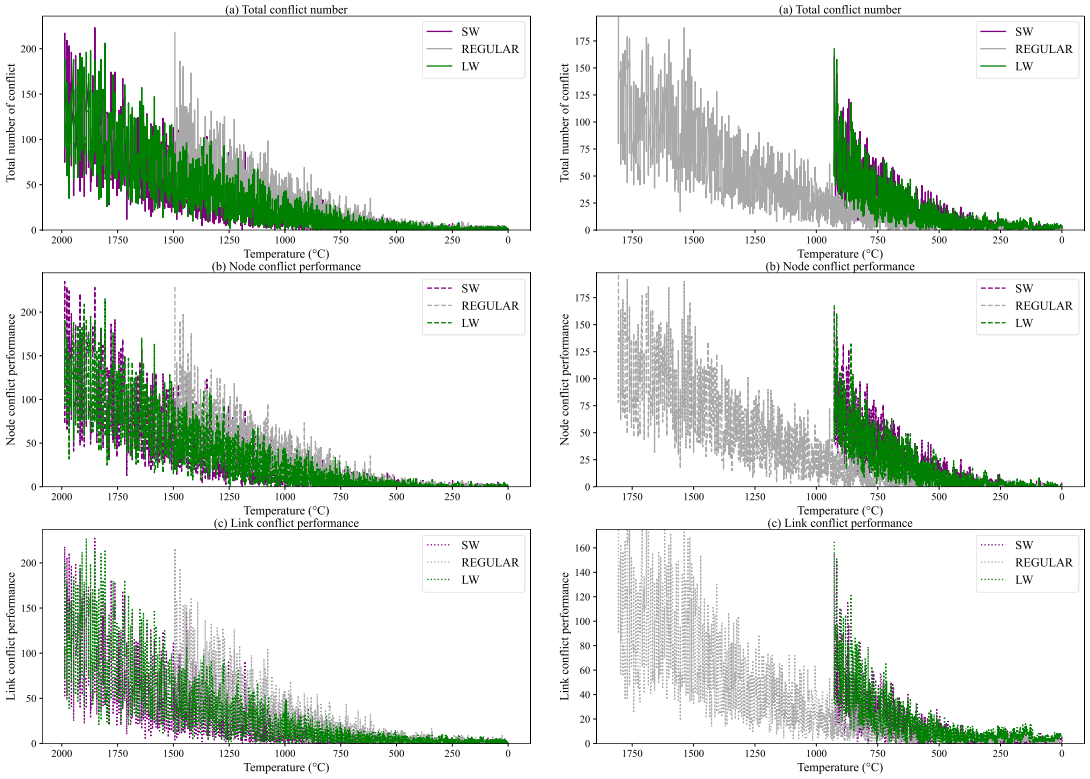

(a) Conflict performance of Scenario 4 (b) Conflict performance of Scenario 7

Figure 6-7. Iteration of conflict performance for Scenarios 4 and 7 in **Table 6-4** in the process of temperature decrease.

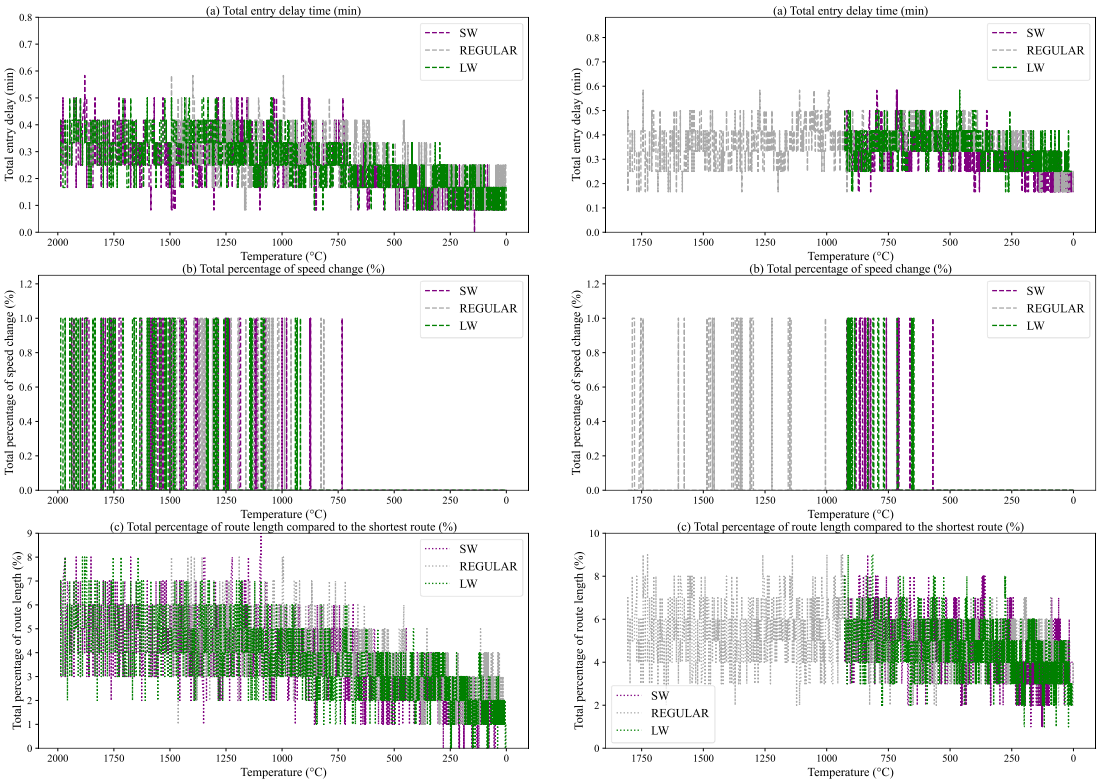

(a) Change of decision variables of Scenario 4 (b) Change of decision variables of Scenario 7

Figure 6-8. Iteration of decision variables of Scenarios 4 and 7 in **Table 6-4** in the optimisation process.

The distributions of flight numbers under the optimised solutions for Scenario 4 are also specified in **Figure 6-9** across these three distinct wake separation matrices. **Figure 6-9**(a) indicates that implementing the reduced wake separations during the final approach can decrease the extreme arrival delay from 60 minutes to 20 minutes while also increasing the proportion of flights arriving without delay by 12.5%. Regarding TMA entry time deviation, **Figure 6-9**(b) also shows that the "SW" wake matrix exhibits a more concentrated distribution around the zero-deviation mark, implying the flights experience less variability in their entry time following the flight speed control in **Figure 6-9**(c).

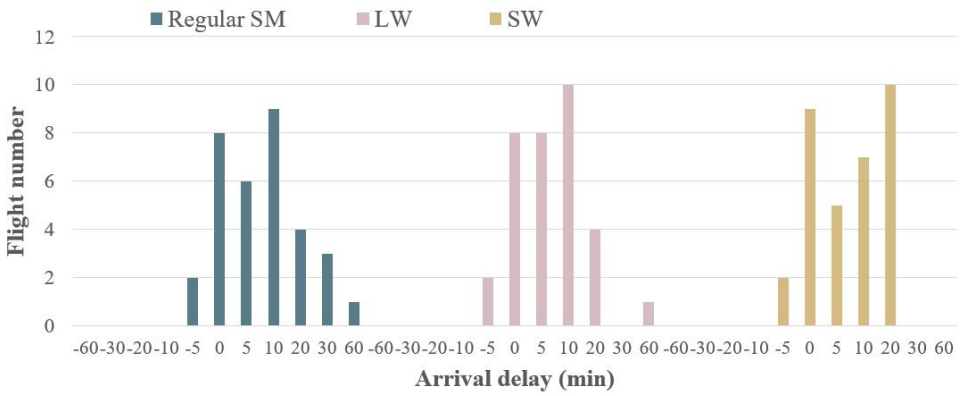

(a) Arrival delay

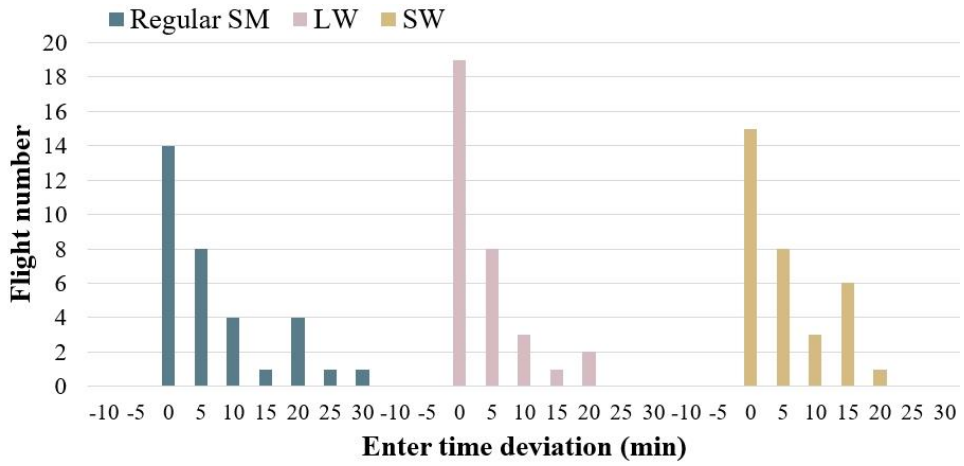

(b) Entry time deviation

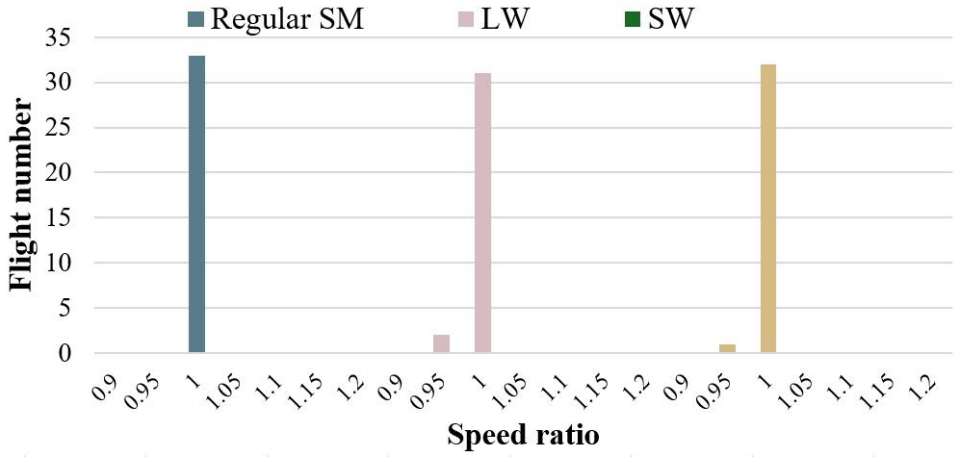

(c) Average speed change

Figure 6-9. Deviations in average flight delay, TMA entry time and the flight speed of Scenario 4 under 3-level wake separation matrices in **Table 6-4**.

In addition, this study has also explored the performance impact of employing the earliest TMA entry time strategies for heavy traffic scenarios in **Table 6-5**. It is evident that allowing for an earlier entry time into the TMA, specifically 5 minutes and 10 minutes ahead of schedule, results in a more significant reduction in total arrival time compared to the scenarios presented in **Table 6-4**. This reduction is particularly pronounced under the "SW" separation scenario, where a 10.43% decrease is observed for Scenario 4 and an 11.95% decrease for Scenario 8. These percentages indicate a substantial improvement in overall traffic flow management and more efficient use of airspace during peak traffic periods. Despite the reduction in total arrival time, the average flight delay does not experience a substantial increase. This suggests that the strategy of adjusting the entry time into the TMA can effectively manage traffic without significantly impacting individual flight delays. It is noteworthy that the performance increase under the "LW" matrix is not as pronounced as under the "SW" matrix. This can be attributed to the conservative nature of the "LW" separation matrix values.

Figure 6-10 visualises the distribution of flights on flight delay time, entry time deviations, and average speed changes for Scenario 4, allowing aircraft to earlier enter TMA by up to 10 minutes. By enabling more flights to enter the TMA earlier (**Figure 6-10**(b), the system reduces the overall arrival delay, with especially a noticeable decrease in the number of flights under extreme delay ranges (beyond 10 minutes). Furthermore, the reduction in speed changes contributes to a more predictable flight environment, which in turn reduces the burden of ATCOs and pilots. Finally, the wake separation reduction has the potential to offer a promising approach to optimising air traffic flow, enhancing punctuality, and improving overall airspace management.

Table 6-5. Performance effect of the earliest TMA entry time for heavy traffic scenarios on February 20, 2019.

Scenarios/Time interval / Aircraft number	Entry time period (min)	Separation scenarios	Total arrival time (s)	Average flight delay (min)	Average entry time delay (min)	Average speed change percentage	Shortest route percentage
4 13:00-14:09 (33)	[-5, 30]	REGULAR	4336	6.43	5.17	-0.21%	72.72%
		LW	4131 (4.72%)	6.98	5.52	-0.09%	75.75%
		SW	**3980 (8.21%)**	**5.03**	**4.69**	**-0.36%**	**63.63%**
	[-10, 30]	REGULAR	4296	6.84	6.86	-0.65%	57.57%
		LW	3883 (9.61%)	6.48	7.01	-0.12%	75.75%
		SW	**3848 (10.43%)**	**7.54**	**8.09**	**-0.27%**	**69.69%**
8 17:40-18:44 (37)	[-5, 30]	REGULAR	4322	7.66	7.36	-0.89%	45.94%
		LW	3997 (7.52%)	5.88	6.40	-0.64%	62.16%
		SW	**3954 (8.51%)**	**6.08**	**6.32**	**-0.64%**	**54.05%**
	[-10, 30]	REGULAR	4157	8.60	9.50	-0.35%	43.24%
		LW	4018 (3.34%)	6.68	7.22	-0.59%	40.54%
		SW	**3660 (11.95%)**	**7.02**	**8.03**	**-0.56%**	**67.56%**

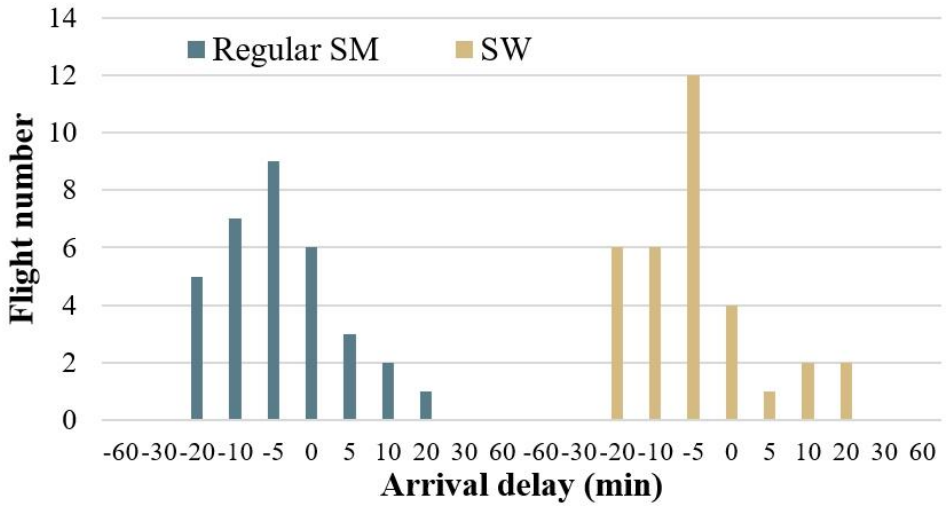

(a) Average flight delay

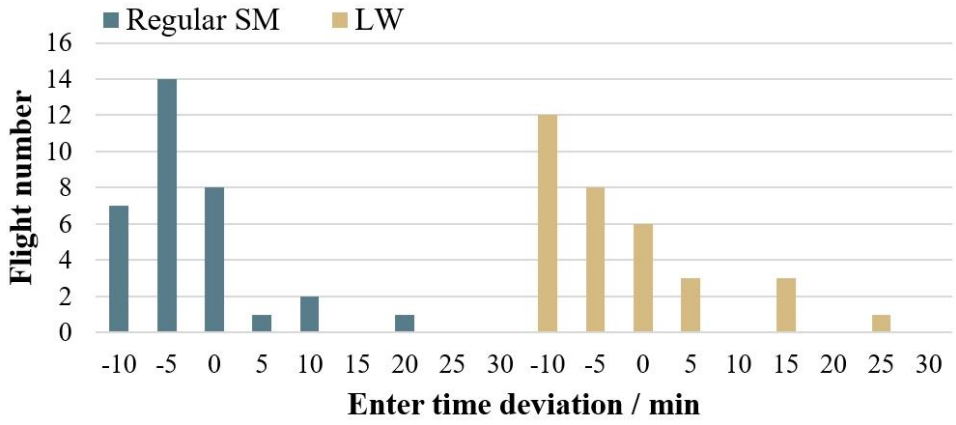

(b) Entry time deviation

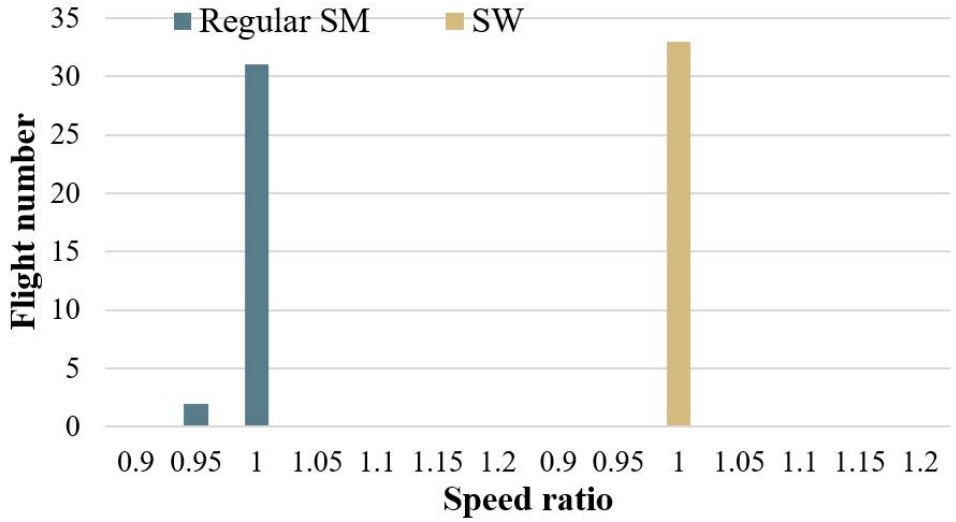

(c) Average speed change

Figure 6-10. Deviations in average flight delay, TMA entry time and flight speed of Scenario 4 under the early three levels of the wake separation matrix and the early entry.

Table 6-6 compares the performance impacts of employing three different wake separation matrices under non-peak traffic scenarios on February 20, 2019. It indicates that the implementation of reduced wake separation matrices (LW and SW) does not significantly affect the overall operational intervals and arrival times of flights. The ample runway capacity and larger time buffers during off-peak hours mitigate the need for resource-intensive efforts to further reduce separation intervals. This also suggests that air traffic management strategies of dynamic wake separation can be tailored to

traffic density.

Table 6-6. Performance comparison of 3-level wake separation matrices under non-peak traffic scenarios on February 20, 2019.

Scenarios / Time interval / Aircraft number	Separation scenarios	Total arrival time (s)	Average flight delay (min)	Average entry time delay (min)	Maximum speed change	Shortest route percentage
14 2:00-3:00 (8)	REGULAR	3166	4.05	4.68	-0.12%	75%
	LW	3153	4.08	4.70	-0.37%	100%
	SW	3154	4.25	4.33	-0.25%	87.5%
15 4:00-5:01 (11)	REGULAR	2766	4.03	4.62	0%	90.90%
	LW	2768	3.50	3.68	-0.72%	81.81%
	SW	2769	3.20	4.78	-0.81%	72.72%
16 5:02-6:59 (15)	REGULAR	3327	2.48	4.25	-0.33%	93.33%
	LW	3369	2.27	4.42	-0.4%	80%
	SW	3376	2.38	4.5	-0.26%	93.33%

6.4.4. Performance of dynamic wake separation in large-scale scenarios

In addition to the previously discussed static wake separation reductions relative to the RECAT-EU standard, this study explores the potential of dynamic pairwise wake separation in large-scale scenarios. **Table 6-7** compares the performance of three levels of static wake separation matrices with the dynamic wake separation (DW) matrix. The DW separation is tailored to pairwise approaching aircraft and varying crosswind conditions as depicted in **Figure 6-4**, with wake separation values predicted by TCN model and the final approach separation determined by Eq. (1).

During the time interval from 10:00 to 11:00 (Scenario 11), crosswind values are noted at around 3-5 m/s. Under these conditions, the DW standard demonstrates a significant improvement in total arrival time compared to the REGULAR standard, achieving a 7.97% reduction. However, it demonstrates less efficiency enhancement when compared to the SW standard, which yields a 10.89% reduction. In Scenarios 12 and 13, crosswinds increase between 11:00 and 13:00, prompting the TCN model to

predict dynamic wake separation intervals that align more closely with minimum separation requirements in strong crosswinds. Consequently, the efficiency gains for both DW and SW standards become comparable. Moreover, the DW standard exhibits superior runway efficiency compared to both REGULAR and LW standards, highlighting its potential as an effective strategy in air traffic management for optimizing safety and efficiency under dynamic atmospheric conditions.

Table 6-7. Simulation results of dynamic wake separation under heavy traffic scenarios of February 20, 2019.

Scenarios / Time interval / Aircraft number	Separation scenarios	Total arrival time (s)	Average flight delay (min)	Average entry time delay (min)	Average speed change percentage	Shortest route percentage
11 10:01-10:58 (31)	REGULAR	3579.56	10.10	6.51	-0.38%	41.93%
	LW	3483.68 (2.67%)	7.49	6.04	-0.22%	48.38%
	DW	**3293.98 (7.97%)**	7.89	6.53	-0.38%	61.29%
	SW	3189.73 **(10.89%)**	9.18	5.84	-0.45%	48.38%
12 11:00-11:59 (27)	REGULAR	3627.45	4.32	4.00	-0.37%	55.55%
	LW	3652.40	3.56	5.14	-0.37%	81.48%
	DW	3538.93 **(2.44%)**	3.39	4.05	-0.59%	77.77%
	SW	3515.17 (3.09%)	2.65	3.75	-0.40%	62.96%
13 12:01-12:58 (33)	REGULAR	3605.37	6.25	6.21	-0.45%	75.75%
	LW	3629.70 (0.44%)	7.10	6.28	-0.42%	60.60%
	DW	3466.24 **(3.85%)**	6.42	5.96	-0.15%	66.66%
	SW	3460.07 (4.03%)	6.05	5.56	-0.24%	57.57%

Compared to the general SA algorithm for optimising aircraft based on the TMA entry sequence, which is the FCFS sequence, **Table 6-8** also explores the performance of the K-CPS SA algorithm for Scenario 4 under strong-wind wake separation conditions. The K-CPS strategy generates several alternative aircraft optimisation

sequences based on the FCFS entry order and a defined K value, which constrains the maximum positional displacement of the aircraft relative to its original position. As the K value increases, the number of alternative aircraft sequences increases exponentially, resulting in excessive time to traverse these decision sequences. Therefore, we randomly selected 100 sequences for performance evaluation under limited CPU conditions. The values in parentheses of the "Makespan" column are the percentages decrease compared to the K=0 scenario. Compared with the determined optimisation sequence, the performance of the K-CPS-based SA algorithm tends to improve with increasing K values. By limiting the range of position shifts, K-CPS promotes broader exploration of scheduling sequences, enhancing solution diversity and avoiding local optima. For example, with 11 aircraft, the “Makespan” (last arrival time decreases the earliest arrival time) at K = 2 and 3 exhibit reductions of 14.32% and 13.36%, respectively, compared to the baseline scenario without K-CPS. In the scenario with 20 aircraft, K = 1 and K = 2 demonstrate comparable performance but different computational times, highlighting the need to balance search space exploration and computational efficiency. Notably, for a scenario with 15 aircraft, K = 1 outperformed K = 3, likely due to limitations in the selected sequence sets. We must acknowledge that using the K-CPS algorithm is similar to simulating the single case many times, the CPU time is also doubled compared with only simulating once. Therefore, more time-efficient strategies and mature hardware environments can be implemented to reduce the time burden.

Table 6-8. Performance of the CPS-based SA algorithm for Scenario 4 in strong winds.

Aircraft number	K value in CPS	Alternative sequence number selected/ all sequence number	Makespan (s)	CPU time (s)
5	0	1	410	10.77
	1	8	381 (7.07%)	73.41
	2	31	378 (7.8%)	487.08
	3	78	**367 (10.48%)**	**1247.69**
11	0	1	1250	20.60
	1	144	1116 (10.72%)	2995.02
	2	100/5081	**1071 (14.32%)**	2518
	3	100/60216	**1083 (13.36%)**	**2726**
15	0	1	2045	27.31
	1	100/987	**1966 (3.86%)**	**2760**
	2	100/150639	1983 (3.03%)	3354
	3	100/5284109	2008 (1.8%)	3530
20	0	1	2622	40
	1	100/10946	2434 (7.17%)	3977
	2	100/10423761	**2423 (7.58%)**	**4867**

To facilitate the implementation of the proposed air traffic flow management under dynamic wake separation in large-scale aircraft operations, we have evaluated the overall arrival performance by scheduling in the rolling horizon. **Figure 6-11** illustrates operational runway throughput during heavy traffic on February 20, 2019, with the rolling horizon encompassing one-hour intervals, shifting forward hourly from 10 AM to 7 AM. The data indicates that historical hourly aircraft arrivals, as scheduled by air traffic controllers using the FCFS method, exhibit significant fluctuations, particularly during peak periods. In contrast, the proposed SA algorithm, applied under dynamic wake separation, has the potential to significantly redistribute the arrival patterns,

leading to a more uniform distribution of aircraft arrivals over time. As represented by the light purple bars in the figure, this algorithm markedly increases the number of arrivals in certain hours, effectively optimizing the use of available airspace and runway capacity. Consequently, this results in improved airport throughput and potential reductions in delays for both airlines and passengers. The notable decrease in arrivals between 17:00 and 19:00 can be attributed to the concluding phase of the rolling process, during which later-scheduled flights are not considered.

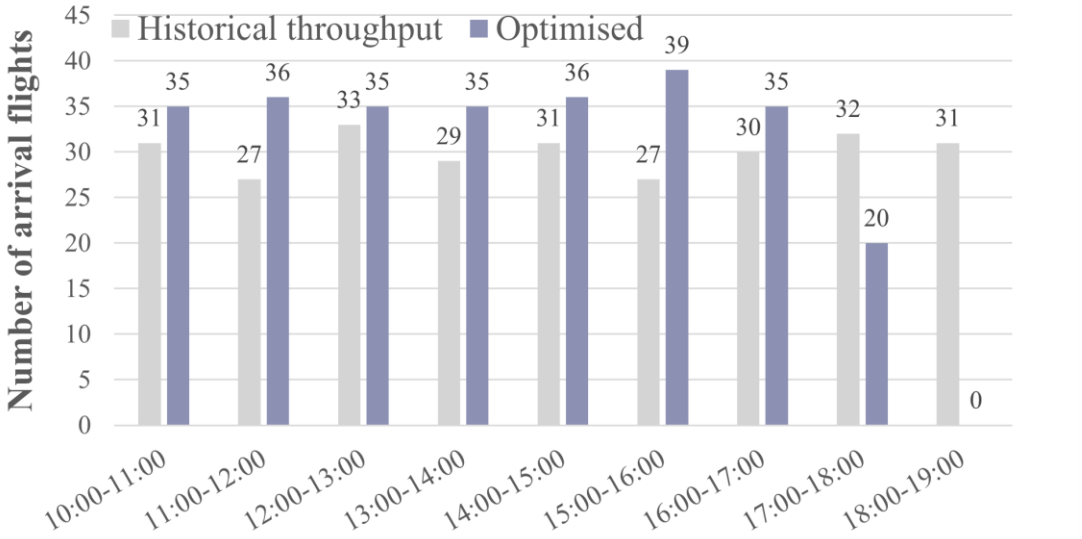

Figure 6-11. Overall runway throughput improvement under rolling horizon and dynamic wake separation compared to actual arrival on February 20, 2019.

6.5. Managerial implications and result discussion

This study presents the integrated terminal traffic flow management and runway scheduling under deep learning-driven dynamic wake separation prediction based on the LiDAR wake detection and ADS-B flight trajectory data at HKIA. The performance of dynamic wake separation in runway efficiency improvement is verified from several aspects. The findings are anticipated to provide the following managerial implications:

1. **Runway resource utilisation and traffic flow enhancement**. The results

indicate that the strong-wind wake separation matrix can bring a significant reduction in maximum delays and an increase in the proportion of on-time flights. It also leads to decreased entry time deviation and a more stable average speed profile. These enhancements collectively reduce the workload for ATCOs and simplify the operational complexity for pilots. Consequently, this approach fosters a more efficient, predictable, and streamlined air traffic management system that leverages existing infrastructure to mitigate challenges associated with the demand-supply imbalance.

2. **Adaptive dynamic wake vortex intervals**. illustrates the efficacy of dynamic wake separation in managing heavy traffic scenarios, particularly under varying crosswind conditions. **Figure 6-11** highlights a significant advancement over the traditional FCFS approach, achieving a more balanced hourly distribution of arriving aircraft and increasing the maximum number of flights accommodated per hour. The dynamic wake vortex intervals can be tailored based on traffic density and weather conditions, thereby increasing the flexibility of air traffic controllers in scheduling. This adaptability allows for real-time adjustments that can accommodate varying levels of traffic and weather-related challenges, enhancing the overall efficiency and safety of air traffic operations.
3. **Integrated terminal and runway scheduling**. By managing the overall flow more effectively, the integrated approach to terminal traffic flow management and runway scheduling greatly alleviates the pressure on the final approach driven by reduced separation. This holistic strategy ensures that the reduction in separation intervals does not compromise safety, leading to an efficient and secure terminal approach.

The explanation of results in this paper and future research are discussed as follows:

- **Table 6-5** and **Figure 6-10** demonstrate the benefits of allowing aircraft to enter the TMA early, which increases the punctuality of arrivals and shortens overall arrival times. However, this strategy also requires coordination with en-route aircraft scheduling and consideration of traffic density and control regulations during that phase. Furthermore, the feasibility and complexities of the dynamic wake separation concept and how it affects controller workload and situational awareness still require to be verified in real-world implementation.
- These dynamic wake separation intervals are totally time-based and are derived based on actual LiDAR data on wake evolution, making them more promising than that in (Morris et al., 2013). However, the current separation matrices are primarily tailored based on stable and strong crosswind conditions to demonstrate their operational performance. To realise higher dimensional dynamic separation, other atmospheric data, such as the headwind and tailwind, can be considered to capture three-dimensional wake transport (Hallock et al., 2018).
- The flight speed adjustments discussed in this paper refer to the overall ground speed of the aircraft from a kinematic perspective. In actual operations, ATCOs' instructions may target at the airspeed, and the true ground speed may be influenced by high-altitude winds. In addition, the headwinds and tailwinds at low altitudes also affect the final approach. The impact of wind could be conducted in future research. Additionally, time-based interval prediction can also be integrated with 4D trajectory prediction to support longer-term and more accurate forecasting and scheduling decisions (Fusaro et al., 2019).

- In fact, **Figure 6-2** shows the STARs in the extended TMA area. The reason we consider the reference arrival time in the objective function is that the developed SA algorithm in this paper optimises decision variables of a single aircraft every time, rather than adjusting all aircraft at the same time. There may exist situations in which the total arrival time is minimal, but the largest arrival time of the last aircraft is not optimal. Therefore, the reference arrival time provides a baseline for the optimisation to maximise the effectiveness of separation reduction and reduce computational burden.

6.6. Conclusion

This study suggests a new deep learning-based and prediction-driven approach for terminal approach path planning and runway sequencing, specifically addressing the challenges associated with dynamic pairwise wake separation. The objectives of this problem are to keep safe and conflict-free flights in the terminal network and improve arrival efficiency. This tailored approach to wake separation reduction under light-wind and strong-wind conditions aims to enhance airspace utilisation while maintaining stringent safety protocols.

Overall, two deep-learning models are proposed to predict pairwise aircraft wake separation utilising historical LiDAR wake data and ADS-B flight trajectory data at HKIA. Two wake separation matrices with reduction under two levels of crosswinds are proposed based on the RECAT-EU standards. Furthermore, dynamic wake separations are customised to fit individual circumstances of aircraft pairs and varying wind conditions. Further, the terminal traffic flow problem under dynamic wake separation is modelled and solved with the proposed K-CPS-based SA algorithm. Finally, the runway operational performances under these three wake separation

matrices and the dynamic wake separation are evaluated on both heavy-traffic and non-peak arrival scenarios. The influence of wake separation reduction in several aspects of operational performance is discussed, including the total arrival time, average flight delay, TMA entry time delay, flight speed change and route selection. The superior performance presented by the proposed algorithm indicates a promising alternative approach for improving runway operational throughput and efficiency for airports with constrained configurations.

Chapter 7. Conclusion

7.1. Conclusion of the thesis

The terminal area and final approach zone are critical for efficient flight dispatch, yet current methods often rely on static, conservative wake separation constraints that hinder optimal traffic flow at airports. These conventional methods prioritise safety but limit capacity and efficiency. With increasing air traffic demands, innovative solutions are essential to enhance runway performance within existing constraints. Dynamic wake separation offers a promising approach by adjusting separation distances based on real-time conditions, potentially improving runway throughput and efficiency. This concept considers the variability in aircraft wake behaviour influenced by meteorological conditions and aircraft types, allowing for more flexible and efficient traffic management. Additionally, the impact of reducing separation distances in the final approach on overall terminal traffic control remains underexplored.

Given the above research context, this thesis presents an innovative approach to enhancing terminal traffic management by leveraging deep learning-driven methodologies for dynamic wake separation prediction and optimisation using LiDAR data and actual meteorological data. By analysing historical wake turbulence data from Hong Kong International Airport, the research will identify patterns and predict dynamic separations, contributing to enhanced operational performance in both runway and terminal airspace. This involves four stages: recognising wake vortex patterns, forecasting their spatiotemporal evolution, and optimising runway and terminal arrivals.

To be more specific, this research formulated a data-driven intelligent strategy for quantifying the dynamic wake separation and scheduling the runway and terminal arrival in a holistic manner. The online and near real-time aircraft wake vortex recognition, and long-term prediction are researched in Chapter 3 and Chapter 4. A

novel two-stage deep convolutional neural network framework is developed for precise and rapid recognition of aircraft wake vortices using LiDAR-scanned images, focusing on vortex location and strength estimation. By integrating DCNN with the ATCN network, the research delivers a robust system for near real-time wake detection and decay forecasting, supporting dynamic time-based separation minima under varying wind conditions. The probabilistic prediction models incorporate spatiotemporal features, enabling accurate and trustworthy assessments of wake vortex evolution. The potential of flight separation reduction in final approach phases is analysed statistically using the predicted vortex spatial-temporal features of aircraft wake vortices, with the effects of crosswind in vortex lateral transport examined.

This study further evaluates the operational impact of dynamic wake separation on runway capacity and throughput, proposing tailored separation matrices for different crosswind scenarios. These findings demonstrate significant improvements in reducing flight delays, enhancing arrival efficiency, and optimising runway utilisation without compromising safety. The proposed K-CPS-based SA algorithm offers an effective solution for terminal traffic flow and runway sequencing under high traffic density, accommodating the unique needs of aircraft pairs and atmospheric variability.

Overall, this research provides a comprehensive framework for integrating advanced machine learning techniques into air traffic operations, offering actionable insights for air traffic controllers and airport managers. It underscores the potential of dynamic separation strategies to address the growing demands of modern aviation. By balancing safety and efficiency, this thesis contributes to the development of a proactive, data-driven decision-support system, paving the way for more resilient and intelligent airspace management solutions.

7.2. Contributions of the thesis

This thesis is expected to provide preconditions for holistic traffic flow management and improve the automation and efficiency of terminal approach dispatch through a dynamic wake separation strategy. The contributions of the above four-aspect research are mainly threefold:

(1) **Online aircraft wake monitoring and encounter risk analysis**. The study introduces a two-stage wake vortex recognition and evolution prediction framework powered by deep learning, achieving both high precision and computational speed. This enables near real-time monitoring of wake vortices and supports onboard decision-making to reduce air traffic controller workload. The probabilistic estimation and decision transparency of the wake prediction models enhance reliability, facilitating safety-critical implementations. This strengthens the ability to predict and manage wake vortex risks dynamically and robustly. The hybrid deep learning framework improves wake vortex state recognition and evolution prediction, supports the development of dynamic flight separation systems and ensures safe traffic flow under complex conditions.

(2) **Improvement of runway operational capacity and throughputs**. The implementation of time-based wake separation standards, aligned with RECAT-EU, under certain wind conditions, allows for reduced approach separation while maintaining safety. This strategy can boost throughput without requiring additional infrastructure. Dynamic wake vortex intervals, tailored to traffic density and weather conditions, enable flexible adjustments that accommodate varying operational scenarios. These intervals increase the number of flights handled per hour, balancing arrivals and improving overall runway utilisation.

(3) **Integrated terminal traffic operational efficiency without sacrificing flight**

safety. The study integrates terminal traffic flow management and runway scheduling using dynamic wake separation models based on LiDAR detection and ADS-B data. This holistic approach effectively manages terminal and runway flow, reduces delays, stabilises flight speed profiles, and simplifies air traffic controller operations without compromising safety. The adaptive scheduling strategies accommodate weather variability and traffic demand, which are expected to enhance overall system efficiency and safety in heavy traffic scenarios, and support rapid recovery from adverse weather and emergencies, ensuring smooth and secure terminal operations.

In conclusion, this research expects to facilitate the development of the near real-time aircraft wake monitoring and dynamic separation suggestion system. A comprehensive understanding of how dynamic wake separation impacts both runway and terminal area operations is evaluated by assessing the trade-offs between dynamic and time-based separation and maintaining safety. Ultimately, the study seeks to quantify the extent of efficiency improvements while adhering to safety and scheduling limitations within the TMA in a unified framework, contributing to more effective and safe air traffic management solutions against operational disruptions by a robust decision-support tool for air traffic controllers.

7.3. Areas of future research

Despite the achievement in this research of integrated terminal approach optimisation under the dynamic wake separation, the completed studies have some limitations for future exploration. The following aspects are proposed as potential directions for future work:

(1) **Exploring the societal impacts of this research**. The societal impacts of this research extend beyond operational efficiencies and safety, particularly in the context of noise pollution and community well-being. As dynamic wake separation strategies are implemented to enhance runway capacity and reduce delays, there is a potential trade-off with increased aircraft noise due to more frequent take-offs and landings. This could disproportionately affect communities living near airports, especially in urban areas with high traffic density. To mitigate these impacts, future studies should explore the relationship between separation enhancement and noise levels, emphasising the need for quieter aircraft design and advanced noise abatement procedures. Collaboration between researchers, aircraft manufacturers, and regulatory bodies will be essential to develop technologies and operational practices that balance capacity improvements with environmental sustainability. By addressing these societal concerns, the aviation industry can ensure that advancements in wake vortex management contribute positively to both operational efficiency and community quality of life.

(2) **Consideration of three-dimensional wake vortex simulation with atmospheric factors**. Future studies should integrate more comprehensive atmospheric conditions, including headwinds, tailwinds, wind shear, and dynamic crosswinds, to develop a more realistic three-dimensional wake vortex simulation. These factors significantly influence vortex transport and decay, especially in high-altitude and low-altitude airspaces. Combining these simulations with physical wake models and computational fluid dynamics will support the development of physics-informed aircraft wake vortex prediction models. These models can capture complex interactions between wake vortices

and dynamic atmospheric conditions, improving the accuracy and reliability of wake separation decisions.

(3) **Model validation across multiple airports**. While this study demonstrates the applicability of wake recognition and evolution prediction models at the Hong Kong International Airport, future research should evaluate model performance across different airports. Factors such as variations in runway configurations (e.g., closely spaced parallel runways or cross runways), traffic density, and regional weather patterns can influence wake vortex behaviour. In these layouts, wake turbulence generated on one runway can significantly impact operations on adjacent runways, wake vortices may drift from one runway to the other under certain wind conditions, requiring increased separation to maintain safety. Similarly, in cross-runway configurations, the interaction of wake vortices with intersecting traffic steams introduces additional complexity. Testing the models under diverse operational and meteorological conditions will verify their robustness, scalability, and generalisability, enhancing their utility for global air traffic management systems.

(4) **Integrating runway configuration switch with dynamic separation**. The combination of runway configuration changes and dynamic wake separation should be investigated to evaluate the overall runway capacity envelope. This approach can optimise departure and arrival sequencing while accommodating fluctuating traffic patterns and weather conditions. By considering both arrival and departure dynamics, future studies can provide a holistic assessment of how dynamic wake separation impacts total runway throughput and operational efficiency. Incorporating these strategies into runway scheduling frameworks will enable a more adaptive and integrated terminal management system.

Appendix I – Flight separation standards

Table 1. ICAO wake separation minima under categories of maximum take-off mass.

Leader/ Follower (NM)	A380	Heavy	Medium	Light
A380	MRS	6	7	8
Heavy	MRS	4	5	6
Medium	MRS	MRS	MRS	5
Light	MRS	MRS	MRS	MRS

Note: MRS refers to the minimum radar separation, which remains 2.5/3NM, and NM represents the nautical mile.

Table 2. RECAT-EU distance-based separation minima on approach.

Leader/ Follower (NM)		Super heavy A	Upper heavy B	Lower heavy C	Upper medium D	Lower medium E	Light F
Super heavy	A	3	4	5	5	6	8
Upper heavy	B	MRS	3	4	4	5	7
Lower heavy	C	MRS	MRS	3	3	4	6
Upper medium	D	MRS	MRS	MRS	MRS	MRS	5
Lower medium	E	MRS	MRS	MRS	MRS	MRS	4
Light	F	MRS	MRS	MRS	MRS	MRS	3

Appendix II – Literature review of flight trajectory prediction

Table 3. Review of dataset of the selected machine learning models for flight trajectory prediction.

Model	Trajectory data source	Trajectory data period	Year of data	Region	Input sequence length	Sampling length	Flight profile	Ref
ML models without deep learning	Radar tracks	2 months	July 2006, Jan 2007	Paris-Orly and Paris-Charles-de-Gaulle airports	11	15s	Climbing phase with longitudinal acceleration and climb rate	(Alligier et al., 2013)
	Radar tracks	1 year	None	City of Paris, France	None	None	En-route flight	(Tastambekov et al., 2014)
	Radar data	2 months	March and May 2012	Incheon International Airport	NS	NS	Approaching phase	(Hong et al., 2015)
	SSR Mode S	4 months	03/06/09/12 2016	Tokyo, Sendai in Japan	NS	NS	Cruise phase	(Takeichi, 2018)
	IFS radar tracks	1 month	April 2016	Barcelona-Madrid, Spanish	None	None	En-route flight	(Georgiou et al., 2020)
	SDPS data	2 months	2019	Guangzhou International Airport	None	None	Approaching phase with ETA estimation	(Gui et al., 2021)
DNN	ADS-B data	1 month	July 2017	TMA of Beijing Capital International Airport	NS	NS	Approaching phase with ETA estimation	(Wang et al., 2018)
	ADS-B data	2 years	2014, 2015	Spain ATC centre	NS	NS	Vertical descent phase with pressure altitude estimation	(Verdonk et al., 2018)
	ADS-B data	NS	NS	Qingdao airport to Beijing Capital International Airport	3s	NS	En-route flight	(Wu et al., 2020)
	ADS-B data	1 month	July 2017	TMA of BCIA	4	None	Approaching phase with ETA estimation	(Wang et al., 2020)
RNN	ADS-B data	4 months	August-November 2018	Baiyun International Airport, China	35 for takeoff; 48 for landing	NS	Landing and take-off phase	(Zeng et al., 2020)

	ADS-B data	5 months	June – November 2017	NS	10	15s	Climbing, cruising, descending/approaching phases	(Shi et al., 2021)
	ADS-B data	12 days	NS	Beijing to Changchun, China	11 days	None	En-route flight	(Han et al., 2021)
	ADS-B data; Flight Radar 24	5 months	February-June 2020	Mumbai airport to Bangalore airport	5	NS	En-route flight	(Sahadevan et al., 2022)
	ADS-B data	1 month	March-April 2019	Singapore	10	15s	En-route flight	(Tran et al., 2022)
	QAR onboard flight data	4 months	Dec 2021- Mar 2022	Chengdu Shuangliu Airport to Guangzhou Baiyun Airport	8	2s, 6s, 10s	En-route flight	(Zhao et al., 2023)
	ADS-B data	8 months	Jan-Aug 2019	Incheon International Airport (ICN), South Korea	None	None	Approaching phase	(Deng et al., 2022)
GAN	ADS-B data	2 months	June-August, 2019	Beijing to Chengdu, China	NS	NS	En-route flight	(Wu et al., 2022)
DGP	NS	1 month	October-November 2018	NS	40	NS	Cruise; heading regulating; climb/descent; acceleration/deceleration	(Chen et al., 2020)
Transformer	ADS-B data	45 days	Feb 1 to Mar 15, 2021	NS	9 (3min)	20s	Climbing; climbing and turning right; descending; maintain; turn; climbing and maintain	(Guo et al., 2023)
Hybrid models	SFDPS messages	2 months	Dec 2018 – Feb 2019	VC Bird International Airport to Miami International Airport	20	12s	En-route flight	(Zhang et al., 2020)
	ADS-B data	4 months	Feb-May 2017	Qingdao to Beijing, China	6	NS	En-route flight	(Ma et al., 2020)
	ADS-B data from OpenSky*	4 years	March 2016 – March 2020	Hartsfield–Jackson Atlanta International Airport	100 timestamps	1 timestamp	Taking-off, landing, and flying over	(Sahfienya et al., 2021; Shafienya et al., 2022)
	ADS-B data	1 year	Mar 2021-Mar 2022	NS	6	5s	En-route flight	(Ding et al., 2022)
	ADS-B data	1 month	May 2019	Guangzhou	NS	1s	Cruise phase	(Zhou et al., 2022)
	ADS-B data	1 year	2018	CAN to NNG	NS	None	En-route flight	(Zhao et al., 2022)
Multiple-flight prediction	NS	1 month	January 2006	Oakland International Airport	20 (100s)	5s	Approaching phase	(Xu et al., 2021)

	Radar tracks	7 days	Aug 2019	KATL airport	20 timestamps	5s	Approaching phase	(Pang et al., 2021; Pang et al., 2022)

Notes: "None" means "not applicable", "NS" denotes "not specified in this research. For the input length column, the value without unit represents the length of sequence.

Table 4. Features of input of the selected machine learning models for flight trajectory prediction.

Trajectory features	Other features	Flight profile	Ref
Thrust law; Mass	Wind; Temperature	Climbing phase with longitudinal acceleration and climb rate	(Alligier et al., 2013)
Latitude; Longitude; Altitude; Speed	Aircraft type	En-route flight	(Tastambekov et al., 2014)
Latitude; Longitude; Altitude; Speed	Aircraft type	Approaching phase	(Hong et al., 2015)
Mach number; Flight distance	Wind; Temperature	Cruise phase	(Takeichi, 2018)
Latitude; Longitude; Altitude	Flight plan; Wind; Temperature; Humidity; Aircraft type	En-route flight	(Georgiou et al., 2020)
Altitude; Longitude; Latitude; Speed; Heading	Historical states (mean flight time, landing runway, etc.); Traffic density; Wind; Metering fix	Approaching phase with ETA estimation	(Gui et al., 2021)
Positions in Cartesian coordinate (X, Y, Z); Heading; Speed	None	Approaching phase with ETA estimation	(Wang et al., 2018)
Latitude; longitude; Flight level; Ground velocity; Descent rate	Aircraft type; Operational procedure (cleared flight levels)	Vertical descent phase with pressure altitude estimation	(Verdonk et al., 2018)
Latitude; Longitude; Altitude; Velocity; Heading; Vertical speed	None	En-route flight	(Wu et al., 2020)
Position in Cartesian coordinate (X, Y, Z); Heading; Ground speed	None	Approaching phase with ETA estimation	(Wang et al., 2020)
Latitude; Longitude; Altitude; Velocity; Course	Aircraft type	Landing and take-off phase	(Zeng et al., 2020)
Latitude; Longitude; Altitude; Heading	Top of climb; Way-points; Takeoff and landing airports	Climbing, cruising, descending/approaching phases	(Shi et al., 2021)
Latitude; Longitude; Height; Airspeed	Time of wheel block	En-route flight	(Han et al., 2021)
Latitude; Longitude; Altitude; Speed; Heading	None	En-route flight	(Sahadevan et al., 2022)
Positions in Cartesian coordinate (X, Y, Z)	Aircraft intents (flight plans; reconstructed trajectory turning points)	En-route flight	(Tran et al., 2022)
Latitude; Longitude; Altitude; Heading; Velocity	Aircraft performance parameters; Wind; Flight phase	En-route flight	(Zhao et al., 2023)

Latitude; Longitude; Altitude; Horizontal and vertical speed	Standard Terminal Arrival Routes	Approaching phase	(Deng et al., 2022)
Positions in Cartesian coordinates (X, Y, Z); Horizontal speed; Vertical speed; Heading	None	En-route flight	(Wu et al., 2022)
Positions in Cartesian coordinate (X, Y, Z)	Flight plan (waypoint sequence, cruise speed and altitude)	Cruise; heading regulating; climb/descent; acceleration/deceleration	(Chen et al., 2020)
Latitude; Longitude; Altitude; Velocity	None	Climbing; climbing and turning right; descending; maintain; turn; climbing and maintain	(Guo et al., 2023)
Latitude; Longitude; Altitude; Horizontal and vertical velocity	Flight plan (4D)	En-route flight	(Zhang et al., 2020)
Latitude; Longitude; Latitude; Velocity; Heading	None	En-route flight	(Ma et al., 2020)
Latitude; Longitude; Altitude; Velocity; Heading; Vertical rate	None	Taking-off, landing, and flying over	(Sahfienya et al., 2021; Shafienya et al., 2022)
Latitude; Longitude; Altitude; velocity	Distance from reference point; Sine and cosine of Angle from reference point	En-route flight	(Ding et al., 2022)
Latitude; Longitude; Altitude; Velocity; Heading	Trajectory intention deviation; Wind	Cruise phase	(Zhou et al., 2022)
Latitude; Longitude; Altitude; Heading; Speed	Weather (temperature, wind direction, wind speed, humidity)	En-route flight	(Zhao et al., 2022)
Latitude; Longitude; Altitude	None	Approaching phase	(Xu et al., 2021)
Latitude; longitude	None	Approaching phase	(Pang et al., 2021; Pang et al., 2022)

Table 5. Literature review of Machine Learning techniques in flight trajectory prediction.

Model	Publish year	Model structure	Prediction time span	Flight phase	Evaluation metrics	Benchmark model(s)	Advantages	Limitations mentioned	Ref
ML models without deep learning	2013	Polynomial regression	10min	Climb phase	RMSE	BADA	Learn unknown parameters of the point-mass model with ML	• Limited class of trajectories utilised; • No comparison with standard ML models	(Alligier et al., 2013)

	2014	Local linear functional regression + wavelet decomposition	10–30 min	En-route flight	RPE	MLR	Regression without physical parameters	Lack observed weather parameters	(Tastambekov et al., 2014)
	2015	Hierarchical clustering with DTW + MLM	NS (short-term)	Approaching phase	RMSE	Regression without clustering	• Include traffic density in regression model; • Identify vectoring patterns of ATCOs	Lack meteorological and other operational features	(Hong et al., 2015)
	2018	GMM + MLR + Adaptive prediction	None	Cruise phase with flight time prediction	RMSE	Static linear prediction	Onboard flight time estimation with adaptive uncertainty prediction	• Without considering ascent and descent trajectories	(Takeichi, 2018)
	2020	Semantic clustering + HMM/ LR/ RT/ DNN	NS (long-term)	En-route flight	MAPE RMSE	Single HMM/ LR/ RT/ DNN without clustering	• Constraint-based waypoint lightweight predictors utilising flight plans; • Nonuniform graph—based grid with low complexity	• Only one flight route considered; • Prediction performed on discrete waypoints; • 3D spatial features predicted individually	(Georgiou et al., 2020)
	2021	K-means with DTW + RF/ XGBoost	None	Approaching phase with ETA estimation	RMSE MAE	Single RF/ XGBoost without clustering	• Multiple stages strategy in data-driven ETA prediction; • consider traffic situations and meteorology conditions	Lack explanation of correlation between fight patterns and flight time estimation	(Gui et al., 2021)

DNN	2018	PCA+DT/ K-means/ DBSCAN + MCNN	None	Approaching phase with ETA estimation	MAE RMSE	Single multiple linear regression	Parallel trajectory prediction for different traffic patterns	• Trajectory resampled into the same length; • Limited time scale of dataset	(Wang et al., 2018)
	2018	PCA + DBSCAN + MLM + PMM/ANN	NS (short-term)	Vertical descent phase	Mean of residuals; RMSE	ANN/PMM model without input of operational procedure	• Comparison of physical model-based prediction with ML methods; • Consider operational factors in ANN	• Made assumption regarding temperature and wind in PMM model; • Consider only two aircraft types	(Verdonk et al., 2018)
	2020	Hierarchical K-means + BPNN	1s	En-route flight	MAX RMSE MAE	SVM	4D trajectory prediction	• Trajectory resampled into the same time interval; • Lack weather and regulatory information	(Wu et al., 2020)
	2020	Clustering + stacked model	None	Approaching phase ETA estimation	MAE RMSE	MLR; BPNN; KNN; GBM; RF	Model stacking to combine high-performance individual models	Lack weather and other factors in prediction	(Wang et al., 2020)
RNN	2020	SS-DLSTM	90s for takeoff; 150s for landing	Landing and take-off	EE ATE CTE Altitude Error	BP-NN; LFR; LSTM	Sequence-to-sequence LSTM for takeoff and landing 4D FTP	Lack weather and other factors in prediction	(Zeng et al., 2020)
	2021	LSTM	1 step (15s)	Climbing, cruising, descending/approaching phases	RMSE MAE MRE DTW	LSTM; SVM; wMM; MM; KF	Embedding flight constraints in loss function of LSTM model for 4D FTP in these flight phases	Lack weather and regulatory factors in prediction	(Shi et al., 2021)
	2021	K-means + online-learning	1 day	En-route flight	RMSE	Single GRU/ LSTM without clustering	Real-time FTP of next day with K-	NS	(Han et al., 2021)

		GRU + LSTM					means clustering to categorise historical trajectories		
	2022	Bi-directional LSTM	5 steps	En-route flight	MAE RMSE MAPE	Uni-directional LSTM; CNN-LSTM; BPNN	• 4D trajectory prediction; • Utilise flight trajectory with variable length without interpolation	Lack weather and other factors	(Sahadevan et al., 2022)
	2022	Encoder (1D Conv) – Decoder (GRU)	1-10 min	En-route flight	RMSE MAE ATE CTE	LSTM with flight constraints embedding in loss function (Shi et al., 2021); BlueSky ATC simulator	• Reconstruct aircraft intents from flight track data; • Predict future trajectories with flexible time horizon	Without considering actual ATC clearance data, or ATCOs management strategies	(Tran et al., 2022)
	2022	Agglomerative hierarchical clustering + DTW; LSTM; ETA	None	Approaching phase	RMSE	K-means; GMM	• LSTM model for trajectory pattern classification; capture complex and diverse flight patterns	Without meteorological data or operational data	(Deng et al., 2022)
	2023	LSTM; XGBoost	1	En-route flight	RMSE MAE	Unbalanced overall prediction model	Consider aircraft performance parameters such as Mach number, pitch angle) in prediction	Individual prediction model for 3D spatial positions.	(Zhao et al., 2023)
GAN	2022	Conv2D-GAN; Conv1D-GAN; LSTM-GAN	NS (long-term)	En-route flight	IS FID MMD MED	None	• Trajectories in RGB image format in modelling; probabilistic 4D FTP	Without considering features of weather or traffic control strategies	(Wu et al., 2022)

DGP	2020	Gaussian process + DNN	3min	Cruise; heading regulating; climb/descent; acceleration/deceleration	Time error; Mean error of DTW; Mean prewarning time	KDA; Kalman; GP	• Probabilistic FTP with application in conflict detection; • Several-stage prediction in altitude, flight time and positions	Only one hidden layer in DGP model; Not end-to-end method in flight altitude and speed prediction	(Chen et al., 2020)
Transformer	2023	Binary encoding + transformer + predictor	20s, 1min, 3min, 5min	Climbing; climbing and turning right; descending; maintain; turn; climbing and maintain	MAE RMSE Average time costs	LSTM; BiLSTM; KF; transformer replaced with LSTM/BiLSTM	Formulate FTP as multi-binary classification problem with trajectory encoded as binary	Prediction model is flight phase-oriented	(Guo et al., 2023)
Hybrid models	2018	Hybrid DNN+ LSTM model + MC Dropout	2 min	En-route flight	RMSE MAE	LR; SVM; DTR; Single RNN	• Prediction based on the trajectory deviation; probabilistic prediction for multiple flights with separation safety measurement	Without consideration of weather conditions	(Zhang et al., 2020)
	2020	CNN(1D)-LSTM	1,3,5	En-route flight	RMSE MAT MAPE	Single BP; single LSTM	1D convolution to extract spatial trajectory features and LSTM to extract temporal dimension	• Prediction model for a single route; • Without considering meteorological conditions and other control orders	(Ma et al., 2020)
	2021	PCA + CNN(3D)-GRU + 3D-CNN + MC Dropout	5 timestamps	Taking-off, landing, and flying over	MAE RMSE	Single CNN; CNN-GRU	3D convolution for both spatial and temporal feature extraction	Lack consideration of other uncertainty sources	(Sahfienya et al., 2021; Shafienya et al., 2022)
	2022	CNN-BiLSTM +dual attention	1	En-route flight	MAE RMSE	BiLSTM; LSTM; CNN-LSTM; F-	• Autotuning hyperparameter	Without considering	(Ding et al., 2022)

		mechanism				CNN-BiLSTM; T-CNN-BiLSTM	with genetic algorithm; • Temporal attention mechanism	other factors affecting trajectory	
	2022	Velocity trend extrapolation; LSTM; stateful-LSTM; BPNN; 1D-ConvNet; KF	1	Cruise phase	MSE	None	Combine several models for 4D FTP according to their advantages in different prediction time horizon	Lack verification of model performance in other flight phases	(Zhou et al., 2022)
	2022	DBSCAN + Gaussian mixture model + LSTM network	None	En-route flight in pre-tactical stage	EE ATE CTE	BPNN; HMM; generic algorithm	Probabilistic FTP with aircraft intention predicting based on Bayesian theory	Aircraft intension is predicted with regard to only meteorological conditions	(Zhao et al., 2022)
Multiple-flight prediction	2021	Social-LSTM network	30 (150s)	Approaching phase	Mean Absolute Point-wise horizontal error; Mean Absolute Point-wise vertical error; APE	Local weighted linear regression; HMM; BPNN; LSTM	FTP of multiple flights with capturing aircraft interaction	Lack consideration of meteorological conditions	(Xu et al., 2021)
	2022	Graph-based spatial transformer module + temporal module	8	Approaching phase	Average Displacement Error; Final Displacement Error	Social LSTM; State refined LSTM; Social attention; TrafficPredict; TAR; Social GAN; Trajectron; STAR-Dropout	• Graph-based spatial transformer module; • trajectory prediction of multiple flights	Without consideration of airspeed, altitude dimensions	(Pang et al., 2021; Pang et al., 2022)

References

Abdelghany, K., Abdelghany, A., & Niznik, T. (2007). Managing severe airspace flow programs: The Airlines' side of the problem. *Journal of Air Transport Management*, *13*(6), 329-337. https://doi.org/https://doi.org/10.1016/j.jairtraman.2007.05.004

Aissi, H., Bazgan, C., & Vanderpooten, D. (2009). Min–max and min–max regret versions of combinatorial optimization problems: A survey. *European Journal of Operational Research*, *197*(2), 427-438. https://doi.org/https://doi.org/10.1016/j.ejor.2008.09.012

Alligier, R., & Gianazza, D. (2018). Learning aircraft operational factors to improve aircraft climb prediction: A large scale multi-airport study. *Transportation Research Part C: Emerging Technologies*, *96*, 72-95. https://doi.org/https://doi.org/10.1016/j.trc.2018.08.012

Alligier, R., Gianazza, D., & Durand, N. (2013). Learning the aircraft mass and thrust to improve the ground-based trajectory prediction of climbing flights. *Transportation Research Part C: Emerging Technologies*, *36*, 45-60. https://doi.org/https://doi.org/10.1016/j.trc.2013.08.006

Alligier, R., Ginazza, D., & Durand, N. (2015). *Machine Learning Applied to Airspeed Prediction During Climb* 11th USA/Europe Air Traffic Management Research and Development Seminar (ATM seminar 2015), https://oatao.univ-toulouse.fr/16837/

Awad, M., & Khanna, R. (2015). Support Vector Regression. In M. Awad & R. Khanna (Eds.), *Efficient Learning Machines: Theories, Concepts, and Applications for Engineers and System Designers* (pp. 67-80). Apress. https://doi.org/10.1007/978-1-4302-5990-9_4

Ayhan, S., & Samet, H. (2016). *Aircraft Trajectory Prediction Made Easy with Predictive Analytics* Proceedings of the 22nd ACM SIGKDD International Conference on Knowledge Discovery and Data Mining, San Francisco, California, USA. https://doi.org/10.1145/2939672.2939694

Balakrishnan, H., & Chandran, B. G. (2010). Algorithms for Scheduling Runway Operations Under Constrained Position Shifting. *Operations Research*, *58*(6), 1650-1665. https://doi.org/10.1287/opre.1100.0869

Barbaresco, F., Juge, P., Klein, M., Canal, D., Ricci, Y., Schneider, J.-Y., Moneuse, J.-F., Lavergne, E., & Mutuel, L. (2013). *Wake vortex detection, prediction and decision support tools in SESAR program*. https://doi.org/10.1109/DASC.2013.6712614

Baren, G. v., Treve, V., & Herrema, F. (2016, 19-21 April 2016). Predicting time to fly on final approach for optimized delivery of separation. 2016 Integrated Communications Navigation and Surveillance (ICNS),

Baren, G. V., Treve, V., Rooseleer, F., Geest, P. V. d., & Heesbeen, B. (2017). *Assessing the severity of wake encounters in various aircraft types in piloted flight simulations* AIAA Modeling and Simulation Technologies Conference, https://arc.aiaa.org/doi/abs/10.2514/6.2017-1084

Barhydt, R. (2013, 22-25 April 2013). Efficient surface operations: Spot and runway departure advisor (SARDA). 2013 Integrated Communications, Navigation and Surveillance Conference (ICNS),

Beasley, J. E., Krishnamoorthy, M., Sharaiha, Y. M., & Abramson, D. (2000). Scheduling Aircraft

Landings—The Static Case. *Transportation Science*, *34*(2), 180-197. https://doi.org/10.1287/trsc.34.2.180.12302

Blasi, L., Barbato, S., & Mattei, M. (2013). A particle swarm approach for flight path optimization in a constrained environment. *Aerospace Science and Technology*, *26*(1), 128-137. https://doi.org/https://doi.org/10.1016/j.ast.2012.02.021

Breitsamter, C. (2011). Wake vortex characteristics of transport aircraft. *Progress in Aerospace Sciences*, *47*(2), 89-134. https://doi.org/https://doi.org/10.1016/j.paerosci.2010.09.002

Burnham, D. C., & Hallock, J. N. (1982). *Chicago monostatic acoustic vortex sensing system : Vol. IV. wake vortex decay* [Tech Report](DOT-TSC-FAA-79-18, IV). D. o. T. o. F. A. Administration. https://rosap.ntl.bts.gov/view/dot/9391

Burnham, D. C., Hallock, J. N., Tombach, I. H., Brashears, M. R., & Barber, M. R. (1978). Ground-Based Measurements of the Wake Vortex Characteristics of a B-747 Aircraft in Various Configurations [Tech Report]. https://rosap.ntl.bts.gov/view/dot/10807

Cai, Z., & Vasconcelos, N. (2018). Cascade r-cnn: Delving into high quality object detection. Proceedings of the IEEE conference on computer vision and pattern recognition,

Casado, E., Civita, M. L., Vilaplana, M., & McGookin, E. W. (2017, 17-21 Sept. 2017). Quantification of aircraft trajectory prediction uncertainty using polynomial chaos expansions. 2017 IEEE/AIAA 36th Digital Avionics Systems Conference (DASC),

Chen, X. H. J. H. Y. (2019). Optimization of CSPRs take-off wake interval based on crosswind effect. *Journal of Safety and Environment*, *19*(02), 411-418. https://doi.org/DOI:10.13637/j.issn.1009-6094.2019.02.008

Chen, Z., Guo, D., & Lin, Y. (2020). A Deep Gaussian Process-Based Flight Trajectory Prediction Approach and Its Application on Conflict Detection. *Algorithms*, *13*(11), 293. https://www.mdpi.com/1999-4893/13/11/293

Cheng, C., Guo, L., Wu, T., Sun, J., Gui, G., Adebisi, B., Gacanin, H., & Sari, H. (2021). Machine Learning-Aided Trajectory Prediction and Conflict Detection for Internet of Aerial Vehicles. *IEEE Internet of Things Journal*, 1-1. https://doi.org/10.1109/JIOT.2021.3060904

Choi, H. C., Deng, C., & Hwang, I. (2021). Hybrid Machine Learning and Estimation-Based Flight Trajectory Prediction in Terminal Airspace. *IEEE Access*, *9*, 151186-151197. https://doi.org/10.1109/ACCESS.2021.3126117

Chu, N., Ng, K. K. H., Liu, Y., & Hon, K. K. (2024). *Analyzing the Potential of Dynamic Aircraft Wake Separation via Data-Driven Aircraft Wake Region Detection* AIAA AVIATION FORUM AND ASCEND 2024, https://arc.aiaa.org/doi/abs/10.2514/6.2024-4249

Chu, N., Ng, K. K. H., Liu, Y., Hon, K. K., Chan, P. W., Li, J., & Zhang, X. (2024). Assessment of approach separation with probabilistic aircraft wake vortex recognition via deep learning. *Transportation Research Part E: Logistics and Transportation Review*, *181*, 103387. https://doi.org/https://doi.org/10.1016/j.tre.2023.103387

Chu, N., Ng, K. K. H., Zhu, X., Liu, Y., Li, L., & Hon, K. K. (2024). Towards dynamic flight separation

in final approach: A hybrid attention-based deep learning framework for long-term spatiotemporal wake vortex prediction. *Transportation Research Part C: Emerging Technologies*, *169*, 104876. https://doi.org/https://doi.org/10.1016/j.trc.2024.104876

Chung, J., Gulcehre, C., Cho, K., & Bengio, Y. (2014). Empirical evaluation of gated recurrent neural networks on sequence modeling. *arXiv preprint arXiv:1412.3555*.

Corjon, A., Stoessel, A., Corjon, A., & Stoessel, A. (2012). Three-dimensional instability of wake vortices near the ground. In *28th Fluid Dynamics Conference*. https://doi.org/10.2514/6.1997-1782

Cortes, C., & Vapnik, V. (1995). Support-vector networks. *Machine Learning*, *20*(3), 273-297. https://doi.org/10.1007/BF00994018

Dastgerdi, K., Mehrshad, N., & Farshad, M. (2015). A new intelligent approach to aircrafts take-off/landing planning at congested single runway airports. *Journal of Soft Computing and Decision Support Systems*, *2*(2), 17-25.

De Visscher, I., Treve, V., & Winckelmans, G. (2016). Characterization of Aircraft Wake Vortex Circulation Decay in Reasonable Worst Case Conditions. In *54th AIAA Aerospace Sciences Meeting*. American Institute of Aeronautics and Astronautics. https://doi.org/doi:10.2514/6.2016-160310.2514/6.2016-1603

Demirel, S. (2023). Comparison of RECAT-EU and ICAO wake turbulence category on the Point Merge System. *The Aeronautical Journal*, 1-15. https://doi.org/10.1017/aer.2023.17

Deng, C., Choi, H.-C., Park, H., & Hwang, I. (2022). Trajectory pattern identification and classification for real-time air traffic applications in Area Navigation terminal airspace. *Transportation Research Part C: Emerging Technologies*, *142*, 103765. https://doi.org/https://doi.org/10.1016/j.trc.2022.103765

Diana, T. (2015a). An evaluation of departure throughputs before and after the implementation of wake vortex recategorization at Atlanta Hartsfield/Jackson International Airport: A Markov regime-switching approach. *Transportation Research Part E: Logistics and Transportation Review*, *83*, 216-224. https://doi.org/https://doi.org/10.1016/j.tre.2015.09.005

Diana, T. (2015b). Measuring the impact of traffic flow management on interarrival duration: An application of autoregressive conditional duration. *Journal of Air Transport Management*, *42*, 219-225. https://doi.org/https://doi.org/10.1016/j.jairtraman.2014.11.002

Ding, W., Huang, J., Shang, G., Wang, X., Li, B., Li, Y., & Liu, H. (2022). Short-Term Trajectory Prediction Based on Hyperparametric Optimisation and a Dual Attention Mechanism. *Aerospace*, *9*(8), 464. https://www.mdpi.com/2226-4310/9/8/464

Dönmez, K., Çetek, C., & Kaya, O. (2022). Aircraft Sequencing and Scheduling in Parallel-Point Merge Systems for Multiple Parallel Runways. *Transportation Research Record*, *2676*(3), 108-124. https://doi.org/10.1177/03611981211049410

Dupuy, M., & Porretta, M. (2007, 21-25 Oct. 2007). Preliminary results for a robust trajectory prediction method using advanced flight data. 2007 IEEE/AIAA 26th Digital Avionics Systems

Conference,

EUROCONTROL. (2018a). *European Wake Turbulence Categorisation and Separation Minima on Approach and Departure*. BRUSSELS: EUROCONTROL Headquarters

EUROCONTROL. (2018b). *RECAT-EU at Paris-CDG, a first in Europe* https://www.eurocontrol.int/press-release/recat-eu-paris-cdg-first-europe

EUROCONTROL. (2020). *Time-Based Separation (TBS) Principles as Alternative to Static Distance-Based Separation for Final Approach*. https://www.eurocontrol.int/sites/default/files/2021-05/eurocontrol-tbs-principles-alt-static-separation-final-approach.pdf

FAA. (2007). *Next generation Air Transport System - NextGen - Concept of Operations, Version 2*, F. J. P. a. D. Office, Washington,DC.

FAA. (2016). *Wake Turbulence Recategorization*. (FAA Order JO 7110.659C). Washington, DC: Federal Aviation Administration

FAA/EUROCONTROL. (2010). *Common TP Structure and Terminology in support of SESAR & NextGen*, FAA/EUROCONTROL, Brussels, Belgium.

Farhadi, F., Ghoniem, A., & Al-Salem, M. (2014). Runway capacity management – An empirical study with application to Doha International Airport. *Transportation Research Part E: Logistics and Transportation Review*, *68*, 53-63. https://doi.org/https://doi.org/10.1016/j.tre.2014.05.004

Frehlich, R., & Sharman, R. (2005). Maximum Likelihood Estimates of Vortex Parameters from Simulated Coherent Doppler Lidar Data. *Journal of Atmospheric and Oceanic Technology*, *22*(2), 117-130. https://doi.org/10.1175/jtech-1695.1

Fusaro, R., Viola, N., Cresto Aleina, S., & Di Meo, G. A. (2019). Innovative time-based separation procedures for civil RPAS integration. *Aircraft Engineering and Aerospace Technology*, *91*(5), 728-735. https://doi.org/10.1108/AEAT-08-2018-0235

Gabrel, V., Murat, C., & Thiele, A. (2014). Recent advances in robust optimization: An overview. *European Journal of Operational Research*, *235*(3), 471-483. https://doi.org/https://doi.org/10.1016/j.ejor.2013.09.036

Gal, Y., & Ghahramani, Z. (2016). Dropout as a bayesian approximation: Representing model uncertainty in deep learning. international conference on machine learning,

Gal, Y., & Ghahramani, Z. (2016). Dropout as a Bayesian Approximation: Representing Model Uncertainty in Deep Learning. *Proceedings of The 33rd International Conference on Machine Learning*, 1050-1059. https://www.scopus.com/inward/record.uri?eid=2-s2.0-85024483419&partnerID=40&md5=fc85184db51ebdb23cdf26b8a62c64a7

Gallo, E., Lopez-Leones, J., Vilaplana, M. A., Navarro, F. A., & Nuic, A. (2007, 21-25 Oct. 2007). Trajectory computation Infrastructure based on BADA Aircraft Performance Model. 2007 IEEE/AIAA 26th Digital Avionics Systems Conference,

Gan, C., Naiyan, W., Yang, Y., Dit-Yan, Y., & Hauptmann, A. G. (2015, 7-12 June 2015). DevNet: A Deep Event Network for multimedia event detection and evidence recounting. 2015 IEEE Conference on Computer Vision and Pattern Recognition (CVPR),

Ge, Z., Liu, S., Wang, F., Li, Z., & Sun, J. (2021). Yolox: Exceeding yolo series in 2021. *arXiv preprint arXiv:2107.08430*.

Georgiou, H., Pelekis, N., Sideridis, S., Scarlatti, D., & Theodoridis, Y. (2020). Semantic-aware aircraft trajectory prediction using flight plans. *International Journal of Data Science and Analytics*, *9*(2), 215-228. https://doi.org/10.1007/s41060-019-00182-4

Gerz, T., Holzäpfel, F., & Darracq, D. (2002). Commercial aircraft wake vortices. *Progress in Aerospace Sciences*, *38*(3), 181-208. https://doi.org/https://doi.org/10.1016/S0376-0421(02)00004-0

Gevorgyan, Z. (2022). SIoU loss: More powerful learning for bounding box regression. *arXiv preprint arXiv:2205.12740*.

Gu, Y., Zhang, J., Zhou, M., & Wang, B. (2022). Data-Driven Analysis of Final Separation Between Successive Landing Aircraft. *Transportation Research Record*, *2676*(7), 786-798. https://doi.org/10.1177/03611981221082559

Guan, X., Zhang, X., Han, D., Zhu, Y., Lv, J., & Su, J. (2014). A strategic flight conflict avoidance approach based on a memetic algorithm. *Chinese Journal of Aeronautics*, *27*(1), 93-101. https://doi.org/https://doi.org/10.1016/j.cja.2013.12.002

Gui, X., Zhang, J., Peng, Z., & Yang, C. (2021). Data-Driven Method for the Prediction of Estimated Time of Arrival. *Transportation Research Record*, *2675*(12), 1291-1305. https://doi.org/10.1177/03611981211033295

Guo, D., Wu, E. Q., Wu, Y., Zhang, J., Law, R., & Lin, Y. (2023). FlightBERT: Binary Encoding Representation for Flight Trajectory Prediction. *Ieee Transactions on Intelligent Transportation Systems*, *24*(2), 1828-1842. https://doi.org/10.1109/TITS.2022.3219923

Hallermeyer, A., Dolfi-Bouteyre, A., Valla, M., Brusquet, L. L., Fleury, G., Thobois, L. P., Cariou, J.-P., Duponcheel, M., & Winckelmans, G. (2016). *Development and assessment of a Wake Vortex characterization algorithm based on a hybrid LIDAR signal processing* 8th AIAA Atmospheric and Space Environments Conference, https://arc.aiaa.org/doi/abs/10.2514/6.2016-3272

Hallock, J. N., & Holzäpfel, F. (2018). A review of recent wake vortex research for increasing airport capacity. *Progress in Aerospace Sciences*, *98*, 27-36. https://doi.org/https://doi.org/10.1016/j.paerosci.2018.03.003

Hammer, J. (2000). Case Study of Paired Approach Procedure to Closely Spaced Parallel Runways. *Air Traffic Control Quarterly*, *8*(3), 223-252. https://doi.org/10.2514/atcq.8.3.223

Han, P., Wang, W., Shi, Q., & Yue, J. (2021). A combined online-learning model with K-means clustering and GRU neural networks for trajectory prediction. *Ad Hoc Networks*, *117*, 102476. https://doi.org/https://doi.org/10.1016/j.adhoc.2021.102476

He, K., Zhang, X., Ren, S., & Sun, J. (2016). Deep residual learning for image recognition. Proceedings of the IEEE conference on computer vision and pattern recognition,

Herrema, F., Curran, R., Hartjes, S., Ellejmi, M., Bancroft, S., & Schultz, M. (2019). A machine learning model to predict runway exit at Vienna airport. *Transportation Research Part E: Logistics and Transportation Review*, *131*, 329-342. https://doi.org/https://doi.org/10.1016/j.tre.2019.10.002

Hochreiter, S., & Schmidhuber, J. (1997). Long Short-Term Memory. *Neural Computation*, *9*(8), 1735-1780. https://doi.org/10.1162/neco.1997.9.8.1735

Hockaday, S. L. M., & Kanafani, A. K. (1974). Developments in airport capacity analysis. *Transportation Research*, *8*(3), 171-180. https://doi.org/https://doi.org/10.1016/0041-1647(74)90004-5

Holzäpfel, F. (2003). Probabilistic Two-Phase Wake Vortex Decay and Transport Model. *Journal of Aircraft*, *40*(2), 323-331. https://doi.org/10.2514/2.3096

Holzäpfel, F., Gerz, T., Köpp, F., Stumpf, E., Harris, M., Young, R. I., & Dolfi-Bouteyre, A. (2003). Strategies for Circulation Evaluation of Aircraft Wake Vortices Measured by Lidar. *Journal of Atmospheric and Oceanic Technology*, *20*(8), 1183-1195. https://doi.org/10.1175/1520-0426(2003)020<1183:Sfceoa>2.0.Co;2

Holzäpfel, F., & Steen, M. (2007). Aircraft Wake-Vortex Evolution in Ground Proximity: Analysis and Parameterization. *AIAA Journal*, *45*(1), 218-227. https://doi.org/10.2514/1.23917

Holzäpfel, F., Strauss, L., & Schwarz, C. (2021). Assessment of dynamic pairwise wake vortex separations for approach and landing at Vienna airport. *Aerospace Science and Technology*, *112*, 106618. https://doi.org/https://doi.org/10.1016/j.ast.2021.106618

Hon, K.-K., & Chan, P.-w. (2022). Historical analysis (2001–2019) of low-level wind shear at the Hong Kong International Airport [https://doi.org/10.1002/met.2063]. *Meteorological Applications*, *29*(2), e2063. https://doi.org/https://doi.org/10.1002/met.2063

Hon, K. K., Chan, P. W., Chim, K. C. Y., De Visscher, I., Thobois, L., Rooseleer, F., & Troiville, A. (2021). Wake Vortex Measurements at the Hong Kong International Airport. In *AIAA SCITECH 2022 Forum*. American Institute of Aeronautics and Astronautics. https://doi.org/doi:10.2514/6.2022-201110.2514/6.2022-2011

Hong, S., & Lee, K. (2015). Trajectory Prediction for Vectored Area Navigation Arrivals. *Journal of Aerospace Information Systems*, *12*(7), 490-502. https://doi.org/10.2514/1.I010245

Hrastovec, M., & Solina, F. (2016). Prediction of aircraft performances based on data collected by air traffic control centers. *Transportation Research Part C: Emerging Technologies*, *73*, 167-182. https://doi.org/https://doi.org/10.1016/j.trc.2016.10.018

Hu, X.-B., Wu, S.-F., & Jiang, J. (2004). On-line free-flight path optimization based on improved genetic algorithms. *Engineering Applications of Artificial Intelligence*, *17*(8), 897-907. https://doi.org/https://doi.org/10.1016/j.engappai.2004.08.015

IATA. (2022). *Climate change*. International Civil Aviation Organisation. https://www.iata.org/en/pressroom/2022-releases/2022-03-01-01/

ICAO. (2005). *Global Air Traffic Management Operational Concept*, ICAO, Montreal, QC, Canada.

ICAO. (2023). *Enhanced wake turbulence separation webinar for the APAC Region*. https://www.icao.int/APAC/Meetings/Pages/2023-RECAT-Webinar.aspx

ICAO. (2024). *Passenger air traffic surpasses pre-pandemic levels*. https://www.icao.int/Newsroom/Pages/Passenger-air-traffic-surpasses-pre-pandemic-levels.aspx

Ikli, S., Mancel, C., Mongeau, M., Olive, X., & Rachelson, E. (2021). The aircraft runway scheduling problem: A survey. *Computers & Operations Research*, *132*, 105336. https://doi.org/https://doi.org/10.1016/j.cor.2021.105336

Jacob, D., Lai, D., Delisi, D., Hutton, D., Barr, K., Shald, S., Hannon, S., & Gatt, P. (2011). *Assessment of Lockheed Martin's Aircraft Wake Vortex Circulation Estimation Algorithms Using Simulated Lidar Data* 3rd AIAA Atmospheric Space Environments Conference, https://arc.aiaa.org/doi/abs/10.2514/6.2011-3196

Jacquillat, A., & Odoni, A. R. (2015). An Integrated Scheduling and Operations Approach to Airport Congestion Mitigation. *Operations Research*, *63*(6), 1390-1410. https://doi.org/10.1287/opre.2015.1428

Jacquillat, A., Odoni, A. R., & Webster, M. D. (2017). Dynamic Control of Runway Configurations and of Arrival and Departure Service Rates at JFK Airport Under Stochastic Queue Conditions. *Transportation Science*, *51*(1), 155-176. https://doi.org/10.1287/trsc.2015.0644

Janic, M. (2008). Modelling the capacity of closely-spaced parallel runways using innovative approach procedures. *Transportation Research Part C: Emerging Technologies*, *16*(6), 704-730. https://doi.org/https://doi.org/10.1016/j.trc.2008.01.003

Jiang, Y., Wang, X., & Zhang, Y. (2023, 26-29 May 2023). Safety Study of Aircraft Dynamic Wake Encounter Based on QAR Data. 2023 6th International Conference on Artificial Intelligence and Big Data (ICAIBD),

Khan, W. A., Ma, H.-L., Ouyang, X., & Mo, D. Y. (2021). Prediction of aircraft trajectory and the associated fuel consumption using covariance bidirectional extreme learning machines. *Transportation Research Part E: Logistics and Transportation Review*, *145*(C). https://doi.org/10.1016/j.tre.2020.102189 (Transportation Research Part E: Logistics and Transportation Review)

Kolos-Lakatos, T. (2017). *A system level study of new wake turbulence separation concepts and their impact on airport capacity*

Kopardekar, P., Green, S., Aston, J., & Roherty, T. (2003). *Miles-in-Trail (MIT): A Perspective* (AIAA's 3rd Annual Aviation Technology, Integration, and Operations (ATIO) Forum, Issue, American Institute of Aeronautics and Astronautics. https://doi.org/10.2514/6.2003-6700

Lea, C., Vidal, R., Reiter, A., & Hager, G. D. (2016). Temporal convolutional networks: A unified approach to action segmentation. Computer Vision–ECCV 2016 Workshops: Amsterdam, The Netherlands, October 8-10 and 15-16, 2016, Proceedings, Part III 14,

Li, J., Li, K., Tian, Q., & Ram Kumar, P. N. (2022). An improved column generation algorithm for the disrupted flight recovery problem with discrete flight duration control and aircraft assignment constraints. *Computers & Industrial Engineering*, *174*, 108772. https://doi.org/https://doi.org/10.1016/j.cie.2022.108772

Li, J., Shen, C., Gao, H., Chan, P. W., Hon, K. K., & Wang, X. (2020). Path integration (PI) method for the parameter-retrieval of aircraft wake vortex by Lidar. *Optics Express*, *28*(3), 4286-4306.

https://doi.org/10.1364/OE.382968

Li, J., Wang, T., Liu, Z., & Wang, X. (2016). Circulation retrieval of wake vortex in fog with a side-looking scanning radar. *IEEE Transactions on Aerospace and Electronic Systems*, *52*(5), 2242-2254. https://doi.org/10.1109/TAES.2016.150635

Li, T., & Wan, Y. (2021). A fuel savings and benefit analysis of reducing separation standards in the oceanic airspace managed by the New York Air Route Traffic Control Center. *Transportation Research Part E: Logistics and Transportation Review*, *152*, 102407. https://doi.org/https://doi.org/10.1016/j.tre.2021.102407

Li, Z., Liu, F., Yang, W., Peng, S., & Zhou, J. (2022). A Survey of Convolutional Neural Networks: Analysis, Applications, and Prospects. *IEEE Transactions on Neural Networks and Learning Systems*, *33*(12), 6999-7019. https://doi.org/10.1109/TNNLS.2021.3084827

Lieder, A., & Stolletz, R. (2016). Scheduling aircraft take-offs and landings on interdependent and heterogeneous runways. *Transportation Research Part E: Logistics and Transportation Review*, *88*, 167-188. https://doi.org/https://doi.org/10.1016/j.tre.2016.01.015

Lin, M., Huang, W., Zhang, Z., Xu, C., & Cui, G. (2017). Numerical study of aircraft wake vortex evolution near ground in stable atmospheric boundary layer. *Chinese Journal of Aeronautics*, *30*(6), 1866-1876. https://doi.org/https://doi.org/10.1016/j.cja.2017.08.012

Lin, X., Zhang, J., Zhu, Y., & Liu, W. (2008, 10-12 Oct. 2008). Simulation study of algorithms for aircraft trajectory prediction based on ADS-B technology. 2008 Asia Simulation Conference - 7th International Conference on System Simulation and Scientific Computing,

Liu, F., Liu, X., Mou, M., & Wei, Z. (2019). Safety assessment of approximate segregated parallel operation on closely spaced parallel runways. *Chinese Journal of Aeronautics*, *32*(2), 463-476. https://doi.org/https://doi.org/10.1016/j.cja.2018.12.009

Liu, Y., Ng, K. K. H., Chu, N., Hon, K. K., & Zhang, X. (2023a). Spatiotemporal Image-Based Flight Trajectory Clustering Model with Deep Convolutional Autoencoder Network. *Journal of Aerospace Information Systems*, *20*(9), 575-587. https://doi.org/10.2514/1.I011194

Liu, Y., Ng, K. K. H., Chu, N., Hon, K. K., & Zhang, X. (2023b). Spatiotemporal Image-Based Flight Trajectory Clustering Model with Deep Convolutional Autoencoder Network. *Journal of Aerospace Information Systems*, *0*(0), 1-13. https://doi.org/10.2514/1.I011194

Lopez-Leones, J., Vilaplana, M. A., Gallo, E., Navarro, F. A., & Querejeta, C. (2007, 21-25 Oct. 2007). The Aircraft Intent Description Language: A key enabler for air-ground synchronization in Trajectory-Based Operations. 2007 IEEE/AIAA 26th Digital Avionics Systems Conference,

Louie, R., Lui, G. N., Tai, T. S., & Liem, R. P. (2023). Data-Driven Analysis of Inefficient Arrival Separation. In *AIAA AVIATION 2023 Forum*. American Institute of Aeronautics and Astronautics. https://doi.org/doi:10.2514/6.2023-3258 10.2514/6.2023-3258

Lundberg, S. M., & Lee, S.-I. (2017). A unified approach to interpreting model predictions. *Advances in neural information processing systems*, *30*.

Lymperopoulos, I., & Lygeros, J. (2010). Sequential Monte Carlo methods for multi-aircraft trajectory

prediction in air traffic management. *International Journal of Adaptive Control and Signal Processing*, *24*(10), 830-849. https://doi.org/https://doi.org/10.1002/acs.1174

Ma, J., Delahaye, D., Sbihi, M., Scala, P., & Mujica Mota, M. A. (2019). Integrated optimization of terminal maneuvering area and airport at the macroscopic level. *Transportation Research Part C: Emerging Technologies*, *98*, 338-357. https://doi.org/https://doi.org/10.1016/j.trc.2018.12.006

Ma, L., & Tian, S. (2020). A Hybrid CNN-LSTM Model for Aircraft 4D Trajectory Prediction. *IEEE Access*, *8*, 134668-134680. https://doi.org/10.1109/ACCESS.2020.3010963

Malik, W., & Jung, Y. C. (2016). Exact and Heuristic Algorithms for Runway Scheduling. In *16th AIAA Aviation Technology, Integration, and Operations Conference*. American Institute of Aeronautics and Astronautics. https://doi.org/doi:10.2514/6.2016-407210.2514/6.2016-4072

Malik, W., Lee, H., & Jung, Y. C. (2016). Runway Scheduling for Charlotte Douglas International Airport. In *16th AIAA Aviation Technology, Integration, and Operations Conference*. American Institute of Aeronautics and Astronautics. https://doi.org/doi:10.2514/6.2016-407310.2514/6.2016-4073

Matayoshi, N., & Yoshikawa, E. (2014). Dynamic wake vortex separation combining with traffic optimization. 29th Congress of the International Council of the Aeronautical Sciences, St. Petersburg, Russia,

Moore, D. W. (1974). A numerical study of the roll-up of a finite vortex sheet. *Journal of Fluid Mechanics*, *63*(2), 225-235. https://doi.org/10.1017/S002211207400111X

Morris, C., Peters, J., & Choroba, P. (2013). Validation of the time based separation concept at London Heathrow Airport. Tenth USA/Europe Air Traffic Management Research and Development Seminar,

Murça, M. C. R., & Müller, C. (2015). Control-based optimization approach for aircraft scheduling in a terminal area with alternative arrival routes. *Transportation Research Part E: Logistics and Transportation Review*, *73*, 96-113. https://doi.org/https://doi.org/10.1016/j.tre.2014.11.004

Mutuel, L., Barbaresco, F., Juge, P., Klein, M., Canal, D., Ricci, Y., Schneider, J.-Y., Moneuse, J.-F., & Lavergne, E. (2014). *ATM Decision Support Tool for Wake Vortex Hazard Management Combining Sensors and Modeling* (Vol. 51). https://doi.org/10.2514/6.2014-2332

NATS. (2015). *Aeronautical Information Circular P 001/2015*.

Neal, R. M. (2012). *Bayesian learning for neural networks* (Vol. 118). Springer Science & Business Media.

Ng, K. K. H., Chen, C.-H., & Lee, C. K. M. (2021). Mathematical programming formulations for robust airside terminal traffic flow optimisation problem. *Computers & Industrial Engineering*, *154*, 107119. https://doi.org/https://doi.org/10.1016/j.cie.2021.107119

Ng, K. K. H., Lee, C. K. M., & Chan, F. T. S. (2017, 10-13 Dec. 2017). A robust optimisation approach to the aircraft sequencing and scheduling problem with runway configuration planning. 2017 IEEE International Conference on Industrial Engineering and Engineering Management (IEEM),

Ng, K. K. H., Lee, C. K. M., Chan, F. T. S., Chen, C.-H., & Qin, Y. (2020). A two-stage robust optimisation for terminal traffic flow problem. *Applied Soft Computing*, *89*, 106048. https://doi.org/https://doi.org/10.1016/j.asoc.2019.106048

Ng, K. K. H., Lee, C. K. M., Chan, F. T. S., & Lv, Y. (2018). Review on meta-heuristics approaches for airside operation research. *Applied Soft Computing*, *66*, 104-133. https://doi.org/https://doi.org/10.1016/j.asoc.2018.02.013

Ng, K. K. H., Lee, C. K. M., Chan, F. T. S., & Qin, Y. (2017). Robust aircraft sequencing and scheduling problem with arrival/departure delay using the min-max regret approach. *Transportation Research Part E: Logistics and Transportation Review*, *106*, 115-136. https://doi.org/https://doi.org/10.1016/j.tre.2017.08.006

Nuic, A., Poles, D., & Mouillet, V. (2010). BADA: An advanced aircraft performance model for present and future ATM systems. *International Journal of Adaptive Control and Signal Processing*, *24*(10), 850-866. https://doi.org/https://doi.org/10.1002/acs.1176

Pan, W., Jiang, Y., & Zhang, Y. (2023). Simulation Study of the Effect of Atmospheric Stratification on Aircraft Wake Vortex Encounter. *Sustainability*, *15*(8).

Pan, W., Wu, Z., & Zhang, X. (2020). Identification of Aircraft Wake Vortex Based on SVM. *Mathematical Problems in Engineering*, *2020*, 9314164. https://doi.org/10.1155/2020/9314164

Pang, Y., Zhao, P., Hu, J., & Liu, Y. (2024). Machine learning-enhanced aircraft landing scheduling under uncertainties. *Transportation Research Part C: Emerging Technologies*, *158*, 104444. https://doi.org/https://doi.org/10.1016/j.trc.2023.104444

Pang, Y., Zhao, X., Hu, J., Yan, H., & Liu, Y. (2021). Bayesian Spatio-Temporal Graph Transformer Network (B-Star) for Multi-Aircraft Trajectory Prediction. *SSRN Electronic Journal*. https://doi.org/10.2139/ssrn.3981312

Pang, Y., Zhao, X., Hu, J., Yan, H., & Liu, Y. (2022). Bayesian Spatio-Temporal grAph tRansformer network (B-STAR) for multi-aircraft trajectory prediction. *Knowledge-Based Systems*, *249*, 108998. https://doi.org/https://doi.org/10.1016/j.knosys.2022.108998

Pang, Y., Zhao, X., Yan, H., & Liu, Y. (2021). Data-driven trajectory prediction with weather uncertainties: A Bayesian deep learning approach. *Transportation Research Part C: Emerging Technologies*, *130*, 103326. https://doi.org/https://doi.org/10.1016/j.trc.2021.103326

Pinol, H., & Beasley, J. E. (2006). Scatter Search and Bionomic Algorithms for the aircraft landing problem. *European Journal of Operational Research*, *171*(2), 439-462. https://doi.org/https://doi.org/10.1016/j.ejor.2004.09.040

Pohl, M., Kolisch, R., & Schiffer, M. (2021). Runway scheduling during winter operations. *Omega*, *102*, 102325. https://doi.org/https://doi.org/10.1016/j.omega.2020.102325

Prakash, R., Piplani, R., & Desai, J. (2018). An optimal data-splitting algorithm for aircraft scheduling on a single runway to maximize throughput. *Transportation Research Part C: Emerging Technologies*, *95*, 570-581. https://doi.org/https://doi.org/10.1016/j.trc.2018.07.031

Proctor, F. (1998). *The NASA-Langley wake vortex modelling effort in support of an operational aircraft*

spacing system 36th AIAA Aerospace Sciences Meeting and Exhibit, https://arc.aiaa.org/doi/abs/10.2514/6.1998-589

Proctor, F., Hamilton, D., & Switzer, G. (2006). *TASS Driven Algorithms for Wake Prediction* 44th AIAA Aerospace Sciences Meeting and Exhibit, https://arc.aiaa.org/doi/abs/10.2514/6.2006-1073

Rahm, S., & Smalikho, I. (2008). Aircraft wake vortex measurement with airborne coherent Doppler lidar. *Journal of Aircraft*, *45*(4), 1148-1155.

Redmon, J., Divvala, S., Girshick, R., & Farhadi, A. (2016). You only look once: Unified, real-time object detection. Proceedings of the IEEE conference on computer vision and pattern recognition,

Redmon, J., & Farhadi, A. (2018). Yolov3: An incremental improvement. *arXiv preprint arXiv:1804.02767*.

Ren, S., He, K., Girshick, R., & Sun, J. (2015). Faster r-cnn: Towards real-time object detection with region proposal networks. *Advances in neural information processing systems*, *28*.

Rey, D., Rapine, C., Fondacci, R., & El Faouzi, N.-E. (2016). Subliminal Speed Control in Air Traffic Management: Optimization and Simulation. *Transportation Science*, *50*(1), 240-262. https://doi.org/10.1287/trsc.2015.0602

Rezaie, R., Li, X. R., & Jilkov, V. P. (2021). Conditionally Markov Modeling and Optimal Estimation for Trajectory With Waypoints and Destination. *IEEE Transactions on Aerospace and Electronic Systems*, *57*(4), 2006-2020. https://doi.org/10.1109/TAES.2021.3075533

Roa, J., Trani, A., Hu, J., & Mirmohammadsadeghi, N. (2020). Simulation of Runway Operations with Application of Dynamic Wake Separations to Study Runway Limitations. *Transportation Research Record*, *2674*(12), 199-211. https://doi.org/10.1177/0361198120953152

Robins, R. E., & Delisi, D. P. (1996). 3-D Calculations Showing the Effects of Stratification on the Evolution of Trailing Vortices. In M. Deville, S. Gavrilakis, & I. L. Ryhming (Eds.), *Computation of Three-Dimensional Complex Flows: Proceedings of the IMACS-COST Conference on Computational Fluid Dynamics Lausanne, September 13–15, 1995* (pp. 264-270). Vieweg+Teubner Verlag. https://doi.org/10.1007/978-3-322-89838-8_35

Robnik-Šikonja, M., & Kononenko, I. (2008). Explaining Classifications For Individual Instances. *IEEE Transactions on Knowledge and Data Engineering*, *20*(5), 589-600. https://doi.org/10.1109/TKDE.2007.190734

Rojas, J. I., Melgosa, M., & Prats, X. (2021). Sensitivity Analysis of Maximum Circulation of Wake Vortex Encountered by En-Route Aircraft. *Aerospace*, *8*(7), 194. https://www.mdpi.com/2226-4310/8/7/194

Roy, K., Levy, B., & Tomlin, C. (2006). Target Tracking and Estimated Time of Arrival (ETA) Prediction for Arrival Aircraft. In *AIAA Guidance, Navigation, and Control Conference and Exhibit*. American Institute of Aeronautics and Astronautics. https://doi.org/doi:10.2514/6.2006-6324

Sahadevan, D., M, H. P., Ponnusamy, P., Gopi, V. P., & Nelli, M. K. (2022). Ground-based 4d trajectory prediction using bi-directional LSTM networks. *Applied Intelligence*.

https://doi.org/10.1007/s10489-022-03309-6

Sahfienya, H., & Regan, A. C. (2021). 4D flight trajectory prediction using a hybrid Deep Learning prediction method based on ADS-B technology: a case study of Hartsfield-Jackson Atlanta International Airport (ATL). *arXiv preprint arXiv:2110.07774*.

Salehipour, A., Modarres, M., & Moslemi Naeni, L. (2013). An efficient hybrid meta-heuristic for aircraft landing problem. *Computers & Operations Research*, *40*(1), 207-213. https://doi.org/https://doi.org/10.1016/j.cor.2012.06.004

Samà, M., D'Ariano, A., Corman, F., & Pacciarelli, D. (2017). Metaheuristics for efficient aircraft scheduling and re-routing at busy terminal control areas. *Transportation Research Part C: Emerging Technologies*, *80*, 485-511. https://doi.org/https://doi.org/10.1016/j.trc.2016.08.012

Samà, M., D'Ariano, A., D'Ariano, P., & Pacciarelli, D. (2017). Scheduling models for optimal aircraft traffic control at busy airports: Tardiness, priorities, equity and violations considerations. *Omega*, *67*, 81-98. https://doi.org/https://doi.org/10.1016/j.omega.2016.04.003

Sankararaman, S., & Daigle, M. (2017). *Uncertainty Quantification in Trajectory Prediction for Aircraft Operations* AIAA Guidance, Navigation, and Control Conference, https://doi.org/10.2514/6.2017-1724

Schuster, W. (2015). Trajectory prediction for future air traffic management – complex manoeuvres and taxiing. *The Aeronautical Journal*, *119*(1212), 121-143. https://doi.org/10.1017/S0001924000010307

Schuster, W., Porretta, M., & Ochieng, W. (2012). High-accuracy four-dimensional trajectory prediction for civil aircraft. *The Aeronautical Journal (1968)*, *116*(1175), 45-66. https://doi.org/10.1017/S0001924000006618

Seah, C. E., Aligawesa, A., & Hwang, I. (2010). Algorithm for Conformance Monitoring in Air Traffic Control. *Journal of Guidance, Control, and Dynamics*, *33*(2), 500-509. https://doi.org/10.2514/1.44839

Selvaraju, R. R., Cogswell, M., Das, A., Vedantam, R., Parikh, D., & Batra, D. (2017). Grad-cam: Visual explanations from deep networks via gradient-based localization. Proceedings of the IEEE international conference on computer vision,

SESAR. (2007). *ATM Target Concept: deliverable D3*, S. Consortium.

Shafienya, H., & Regan, A. C. (2022). 4D flight trajectory prediction using a hybrid Deep Learning prediction method based on ADS-B technology: A case study of Hartsfield–Jackson Atlanta International Airport (ATL). *Transportation Research Part C: Emerging Technologies*, *144*, 103878. https://doi.org/https://doi.org/10.1016/j.trc.2022.103878

Shen, C., Tang, W., Gao, H., Wang, X., Chan, P. W., Hon, K. K., & Li, J. (2023). Aircraft Wake Recognition and Strength Classification Based on Deep Learning. *IEEE Journal of Selected Topics in Applied Earth Observations and Remote Sensing*, *16*, 2237-2249. https://doi.org/10.1109/JSTARS.2023.3243941

Shi, Z., Xu, M., & Pan, Q. (2021). 4-D Flight Trajectory Prediction With Constrained LSTM Network.

Ieee Transactions on Intelligent Transportation Systems, *22*(11), 7242-7255. https://doi.org/10.1109/TITS.2020.3004807

Simonyan, K., Vedaldi, A., & Zisserman, A. (2013). Deep inside convolutional networks: Visualising image classification models and saliency maps. *arXiv preprint arXiv:1312.6034*.

Simonyan, K., & Zisserman, A. (2014). Very deep convolutional networks for large-scale image recognition. *arXiv preprint arXiv:1409.1556*.

Smalikho, I. N., & Banakh, V. A. (2015). Estimation of aircraft wake vortex parameters from data measured with a 1.5-μm coherent Doppler lidar. *Optics Letters*, *40*(14), 3408-3411. https://doi.org/10.1364/OL.40.003408

Smalikho, I. N., Banakh, V. A., Holzäpfel, F., & Rahm, S. (2015). Method of radial velocities for the estimation of aircraft wake vortex parameters from data measured by coherent Doppler lidar. *Optics Express*, *23*(19), A1194-A1207. https://doi.org/10.1364/OE.23.0A1194

Sölveling, G., & Clarke, J.-P. (2014). Scheduling of airport runway operations using stochastic branch and bound methods. *Transportation Research Part C: Emerging Technologies*, *45*, 119-137. https://doi.org/https://doi.org/10.1016/j.trc.2014.02.021

Song, Y., Cheng, P., & Mu, C. (2012, 6-8 June 2012). An improved trajectory prediction algorithm based on trajectory data mining for air traffic management. 2012 IEEE International Conference on Information and Automation,

Subramanian, A., & Mahadevan, S. (2022). Importance sampling for probabilistic prognosis of sector-wide flight separation safety. *Reliability Engineering & System Safety*, *222*, 108410. https://doi.org/https://doi.org/10.1016/j.ress.2022.108410

Sun, J., Ellerbroek, J., & Hoekstra, J. M. (2018). Aircraft initial mass estimation using Bayesian inference method. *Transportation Research Part C: Emerging Technologies*, *90*, 59-73. https://doi.org/10.1016/j.trc.2018.02.022

Sun, J., Ellerbroek, J., & Hoekstra, J. M. (2019). WRAP: An open-source kinematic aircraft performance model. *Transportation Research Part C: Emerging Technologies*, *98*, 118-138. https://doi.org/10.1016/j.trc.2018.11.009

Switzer, G., & Proctor, F. Numerical study of wake vortex behavior in turbulent domains with ambient stratification. In *38th Aerospace Sciences Meeting and Exhibit*. https://doi.org/10.2514/6.2000-755

Takeichi, N. (2018). Adaptive prediction of flight time uncertainty for ground-based 4D trajectory management. *Transportation Research Part C: Emerging Technologies*, *95*, 335-345. https://doi.org/https://doi.org/10.1016/j.trc.2018.07.028

Tastambekov, K., Puechmorel, S., Delahaye, D., & Rabut, C. (2014). Aircraft trajectory forecasting using local functional regression in Sobolev space. *Transportation Research Part C: Emerging Technologies*, *39*, 1-22. https://doi.org/https://doi.org/10.1016/j.trc.2013.11.013

Thipphavong, D. P., Schultz, C. A., Lee, A. G., & Chan, S. H. (2012). Adaptive Algorithm to Improve Trajectory Prediction Accuracy of Climbing Aircraft. *Journal of Guidance, Control, and*

Dynamics, *36*(1), 15-24. https://doi.org/10.2514/1.58508

Thobois, L. P., Krishnamurthy, R., Cariou, J.-P., & Nicolaon, J. P. (2016). Deployment of a next generation and operational LIDAR solution for monitoring wake vortices for supporting new wake turbulence regulations (Invited). In *8th AIAA Atmospheric and Space Environments Conference*. American Institute of Aeronautics and Astronautics. https://doi.org/doi:10.2514/6.2016-327310.2514/6.2016-3273

Tran, P. N., Nguyen, H. Q. V., Pham, D. T., & Alam, S. (2022). Aircraft Trajectory Prediction With Enriched Intent Using Encoder-Decoder Architecture. *IEEE Access*, *10*, 17881-17896. https://doi.org/10.1109/ACCESS.2022.3149231

Treve, V. (2013). *Wake turbulence severity metrics*, EUROCONTROL, Brussels.

van Laarhoven, P. J. M., & Aarts, E. H. L. (1987). Simulated annealing. In P. J. M. van Laarhoven & E. H. L. Aarts (Eds.), *Simulated Annealing: Theory and Applications* (pp. 7-15). Springer Netherlands. https://doi.org/10.1007/978-94-015-7744-1_2

Vaswani, A., Shazeer, N., Parmar, N., Uszkoreit, J., Jones, L., Gomez, A. N., Kaiser, Ł., & Polosukhin, I. (2017). Attention is all you need. *Advances in neural information processing systems*, *30*.

Verdonk Gallego, C. E., Gómez Comendador, V. F., Sáez Nieto, F. J., Orenga Imaz, G., & Arnaldo Valdés, R. M. (2018). Analysis of air traffic control operational impact on aircraft vertical profiles supported by machine learning. *Transportation Research Part C: Emerging Technologies*, *95*, 883-903. https://doi.org/https://doi.org/10.1016/j.trc.2018.03.017

Visscher, I. D., Stempfel, G., Rooseleer, F., & Treve, V. (2018, 23-27 Sept. 2018). Data mining and Machine Learning techniques supporting Time-Based Separation concept deployment. 2018 IEEE/AIAA 37th Digital Avionics Systems Conference (DASC),

Visscher, I. D., Winckelmans, G., Lonfils, T., Bricteux, L., Duponcheel, M., & Bourgeois, N. (2010). *The WAKE4D Simulation Platform for Predicting Aircraft Wake Vortex Transport and Decay: Description and Examples of Application* AIAA Atmospheric and Space Environments Conference, https://arc.aiaa.org/doi/abs/10.2514/6.2010-7994

Wan, S., Liang, Y., & Zhang, Y. (2018). Deep convolutional neural networks for diabetic retinopathy detection by image classification. *Computers & Electrical Engineering*, *72*, 274-282. https://doi.org/https://doi.org/10.1016/j.compeleceng.2018.07.042

Wang, Y. H., Pang, Y. T., Chen, O., Iyer, H. N., Dutta, P., Menon, P. K., & Liu, Y. M. (2021). Uncertainty quantification and reduction in aircraft trajectory prediction using Bayesian-Entropy information fusion. *Reliability Engineering & System Safety*, *212*, Article 107650. https://doi.org/10.1016/j.ress.2021.107650

Wang, Z., Liang, M., & Delahaye, D. (2018). A hybrid machine learning model for short-term estimated time of arrival prediction in terminal manoeuvring area. *Transportation Research Part C: Emerging Technologies*, *95*, 280-294. https://doi.org/https://doi.org/10.1016/j.trc.2018.07.019

Wang, Z., Liang, M., & Delahaye, D. (2020). Automated data-driven prediction on aircraft Estimated Time of Arrival. *Journal of Air Transport Management*, *88*, 101840.

https://doi.org/https://doi.org/10.1016/j.jairtraman.2020.101840

Wartha, N., Stephan, A., Holzäpfel, F., & Rotshteyn, G. (2022). Characterizing aircraft wake vortex position and strength using LiDAR measurements processed with artificial neural networks. *Optics Express*, *30*(8), 13197-13225. https://doi.org/10.1364/OE.454525

Wassaf, H. S., Burnham, D. C., & Wang, F. Y. (2011). Wake Vortex Tangential Velocity Adaptive Spectral (TVAS) algorithm for pulsed Lidar systems [Proceedings]. https://rosap.ntl.bts.gov/view/dot/9150

Weijun, P., Yingjie, D., Qiang, Z., Jiahao, T., & Jun, Z. (2019). Deep Learning for Aircraft Wake Vortex Identification. *IOP Conference Series: Materials Science and Engineering*, *685*(1), 012015. https://doi.org/10.1088/1757-899x/685/1/012015

Woo, S., Park, J., Lee, J.-Y., & Kweon, I. S. (2018, 2018//). CBAM: Convolutional Block Attention Module. Computer Vision – ECCV 2018, Cham.

Wu, S., Zhai, X., & Liu, B. (2019). Aircraft wake vortex and turbulence measurement under near-ground effect using coherent Doppler lidar. *Optics Express*, *27*(2), 1142-1163. https://doi.org/10.1364/OE.27.001142

Wu, X., Yang, H., Chen, H., Hu, Q., & Hu, H. (2022). Long-term 4D trajectory prediction using generative adversarial networks. *Transportation Research Part C: Emerging Technologies*, *136*, 103554. https://doi.org/https://doi.org/10.1016/j.trc.2022.103554

Wu, Z. J., Tian, S., & Ma, L. (2020). A 4D trajectory prediction model based on the BP neural network. *Journal of Intelligent Systems*, *29*(1), 1545-1557. https://doi.org/10.1515/jisys-2019-0077

Xu, B. (2017). An efficient Ant Colony algorithm based on wake-vortex modeling method for aircraft scheduling problem. *Journal of Computational and Applied Mathematics*, *317*, 157-170. https://doi.org/https://doi.org/10.1016/j.cam.2016.11.043

Xu, Z., Li, D., & Cai, J. (2023). Long-wave deformation of in-ground-effect wake vortex under crosswind condition. *Aerospace Science and Technology*, *142*, 108697. https://doi.org/https://doi.org/10.1016/j.ast.2023.108697

Xu, Z. F., Zeng, W. L., Chu, X., & Cao, P. W. (2021). Multi-Aircraft Trajectory Collaborative Prediction Based on Social Long Short-Term Memory Network. *Aerospace*, *8*(4), Article 115. https://doi.org/10.3390/aerospace8040115

Yamashita, R., Nishio, M., Do, R. K. G., & Togashi, K. (2018). Convolutional neural networks: an overview and application in radiology. *Insights into Imaging*, *9*(4), 611-629. https://doi.org/10.1007/s13244-018-0639-9

Yang, Y., Gao, Z., & He, C. (2020). Stochastic terminal flight arrival and departure scheduling problem under performance-based navigation environment. *Transportation Research Part C: Emerging Technologies*, *119*, 102735. https://doi.org/https://doi.org/10.1016/j.trc.2020.102735

Yu, Y., Yao, H., & Liu, Y. (2019). Aircraft dynamics simulation using a novel physics-based learning method. *Aerospace Science and Technology*, *87*, 254-264. https://doi.org/https://doi.org/10.1016/j.ast.2019.02.021

Zeng, W., Quan, Z., Zhao, Z., Xie, C., & Lu, X. (2020). A Deep Learning Approach for Aircraft Trajectory Prediction in Terminal Airspace. *IEEE Access*, *8*, 151250-151266. https://doi.org/10.1109/ACCESS.2020.3016289

Zhang, J., Liu, J., Hu, R., & Zhu, H. (2018). Online four dimensional trajectory prediction method based on aircraft intent updating. *Aerospace Science and Technology*, *77*, 774-787. https://doi.org/https://doi.org/10.1016/j.ast.2018.03.037

Zhang, X., Guan, X., Zhu, Y., & Lei, J. (2015). Strategic flight assignment approach based on multi-objective parallel evolution algorithm with dynamic migration interval. *Chinese Journal of Aeronautics*, *28*(2), 556-563. https://doi.org/https://doi.org/10.1016/j.cja.2015.01.012

Zhang, X., & Mahadevan, S. (2020). Bayesian neural networks for flight trajectory prediction and safety assessment. *Decision Support Systems*, *131*, 113246. https://doi.org/https://doi.org/10.1016/j.dss.2020.113246

Zhang, Y.-F., Ren, W., Zhang, Z., Jia, Z., Wang, L., & Tan, T. (2022). Focal and efficient IOU loss for accurate bounding box regression. *Neurocomputing*, *506*, 146-157.

Zhao, Y., & Li, K. (2023). A Fractal Dimension Feature Model for Accurate 4D Flight-Trajectory Prediction. *Sustainability*, *15*(2), 1272. https://www.mdpi.com/2071-1050/15/2/1272

Zhao, Z., Zhang, L., & Mao, J. (2022, 8-10 April 2022). A Deep Learning Approach for Aircraft Trajectory Prediction in Pre-Tactical Stage. 2022 5th International Symposium on Autonomous Systems (ISAS),

Zhou, B., Khosla, A., Lapedriza, A., Oliva, A., & Torralba, A. (2016). Learning deep features for discriminative localization. Proceedings of the IEEE conference on computer vision and pattern recognition,

Zhou, J., Zhang, H., Lyu, W., Wan, J., Zhang, J., & Song, W. (2022). Hybrid 4-Dimensional Trajectory Prediction Model, Based on the Reconstruction of Prediction Time Span for Aircraft en Route. *Sustainability*, *14*(7), 3862. https://www.mdpi.com/2071-1050/14/7/3862

Zintgraf, L. M., Cohen, T. S., Adel, T., & Welling, M. (2017). Visualizing deep neural network decisions: Prediction difference analysis. *arXiv preprint arXiv:1702.04595*.